UNIVERSITY OF TASMANIA

Emtins: Novel Peptides Derived from Metallothionein-II as Potential Therapeutics in Alzheimer's Disease

By

Emma Dawn Eaton, B.Sc. (Hons)

Submitted in partial fulfilment for the

Degree of Doctor of Philosophy (Medicine)

University of Tasmania, March 2016

Declaration of originality

This thesis contains no material which has been accepted for a degree or diploma by the University of Tasmania or any other institution, except where acknowledged, and by way of background information and duly acknowledged in the thesis, and to the best of my knowledge and belief no material previously published or written by another person except where due acknowledgement is made in the text of the thesis, nor does the thesis contain any material that infringes copyright.

Emma Eaton

Authority of Access

This thesis may be made available for loan and limited copying and communication in accordance with the Copyright Act 1968.

Emma Eaton

Statement of Ethical Conduct

The research associated with this thesis abides by the international and Australian codes on human and animal experimentation, the guidelines by the Australian Government's Office of the Gene Technology Regulator and the rulings of the Safety, Ethics and Institutional Biosafety Committees of the University.

Emma Eaton

Acknowledgements

I would like to acknowledge the work carried out by Paul Adlard and his colleagues Charlotte Jordan and Kali Perronnes at the Florey Institute, in Victoria, Australia, who carried out a preliminary Y-maze study looking at cognitive differences in APPswe/PS1ΔE9 and wildtype B6 mice and provided me with the graphed data (Figure 5.3). They also administered the EmtinB peptide to our cohort of APPswe/PS1ΔE9, carried out the behavioural study with chi-square analysis (Figure 5.4), and collected the tissues for me to analyse in this thesis. You did a wonderful job and I thank you.

I would like to acknowledge Dr Ashley Townsend, Deputy director of the central science laboratory (CSL) and senior research fellow at the University of Tasmania. Dr Townsend carried out the ICP-MS analysis on my samples and instructed me on the principles and practice of ICP-MS. Thank you, Ashley, you are a great scientist and an excellent person. I appreciate your help and support.

I would also like to acknowledge Julie Wills (School of Medicine, University of Tasmania) who carried out the linear regression analysis in Chapter 5.

Thanks must go to my supervisors:

Emeritus Professor Adrian West – Thank you for your guidance, wisdom and positivity. Your optimism is something I aspire to. Thank you also for sticking with me even after you retired; it really means the world to me to finish this journey with you.

Professor Roger Chung – Your enthusiasm for science has and always will inspire me. Thank you for introducing me to the world of neuroscience as an RA all those years ago and for taking me on as a PhD student; you changed my life.

Dr Bill (Bilbo Baggins) Bennett – Rarely (by which I mean never) have I met someone as talented as you are in the lab. I don't think there has been a single issue I've had that you have not been able to make a sensible suggestion about. Thank you for your help, both in the lab and with writing this thesis. Thank you also for all of our wonderful conversations about terrible movies and fried foods, they contributed to getting me through this PhD.

Dr Anna King – You have been a source of both comfort and motivation for me at times when I wasn't quite sure I could keep going. Thank you for joining my supervisory team.

Thanks must also go to the members of the MT group, where my journey started:

Ros Herbert - Thanks for being my cell culture buddy and duet companion. You are a rock-star.

Dr Kate Lewis - Thank you for your compassion and kindness. Oh, and you are super clever!

Dr Lila Landowski – You may be the most thoughtful person in the world. Thanks for all the notes, gifts, and love.

Dr Jackie Leung – Thanks for the lunches, the chats and the caring.

Deb Orchard and Dr Julie Harris – Thank you for being my lab mums. It's helped more than you might think.

Thanks to the Wicking Dementia Research and Education Centre, who have adopted me, welcomed me, and supported me through the end of my PhD. I am forever grateful. In particular, thanks go to:

Professor James Vickers – for listening and helping.

Dr Carmen Fernandez-Martos – for being a friend and giving great western blot advice.

Justin Dittman – who helps everyone, all the time, because that's the kind of guy he is.

My desk buddies and fellow students Jess Collins, Kelsey Hanson, Andy Phipps, Aidan O'Mara, Kim Stuart, Rachel Atkinson and James Bender for keeping me sane, helping me through all manner of tiny and large problems, and just being all-round great people. Aidan O'Mara gets extra thanks for his help with statistics and for developing the random forest segmenter used to analyse plaque load in chapter 5.

Thanks must also go to my family who have done this PhD along-side me:

My husband, Dr Adam James – Who moved in with me, proposed to me, bought a house with me, married me and had a baby with me all in the space of this PhD. There isn't enough acknowledgement in the world for you. Thank you for taking care of me, the kids, the house, the pets, legal battles and…well, EVERYTHING. Your patience has been inexhaustible. You are amazing.

My big little girl, Lara O'Neill – You've been through my degree, honours and a PhD with me. It's been tough but you have been amazing. Thank you for being the patient, caring, thoughtful, well-behaved, clever and funny child that you are. You make me a better person.

My little little girl, Isabella James – My PhD baby, born halfway through the PhD. I promise mamma is going to be less busy now. Thank you for those moments of adorable that you gifted me with over the past two years. You have been a light in dark places for me.

My mother, Vicki Franklin – Thank you for teaching me, by example, to work hard at everything I do. If it's worth doing, it's worth doing properly!

Dwayne, Max and Rosie O'Neill – For choosing to be my family. You've looked after me in a million different ways over the course of my college and university education.

Kate and Peter Goldstone-James – It has been a tough few years but you have always been there to lean on. Thank you for your help, support and understanding.

Sandessa Foster, Kathleen Downey and Carol Bussey. I wouldn't be here if it weren't for your help during honours. I have not, and will not, ever forget that you were there for me.

To my friends – You know who you are. Thank you for your patience and love.

Special mentions to Trudy Beadman (who cooked for me – a lot). Jarrod Coad and Stephanie Young (who listened – a lot), Ian and Lindsay Little (who cared with wine, chocolate and boardgames). Susan Davis (who understood). Bec Irwin (who reminded me to laugh).

Abstract

Alzheimer's disease (AD) is a common neurodegenerative disease that is characterised by the extracellular accumulation of plaques, comprised predominantly of the β-amyloid (Aβ) peptide. These Aβ peptides have demonstrated toxic effects on neurons under a variety of experimental conditions. Metallothioneins (MTs) are a family of low molecular weight, metal binding proteins that have demonstrated neuroprotective and neuroregenerative properties. Recently MTs have been shown in neuronal cultures to be protective against a toxic, copper-bound form of Aβ (CuAβ). MTs have been proposed as a potential therapeutic for the treatment of AD, however, MT does not cross the blood brain barrier (BBB) to an appreciable degree, which limits its capacity as an AD therapeutic. More recently, synthetic peptides based on the MT sequence, termed emtins, have been developed. Emtins have not only reproduced some of the properties of MT but, importantly, one peptide has been demonstrated to cross the mouse BBB, indicating that emtins may represent a novel therapeutic for the treatment of AD.

This thesis investigates the capacity of two emtins, EmtinB and EmtinAc, to protect cultured rat hippocampal neurons against CuAβ with the aim of determining the most effective peptide for ongoing studies. EmtinB was the more effective of the two emtins tested in this toxicity model. Furthermore, in a comparison of two EmtinB forms; a tetrameric, 4 -peptide form and a dimeric, 2-peptide form, the dimeric EmtinB peptide was shown to be considerably more protective than the tetrameric form.

Three potential mechanisms by which EmtinB might protect cultured rat neurons against CuAβ were investigated: removal of copper from CuAβ to prevent formation of free radicals, direct scavenging of free radicals by EmtinB, and improved neuronal survival *via* activation of the LRP family of receptors. While no conclusion was reached on its primary mechanistic action, this thesis will show that EmtinB is able to bind metals such as copper and zinc, and can remove

copper from the CuAβ complex. Further investigations into mechanism show that EmtinB is also able to protect cultured rat neurons against hydrogen peroxide (which can be generated by CuAβ) and that EmtinB is unable to protect against CuAβ in the presence of an inhibitor of the LRP family of receptors suggesting that EmtinB may potentially be interacting with hippocampal neurons via the LRP family of receptors.

The *in vivo* protective capacity of EmtinB was also investigated in this thesis using the APPswe/PS1Δ E9 mouse model of AD. In this model, EmtinB treatment was shown to improve cognitive outcomes, as measured by Y-maze, and also reduced astroglial activation, as measured by GFAP levels, but did not reduce levels of activated microglia. Although EmtinB treatment appeared to reduce plaque load, these changes were not statistically significant and soluble levels of Aβ remained unchanged.

This thesis investigates the activity of emtin peptides to protect cultured hippocampal neurons against a toxic copper-bound form of Aβ and the ability of EmtinB to reduce cognitive deficits and alter pathological markers of AD in the APPswe/PS1ΔE9 mouse model of AD. Emtin peptides have demonstrated beneficial outcomes in both *in vivo* and *in vitro* models of AD, but as yet a single definitive mechanism cannot be ascribed.

Table of Contents

Abbreviations

°C	degrees Celsius
µL	microlitres
µM	micromoles per litre
AA	amino acids
AD	Alzheimer's disease
Akt	serine/threonine kinase
ANOVA	analysis of variance
APP	amyloid precursor proteins
Aβ	β-amyloid
BBB	blood-brain barrier
BCA	bicinchoninic acid
CNS	central nervous system
CREB	cAMP response binding element
CSF	cerebral spinal fluid
CuAβ	copper-bound Aβ
DHA	dexahexanoic acid
DIV	days *in vitro*
EDTA	ethylenediaminetetraacetic acid
ERC	entorhinal cortex
ERK	extracellular signal-regulated kinase
GFAP	glial fibrillary acidic protein
g	grams

hAβ1-42	human β-amyloid 1-42
HBSS	Hank's buffered salt solution
ICC	immunocytochemistry
ICP-MS	inductively coupled plasma - mass spectrometry
IHC	immunohistochemistry
kg	kilograms
L	litres
LDLR	low density lipoprotein receptor
LRP	low density lipoprotein receptor-related protein
MAPK	mitogen activated protein kinase
mg	milligrams
mL	millilitres
mM	millimoles per litre
mm	millimetres
mol	moles
MT	metallothionein
MT1	metallothionein 1
MT2	metallothionein 2
MT3	metallothionein 3
MT4	metallothionein 4
MTKO	metallothionein knock-out
MW	molecular weight
PBS	phosphate buffered saline
PFA	paraformaldehyde
PI3K	phosphoinositide 3-kinase

PKB	protein kinase B
ppb	parts per billion
PSD95	post synaptic density-95
RAP	receptor related protein
ROS	reactive oxygen species
rpm	revolutions per minute
SDS	sodium dodecyl sulfate
SDS-PAGE	sodium dodecyl sulfate-polyacrylamide gel electrophoresis
SEM	standard error of the mean
siRNA	small interfering RNA
SSV	sterile saline vehicle
TBS	Tris-buffered saline
TFA	trifluoroacetic acid
TFE	trifluoroethanol
VLDLR	very low density lipoprotein receptor
ZnAβ	Zinc-bound Aβ

Table of Figures and Tables

Introduction

1.1 Metallothionein

Metallothioneins (MTs) are a family of low molecular weight proteins that are characterised by a high proportion of cysteine residues. Since the 1957 discovery of a metallothionein protein in equine kidney [1], there has been intense interest in the physical and biochemical properties of the MT family [2]. The ubiquitous expression of MTs in eukaryotes and expression of related proteins in some prokaryotic species [3, 4] suggests a pivotal biological role for the MT family of proteins yet, while studies have uncovered multiple functions of metallothionein, a primary biological function of MTs remains to be unambiguously determined.

There are four main isoforms of MT that are expressed in mammalian species; metallothionein I (MT1), metallothionein II (MT2), metallothionein III (MT3) and metallothionein IV (MT4) [3]. Metallothionein 1 and 2 are expressed in almost all tissues and have similar expression profiles. The action and expression of the two are sufficiently similar that they are often treated as a single isoform and, for practical reasons, viewed as a single entity, referred to simply as MT1/2. MT3 and MT4 are MT isoforms that have a degree of tissue specificity. MT-3 is expressed mainly in the central nervous system, predominantly in neurons [5], but also in glia [6, 7] and in the reproductive system [8]. MT-4 is expressed exclusively in squamous epithelia [9].

The elusive function of MTs has been extensively researched in laboratory rodents, such as the mouse. The mouse metallothionein gene family consists of four members clustered on chromosome 8, each expressing one of the MT isoforms (MT1-MT4) [10-12]. In humans, however, metallothionein gene expression is more complex with around 18 genes in the MT gene family [13-16]. These genes encode multiple variants of MT and are found mostly on

chromosome 16 [13, 14]. While humans and mice have a single copy of MT2, MT3, and MT4 genes, humans differ to mice in that they contain a large number of genes encoding MT1 variants, seven of which are active in producing MT1 protein isoforms [15]. MT2 is coded for by a single active gene, *MT2A*, and is the most widely expressed of the metallothionein family in humans, constituting around 80% of MT in the body (reviewed in [17]).

Early theories on the primary biological function of MTs revolve around their metal binding capacity. Metallothioneins bind a wide range of physiological metals, such as zinc and copper, as well as xenobiotic metals, such as cadmium and mercury. Metallothioneins bind metals through the thiol groups (-SH groups) of their cysteine residues. Mammalian MTs contain 61-68 amino acids and typically have 20 cysteine residues found at conserved positions [18] (see Figure 1). The conserved cysteine residues are distributed between two globular domains, the α-domain and β-domain, which bind 4 and 3 divalent metal ions, respectively, and form two distinct metal-thiolate structures [19] (see Figure 1.1). MT has a metal-binding capacity of up to 7 divalent metal ions, typically Zn(II), in an exclusively tetrahedral metal co-ordination, or up to 12 monovalent metal ions, such as Cu(I).

1.2 Actions of metallothionein

1.2.1 Sequestration and transfer of bio-metals to apo-proteins

Bio-metals, such as copper and zinc, are essential micronutrients for plants and animals, however, these metals can also be toxic to living organisms. In response to this apparent paradox, plants and animals alike have developed mechanisms such as chelation and sequestration for managing these metals [20]. Chelation and sequestration of metals prevents unwanted actions of the metal ions while keeping them proximal and accessible within the cell. One theory of MT function suggests that MT could chelate metals and subsequently act as

Figure 1.1 Human metallothionein 1-4 amino acid sequences and structure of human metallothionein 2 (cadmium bound)

A) Aligned amino acid sequences of human metallothioneins MT1A, MT2, MT3 and MT4 [21]. Amino acid sequences of mammalian metallothioneins contain 61-68 amino acids with 20 cysteines at conserved positions. Cysteines highlighted in yellow. B) NMR derived structure of human metallothionein 2A bound to 7 divalent cadmium ion (sequence established by [22] , image adapted from [23]). Mammalian MTs have two distinct globular domains, the α-domain and the β-domain which bind 4 and 3 divalent metal ions, respectively.

A

```
MT1A MDP-NCSCATGGSCTCTGSCKCKECKCTSCKKSCCSCCPMSCAKCAQGCICKG------ASEKCSCCA
MT2  MDP-NCSCAAGDSCTCAGSCKCKECKCTSCKKSCCSCCPVGCAKCAQGCICKG------ASDKCSCCA
MT3  MDPETCPCPSGGSCTCADSCKCEGCKCTSCKKSCCSCCPAECEKCAKDCVCKGGEAAEAEAEKCSCCQ
MT4  MDPRECVCMSGGICMCGDNCKCTTCNCKTYWKSCCPCCPPGCAKCARGCICKG------GSDKCSCCP
```

B

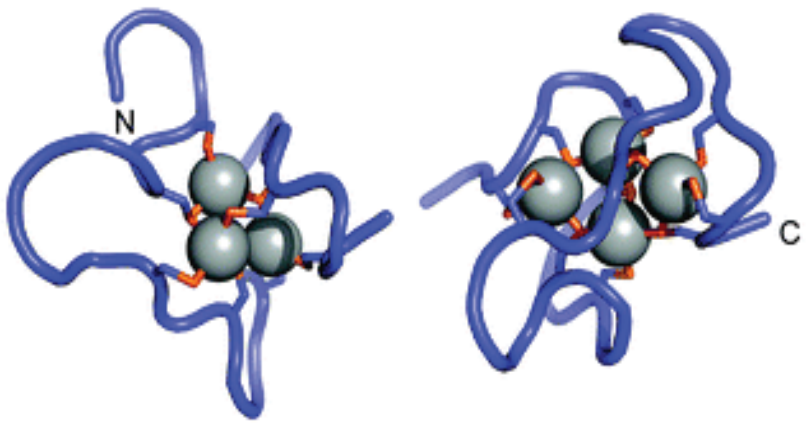

a metal chaperone, therefore playing a role in the production of metalloproteins (reviewed in [4]). *In vitro* investigation of MT interaction with zinc shows that MTs are able to donate zinc to zinc-requiring apo-enzymes [24], receptors [25] and transcription factors [26], while a more recent *in vivo* study utilising ^{65}Zn and metallothionein knockout (MTKO) mice showed that zinc-bound MT can directly transfer zinc to the protein m-aconitase, supporting the theory that MTs act as zinc chaperones *in vivo* [27].

While there is considerable evidence that MTs are capable of acting as a metal chaperone, this capacity does not appear to be an essential function of MTs. Bio-metals play an important role in catalytic, structural and regulatory functions and, as such, homeostasis is not just regulated by MTs but by a variety of proteins [28, 29]. Evidence for a non-essential role of MT's in metal homeostasis comes from cultured yeast and mammalian cells in which MT has been ablated, with these cells able to grow and prosper to the same degree as cells expressing normal levels of MT (reviewed in [30]). Furthermore, in mammalian cells, zinc exchange between metalloproteins and extracellular zinc occurs in the absence of MT and the rate of this zinc transfer is minimally affected by restoring MT [4]. In addition to *in vitro* evidence, mice in which MT has been knocked out are physiologically and developmentally normal [31], strengthening the contention that MT does not play an essential role in metal transfer. While MT does not appear to be essential for development and survival, there is accumulating evidence that MT provides a benefit to an organism under circumstances of abnormal physiology such as heavy metal toxicity, oxidative stress or neurodegenerative disease.

1.2.2 Heavy metal detoxification

Many studies of metallothionein function have supported a role for MT in heavy metal detoxification. Early studies demonstrated that MTs are induced by heavy metals *in vitro* [32, 33] and *in vivo* [34, 35], and metal binding studies have shown that, while zinc is the primary metal ion bound to the major MT isoforms under normal physiological conditions [36], zinc is

highly displaceable and MT binds to toxic heavy metals such as Cu and Cd with a much greater affinity (reviewed in [4, 37]). Accordingly, cells with decreased MT levels are susceptible to heavy metal toxicity and show increased sensitivity to copper (in single cell eukaryotes) and cadmium (in mice and mammalian cell-lines) while increased expression of MT protects against toxicity of these metals (reviewed in [4, 30]). Furthermore, in a study of metal toxicity using MT-null mice and wild-type controls, MT-null mice were more susceptible to cadmium, zinc and copper toxicity than the wild-type counterparts[38]. Taken together, these data suggest that MTs could play a significant role in protecting organisms against heavy metal toxicity, however, many authors believe that this capacity to scavenge toxic heavy metals, while advantageous, does not represent the primary physiological role of MTs [39] [4]. This view is based on the expression profile of MTs, their tissue distribution, and the fact that exposure to high levels of toxic heavy metals such as cadmium and mercury are, for mammals, a relatively recent phenomenon.

1.2.3 Protection against oxidative stress

The production of reactive oxygen species (ROS) is a normal occurrence in the body. ROS are continually produced in tissues by the mitochondria and can be additionally produced for beneficial purposes, such as an immune response, or as part of cell signalling systems [40]. The endogenous antioxidant defence system is responsible for counteracting the effects of ROS, and contains both enzymatic and non-enzymatic antioxidants [41]. Enzymatic antioxidants include catalase, which catalyses the breakdown of hydrogen peroxide (H_2O_2) to H_2O and O_2; superoxide dismutase (SOD), which catalyses the dismutation of the super anion (O_2^-) to O_2 or H_2O_2; and glutathione peroxidases, which reduce lipid hydroperoxides and also reduce H_2O_2; ceruloplasmin, a copper transport protein that has antioxidant capacity [42-44]. Non-enzymatic antioxidants include reduced glutathione (GSH), which is able to donate a reducing equivalent (H^+ or e^-) to unstable molecules [45]. These antioxidants, along with other

endogenous and exogenous antioxidants, are responsible for maintaining an oxidative balance and oxidative stress is caused when ROS are produced in amounts that exceed the neutralising capacity of the antioxidant defence system [46].

Evidence suggests that MTs might act to bolster the endogenous antioxidant defence system. MT is inducible in response to oxidative stress both *in vitro* and *in vivo*. *In vitro*, MT is induced in various cell culture models in response to hydrogen peroxide [47], ionizing radiation [48], and paraquat [49], all of which are known to promote the formation of free radicals. In animal models, oxidative stress induces metallothionein expression [50] and regulates MT gene expression [51]. MT upregulation has been observed in response to alkylating agents, which cause lipid peroxidation; in response to chemotherapy drugs such as cisplatin and bleomycin, which are believed to work through production of free radicals; after administration of radical forming organic solvents such as carbon tetrachloride (CCl_4); and in response to free-radical inducing cytokines such as tumour necrosis factor alpha (TNFα) and interleukin-6 (IL-6) (for a thorough review see [50]).

Furthermore, susceptibility to oxidative stress is correlated to MT levels in cell culture models and in rodent models. For example, MTKO hepatocytes and embryonic stem cells, as well as MT-null cell lines, are more susceptible to oxidative stress [52-54] and cells overexpressing MT are more resistant to oxidative stress [55, 56]. *In vivo*, MTKO mice are more susceptible to a number of oxidative stressors while MT overexpressing mice have improved outcomes in a number of oxidative stress models (reviewed in [2]).

Direct evidence for MT's antioxidant capacity comes from *in vitro* studies in which metallothionein has variously been shown to dismutate superoxide [57, 58] and scavenge hydroxyl radicals ([57] [59]), 1,1-diphenyl-2-picrahydrazyl radicals [59], nitric oxide [60] and hydrogen peroxide [61]. Much like its metal binding capabilities, MT antioxidant activity appears to be dependent on cysteine residues [57]. Metallothionein is predominantly bound to

zinc under physiological conditions [62]. When MT is oxidised by ROS, cysteine sulfhydryl groups are oxidised to disulphides and zinc is lost from the cysteine [2](see Figure 1.2). Oxidised MT is either degraded or, in the presence of a selenium catalyst, can be reduced back into free-thiol form by glutathione [2, 62].

MT's capacity for reducing oxidative stress may play an important role in the central nervous system [63, 64], where both injury [65] and neurodegenerative diseases [64, 66] are associated with oxidative stress. Neuronal cells are particularly sensitive to oxidative stress [67]. In traumatic brain injury, much of the damage that occurs in the CNS following trauma is due to the secondary effects of glutamate excitotoxicity, Ca^{2+} overload, and oxidative stress [68]. Both necrotic and apoptotic cell death have been observed in mouse and rat models following traumatic CNS injury [69-71], and improved functional recovery is observed in response to inhibition [72] and scavenging [73] of ROS, suggesting that increased ROS production contributes to injury-mediated neuronal cell damage and neurological dysfunction [74]. Notably, MTKO mice show increased oxidative stress and apoptosis following brain injury compared with wild-type [75]. A further study shows MT overexpressing mice have reduced cell death and oxidative tissue damage after brain injury [76]. Addition of exogenous MT also improved outcomes after brain cryolesion in a rat model of brain injury, improving both wound healing and reactive axon growth [77], and reduced neuronal apoptosis and injury-induced oxidative stress after cryolesion in both normal and MTKO mice [76].Thus, the data suggest a protective role of MTs in the CNS under circumstances of increased oxidative stress, and this protective effect could be achieved by administration of exogenous MT.

1.2.4 Neuroprotection and neuroregeneration

While modulation of oxidative stress is clearly implicated as a mechanism of MT protection in the CNS, recent studies have suggested that MT could also be functioning through direct interaction with neurons or glial cells.

Figure 1.2 Metallothionein oxidation in response to oxidative stressors

After synthesis, the MT apo-protein (A) acquires metals, such as zinc, which bind to sulfhydryl groups of cysteine residues (B). Metallothionein can become oxidised in response to oxidative stressors, such as hydrogen peroxide (H_2O_2), which results in the formation of a disulphide bond between two sulfurs. Oxidised MT (C) is often degraded but, in the presence of selenium (Se), can also be reduced back to the free thiol form (A), by glutathione (GSH)/glutathione disulfide (GSSG). Adapted from [2, 37].

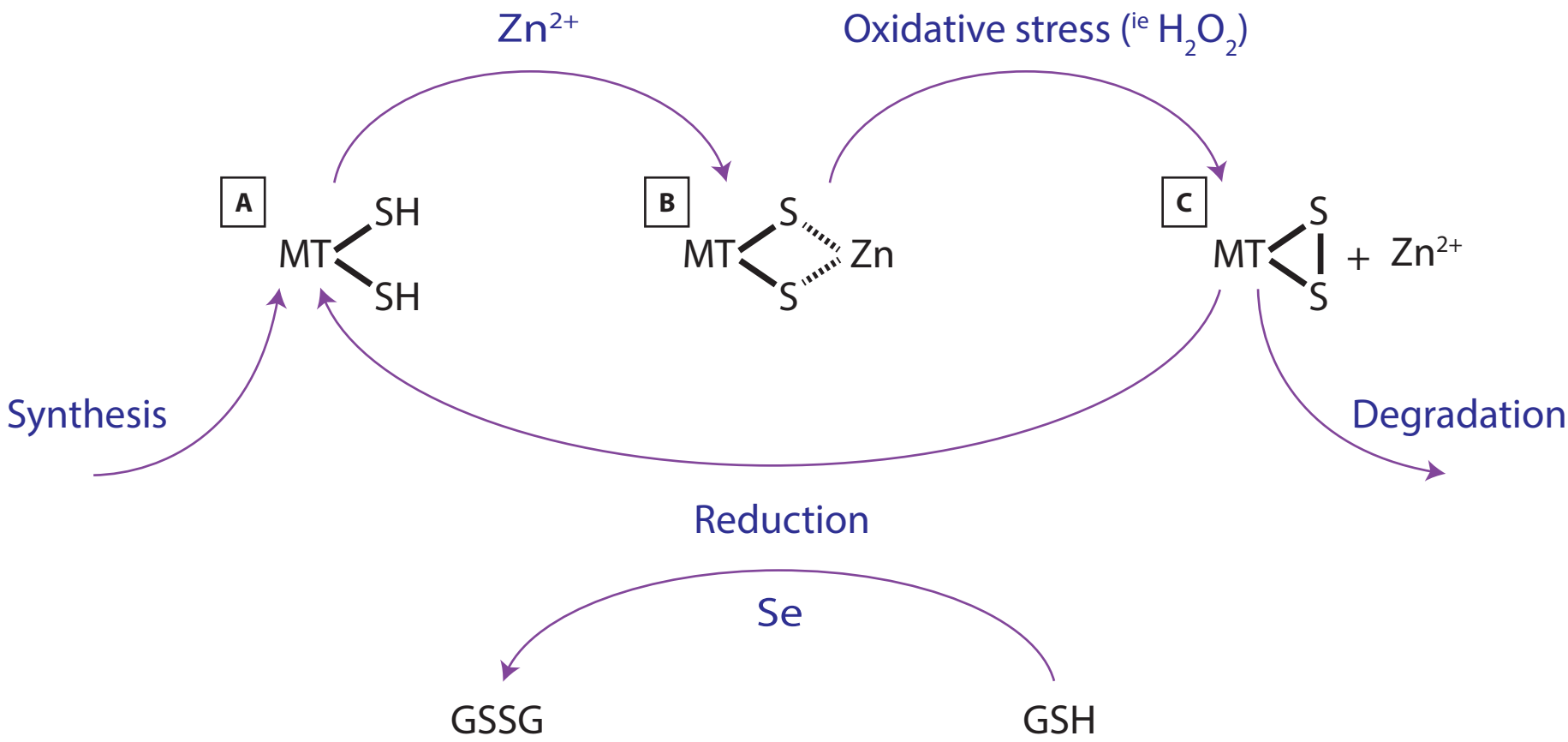
Zn2+
Oxidative stress (ie H2O2)
A
SH
MT
SH
B
S
MT
Zn
S
C
S
MT
+ Zn2+
S
Synthesis
Degradation
Reduction
Se
GSSG
GSH

In neurons, MT has been found to promote survival and regeneration when added exogenously. In culture, MT added directly to neuronal cultures promotes neurite outgrowth [77, 78], and reactive neurite sprouting after injury [77]. Exogenous MT application also promoted neuronal survival in hippocampal neurons after toxic insult with 6-hydroxydopamine [78] and in cerebellar granule neurons after potassium withdrawal [79]. *In vivo*, exogenous MT administered to brain regions damaged by needlestick injury promoted axonal growth into the lesion site [77], and MT administered to the eye after transection of the optic nerve dramatically improved axonal regeneration [80].

In glia, exogenous MT has been shown to modulate the reactive nature of these supportive cells. Astrocytes become reactive after CNS insult or injury, inhibiting neuronal growth [81]. In cultured astrocytes, exogenous MT application altered the reactive phenotype, promoting a phenotype which was permissive to neuronal growth [82]. Similarly, microglial inflammatory response is also attenuated by MT both *in vitro* [83] and *in vivo* in traumatic brain injury models [84], and after treatment with neurotoxic quinolinic acid [83].

MT was originally thought to function purely as an intracellular protein as it contains no signal motif for transport [85], however extracellular MT has been detected in the injured brain and cultured astrocytes have been shown to actively excrete metallothionein in response to zinc [80]. Importantly, recent evidence suggests MT binds to receptors on the surface of CNS cells such as astrocytes [86, 87], neurons [88-90] and microglia [91, 92].

Metallothionein has been found to bind members of the low density lipoprotein receptor (LDLR) family of receptors, low-density lipoprotein receptor-related proteins 1 (LRP1) and 2 (LRP2). LRP1 and LRP2 are thought to play significant roles in the CNS where they are widely expressed in neurons and glia [85]. Family members of the LDLR type are structurally similar, single span transmembrane proteins, comprising an extracellular domain, a transmembrane domain, and an intracellular domain (See Figure 1.3). The extracellular domains of LDLR family

members are composed of repeats of distinct motifs; a ligand binding region, an epidermal growth factor (EGF)-precursor homology region, a region of O-linked sugars which is absent in LRP1 and LRP2 (See Figure 1.3) [86]. The cytosolic domain contains an NPxY motif which is important in the endocytic function of the LDLR family. The LDLR family were originally thought to function purely as endocytic receptors, internalising extracellular ligands for cellular use and degradation [87]. However, some members of this family, such as LRP1 and LRP2 can also act as signal transducers, activating intracellular signalling pathways *via* interaction with adaptor proteins such as disabled-1 (DAB1) and post-synaptic density-95 (PSD-95) [88].

Both protective and regenerative actions of metallothionein have been shown to be mediated through LRP receptors [79, 80, 89, 90]. Fitzgerald et al. [90] showed that the capacity of MT2 to promote neurite outgrowth in cultured retinal ganglion cells could be blocked using anti-LRP antibodies and further investigation by Chung et al. [80] demonstrated that LRP-directed siRNA ablated the ability of MT2 to promote regenerative sprouting in cultured cortical neurons. Extending on this, Ambjorn et al. [79] used surface plasmon resonance to show MT2 was able to bind to both LRP1 and LRP2 on the surface of cultured cerebellar granule neurons, and that this binding was inhibited by receptor associated protein-1 (RAP), a competitive inhibitor of the LDLR family. In this study, MT was able to protect cerebellar granule neurons against apoptotic death caused by potassium deprivation and this MT-mediated cell survival was absent in the presence of the LRP inhibitor RAP, indicating that MT mediates survival through members of the LDLR family (see Figure 1.4). Further investigation showed that in cerebellar granule neurons, MT treatment activated the signalling molecule's extracellular signal-regulated kinase (ERK), protein kinase B/serine threonine kinase (PKB/AKT) and cAMP response binding protein (CREB). Both ERK, which is part of the mitogen activated protein kinases (MAPK) signalling pathway, and PKB/Akt, which belongs to the PI3K signalling pathway, have been implicated in anti-apoptotic intracellular signalling [91, 92], suggesting that MT can activate at least two pathways which are able to directly regulate apoptosis [79].

Figure 1.3 LRP1 and LRP2 are members of the structurally similar low-density lipoprotein receptor (LDLR) family

Low-density lipoprotein receptor-related protein 1 (LRP1) and 2 (LRP2) are members of the low-density lipoprotein receptor (LDLR) LDLR family. LRPs are so named because they contain structural domains found in the low density lipoprotein receptor (LDLR). This family of receptors comprise an extracellular domain (ECD), a transmembrane domain (TMD), and an intracellular domain (ICD). The extracellular domains of LDLRs consist of three distinct regions: cysteine rich ligand binding domains, EGF precursor-like domain and glycosylated region. These regions are found in the ECD of other LDLR family members in a varying number of repeats. The intracellular domain contains important NPXY motifs which mediate endocytosis. Figure adapted from [93] and [86].

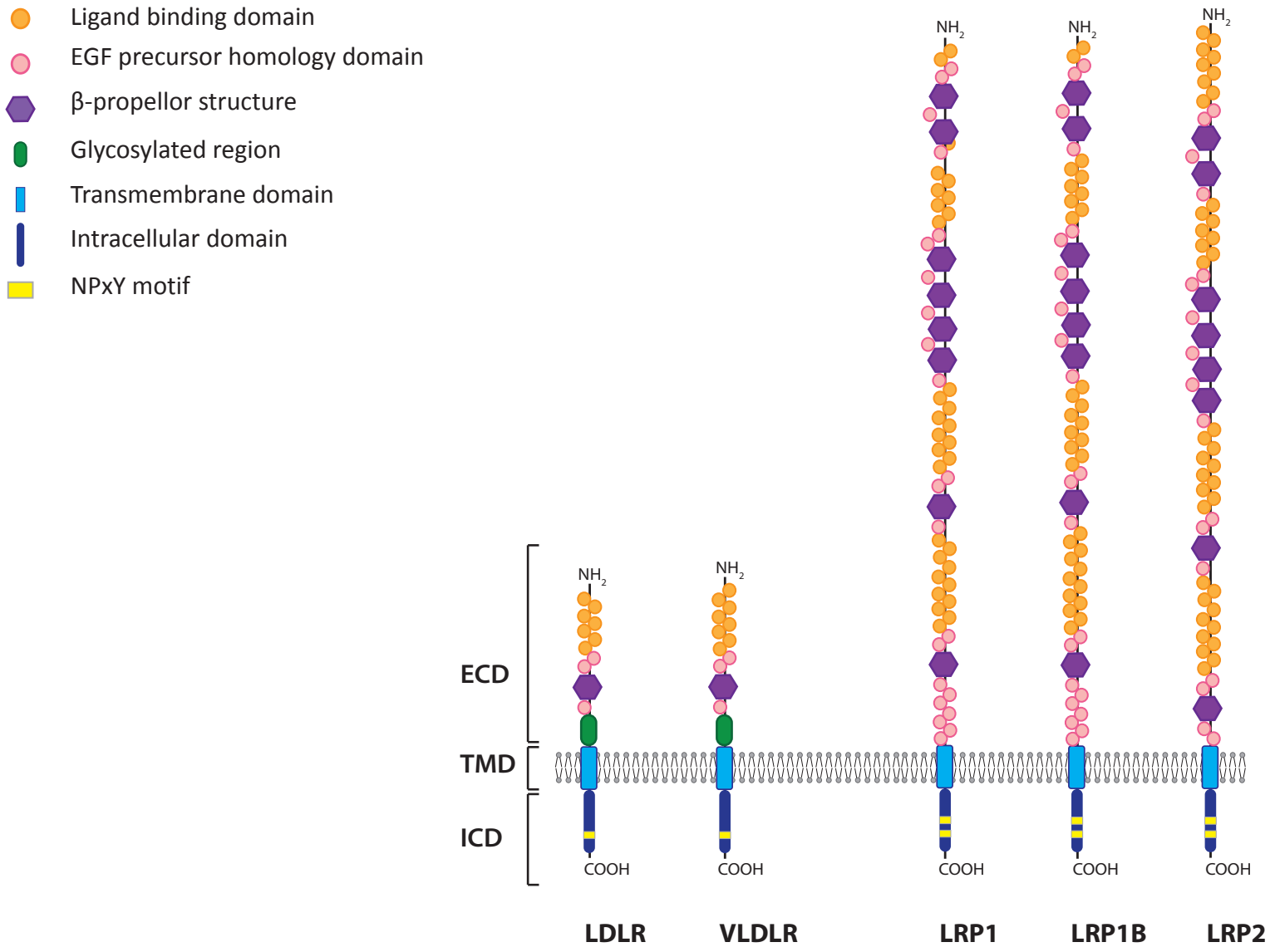
Ligand binding domain
EGF precursor homology domain
β-propellor structure
Glycosylated region
Transmembrane domain
Intracellular domain
NPxY motif
NH2
COOH
ECD
TMD
ICD
LDLR
VLDLR
LRP1
LRP1B
LRP2

Figure 1.4 Metallothionein promotes neurite outgrowth and cell survival *via* interaction with LRP receptors

Metallothionein has been shown to promote neurite outgrowth, regenerative neurite sprouting and cell survival *via* LRP receptors [80, 89, 90, 94]. LRPs are able to activate intracellular cascades and while the exact pathways remain to be elucidated, MT binding to LRP receptors has been shown to increase phosphorylation of Akt, CREB and ERK [94]. Receptor associated protein-1 (RAP) is an inhibitor of the LDL-family of receptors, including the LRP receptors. In the presence of RAP, MT is unable to promote cell survival or neurite outgrowth [94].

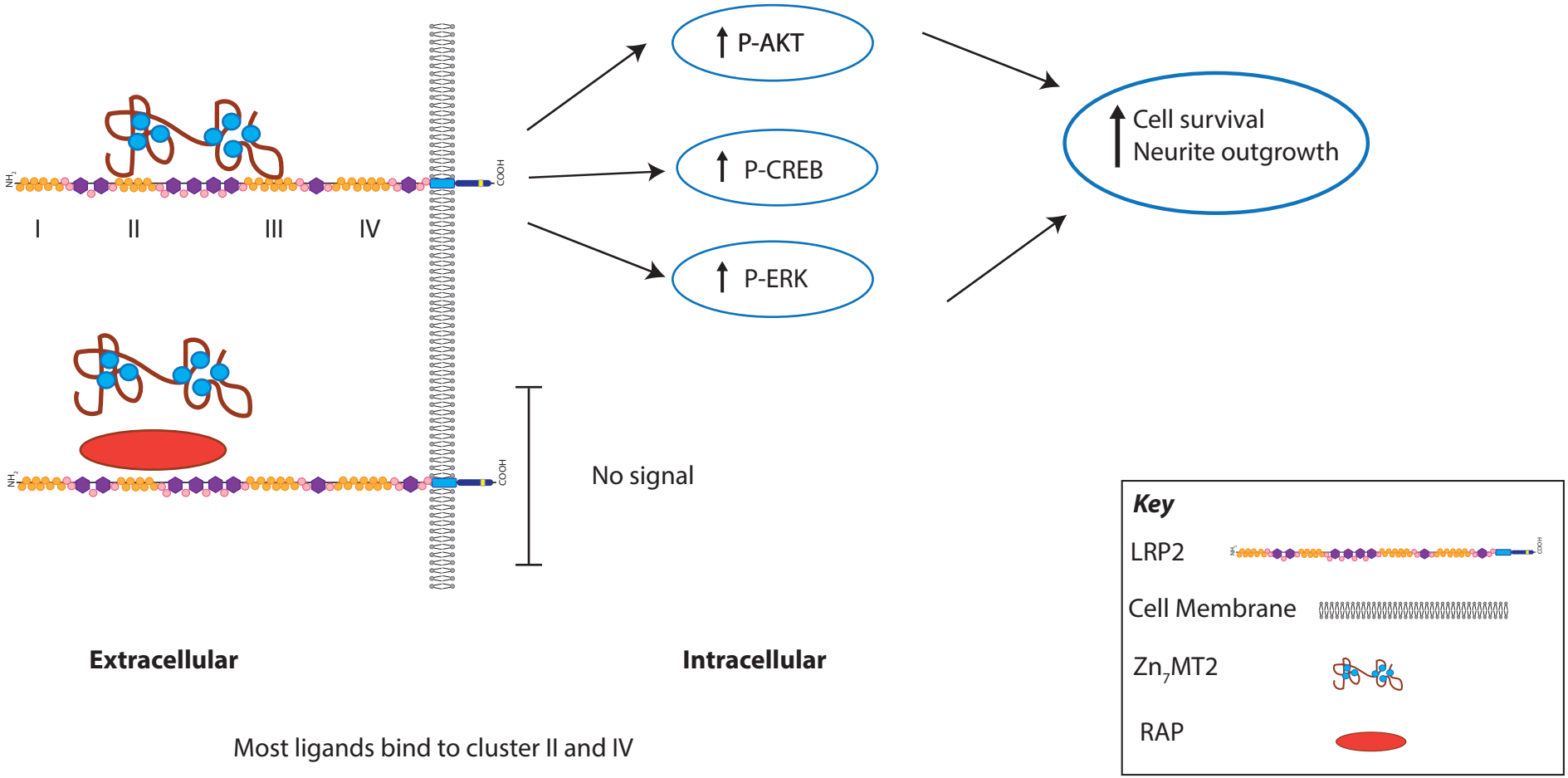
P-AKT
P-CREB
P-ERK
Cell survival
Neurite outgrowth
I
II
III
IV
NH2
COOH
No signal
Extracellular
Intracellular
Most ligands bind to cluster II and IV
Key
LRP2
Cell Membrane
Zn7MT2
RAP

Investigation into MT binding to LRP receptors has demonstrated that MT binding to LRP2 could be out-competed with a small peptide similar to MT2 which contained a CKCK motif [79, 89], suggesting that the CKCK motif may be important for LRP-mediated signalling.

The accumulated evidence, that MT can be neuroprotective and neuroregenerative *in vitro* and *in vivo,* has given rise to speculation that aspects of MT biology may be useful in developing a treatment or therapeutic agent for Alzheimer's disease.

1.3 Metallothionein and Alzheimer's disease

1.3.1 Alzheimer's disease

Alzheimer's disease (AD) is a common neurodegenerative disease and is characterised by the extracellular accumulation of plaques comprised predominantly of fragments of the β-amyloid peptide (Aβ). The Aβ peptide is generated through the proteolytic processing of the amyloid precursor protein (APP) (for reviews see [95, 96]). APP is a single-pass transmembrane protein comprised of a significant N-terminus ectodomain, an intramembrane domain, and a short intracellular domain [95, 96]. APP is highly expressed in the brain [95] and yet, despite numerous purported functions, the physiological function of APP *in vivo* remains unclear. There is some evidence that APP positively modulates synapse formation and maintenance [97], as well as learning and memory [98], and a potential trophic function has also been suggested since APP has been demonstrated to stimulate neurite outgrowth in cultured hippocampal neurons [99]. More recently, APP has been implicated in metal homeostasis, with evidence suggesting that APP acts by stabilising ferroportin, an iron transport protein, at the cell surface [100]. Notwithstanding these findings, there is currently no consensus on the physiological role of APP and its seminal function remains to be elucidated.

Processing of APP occurs through proteolytic cleavage by α, β and γ secretases *via* two distinct processing pathways [95, 101] (see Figure 1.5). Both of the APP processing pathways use a

two-step sequential cleavage of APP, using either α or β-secretase to cleave within the N-terminus ectodomain, followed by a second cleavage with γ-secretase in the transmembrane region; however only one pathway leads to the generation of amyloidogenic peptides [101].

Three non-toxic peptides are produced through APP cleavage with α and γ-secretases; APPsα, p3 and AICD - none of which are amyloidogenic [101]. Aβ peptides are derived from APP *via* the amyloidogenic processing pathway using β and γ-secretases. Cleavage by β-secretase in the ectodomain generates the APPsβ peptide [101]. Subsequent cleavage by γ-secretase liberates AICD protein and the amyloidogenic Aβ peptide[101]. Notably, alternate cleavage by β-secretase and γ-secretase gives rise to the variety of Aβ peptides observed *in vivo,* with Aβ peptides ranging in length from 39-42 amino acids [102] and of these, the Aβ1-40 and 1-42 peptides are most common in the human brain [103]. Studies have now established that various biochemical forms of Aβ that specifically accumulate in the AD brain are toxic to neurons. While the cause of AD remains unknown, factors associated with its pathogenesis include oxidative stress, metal dyshomeostasis and neuronal cell loss.

1.3.2 Oxidative stress in Alzheimer's disease

Oxidative stress is a key feature of the AD brain [104]. Studies have shown increased lipid peroxidation products, DNA and RNA oxidation products, and markers of protein oxidation, in AD brain (reviewed in [104, 105]).

Aβ induces oxidative stress *in vitro* and *in vivo* (reviewed in [106]). Aβ peptide has been shown to generate free radicals in aqueous solution [107] and cause high levels of H_2O_2 and lipid peroxides in cells [108]. Exacerbating this increase in free radical production is the change in activity of endogenous antioxidant enzymes. Decreases in the activity of endogenous antioxidant enzymes SOD, catalase and glutathione peroxidase have been demonstrated in

Figure 1.5 The processing pathways of amyloid precursor protein (APP) by secretase cleavage

The APP protein is a single-pass transmembrane protein that contains the peptide sequence for β-Amyloid (Aβ). Processing of APP occurs *via* proteolytic cleavage of the APP protein by α, β, and γ secretases. Processing of APP occurs through two distinct pathways; the non-amyloidogenic pathway and the amyloidogenic pathway. Non-amyloidogenic processing of APP involves sequential cleavage of APP by α-secretase followed by cleavage in the transmembrane region of APP by γ secretase. This produces secreted APPα (APPsα), the p3 peptide and the APP intracellular domain (AICD). Amyloidogenic processing of APP occurs through a similar mechanism, with APP sequentially cleaved by β then γ secretases to produce secreted APPβ (APPsβ) the AICD and the Aβ peptide. As γ-secretase can cleave at either of two positions in the transmembrane domain, the resulting Aβ peptide can be comprised of either 40 or 42 amino acids, denoted Aβ1-40 and Aβ1-42 respectively.

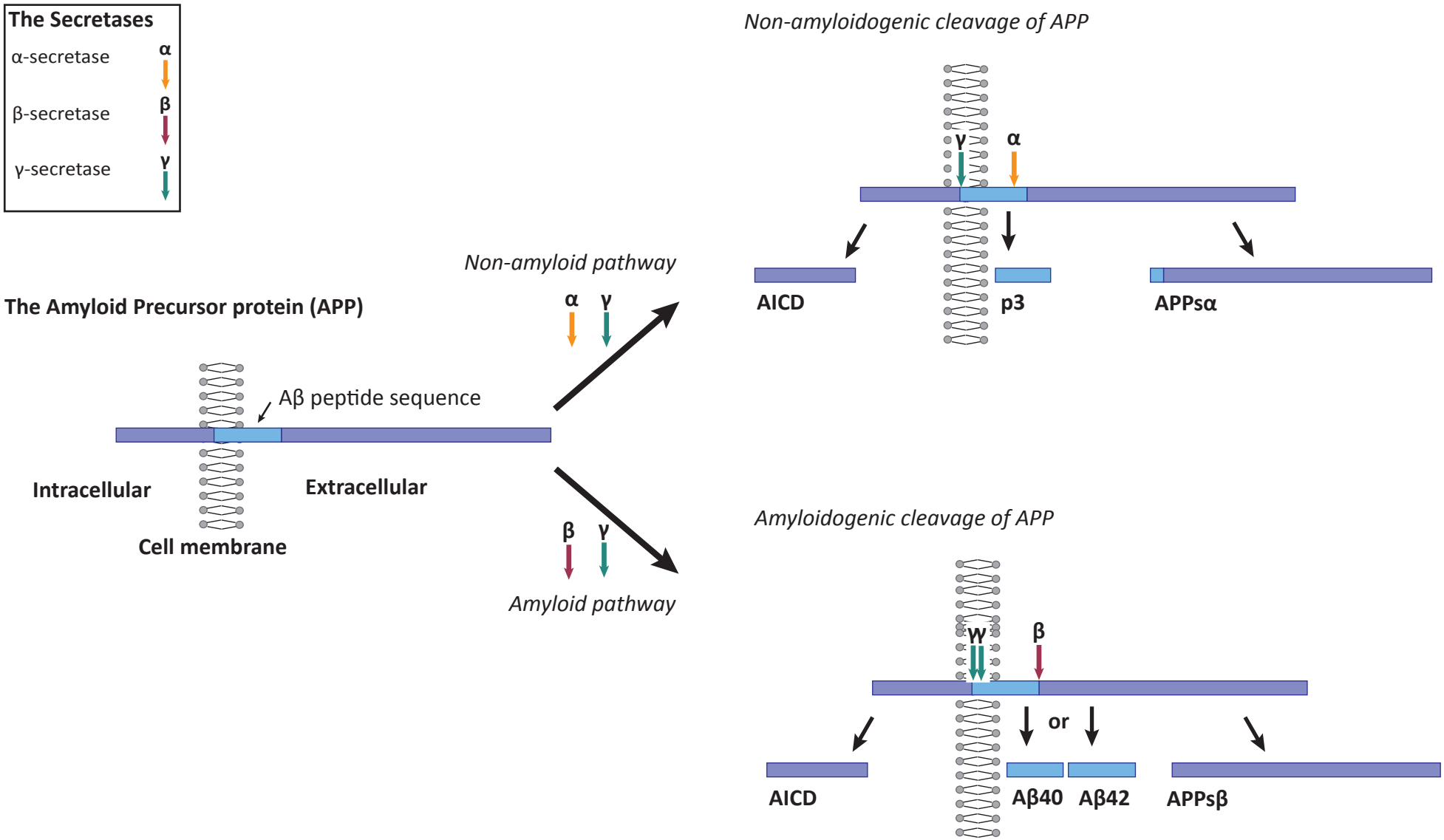
The Secretases
α-secretase
β-secretase
γ-secretase
α
β
γ
The Amyloid Precursor protein (APP)
Aβ peptide sequence
Intracellular
Extracellular
Cell membrane
Non-amyloid pathway
α γ
β γ
Amyloid pathway
Non-amyloidogenic cleavage of APP
γ α
AICD
p3
APPsα
Amyloidogenic cleavage of APP
γ β
or
AICD
Aβ40
Aβ42
APPsβ

various AD brain regions [109, 110]. Furthermore, decreased SOD and catalase is associated with neurofibrillary tangles and plaques in the AD brain [111].

Further studies have shown that not only does excess Aβ promote oxidative stress, but oxidative stress has been shown to increase Aβ production *via* alterations to secretases associated with APP processing (reviewed in [104]), suggesting that perhaps oxidative stress is maintained in the AD brain by a positive feedback system involving both oxidative stress and Aβ production [112].

Interestingly, studies into antioxidant interventions in AD, using vitamin supplementation, have shown positive benefits (reviewed in [113]). Vitamin E administration reduced lipid peroxidation and Aβ levels in transgenic mice [70], and slowed disease progression in AD patients [114, 115], while vitamin B_{12} was shown to improve cognitive function in AD patients [116]. These studies suggest that oxidative stress plays a key role in AD progression and, furthermore, oxidative stress-directed therapies may prove viable for the treatment of AD.

1.3.3 Metal dysregulation in Alzheimer's disease

A role for metals in amyloid toxicity has become increasingly supported in the literature. Metal ions such as Fe^{2+}, Zn^{2+} and Cu^{2+} are found in senile plaques *in vivo* [117] and are thought to promote aggregation of Aβ and enhance toxicity (reviewed in [118, 119]). Of particular interest in Alzheimer's pathology is the interaction of copper with Aβ. Copper ion levels are increased in the AD brain and are found co-ordinated directly to Aβ peptides in senile plaques (reviewed in [119]). Copper is a redox active metal and it has been shown that copper binding to Aβ both enhances the formation of Aβ aggregates and promotes generation of reactive oxygen species (ROS) [120, 121] *via* Fenton chemistry [122].

Recent studies have suggested that dysregulation of copper in the AD brain not only plays an important role in AD pathogenesis, but represents a novel therapeutic target [122-125]. In

support of this concept, early studies utilising 8-hydroxyquinone (8-OHQ) analogues, which are established copper chelating compounds, have demonstrated decreased Aβ deposition [126], as well as improved cognitive outcomes and lower levels of soluble Aβ [125] in the brains of transgenic mice. Similarly, treatment with 8-OHQ decreased cognitive decline and lowered plasma Aβ1-42 levels in AD patients [127, 128].

1.3.4 Neurodegeneration in Alzheimer's disease

A prominent characteristic of the AD is brain atrophy which results from neuronal loss in areas such as the cerebral cortex and hippocampus [129]. While the exact mechanism of cell death remains unknown [130], direct toxicity of Aβ peptide has been implicated.

It is apparent that under certain conditions the Aβ peptide forms aggregates, leading to the production of a variety of soluble and insoluble protein assemblies, some of which have demonstrated neurotoxic properties. Despite over thirty years of research on amyloid protein and its variants, the answer to the fundamental question of which of the Aβ assemblies is the primary pathogenic form *in vivo* remains unanswered. Indeed, the intense investigation into Aβ toxicity has led to the discovery of previously undetected toxic Aβ aggregates and, subsequently, several Aβ species are now frontrunners in the toxicity debate.

Historically, it was believed that the senile amyloid-containing plaques were the toxic assembly of Aβ responsible for neuropathology and degeneration in the Alzheimer's brain [131]. More recently, however, this theory has fallen into disfavour as new evidence raises a number of points of contention. Most central is the debate over how well amyloid plaque load corresponds with cognitive decline. Studies using AD patients and non-dementia control patients have generated evidence both for [132] and against [133] a significant correlation between Aβ deposition and cognitive deficit, leaving only a tenuous link between plaque formation and clinical symptoms of AD. Additionally, studies using transgenic animals have

been unable to demonstrate a clear link between plaque deposition and neuronal cell loss [134].

Smaller fibrillar species of Aβ that are involved in the eventual deposition of amyloid into plaques were formerly favoured among researchers as the key toxic form of AB. These insoluble units of amyloid plaques were found to be toxic *in vitro* [135-137]and *in vivo* [138]. Additionally, Aβ1-42 is known to be the more fibrillogenic Aβ peptide [139], and increases in the ratio of Aβ1-42 to Aβ1-40 are linked to early onset familial AD [140]. However, insoluble Aβ levels correspond poorly with neurodegeneration and clinical pathology, and the more recent discovery of soluble toxic forms of Aβ has led to a revision of the amyloid hypothesis.

Soluble oligomers are defined as any Aβ form that is detectable in an aqueous buffer after centrifugation [141] and are now argued to be the primary toxic form of Aβ in the AD brain [139, 142-145]. Soluble oligomers are demonstrated to be toxic *in vitro* [139, 143, 146, 147] and *in vivo* [138] and have been detected in brain plasma [148] and CSF [149]. Furthermore, not only do soluble oligomer levels correlate better to cognitive impairment than plaque deposition cited in [118, 150-152] but small oligomers have been found to be more toxic than their larger fibrillar counterparts [139, 141, 153, 154].

In summary, key pathological aspects of AD are oxidative stress, metal dysregulation and neuronal degeneration. In contrast, MT has been proven to protect against oxidative stress in a number of models, is capable of binding metals implicated in AD pathogenesis and has demonstrated neuroprotective and neuroregenerative properties. Given the obvious overlap in Aβ pathology and MT action, MT has been suggested as a viable potential therapeutic for the treatment of AD.

1.3.5 Evidence for MT protection in AD

MT exhibits a number of biological capabilities which could prove beneficial against AD pathology. As previously discussed, MT is involved in copper and zinc metabolism, has ROS scavenging capabilities, and improves regenerative sprouting of neurons after injury. The significance of MT in Alzheimer's disease is suggested by a number of studies which show that MT is upregulated in animal models of AD [155, 156] and in humans [157]. Furthermore, MT has been found to protect cortical neurons from Aβ induced toxicity [78, 158] and prevent to formation of insoluble Aβ aggregates [159, 160].

A recent example of *in vitro* MT neuroprotection in an AD-relevant model is the work of Meloni et al. [160], who investigated the capacity of one metallothionein family member, MT3, to protect primary neurons in a cell culture model that incorporated Aβ peptide, AD-associated metals, oxidative stress, and neuronal death. It was shown that copper-bound Aβ (CuAβ) is redox active and kills cells *via* the production of ROS, *via* Fenton-like chemistry [160]. MT3, which carries endogenous zinc, was able to protect cultured primary neurons from CuAβ by mediating a metal swap to produce copper-bound MT3 and non-redox active ZnAβ. While this did suggest a role for metallothionein in AD therapy, MT3 is not a viable therapeutic molecule as, unlike MT1/2, MT3 inhibits the regenerative growth of neurons (reviewed in [161]).

Chung et al. [159] extended this work, investigating the capacity of the protective and regenerative MT family member, MT2, to protect against CuAβ-induced toxicity in cultured cortical neurons. In this study, MT2 was also able to protect neurons from CuAβ toxicity *via* the same copper-swap mechanism demonstrated in the work of Meloni's et al. (Figure 1.6). These studies strengthen the evidence that MT could be a potential therapeutic for AD.

1.3.6 Issues with MT as an AD therapeutic

One obstacle in the development of MT as a treatment for neurodegenerative illnesses of the CNS, is the difficulty involved in delivering the exogenous MT to its neuronal target. Despite generating interest as a potential therapeutic, to date there are no studies published reporting that peripherally administered metallothionein can cross the blood-brain barrier (BBB) to an appreciable degree [162]. As crossing the BBB is an essential requirement for any neuronal directed target, this limitation significantly impacts the potential of MT as a therapeutic in neurodegenerative disorders. However, the recent development of synthetic metallothionein analogues gives new direction for a possible therapeutic for the treatment of Alzheimer's disease.

1.4 Emtin Peptides – synthetic metallothionein analogues

1.4.1 Synthetic peptides

Peptides have emerged as one of the major classes of therapeutic molecules [163-165]. Peptides and peptide analogues have been developed to mimic naturally occurring molecules, such as hormones and growth factors, for drug delivery and immune prophylactics/diagnosis [163].

Peptides for therapeutic use are historically derived from natural peptides from plant, animal or human origins; from genetic or recombinant peptide libraries; or from peptides discovered from chemical libraries [163]. While these peptides have an advantage over small molecules and antibodies, they also have limitations which can inhibit their use as mainstream drugs, such as low potency, rapid renal clearance, and lack of stability *in vivo* due to protease degradation [163, 165]. To overcome these limitations, researchers have turned to the development of synthetic peptides. Synthetic peptides have become popular as ease of

Figure 1.6 Zinc-bound MT2 (Zn_7MT2) undergoes a metal swap with copper-bound Aβ (CuAβ) to prevent Aβ-mediated free radical formation

The Aβ1-40 and Aβ1-42 peptides can bind to copper ions, forming the redox active CuAβ. CuAβ produces free radicals *via* Fenton-like chemistry and has demonstrated toxicity in neuronal cell cultures [159, 160]. Zn_7MT2 can undergo a metal swap with CuAβ to form ZnAβ, a less toxic form of Aβ [159, 160].

A) Production of free radicals by copper-bound Aβ

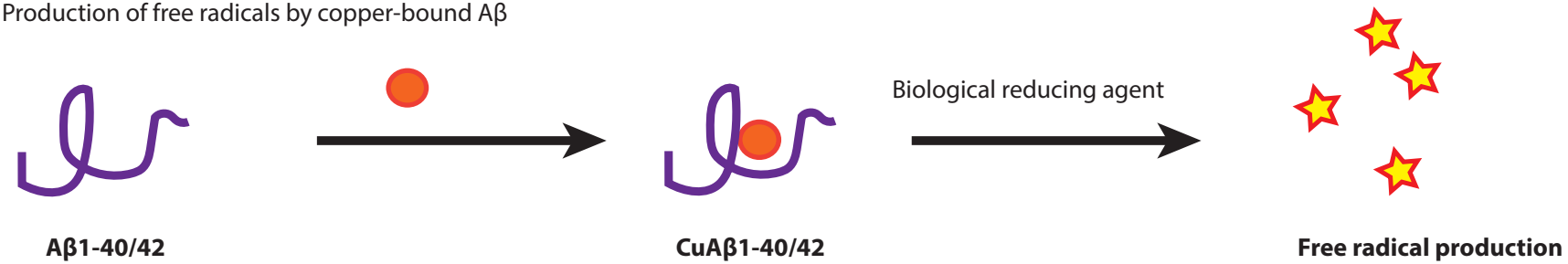

B) MT prevents free radical production by removing copper from CuAβ to produce zinc-bound Aβ

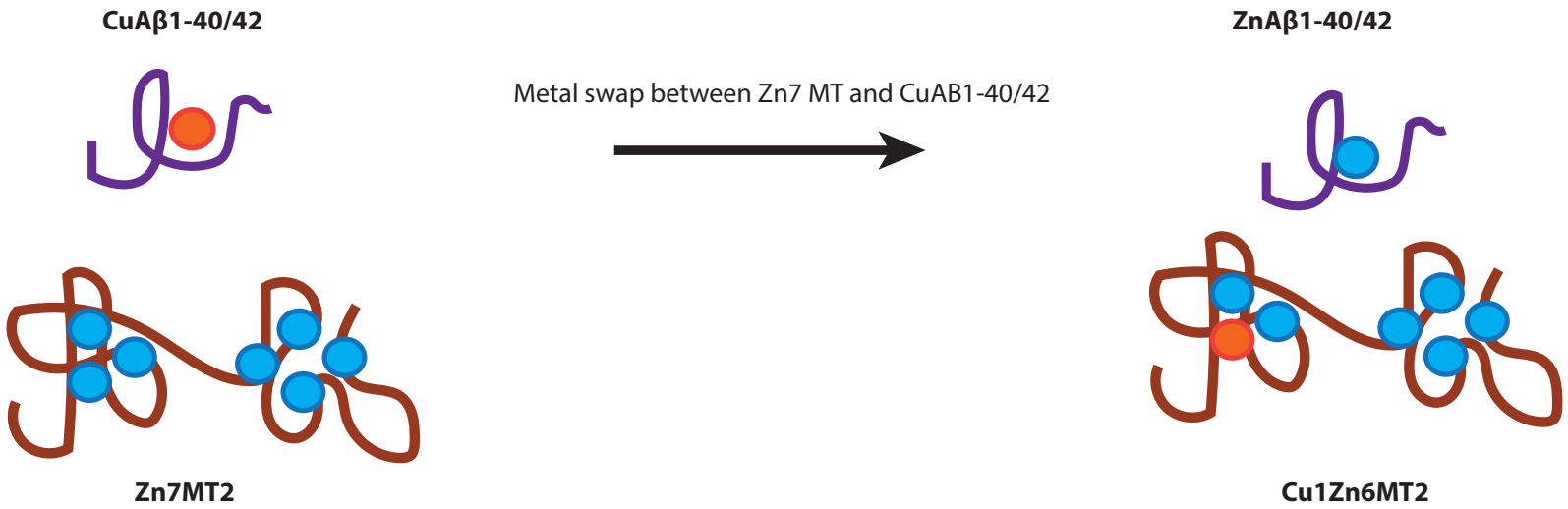

synthesis increases, enabling large scale synthesis and modification to the peptide sequence [163]. Importantly, peptide synthesis has evolved to enable production of multiple antigen proteins (MAPs), where synthetic peptides are tethered together using a core which is often lysine but alternatively, carbohydrate, calixarene, phosphorus or silicone based [166]. The tethering of multiple peptides to a core structure results in a branched, globular peptide, termed a dendrimer, which has multiple reactive end groups at the surface, with the aim of promoting synergistic enhancement of selected functions [166].

Dendrimers were first developed by Fritz Vögtle in 1978 (reviewed in [167]). Synthetic methods of producing dendrimers were improved using a novel convergent synthetic approach introduced by Hawker and Fréchet in 1990 [168], resulting in a rapid expansion of the synthetic peptide literature [169]. Peptide dendrimers are broadly defined as any compound containing peptides as branching elements, and can vary in complexity producing a range of molecules ranging from very low to very high molecular weight [170]. Dendrimers have many biomedical applications, such as protein mimics, drug delivery vehicles and, more recently, have also been used as gene transfection reagents [170, 171].

For dendrimers to be successful for medical applications they must fulfil several important criteria of biological importance [166]. The dendrimers should be non-toxic, non-immunogenic (if not required for vaccine), able to cross bio-barriers such as intestine, BBB, cell membranes, and be able to stay in circulation for the required time needed to have a clinical effect [166, 172].

The pharmacological properties of peptide dendrimers inform the therapeutic potential of these molecules. In general, synthetic peptides are less immunogenic than proteins or antibodies [173, 174] and, as small molecular weight substances are established to have low immunogenicity [175], low molecular mass dendrimers are less immunogenic than high molecular mass dendrimers [170]. A study by Francis et al. 1991 [176] investigated the

immunogenicity of dimers, tetramers and octapeptide dendrimers, finding that dimeric peptides were significantly more immunogenic than monomers, and that tetramers are 5-10 fold greater than dimers. In some cases, such as immunochallenge, immunogenicity is desirable [166] and immunogenicity would be a positive attribute. Thus, dendrimeric peptides may be immunogenic or non-immunogenic depending on the specific properties of the dendrimer and this can be modulated by manipulating the size of the dendrimer.

Peptide dendrimers have been shown to be more resistant to proteases, and therefore more stable, than monomeric peptides. An *in vitro* study showed that tetra-branched peptide dendrimers were detectable in human plasma and serum after 24 hours incubation, while monomeric peptides were degraded within two hours [177]. An *in vitro* study of monomeric, dimeric, trimeric and tetrameric peptides administered intraperitoneally to mice showed monomeric peptides were degraded quickly in plasma with around 50% loss in two hours, while multivalent constructs were more stable with minimal degradation in the first 12-24 hours [105].

The toxicity of synthetic peptide dendrimers is determined by the characteristic of each dendrimer. While some dendrimers exhibit toxicity (for a review see [166]) (notably cationic dendrimers which destabilise the cell membrane [178]) many peptide dendrimers have been found to have no or low toxicity [178-181]. Dendrimeric peptides also have a high level of efficacy (reviewed in [163]) explainable by an increase in avidity. Avidity describes the binding strength of a molecule with multiple binding sites. Multivalent molecules have increased avidity as a result of cooperative interactivity where the dissociation of a ligand from its receptor is less favoured [182].

Additionally, the small size of peptide dendrimers increases the possibility that these molecules can be effectively delivered to tissue. Indeed, some dendrimers have been shown to cross biological barriers such as the intestine [183] and blood-brain barrier [184]. Thus,

synthetic peptides have shown potential as non-toxic, high efficacy biological barrier permeating, high stability, peptide mimetics.

1.4.2 The emtin peptides

The laboratory of Berezin and Bock, at the University of Copenhagen, has produced synthetic peptides based on the amino acid sequence of human MT2 [94]. Four such peptides have been produced, with each peptide being 14 amino acids in length and corresponding to either the C-terminus or N-terminus amino acid sequences of the α-domain or β-domain [185] (Figure 1.7). These peptides are termed 'emtins' and their nomenclature is based on the MT domain and terminus that each individual emtin is modelled upon. Thus, the emtins corresponding to the C-terminus and N-terminus of the α-domain are termed EmtinAc and EmtinAn respectively and, similarly, the emtins corresponding to the C-terminus and N-terminus of the β-domain are termed EmtinB and EmtinBn respectively (See Figure 1.7) [185]. EmtinB nomenclature is slightly different to the other peptides, as EmtinB was the first emtin to be developed and the terminus was not specified in the naming. The emtin peptide sequences are not identical to their MT2 template. MT has a high number of cysteine residues and, to prevent unwanted bridge formation between cysteines in the peptides during synthesis, the amino acid sequence has been altered slightly from native MT2 sequence by substituting some of the cysteine residues for serine residues [94, 185] (See Figure 1.7).

These synthetic protein analogues can be produced as monomers, dimers linked by a single lysine, or dendrimeric tetramers linked by a three lysine backbone (see Figure 1.7) [186]. Experiments by the Berezin and Bock laboratory using the emtin peptides have been carried out with the tetrameric forms [94, 184, 185], likely because earlier work with other dendrimers showed that tetramers are most effective in producing the mimetic effect [186].

The emtin family of metallothionein-derived peptides was developed with the aim of producing an MT-mimetic peptide. As discussed previously, MT2 is noted for having

neuroprotective, neuritogenic and anti-apoptotic properties which underpin positive effects in the CNS after injury and during illness, and these properties form the basis for its speculative potential as a CNS therapeutic. For emtins to exhibit validity as a potential therapeutic in neurodegenerative disorders it must first be shown that they can mimic these properties of MT2 and early evidence suggests that at least some of the emtins exhibit metallothionein-like properties *in vitro* [94, 185].

Ambjorn et al. [94] investigated the properties of the tetrameric form of the peptide modelled on the c-terminus of the β-domain, EmtinB. EmtinB, when administered *in vitro* to primary cultures cerebellar granule neurons, was found to stimulate neurite outgrowth with an efficacy equivalent to that of MT, and to promote cell survival with greater efficacy than MT [94].

EmtinB administration resulted in increased activation of ERK and PKB/Akt (which are involved in neurite outgrowth and cell survival) two kinases which are known to be activated by MT [94]. It was further demonstrated that EmtinB was acting through the LRP family of receptors, which are putative receptors for metallothionein [80, 90, 94]. Thus it appears that EmtinB is an MT-mimetic peptide capable of reproducing at least some of the biological effects demonstrated by MT *in vitro* [184].

Asmussen et al. [185] extended this work by investigating Emtins Ac, An, and Bn, and their capacity to achieve the same MT-mimetic results. EmtinBn exhibited no capacity for neurite extension, however EmtinAc and EmtinAn were both found to promote neurite extension and cell survival. Intriguingly, while both EmtinAc and EmtinAn were both found to activate ERK and PKB/Akt, only Emtin Ac was found to act through the LRP family of receptors [185]. Thus, while EmtinB, EmtinAc and EmtinAn all promote neurite extension and survival, only EmtinB and EmtinAc act through LRP receptors (the putative MT receptor) suggesting that, of the four produced peptides, EmtinB and EmtinAc are most similar in action to the parent protein MT2.

Figure 1.7 Sequence of emtin peptides compared with human MT2 sequence and schematic of emtin dimer and tetramer structure on lysine backbone

A) Emtins are short 14-15AA peptides based on the α-domain or β-domain of the human MT2 sequence. Amino acid sequences for EmtinB, EmtinBn, EmtinAc and EmtinAn are aligned with the human MT2 sequence and denoted in black, green, pink, and blue respectively. Amino acid sequences do not exactly match the sequence for MT2; some cysteine residues present in MT2 have been substituted for serine in emtin sequences to prevent aggregation of the peptides. Substituted serine residues are highlighted in bold (adapted from [185]). B) Emtin peptides have been produced in both dimeric and tetrameric form. Dimeric emtin peptides are produced by tethering two of the same peptide sequence together using a single lysine backbone. Tetrameric emtins are produced using four peptides tethered to a 3 lysine backbone (adapted from [186]).

A

β-domain α-domain

Human MT2

MDPNCSCAAGDSCTCAGSCKCKECKCTSCKKSCCSCCPVGCAKCAQGCICKGASDKCSCCA

MDPNCSCAAGDS**S**T**S**AGSCKCKE**S**K**S**TS KKS**S**CSC**S**PVG**S**AK AQG**S**ICKGASDK**S**S

EmtinBn 1-14 EmtinB 15-28 EmtinAn 30-43 EmtinAc 45-58

B

Dimer

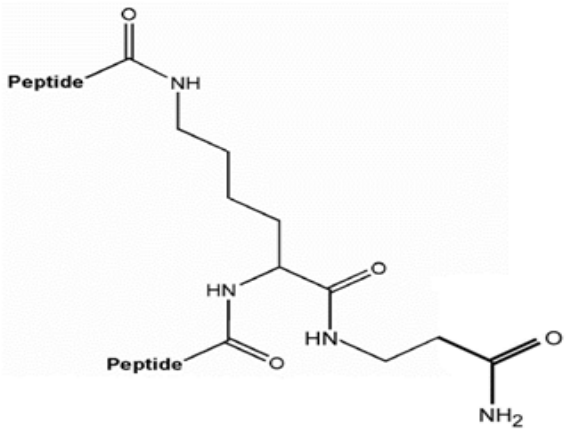

Tetramer

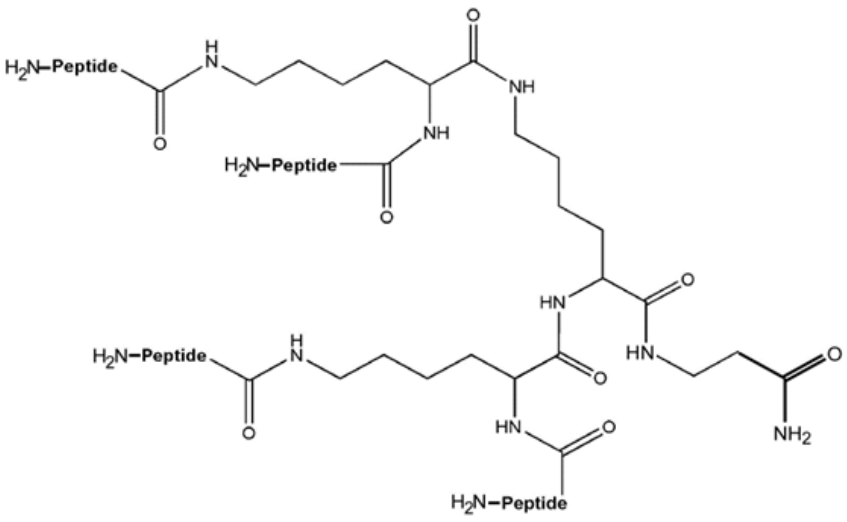

More recently it has been demonstrated, using an animal model of epilepsy, that EmtinB has a significant neuroprotective effect *in vivo*. MTKO mice are more susceptible to seizures induced by kainic acid than their wild-type counterparts [184]. Kainic acid induction of seizures is a model currently used for screening potential anti-epileptic drugs. EmtinB was found to not only attenuate kainic acid-induced seizures, but to ameliorate kainic acid-induced neuropathology in the hippocampi of treated mice [184]. Arguably the most fascinating finding from this work was that, despite being administered subcutaneously, EmtinB was able to affect the target neurons in the hippocampal region of the brain. Analysis of the CSF of treated and non-treated mice demonstrated that Emtin B is able to cross the blood-brain barrier [184]. The ability of other Emtins to cross the blood-brain barrier is yet to be established; however, given that the emtins are all of very similar size and construction, there is a high likelihood that other emtins could share this attribute.

Taken together, the evidence indicates that EmtinAc and EmtinB are good candidates for MT-mimetic peptides as they most closely recapitulate the properties of MT. EmtinAc and EmtinB exhibit both neuroprotective and neuroregenerative properties and, additionally, EmtinB readily crosses the blood-brain barrier, fulfilling a crucial requirement of a neuronal therapeutic (See Table 1.1).

Table 1.1 Metallothionein-like properties of the emtin peptides

Protein/peptide	Neurite outgrowth	Neuronal survival	Bind LRP receptors	Bind copper	Cross BBB
MT2	Yes [77, 79]	Yes [79]	Yes [79]	Yes [187]	No
EmtinB	Yes [79]	Yes [79]	Yes [79]	?	Yes
EmtinBn	No [185]	Yes [185]	Yes [185]	?	?
EmtinAc	Yes [185]	Yes [185]	Yes [185]	?	?
EmtinAn	Yes [185]	Yes [185]	No [185]	?	?

1.5 Thesis aims

The metal binding, radical scavenging and neuroprotective properties of metallothionein have identified MTs as a potential therapy for the treatment of Alzheimer's disease. However, the inability of MT to cross the BBB makes it an unlikely candidate for CNS-directed therapy. Some emtin peptides, in particular EmtinAc and EmtinB, have been able to reproduce some of the neuroprotective and neuritogenic actions of MT, and one of the peptides, EmtinB, has been shown to cross the BBB. We hypothesise that emtin peptides can act as MT-mimetics and rescue cultured neurons from CuAβ-mediated toxicity and, furthermore, this neuroprotective capacity will improve cognitive outcomes and pathological markers of AD *in vivo* in the APPswe/PS1ΔE9 mouse model of AD.

Accordingly, this thesis will evaluate the potential of EmtinAc and EmtinB to recapitulate the neuroprotective effects of MT when applied to a culture model relevant to Alzheimer's disease, and to modulate cognitive and neuropathological outcomes when administered to an animal model of Alzheimer's disease.

Aim 1: Determine the capacity of EmtinAc and EmtinB to protect primary cultured hippocampal neurons in the established CuAβ model of neuronal Aβ insult.

Aim 2: Determine the mechanism of emtin protection in the CuAβ model of neuronal Aβ insult.

Aim 3: Investigate the effect of emtins on pathological traits in the APPswe/PS1ΔE9 model of AD.

Chapter 2 – Materials and Methods

2.1 media, buffers and solutions

2.1.1 Subsequent media

Neurobasal media (Gibco, USA) supplemented with 2% (v/v) B27 (Gibco) and 0.1% (v/v) gentamycin solution (Gibco, USA) and 0.5mM L-glutamine (Gibco, USA). Stored at 4°C.

2.1.2 Initial media

Subsequent media with 10% fetal bovine serum (Gibco, USA). Stored at 4°C.

2.1.3 Ascorbate (0.03M solution)

A 0.03M solution of ascorbate was prepared by dissolving 0.05g of sodium ascorbate in 10mL of distilled water. 1µL of 0.03M ascorbate was added to each 100µL reaction tube to achieve a final concentration of 300µM.

2.1.4 Hank's Buffered Salt Solution (HBSS)

HBSS solution was prepared by adding 0.35g of $NaHCO_3$ and 1 bottle (9.8g) of Hanks' Buffered Salts Solution (HBSS; Gibco, USA) in 950mL in MilliQ water. The pH was adjusted to 7.2 before adjusting the volume to 1L. HBSS was filter sterilised into a sterile bottle and stored at 4°C.

2.1.5 Phosphate Buffered Saline (PBS; 0.01M)

PBS was prepared by combining 10mL of 31.2% $NaH_2PO_4 \cdot 2H_2O$ solution, 40mL of 28.4% Na_2HPO_4 solution and 100mL of 9% NaCl. The solution was made to a volume of 1L by adding 850mL of MilliQ water and the pH was adjusted to 7.2. PBS was filter sterilised and stored at 4°C.

2.1.5.1 $NaH_2PO_4.2H_2O$ solution (31.2%)

31.2g of $NaH_2PO_4.2H_2O$ in1L of MilliQ water. Stored at room temperature.

2.1.5.2 Na_2HPO_4 solution (28.4%)

28.4g of Na_2HPO_4 in 1L in MilliQ. Stored at room temperature.

2.1.5.3 NaCl solution (9%)

90g of NaCl in 1L MilliQ. Stored at room temperature.

2.1.6 Phosphate Buffered Saline with 0.05% Tween20 (PBS-T; 0.01M)

PBS (method 2.1.5) with 0.05% tween-20. Store at 4°C.

2.1.7 Tris Buffered Saline 10x stock (10 x TBS)

Tris base was prepared by dissolving 60.5g of Tris base and 87.6g of NaCl in 950mL of MilliQ water. The pH was adjusted to 7.5 and made to a final volume of 1L with MilliQ water. Stored at 4°C.

2.1.8 Tris Buffered Saline with 1% Tween20 (1 x TBS-T)

To make a working solution of TBS, 100mL of 10x TBS stock solution was added to 900mL of MilliQ water. To make TBS-T, 1mL of Tween-20 was added and mixed thoroughly. Stored at 4°C.

2.1.9 Trypsin (2.5%)

Stock 2.5% trypsin (Gibco, USA) was stored in 500µL aliquots at -20°C. Stock was diluted to 0.1% for use.

2.1.10 Tris buffer

Tris buffer was prepared by dissolving 0.315g of Tris-HCl and 0.584g of NaCl in 95mL of water. The pH was adjusted to 7.4 and the solution made to a volume of 1L with distilled water. Stored at 4°C.

2.1.11 Nuclear Yellow stock solution

10mg of nuclear yellow dye (Invitrogen, Thermofisher Scientific, MA, USA) was dissolved in 1mL of MilliQ water to give a 10mg/mL concentrated stock solution (stored at 4°C). A working solution of 1μg/mL was prepared by dilution in PBS.

2.1.12 EmtinB preparation for cell culture experiments

EmtinB (Neoloch, Hellerup, Denmark) was prepared at 10mg/mL in sterile MilliQ water. This was diluted in warm subsequent media to the required concentration.

2.1.13 Ethylenediaminetetraacetic acid (EDTA; 100mM)

EDTA solution was prepared by dissolving 37.5mg of $Na_2EDTA{\cdot}2H_2O$ in 1mL of sterile MilliQ water. The pH was adjusted to 8 and the solution stored at 4°C.

2.1.14 Paraformaldehyde (PFA; 4%)

40g paraformaldehyde was dissolved in 500mL of MilliQ water at 60°C. A solution of 10M sodium hydroxide was added drop-wise until the PFA solution became clear. The PFA solution was then added to 500mL 2X PBS (2x PBS is prepared using the method for 1x PBS described in 2.1.5 made to a total volume of 500mL instead of 1L). Stored at 4°C.

2.1.15 Preparation of 200μM copper-bound Aβ

1mg of Aβ1-40 was dissolved in 1.15mL of sterile distilled water to give a concentration of 200μM. A 20mM solution of copper chloride was prepared in sterile MilliQ and 1μL was added

for every 100µL of Aβ required. The mixture was incubated at room temperature for 30 minutes (no shaking required).

2.1.16 Preparation of a 1mg/mL sample of EmtinB in PBS

A 10mg/mL stock of EmtinB (Neoloch, Hellerup, Denmark) was prepared by reconstituting 10mg of EmtinB dimer. To make a 1mg/mL EmtinB sample, 100µL of the 10mg/mL stock was added to 900µL of sterile PBS.

2.1.17 Zinc saturated solution (67mM)

A saturated (approximately 67mM) solution of $ZnCl_2$ was prepared by dissolving 0.0913g of $ZnCl_2$ in 10mL of sterile PBS. Stored at 4°C.

2.1.18 Copper saturated solution (67mM)

A saturated (approximately 67mM) solution of $CuCl_2$ was prepared by dissolving 0.1142g of $CuCl_2 \cdot 2H_20$ in 10mL of sterile PBS. Stored at 4°C.

2.1.19 $CuCl_2$ for copper swap (20mM)

20mM $CuCl_2$ was prepared by dissolving 0.034g of $CuCl_2$ in 10mL of MilliQ water. Stored at 4°C.

2.1.20 Aβ1-42 for copper swap (30.4µM)

1mg of Aβ1-42 was resuspended in 7.284mL of tris buffer. To get a final concentration of 25µM, 82.2µL of 30.4µM Aβ1-42 was added to each 100µL reaction. Stored at -20°C.

2.1.21 Hydrogen peroxide stock solution (100mM)

10.2µL of 30% H_2O_2 (9.8M) was made to 1mL with sterile MilliQ water to give a concentration or 100mM. This was diluted in warmed Neurobasal media to give an in-media concentration of 100µM.

2.1.22 Receptor Associated Protein (RAP) stock solution

RAP (250µg; Progen Biotechnik, Heidelberg, Germany), was dissolved in sterile MilliQ at 10µM. RAP was diluted to 1µM in warmed subsequent media for use. Stored at -20°C.

2.1.23 Reconstitution of siRNA

siRNA directed at LRP1 (ON-TARGETplus Rat Lrp1 (299858) siRNA; Dharmacon, CO, USA), LRP2 (ON-TARGETplus Rat Lrp2 (29216); Dharmacon, CO, USA), and a non-targeting control siRNA (Non-targeting siRNA #2 ; Dharmacon, CO, USA) were reconstituted in RNase free water (Dharmacon, CO, USA) to a concentration of 5µM according to manufacturer's instructions. In brief, siRNA was re-suspended in 1mL of water and pipetted gently before incubation in an orbital mixer for 30 minutes at room temperature. The siRNA was then centrifuged briefly to collect all liquid. RNA was stored in 10µL aliquots at -20°C.

2.1.24 Coomassie brilliant blue

Coomassie brilliant blue stain was prepared by dissolving 0.5g of Coomassie brilliant blue (Sigma, USA) in a solution of 45% water, 45% methanol and 10% acetic acid. The resulting solution was stirred for 4 hours before filtering through filter paper (Whatman 18.5cm diameter, qualitative; Sigma, USA). Coomassie stain was stored at room temperature.

2.1.25 Coomassie destain solution

Coomassie detain solution was prepared by combing 10% glacial acetic acid, 10% methanol and 80% MilliQ water. Stored at room temperature.

2.1.26 HEPES (10mM)

HEPES solution was prepared by dissolving 1.1915g of HEPES (Sigma, USA) in 500mL 0.01M PBS. The pH was adjusted to 7.2 and the solution was filter sterilised into a sterile bottle. Stored at 4°C.

2.1.27 Laemlli 4 x sample buffer (reducing)

5mL of 1M Tris-HCl pH 6.8, was combined with 2mL of 20% SDS, 2mL of glycerol, 2mL of β-mercaptoethanol and 0.02% bromophenol blue. Stored at -20°C.

2.1.28 Western Blot Running buffer

NuPAGE MES SDS running buffer (NP0002; 20x; Invitrogen, Thermofisher Scientific, MA, USA) was diluted 1:20 in MilliQ water.

2.1.29 Western Blot Transfer buffer

Transfer buffer was prepared by dissolving 11.5 grams of Glycine and 2.4 grams of Tris base in 600mL of MilliQ water. 160mL of methanol was added to give a final volume of 800mL. Stored at room temperature.

2.1.30 Western Blot Blocking solution

5g of Aptamil gold infant formula milk powder (Woolworths, TAS. AUS) was dissolved in 100mL of TBS-T (method 2.1.8).

2.1.31 Immuno diluent

0.3% TritonX in PBS (method 2.1.5).

2.1.32 Immuno wash solution

0.25% TritonX in PBS (method 2.1.5).

2.1.33 RIPA Lysis buffer

RIPA lysis buffer was prepared by combining 50mM Tris-HCl (0.394g), 150mM NaCl (0.4383g), 1mM EDTA (0.0186g), 1% triton (0.5mL), 1% Sodium deoxycholate (0.5g), and 0.1% SDS in 50mL of MilliQ water. The pH was adjusted to 7.4. To prevent protein degradation, 1%

protease inhibitor cocktail (Thermofisher scientific, MA, USA) was added immediately prior to use.

2.2 Methods

All procedures carried out on animals were approved by the University of Tasmania Animal Ethics Committee and were carried out in accordance with the Australian Code of Practice for the Care and Use of Animals for Scientific Purposes (2004). Rat tissue was obtained from Sprague-Dawley rats and mouse tissue was obtained from APPswe/PS1ΔE9 double transgenic mice or control wild-type C57 black 6 (B6) mice. All cultures were grown in an incubator at 37°C with 5% CO_2.

2.2.1 Hippocampal neuron culture

Hippocampal neurons were cultured from E17/18 rat embryos. Embryos were removed from the uterus of mothers euthanized by CO_2 asphyxiation, removed from the embryonic sacs and decapitated. Heads were placed on ice while awaiting dissection. Embryonic brains were removed using tweezers to cut along the midline of the embryo skull and applying lateral pressure to the head to force the brain out of the cranium. The brain was then placed into HBSS and dissected under microscope. Firstly, the cerebellum was dissected out and discarded. The brain was then cut along the corpus callosum to separate the hemispheres. The thalamus and hypothalamus were removed from each hemisphere, revealing the hippocampus. The meninges were peeled back and removed to expose the hippocampus, which was then dissected out. The hippocampal tissue was transferred to 5mL of ice-cold HBSS. When all brains were thus dissected, 200µL of 2.5% trypsin (Sigma, USA) was added and the tube inverted gently to mix before incubating at 37°C for 5 minutes in a water bath. The HBSS/0.1% trypsin mixture was removed and 1mL of initial plating media was added to the trypsinised tissue. The tissue was gently triturated using a 1mL pipette to form a cell suspension. This cell suspension was filtered through gauze to give a single cell suspension.

Trypan blue (Sigma, USA) was used to perform a cell count. Cells were plated at $1x10^5$ cells per well and maintained in an incubator at 37°C with 5% CO_2.

Cells were changed from initial medium to subsequent medium after 24 hours and media relaced every 2-4 days thereafter.

2.2.2 Trifluoroacetic acid (TFA) and trifluoroethanol (TFE) monomerisation of Aβ

1mg of Aβ1-42 peptide resuspended in 1mL of TFA followed by evaporation of TFA under a stream of nitrogen. The peptide was then washed three times in TFE (1mL) using the same evaporation method as for TFA. Monomerised peptide was stored at -20°C.

2.2.3 Gel Coomassie staining

Gels were incubated in Coomassie brilliant blue (method 2.1.24 Coomassie brilliant blue) overnight with gentle shaking on an orbital mixer at room temperature. Gels were then transferred to destain solution (method 2.1.25) and incubated with gentle shaking on an orbital mixer at room temperature until the bands became clear. Gels were imaged on a Carestream image station 4000MM Pro (Carestream Molecular imaging, CT, USA) using Carestream MI SE software (v4.5.2).

2.2.4 AlamarBlue® assay

AlamarBlue assay was carried out as per the manufacturer's instructions: a 10% solution of alamarBlue (Invitrogen, Thermofisher scientific, MA, USA) was prepared in warmed subsequent media. The experimental media was removed from wells and 300µL of the 10% alamarBlue in media solution was added to cells. After 1.5 hours incubation under cell culture conditions, 50µL of the media was removed from each well and transferred to a clear bottom

96-well plate. The blank used was 10% alamarBlue in subsequent media, incubated under the same conditions for an equal amount of time.

The fluorescence of the media was read using a SpectraMax M2 plate reader (Molecular Devices) and SoftMax Pro computer program (v 4.8). Samples were blank subtracted before analysis.

2.2.5 Protein extraction from primary cultured neurons

To produce lysates for protein analysis, cells (which were plated at 1 x 10^5 cells per well) were washed twice with ice-cold PBS, and 100µL of RIPA buffer (method 2.1.33) was added to each well.

Cells were incubated in RIPA buffer on ice, with shaking for 15 minutes. Cells were then collected and mixed by vortex for ten seconds followed by incubation on ice for a further 15 minutes. Cells were centrifuged at 10,000rpm at 4°C for 10 minutes and the supernatant collected.

2.2.6 Immunocytochemistry (ICC) on neuronal cultures

Hippocampal neurons were fixed in 4% PFA prior to immunostaining. All primary antibodies were incubated in immuno diluent (method 2.1.31) for 1 hour at room temperature or overnight at 4°C. Secondary antibodies were incubated in PBS for 1 hour at room temperature. Cells were washed 3 times for ten minutes after each antibody incubation using immuno wash solution (method 2.1.32) Antibodies used are described in Table 2.1.

Table 2.1 Antibodies used in ICC of neuronal cells.

Target	Antibody	Concentration
LRP1	**Rabbit anti-LRP1 (L2170, Sigma, MO, USA)**	**1:1000**
Tau	**Rabbit anti-Tau (A0024, Dako, NSW, AUS)**	**1:2500**
GFAP	**Rabbit anti-GFAP (20334, Dako, NSW, AUS)**	**1:2500**
Rabbit antibody	**Goat anti-rabbit Alexa 594-conjugated (Molecular probes, OR, USA)**	**1:1000**
Mouse antibody	**Goat anti-mouse Alexa 488-conjugated (Molecular probes, OR, USA)**	**1:1000**

2.2.7 BCA protein assay

Quantitation of protein was carried out using the Pierce BCA Protein Assay Kit (#23225; Thermofisher scientific, MA, USA) according to the manufacturer's instructions. Briefly, in a 96 well plate either 10 or 25µL of sample was combined with 200µL of Working Reagent (a solution comprising 1 part kit reagent A to 50 parts kit reagent B). A standard curve was prepared on the same plate using an appropriate protein standard. Samples and standards were incubated for 30 minutes at 37°C before the absorbance was recorded at 562nm on a SpectraMax M2 plate reader (Molecular Devices) and SoftMax Pro computer program (v 4.8).

2.2.7.1 BCA analysis of protein in neuronal cell extracts

Analysis of protein in neuronal cell extracts in RIPA buffer was carried out according to 2.2.7 with the following specific detail. In brief, 10µL of each sample was added to a 96 well plate along with the following standards: 0, 25, 125, 250, 500, 750, 1000, 1500 and 2000µg/mL Bovine serum albumin (BSA) diluted in RIPA buffer (method 2.1.33). Sample concentrations were determined using the BCA standard curve equation of the line.

2.2.7.2 BCA analysis of protein in column fractions

Analysis of protein in the column fractions was carried out using a BCA Protein Assay. The BCA assay was carried out according to 2.2.7. In brief, 25µL of each column fraction was added to a 96 well plate along with the following standards: 0, 0.031, 0.062, 0.125, 0.25, and 0.5. 1.0, and 2.0mg/mL of Apo-EmtinB. Sample concentrations were determined using the EmtinB standard curve equation of the line calculated from the standard curve constructed on each plate.

2.2.7.3 BCA analysis of extracts from whole brain hemispheres and hippocampal enriched samples

Analysis of protein in brain extracts in RIPA buffer was carried out according to 2.2.7 with the following specific detail. Samples were diluted 1:10 to reduce protein concentration before 10µL of each sample was added to a 96 well plate along with the following standards: 0, 25, 125, 250, 500, 750, 1000, 1500 and 2000µg/mL Bovine serum albumin (BSA) diluted in RIPA buffer (method 2.1.33). Sample concentrations were determined using the BCA standard curve equation of the line calculated from the standard curve constructed on each plate.

2.2.8 Preparation of 5mg/mL biotinylated EmtinB

Biotinylation of EmtinB was carried out using the ImmunoProbe Biotinylation kit (Sigma-Aldrich, MA, USA) as per the manufacturer's instructions. In brief, EmtinB dimer was dissolved in sterile MilliQ water at an approximate concentration of 10mg/mL. Equal volumes (500µL) of 10mg/mL EmtinB and BAC-sulfo biotin ester in 6% DMSO/94% PBS were combined together and incubated on ice for 2 hours with gentle shaking.

The provided column was equilibrated with 6 x 5mL of PBS (method 2.1.5) before the reaction mixture was applied. Biotinylated EmtinB was eluted from the column in 10 x 1mL fractions and quantified using BCA assay. Biotinylation of EmtinB was confirmed by dot blot.

2.2.9 Mouse subcutaneous injection and gavage protocol

Animals were sedated with isofluorane before they were injected or gavaged with the appropriate volume of 5mg/kg biotinylated EmtinB peptide. Previous work using injection of EmtinB [184] and oral administration of peptides [188] suggested that protein should be detectable in serum approximately 45 minutes after administration. Based on these papers the mice were sedated 45 minutes post administration for sample collection. Based on this work, the mice were terminally anaesthetised with a lethal dose of pentabarbitone, >100mg/kg given intraperitoneally, 45 minutes after administration of EmtinB.

When mice had reached a plane of full surgical anaesthesia, as assessed by loss of pedal reflex, blood was extracted *via* intra-cardiac puncture using 1mL syringe and 22G needle coated with EDTA (0.5M, pH 8.0; method 2.1.13) and put into an EDTA coated eppendorf for plasma collection (approximately 2μL of EDTA per 100μL of blood). The EDTA/blood mixture was kept chilled at 4° C while the rest of the procedure and tissue collection was performed then centrifuged at 4°C for 15 minutes at 200g (5000rpm) and the supernatant was collected.

2.2.10 Protein extraction from EmtinB injected and control APPswe/PS1ΔE9 brains

Proteins from frozen brain samples were extracted in RIPA buffer with protease inhibitor. Cortical and whole hemisphere samples were ground under liquid nitrogen in a mortar and pestle. A small amount of the ground brain was then transferred to a chilled Eppendorf tube and 300μL of RIPA buffer (method 2.1.33) added. Tubes were homogenized using a T10 basic ultra-turrax (IKA, Selangor, Malaysia) on setting 3 for short bursts until thoroughly mixed. The mixtures were then centrifuged at 4°C for 15 minutes at 13,000rpm. The supernatant was collected and the pellet discarded.

2.2.11 Western blot analysis and quantitation

Western blot gels were run at 200 volts for 20-30 minutes using western blot running buffer (method 2.1.28). Transfer of proteins to a membrane used western blot transfer buffer (method 2.1.29). For visualisation of protein bands, blots were incubated in chemiluminescent substrate (EMD Millipore, MA, USA) for five minutes before imaging using a Carestream image station 4000MM Pro (Carestream Molecular imaging, CT, USA) using Carestream MI SE software (v4.5.2).

2.2.11.1 Western blot analysis of mouse serum samples from injected and gavaged mice

Western blots were carried out using The Novex® NuPAGE® SDS-PAGE Gel System (Thermofisher scientific, MA, USA). Protein samples were run on Nupage gels using Nupage MES SDS running buffer (Invitrogen Thermofisher scientific, MA, USA)

Samples were prepared by mixing 50% serum with 50% Laemlli reducing sample buffer (method 2.1.27). A control sample of biotinylated EmtinB dimer was prepares using 50ng in 50% MilliQ/50% Laemlli reducing sample buffer. Gels were run on a NuPAGE 4-12% bis-tris gel (Invitrogen, Thermofisher scientific, MA, USA) and transferred to nitrocellulose membrane (Thermofisher scientific, MA, USA) at 30 volts for 1 hour. Blots were blocked western blot blocking solution (method 2.1.30) overnight at 4°C before incubating in avidin-HRP (Invitrogen, Thermofisher scientific, MA, USA) for four hours at room temperature.

2.2.11.2 Western blot analysis of mouse brains from injected and gavaged mice

Cortical and whole hemisphere samples were analysed by western blot for the presence of biotinylated EmtinB. Protein extract from cortex and whole hemisphere brain samples were analysed for protein content by BCA assay. Equal total protein amounts of hemisphere samples

(127µg) and cortex samples (30µg) were prepared in a 10µL volume, and then 1.5µL of NuPAGE reducing agent (Invitrogen, Thermofisher scientific, MA, USA) and 3.5µL of LDS sample buffer (Invitrogen, Thermofisher scientific, MA, USA) were added. The samples were heated at 80°C for 15 minutes before running on a NuPAGE 4-12% bis-tris gel (Invitrogen, Thermofisher scientific, MA, USA). Blots were transferred to polyvinylidene fluoride (PVDF) membrane at 20 volts for 1 hour then blocked in western blot blocking solution (method 2.1.30) overnight at 4°C.Blots were incubated in avidin-HRP (Invitrogen, Thermofisher scientific, MA, USA) for four hours at room temperature.

2.2.11.3 Western blot analysis of EmtinB trial brains

Whole hemisphere and hippocampal extracts were analysed by western blot. RIPA extracts were analysed for protein content by BCA assay and equal total protein amounts of hemisphere samples (20µg) and hippocampal samples (12µg) were prepared in a 6.5µL volume, then 1µL of NuPAGE reducing agent (Invitrogen, Thermofisher scientific, MA, USA) and 2.5µL of NuPAGE LDS sample buffer (Invitrogen, Thermofisher scientific, MA, USA) were added. Samples were heated at 80°C for 15 minutes before running on a NUPAGE 4-12% bis-tris gels (Invitrogen, Thermofisher scientific, MA, USA) and transferring to a PVDF membrane. The membrane was blocked in western blot blocking solution (method 2.1.30) for one hour at room temperature.

2.2.11.4 Antibodies for western blotting

Primary antibodies were incubated in western blot blocking solution (method 2.1.30) overnight at 4°C and then washed 3 x 10 minutes in PBS-T (method 2.1.6) at room temperature. Secondary goat anti-mouse (P0447) and goat anti-rabbit (P0448) antibodies were purchased from Dako (Glostrup, Denmark), and were incubated in 5% milk formula (Woolworths, Tas) powder for two hours at room temperature, then washed in PBS-T three times for ten minutes. For antibody details see Table 2.2.

Table 2.2 Primary and secondary antibodies used in western blotting

Target	Primary antibody	Concentration	Secondary antibody	Concentration
EmtinB dimer (biotinylated)	Streptavidin-HRP conjugate (SNN1004, Invitrogen, Thermofisher scientific, MA, USA).	1:1000	None	None
APP	Mouse anti-APP (MAB348, EMD Millipore, MA, USA)	1:1000	Anti-mouse HRP	1:10000
LRP1	Rabbit anti-LRP1 (L2170, Sigma, USA)	1:1000	Anti-rabbit HRP	1:10000
IBA1	Rabbit anti-IBA1 (01919741, Wako, VA, USA)	1:500	Anti-rabbit HRP	1:10000
GFAP	Rabbit anti-GFAP (20334, Dako, Glostrup, Denmark)	1:1000	Anti-rabbit HRP	1:10000
Synaptophysin	Rabbit anti-Synaptophysin (9272, EMD Millipore, MA, USA)	1:2000	Anti-rabbit HRP	1:7000
PSD95	Mouse anti-PSD95 (75-028, NeuroMab, CA, USA)	1:1000	Anti-mouse HRP	1:7000
β(III)-tubulin	Mouse anti-β(III)-tubulin (G7121, Promega, WI, USA)	1:2000	Anti-mouse HRP	1:20000
β-actin	Mouse anti-β-actin (A2228, Sigma, USA)	1:2500	Anti-mouse HRP	1:20000

2.2.11.5 Quantitation of western blots

Image files (.tiff format) were imported into ImageJ (NIH, MD, USA) and analysed using the following protocol:

1. Flip image so that the first sample on the gel is on the left hand side of the image.
2. Ensure the image shows white bands on a black background.
3. Convert the image to 8 bit greyscale.
4. Subtract the background using a rolling ball radius of 50 pixels.
5. Set the scale to pixels.
6. Set the measurements to area and integrated density
7. Using the ROI manager, place a box around each band and add it to the list of items to be analysed.
8. Measure the integrated density of each band.

The integrated density of each band was obtained and normalised to the control samples on each gel. Each band was then normalised to the actin control. All samples were then represented as a percentage of the SSV control.

Significance was determined using a one-way ANOVA with Tukey Post-test and PRISM software (GraphPad Prism, version 6, La Jolla, CA, USA) for analysis of trial brains, while a t-test was used for comparison between B6 control mice and APPswe/PS1ΔE9 mice.

Chapter 3 – Emtins protect against CuAβ mediated toxicity in primary rat hippocampal neurons

3.1 Introduction

Oxidative stress is a key feature of the AD brain. While the source of excess free radicals is still under debate, there is some evidence that free radical generating, redox active metals are involved. Consistent with this idea, redox active metals, such as copper, are enriched in amyloid plaques in the AD brain [189]. Investigation into copper involvement in AD, using *in vitro* studies, has shown that Aβ peptides bind copper with high affinity and, under culture conditions, copper-bound Aβ (CuAβ) produces reactive oxygen species which are toxic to neurons [108, 121, 160]. Two members of the metallothionein family of proteins, MT2 and MT3 have been shown to be protective against toxic CuAβ species in cultured neurons, and this has led to speculation that MTs could represent a potential therapeutic for the treatment of AD [159, 160]. One of the key requirements of a potential AD therapeutic is the ability to reach targets within the brain by crossing the protective blood-brain barrier and consequently the pharmacokinetics of MT has been of great interest to researchers. While MTs have demonstrated promising neuroprotective capabilities in cell culture models, recent *in vivo* work looking at subcutaneous injection of MT into mice concluded that systemic administration of MT does not result in any detectable level of MT crossing the blood-brain barrier and entering the CNS [162], and thus the therapeutic value of MT is limited.

More recently, synthetic peptides, termed emtins, have been produced that are based upon the short AA sequences of the MT2 protein. Emtins have demonstrated some capacity to act as MT-mimetics; emtins bind to the same family of receptors of MT2, promote neurite outgrowth, and improve neuronal survival (see Table 1.1). Unlike MT, there is evidence that these synthetic peptides are able to cross the blood-brain barrier. Biotinylated EmtinB peptide,

in tetrameric form, has been detected in CSF of C57BL/6J mice by western blot 30 minutes after intraperitoneal injection [184]. Given that the emtin peptides can reproduce some of the neuroprotective effects of MT, the capacity for EmtinB to cross the blood-brain barrier raises the potential therapeutic value of emtin peptides as candidate AD therapeutics. However, it is not currently known if emtins are able to protect neurons in an AD relevant model of neuronal toxicity, such as CuAβ-induced toxicity.

Of the four emtin peptides produced, EmtinB and EmtinAc are the most MT-mimetic (see Table 1.1). EmtinB and EmtinAc bind LRP receptors, improve neuronal survival and promote neurite outgrowth. This chapter will investigate the potential of EmtinB and EmtinAc tetramers and dimers (see Figure 1.7) to protect cultured hippocampal neurons from CuAβ-induced toxicity.

3.2 Methods

3.2.1 Hippocampal neuron culture

Hippocampal neurons were cultured as described in Chapter 2 with the following specific detail: 1) between 5 and 8 E17/18 Sprague-Dawley rat embryos were used per culture 2) cells were grown in 24-well plates at a cell density of $1x10^5$ cells per well, 3) cells were maintained in subsequent media for 7 days. In previous work, immortalised cells [160] and primary rat cortical neurons at 3 days *in vitro* (DIV) were utilised [159]. In this study, hippocampal neurons were treated at 7DIV. In primary neuronal cultures, synapses are just beginning to form at 3 DIV [190] and at 7DIV, neurons are more mature [190, 191]. After 7 DIV, neurons in culture begin to undergo neuronal pruning [192] and, for this reason, treating neurons after 7 DIV was avoided to prevent introducing variability from natural cell loss.

3.2.2 Treatment of hippocampal neurons with CuAβ, Emtins and MT2

Hippocampal neurons were grown to 7DIV to produce a network of neurons. Vehicle and treatments were administered on day 7 in subsequent media containing 300µM ascorbate. The redox cycling of CuAβ is catalysed by cellular reductants such as ascorbate [160]. Ascorbate was added at a final concentration of 300µM as this approximates the ascorbate concentration found in the CSF and extracellular space within the brain [160]. In experiments using CuAβ1-40 as the toxic insult, cells received media containing either 10µM CuAβ-only, or 10µM CuAβ with the addition of MT2, EmtinAc or EmtinB at a concentration of 10 or 25µM. The concentration of emtins used *in vitro* has been selected based on producing an experiment where there were equal ratios of CuAβ and EmtinB/metallothionein. EmtinB concentrations were based on previous metallothionein and CuAβ experiments where copper swap mechanism was the main mechanism of action and this worked effectively as equimolar concentrations. The concentration of Aβ was selected based on published studies [159, 160] and previous work within the lab using metallothionein as a therapeutic against CuAβ toxicity. Control cells received the ascorbate enriched media containing sterile MilliQ water vehicle. In CuAβ1-42 treated cells, cells received either media containing 25µM CuAβ or 10µM CuAβ with the addition of tetrameric EmtinB (25µM) or dimeric EmtinB (20, 25 or 100µM). After treatment, hippocampal neuron cultures were incubated at 37°C with 5% CO_2 for 24 hours, after which cell viability was assessed using alamarBlue assay. Cells were visualised by fixing cells in 4% PFA and immunostaining for tau protein. In this thesis, graphs with a single column per treatment represent a single experiment carried out in a 24-well plate using mixed neurons from 5-8 embryonic Sprague-Dawley rat pups. Graphs with multiple columns per treatment represent repeat experiments from different culture days using the same experimental design, and patterned columns denote a single experimental culture.

3.2.3 Microscopy

Photographs were taken using a 20x objective on an Olympus BX50 microscope using a Photomatrix Cool Snap HQ2 camera.

3.2.3 Statistical analysis

Analyses were carried out using GraphPad PRISM version 4 (La Jolla, CA, USA). All plates were analysed individually using One-way ANOVA with Tukey post-test.

3.3 Results

3.3.1 Tetrameric emtins attenuate CuAβ1-40 toxicity in hippocampal neurons

The capacity for tetrameric EmtinAc to protect neurons against CuAβ-induced toxicity was tested in an *in vitro* CuAβ toxicity model using 7DIV primary rat hippocampal neurons. Treatment of neurons with 10µM CuAβ1-40 alone resulted in a significant decrease in neuronal viability compared to control neurons (Figure 3.1). To determine if the synthetic peptide, EmtinAc, has any efficacy as a protective agent against CuAβ-induced cell loss, 7DIV neurons were treated with CuAβ1-40 in combination with either 10µM or 25µM EmtinAc. While 25µM EmtinAc was able to significantly protect the hippocampal neurons from the CuAβ-induced toxicity (Figure 3.1), 10µM EmtinAc was not able to attenuate CuAβ-mediated toxicity.

EmtinB tetramer was also tested in the CuAβ toxicity model using 7DIV hippocampal neurons. Consistent with results from the EmtinAc peptide, EmtinB was shown to significantly rescue cell viability at 25µM compared to treatment with CuAβ1-40 alone (Figure 3.2). Interestingly, 10µM EmtinB also improved cell viability compared with neurons treated only with CuAβ1-40 (Figure 3.2), showing protective capacity at lower concentration compared to EmtinAc. This

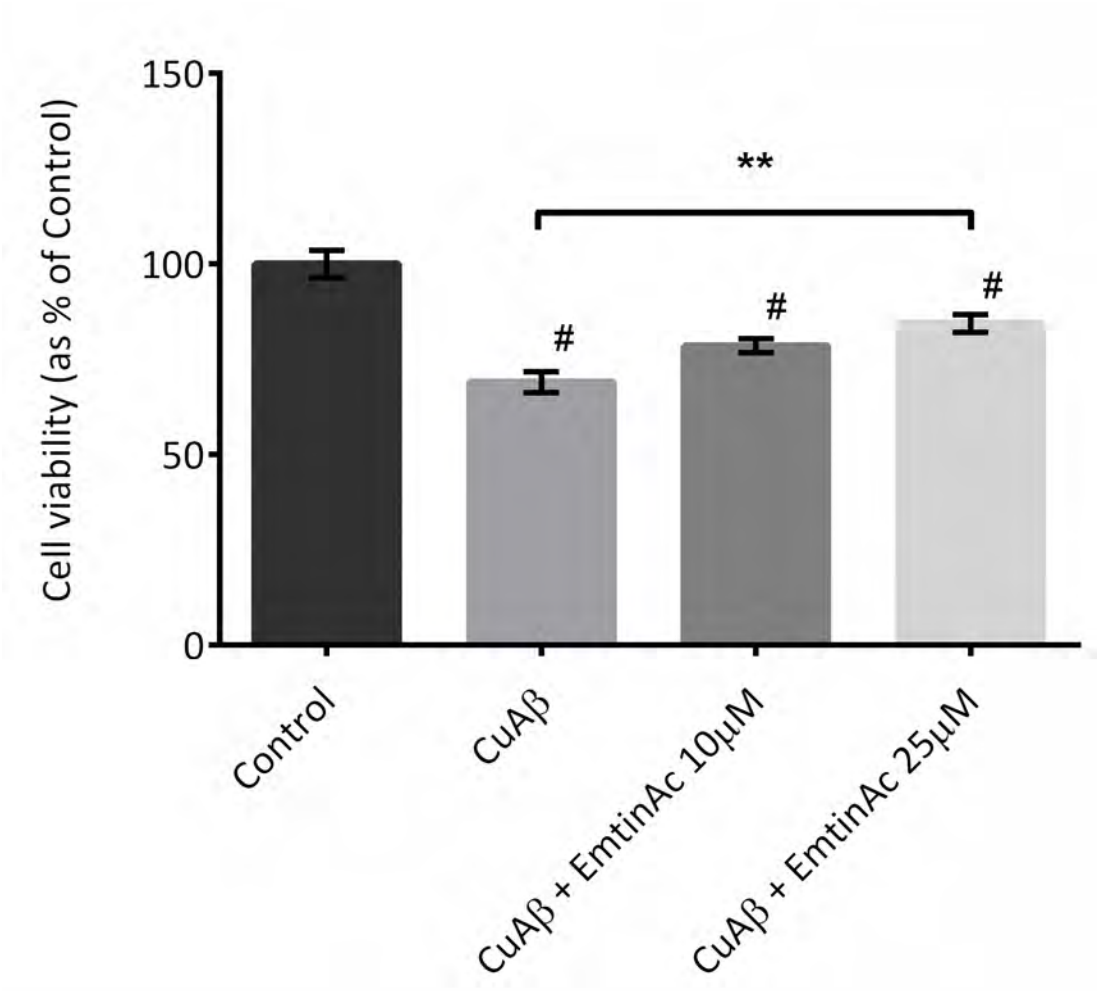

Figure 3.1 EmtinAc protects against CuAβ1-40 induced toxicity in hippocampal neurons

Addition of CuAβ1-40 at 10μM (n=6) significantly decreased the viability of cultured hippocampal neurons relative to control cells treated with MilliQ water vehicle (n=6). Tetrameric EmtinAc at 10μM (n=6) did not significantly rescue cultured hippocampal neurons from 10μM CuAβ1-40 mediated toxicity. However, EmtinAc at 25μM (n=6) did significantly rescue the viability of CuAβ1-40 treated cells. One-way ANOVA with Tukey post-test. # = significantly different to control neuron viability ($p<0.05$). ** = $p<0.01$. All data are means and SEM.

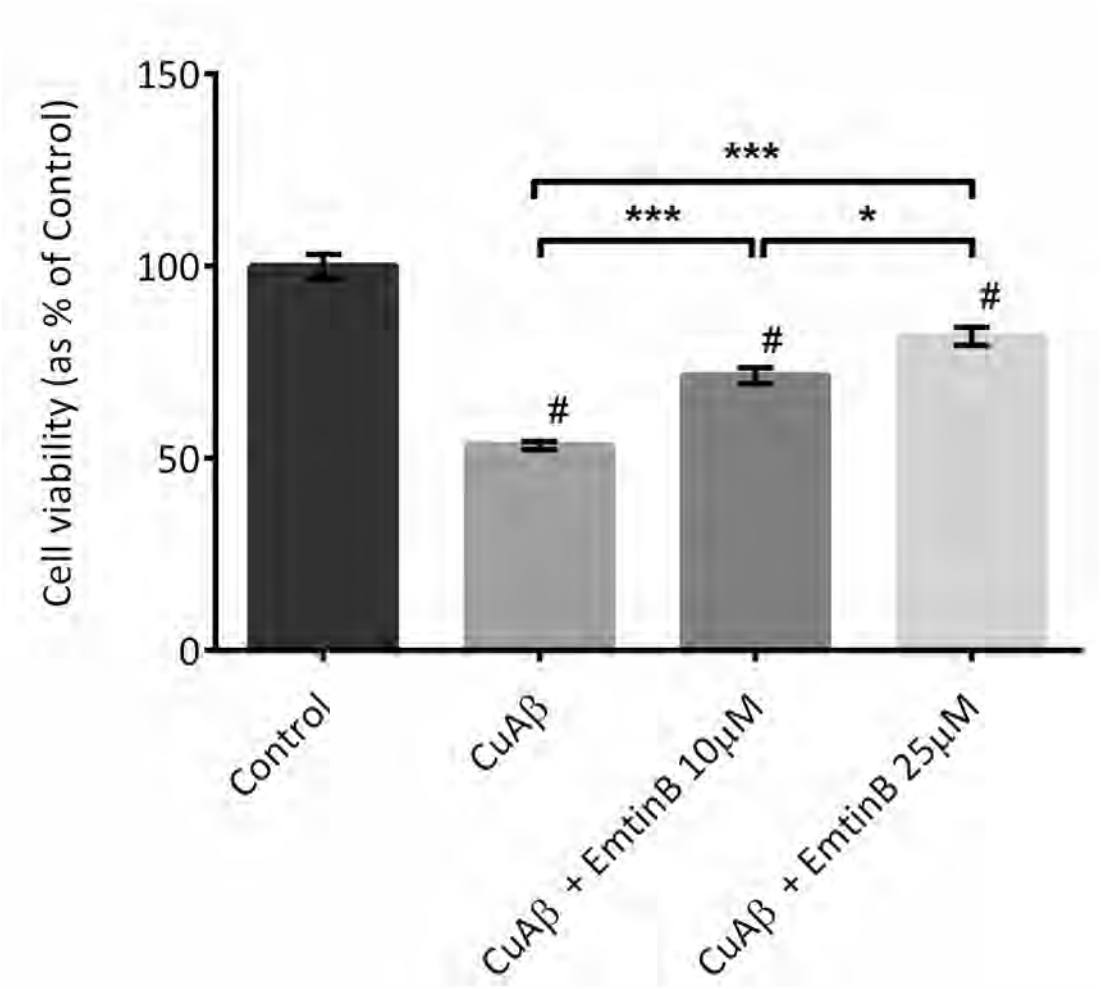

Figure 3.2 EmtinB protects against CuAβ1-40 induced toxicity in hippocampal neurons

CuAβ1-40 (10μM, n=6) significantly reduces neuronal viability of cultured hippocampal neurons compared with vehicle-treated controls (n=6). At 10μM, tetrameric EmtinB (n=6) significantly improves the viability of CuAβ1-40 treated neurons. 25μM EmtinB (n=6) also improves the viability of CuAβ1-40 treated neurons compared to CuAβ1-40 treated cells, and is more effective at improving neuronal viability of CuAβ1-40 treated cells than 10μM EmtinB. One-way ANOVA with Tukey post-test. # = significantly different to control neuron viability ($p<0.05$), * = $p<0.05$, ** = $p<0.01$, *** = $p<0.001$. All data are means and SEM.

suggests that EmtinB is more effective in the protection of neurons in the CuAβ model. Accordingly, future experiments in this thesis will focus on the capabilities of EmtinB as a potential therapeutic for AD.

3.3.2 Tetrameric EmtinB protects cultured neurons from CuAβ1-40 toxicity with the same efficacy as MT2

The potential of EmtinB to act as a therapeutic lies not only in its ability to be MT-mimetic, but also in its ability to act with similar efficacy to MT. To test the relative efficacy of EmtinB and MT2, a direct comparison of protective capacity was carried out using the CuAβ model of amyloid toxicity.

Consistent with previous experiments (see Figure 3.2), co-administration of 10μM EmtinB tetramer and 10μM CuAβ to hippocampal neurons significantly increased cell viability compared with CuAβ only treatment (Figure 3.3). Similarly, co-administration of 10μM MT2 and 10μM CuAβ produced a significant increase in cell viability compared with the CuAβ alone treatment. A comparison of MT2 and EmtinB efficacy in this experiment showed there was no statistical difference between MT2-induced increases in cell viability and EmtinB-induced increases in cell viability ($p>0.05$).

3.3.3 CuAβ1-40 and CuAβ1-42 have comparable toxicity in hippocampal neurons

Initial testing of EmtinB neuroprotective capacity (see 3.3.1 and 3.3.2) utilised the more easily obtainable Aβ1-40 at 10μM. A concentration of 10μM is relatively mild for synthetic Aβ which, in other publications [159, 160], has been used at much higher concentrations to promote toxicity. Using a higher concentration of Aβ than the 10μM currently employed would likely produce a more severe insult and have a greater impact on the viability of the neuron cultures, therefore allowing the protective capabilities of EmtinB peptides to be more rigorously tested.

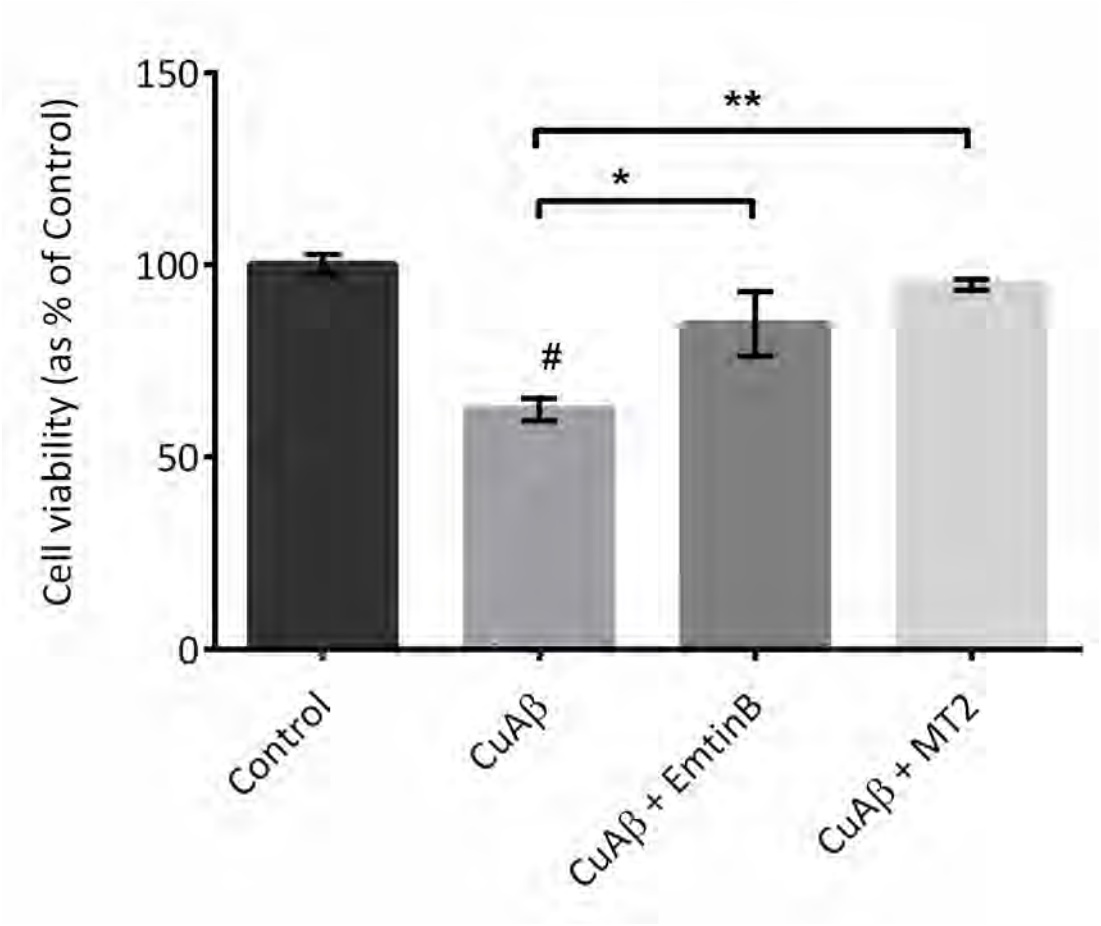

Figure 3.3 EmtinB and Zn_7MT2 protect against CuAβ1-40 toxicity with equal efficacy

Viability of hippocampal neurons was significantly decreased by treatment with 10µM CuAβ1-40 (n=4) compared with vehicle treated control neurons (n=4). Both 10µM EmtinB (n=4) and 10µM Zn_7MT2A (n=4) significantly improved the viability of CuAβ1-40 treated neurons and were equally efficacious in protecting neurons against CuAβ1-40 toxicity, with no significant difference in neuronal viability between Zn_7MT2 and tetrameric EmtinB treated cells. One-way ANOVA with Tukey post-test. # = significantly different to control neuron viability ($p<0.05$). * = $p<0.05$, ** = $p<0.01$. All data are means and SEM.

To this end, a higher concentration of CuAβ was used in further studies to achieve a more robust toxicity. Additionally, the type of Aβ used was changed from the Aβ1-40 to the Aβ1-42 fragment. This was to determine the efficacy of EmtinB against this more aggregation-prone and, reportedly, more toxic fragment. Furthermore, the Aβ1-42 fragment is a more appropriate *in vitro* Aβ investigative target for EmtinB neuroprotection studies, as future experiments will extend to animal trials using the APPswe/PS1ΔE9 mouse model of AD which overexpress the Aβ1-42 fragment. To determine an appropriate toxicity to use, and to investigate the relative toxicities of the Aβ1-40 and 1-42 fragments, a small concentration curve was constructed on 7DIV hippocampal neurons using 10, 25 and 40μM CuAβ1-40 and CuAβ1-42. In this experiment, the CuAβ1-40 and 1-42 fragments have comparable toxicity, with no statistical difference ($p>0.05$) between Aβ1-40 and Aβ1-42 at each concentration (Figure 3.4). From this experiment a concentration of 25μM CuAβ1-42 was selected for future experiments as it shows a strong toxicity, but is not sufficiently toxic to kill all of the cells.

3.3.4 TFA/TFE monomerisation of Aβ1-42 produces no toxic residues.

A unique problem encountered when using synthetically produced Aβ1-42 peptide is the notorious variability in its toxicity, a property which makes it unpredictable and limits its effectiveness as a research tool [193]. In our laboratory it has been observed that Aβ1-42 re-suspension is variable, with the Aβ1-42 suspensions varying in opacity by visual inspection. Given the aggregation-prone nature specific to the Aβ1-42 fragment, and the fact that this variability in toxicity and in clarity has not been observed in this lab when using the Aβ1-40 fragment, we deduce that the variability in Aβ1-42 toxicity is potentially caused by the peptide fragment already having aggregated prior to re-suspension. In an attempt to limit variability between experimental replicates, and to ensure a more reproducible toxic effect using the Aβ1-42 peptide fragment, each vial of Aβ1-42 peptide was thus monomerised by a process

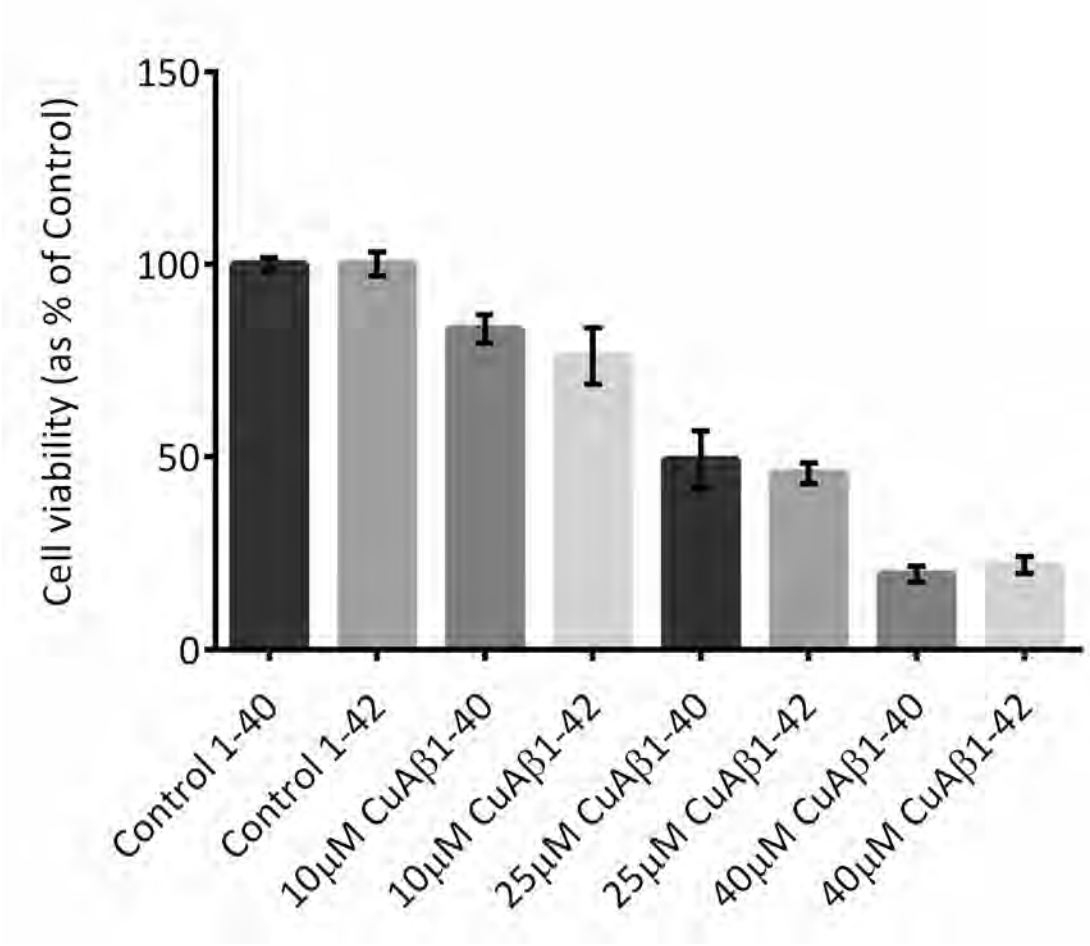

Figure 3.4 CuAβ1-40 and CuAβ1-42 have comparable toxicity in cultured hippocampal neurons

CuAβ1-40 and CuAβ1-42 were applied to hippocampal neurons at 10μM, 25μM and 40μM for 24 hours and subsequent cell viability assessed using alamarBlue assay. No significant difference in cell viability was apparent between the two peptides at any concentration investigated. One-way ANOVA with Tukey post-test. All data are means and SEM.

which uses the solvents trifluoroacetic acid (TFA) and trifluoroethanol (TFE) (see method 2.2.2). Both TFA and TFE are toxic to living organisms, thus it is essential to ensure, prior to using the peptide in cell culture, that no toxic residues remain after the monomerisation process. To confirm the absence of toxic residues, a TFA blank was prepared. The TFA blank underwent the same chemical process as monomerised Aβ, in the absence of the Aβ peptide. This TFA blank was resuspended in an identical manner to the Aβ1-42 peptide and tested for toxicity using 7DIV hippocampal neurons. TFA/TFE treatment produced no toxic side effects for cultured hippocampal neurons, with no change in cell viability for blank treated cells compared to control cells treated with sterile MilliQ vehicle (Figure 3.5), whilst the TFA/TFE monomerised CuAβ1-42 (25μM) showed a significant decrease in cell viability relative to both control and TFA/TFE blank treated neurons (Figure 3.5).

3.3.5 EmtinB dimers and tetramers have no effect on the viability of untreated primary cultured hippocampal neurons.

Prior to determining the protective effect of EmtinB peptides in the CuAβ1-42 toxicity model, it was necessary to determine if EmtinB alters the viability of neurons under basal conditions. EmtinB dimer (25-100μM) and tetramer (25μM) were administered to 7DIV hippocampal neurons for 24 hours and subsequent cell viability assessed by alamarBlue assay. Neither EmtinB dimer nor EmtinB tetramer altered the viability of the cultured neurons relative to the untreated control neurons (Figure 3.6), suggesting that the increase in cell viability observed in the CuAβ treated neurons is a protective effect against CuAβ toxicity.

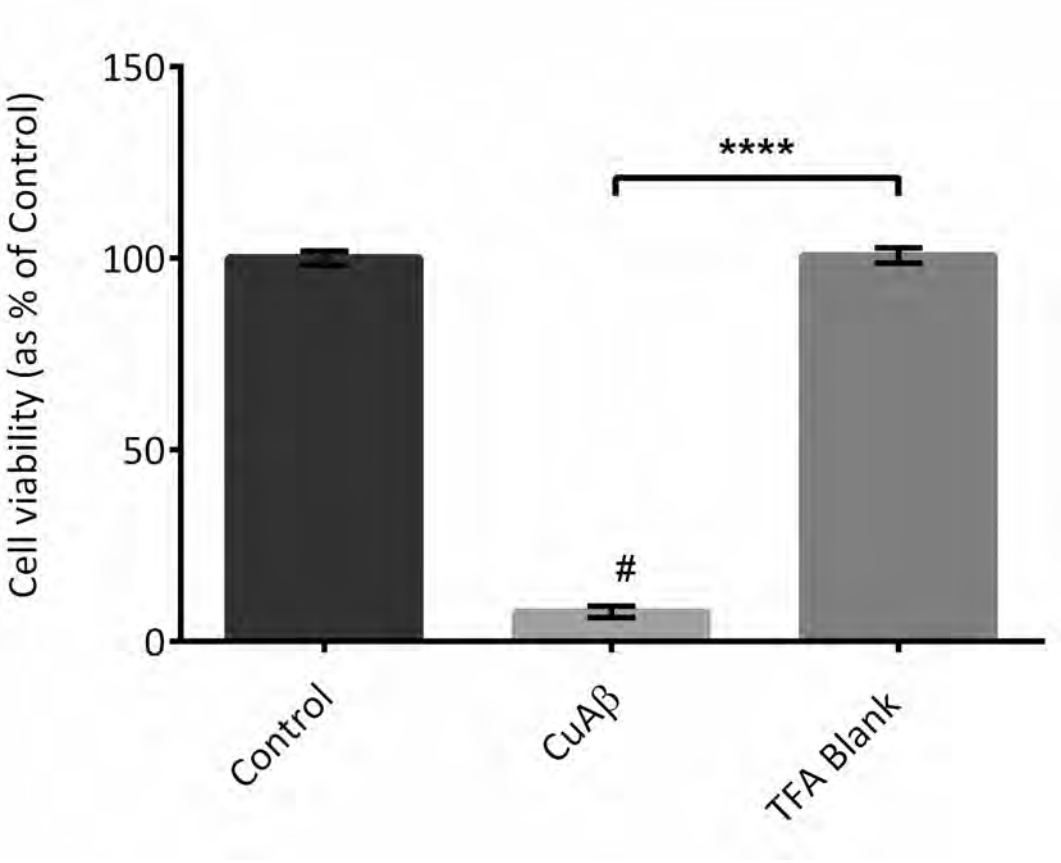

Figure 3.5 TFA monomerised CuAβ1-42, but not the TFA blank, is toxic to cultured hippocampal neurons

TFA monomerised CuAβ1-42(n=5) reconstituted in MilliQ water at 25µM induces significant neuronal cell death in 7DIV cultured hippocampal neurons compared with vehicle control neurons (n=4). The TFA Blank, prepared in the absence of Aβ and resuspended in MilliQ water, exhibits no toxicity in the cultured neurons (n=4) compared with vehicle control cells. One-way ANOVA with Tukey post-test. # = significantly different to control neuron viability ($p<0.05$), **** = $p<0.0001$. All data are means and SEM.

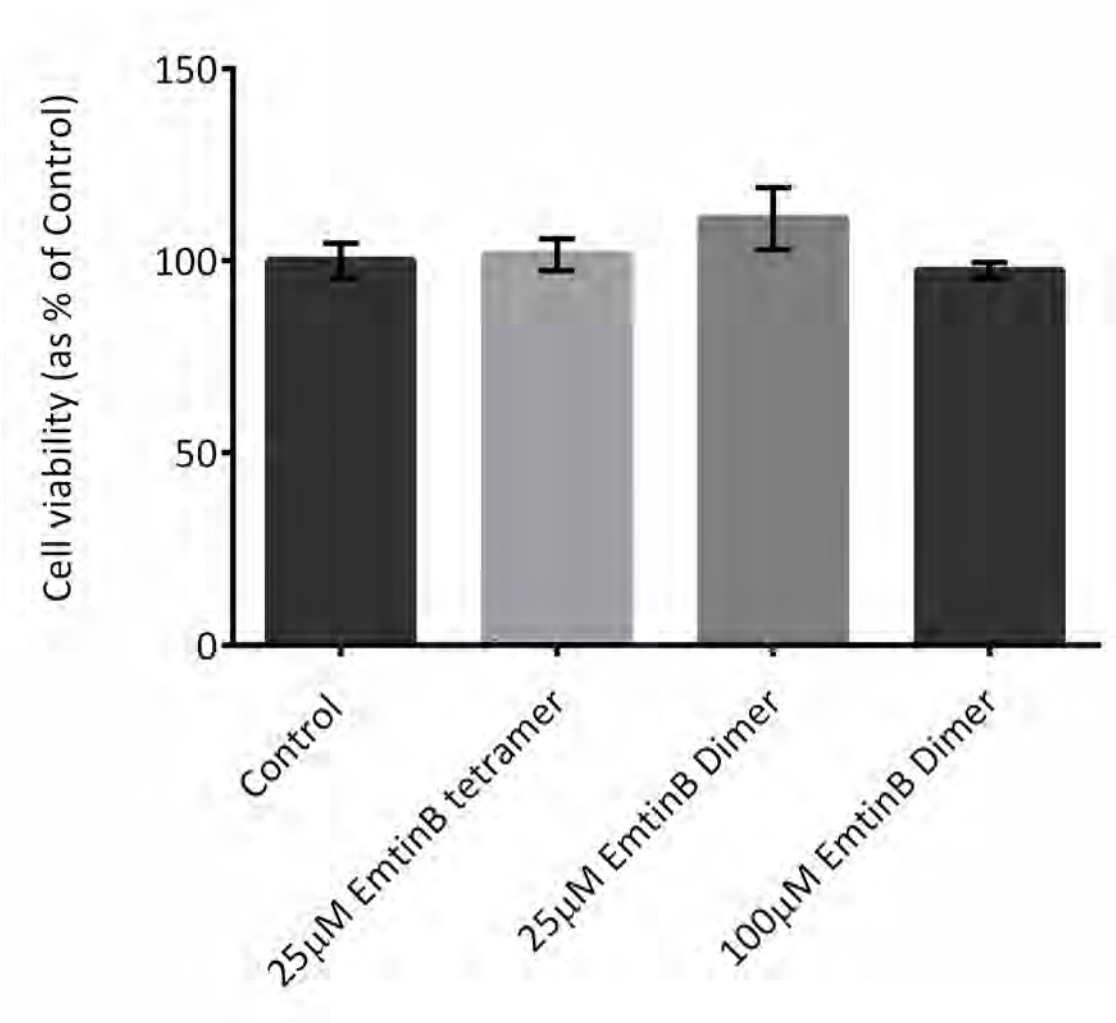

Figure 3.6 EmtinB dimers and tetramers have no effect on the viability of cells under basal conditions

EmtinB tetramer at 25µM (n= 3) had no effect on hippocampal cell viability compared with vehicle control neurons (n=3). Additionally, neither 25µM (n=4) nor 100µM (n=3) EmtinB dimer altered neuronal viability compared with control neurons. One-way ANOVA with Tukey post-test. All data are means and SEM.

3.3.6 EmtinB tetramers are protective against CuAβ1-42 toxicity in primary cultured hippocampal neurons.

The ability of EmtinB tetramer to protect hippocampal neurons against CuAβ1-42 toxicity at a 25µM concentration was investigated in three separate experiments. In all three experiments, 25µM CuAβ1-42 reduced cell viability compared to vehicle control cells (Figure 3.7). Tetrameric EmtinB significantly rescued neuronal viability of CuAβ1-42 treated neurons compared to CuAβ1-42-only treated neurons (Figure 3.7).

3.3.7 EmtinB is significantly more protective in dimeric form compared to tetrameric form

While previous studies by Ambjorn [94], Asmussen [185] and Sonn [184] have investigated the properties of the tetrameric forms of the emtin peptides, less is known about the dimeric forms of the peptide. The protective capacity of the EmtinB dimeric peptides was established in the CuAβ model of toxicity herein. In two experiments 25µM CuAβ1-42 induced toxicity significantly reduced neuronal viability of hippocampal neurons relative to vehicle control neurons (Figure 3.8). In both experiments, EmtinB dimer (25µM) completely abrogated CuAβ1-42 induced neuronal toxicity (Figure 3.8).

In a direct comparison of dimer and tetramer, EmtinB tetramer (25µM) significantly increased cell viability of CuAβ1-42 treated cells compared to CuAβ1-42-only treated neurons (Figure 3.9). EmtinB dimer was significantly more effective in protecting against CuAβ induced toxicity compared with tetramer (Figure 3.9), and subsequently only EmtinB dimer was selected for further investigation.

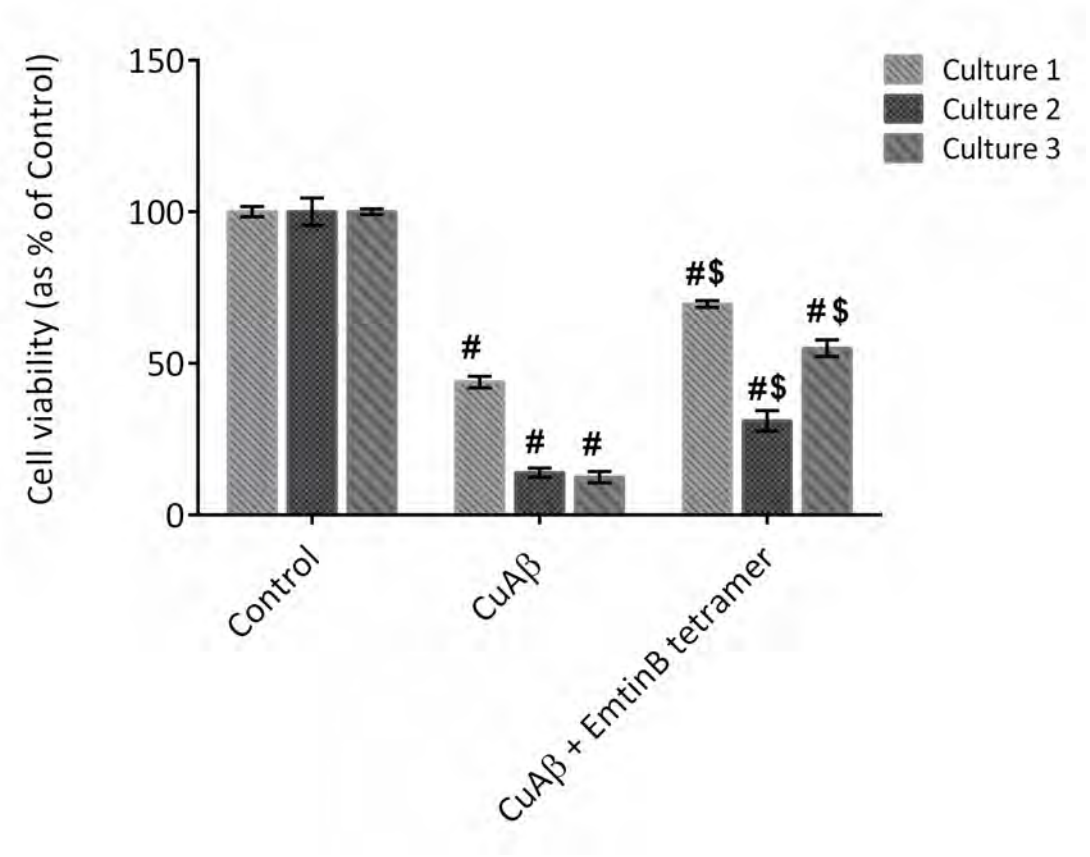

Figure 3.7 EmtinB tetramer protects hippocampal neurons against CuAβ1-42

25μM CuAβ1-42 reduced cell viability of cultured hippocampal neurons after a 24 hour treatment. Tetrameric EmtinB (25μM) improves the viability of 25μM CuAβ1-42 treated hippocampal neurons compared to CuAβ1-42 treatment alone. Each culture was analysed by one-way ANOVA with Tukey post-test. Comparisons denoted # or $ were made within cultures and no comparisons were made between cultures. # = significantly different to control neuron viability ($p<0.05$), $ significantly different from CuAβ. All data are means and SEM.

Figure 3.8 EmtinB dimer significantly protects against CuAβ toxicity in hippocampal neurons

Hippocampal neurons were treated with 25µM CuAβ alone or concurrently with 25µM EmtinB dimer for 24 hours and cell viability was assessed using alamarBlue assay. PFA fixed neurons were immunostained with tau. CuAβ treatment significantly decreased cell viability (A) and resulted in cell loss (B) compared with vehicle control cells. Dimeric EmtinB rescued cell viability (A) and prevented neuronal loss (B). Cultures were analysed by one-way ANOVA with Tukey post-test. Comparisons were made within experiments only; no comparisons were made between cultures. # = significantly different from control, $ significantly different from CuAβ ($p<0.05$). 20x magnification. Scale bar = 50µm.

A

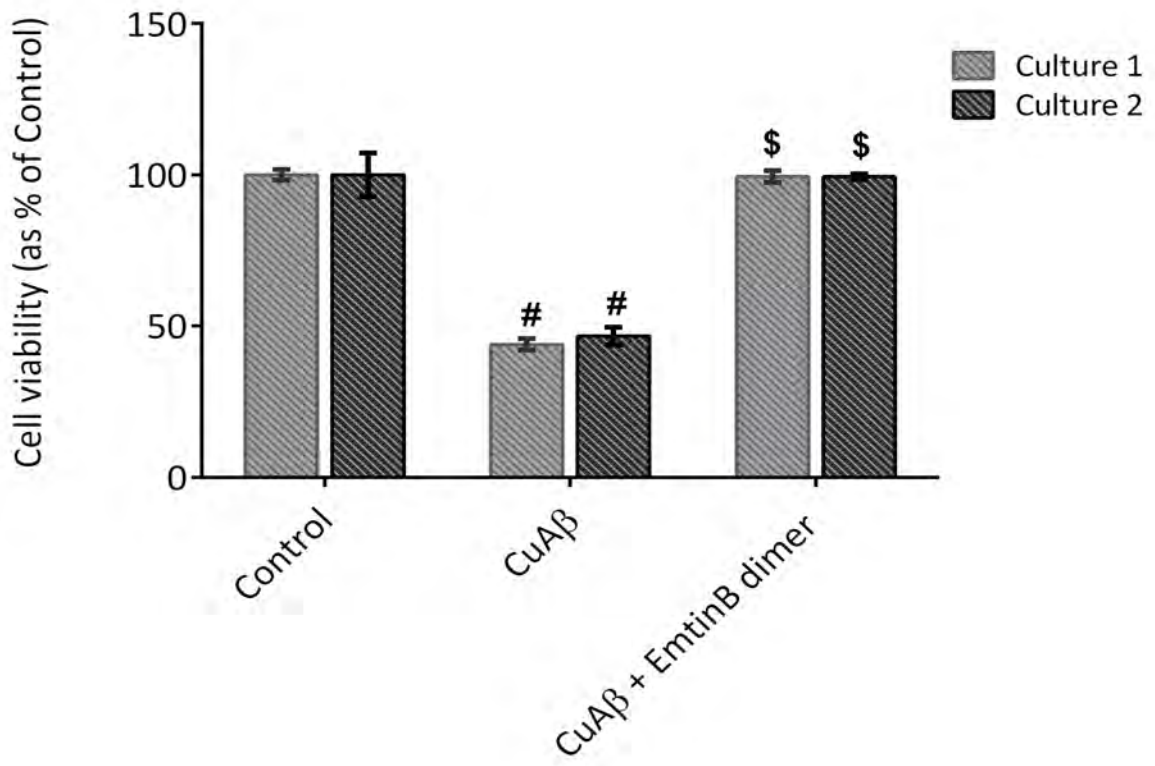
Cell viability (as % of Control)
150
100
50
0
Culture 1
Culture 2
#
#
$
$
Control
CuAβ
CuAβ + EmtinB dimer

B

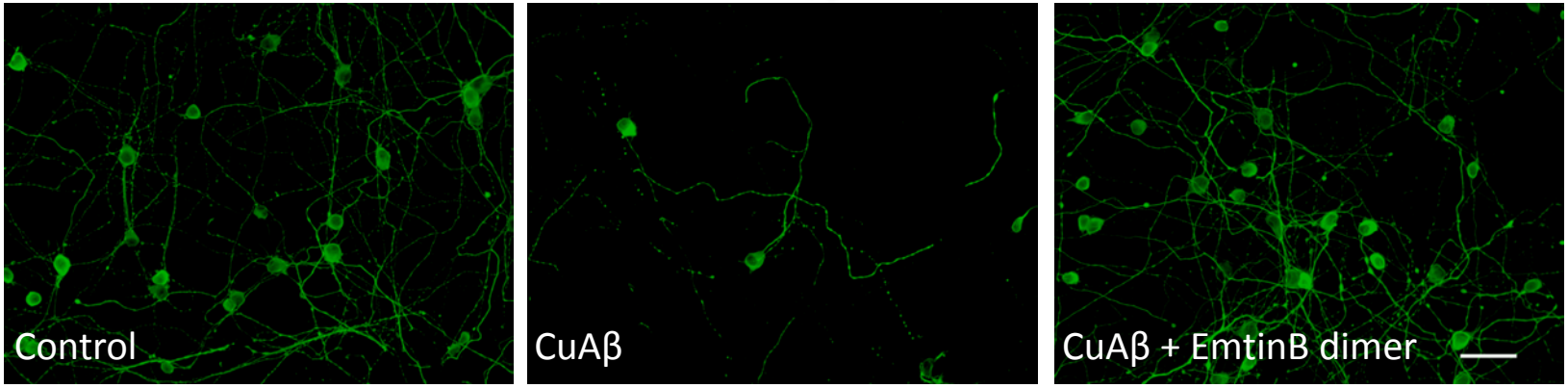
Control
CuAβ
CuAβ + EmtinB dimer

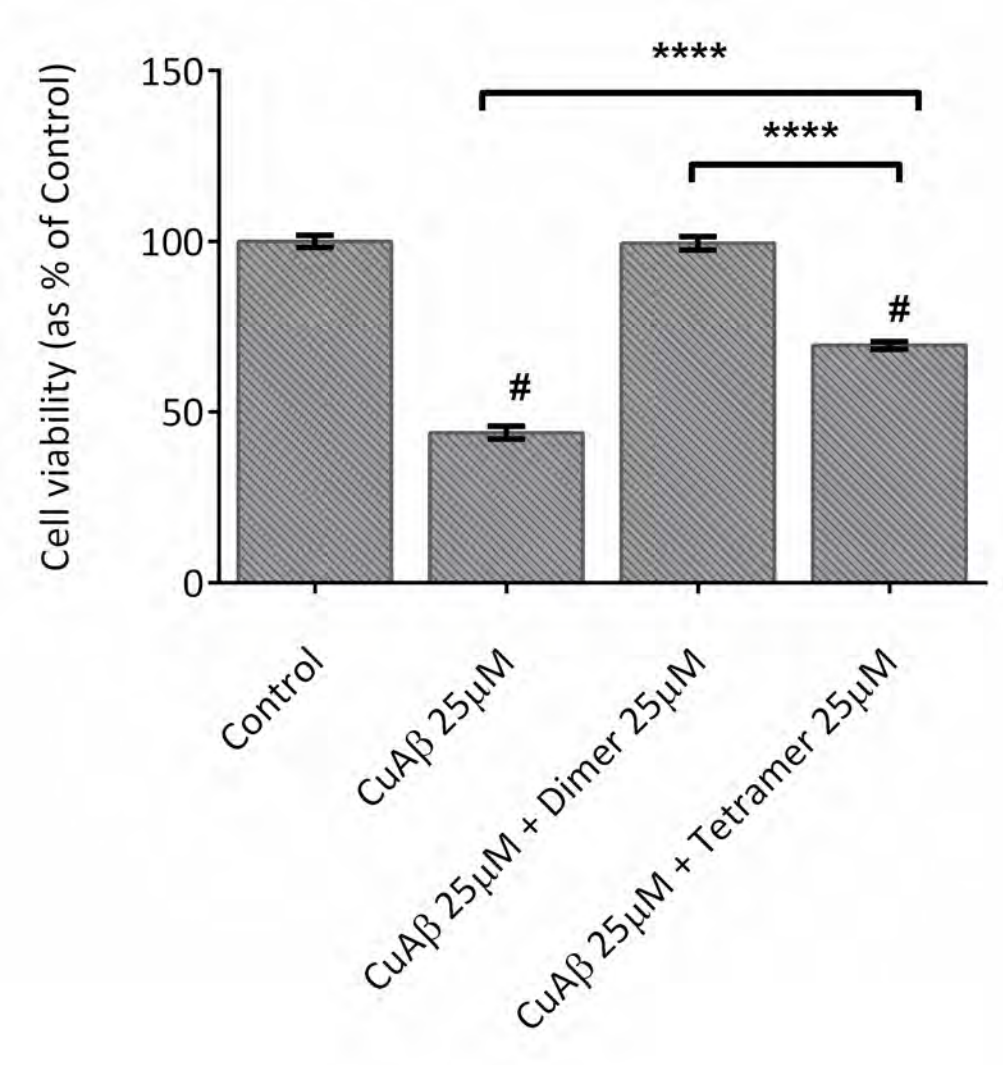

Figure 3.9 EmtinB dimer is more effective than tetramer against CuAβ1-42 toxicity in hippocampal neurons

CuAβ1-42 treatment (n=5) significantly reduces neuronal viability of hippocampal neurons compared with vehicle control neurons (n=4). Both dimeric (n=5) and tetrameric (n=5) EmtinB forms improved cell viability compared to neurons treated with CuAβ1-42 alone. Dimeric EmtinB improved cell viability significantly more than the tetrameric EmtinB. # = significantly different to control neuron viability, ($p<0.05$) **** = $p<0.0001$. One-way ANOVA with Tukey post-test. All data are means and SEM.

3.3.8 EmtinB dimer effect is concentration dependent

To determine if EmtinB dimer protection against CuAβ-mediated toxicity is concentration dependant, hippocampal neurons were treated with 25µM CuAβ1-42 or with 25µM CuAβ1-42 concurrently with EmtinB dimer (20 or 100µM).

In all experiments 25µM CuAβ1-42 reduced cell viability after 24 hours incubation on primary hippocampal neurons (Figure 3.10). At 20µM EmtinB dimer was able to significantly increase the viability of hippocampal neurons relative to 25µM CuAβ1-42 treated neurons, although the effect size was small (Figure 3.10). Addition of 100µM EmtinB with CuAβ1-42 significantly increased cell viability relative to CuAβ1-42-only treated neurons, and neurons that were treated with CuAβ1-42 and 20µM EmtinB (Figure 3.10).

3.3.9 High EmtinB concentrations are less effective at protecting cultured neurons from CuAβ1-42 toxicity

To determine an optimal dosing concentration for EmtinB dimer, a concentration curve was constructed using EmtinB dimer at 25, 75 and 125µM on 7DIV hippocampal neurons.

CuAβ1-42 (25µM) significantly reduced neuronal viability as measured by alamarBlue assay. Addition of 25µM and 75µM EmtinB significantly improved neuronal viability relative to CuAβ1-42 treated cells compared with CuAβ1-42-only treated neurons (Figure 3.11). At these concentrations, neurons were restored to full viability as compared to vehicle control neurons. 125µM EmtinB also significantly improved cell viability relative to CuAβ1-42-only treated cells; however, unlike 25µM and 75µM EmtinB dimer, cells treated with 125µM EmtinB did have significantly lower viability compared with control cells (Figure 3.11).

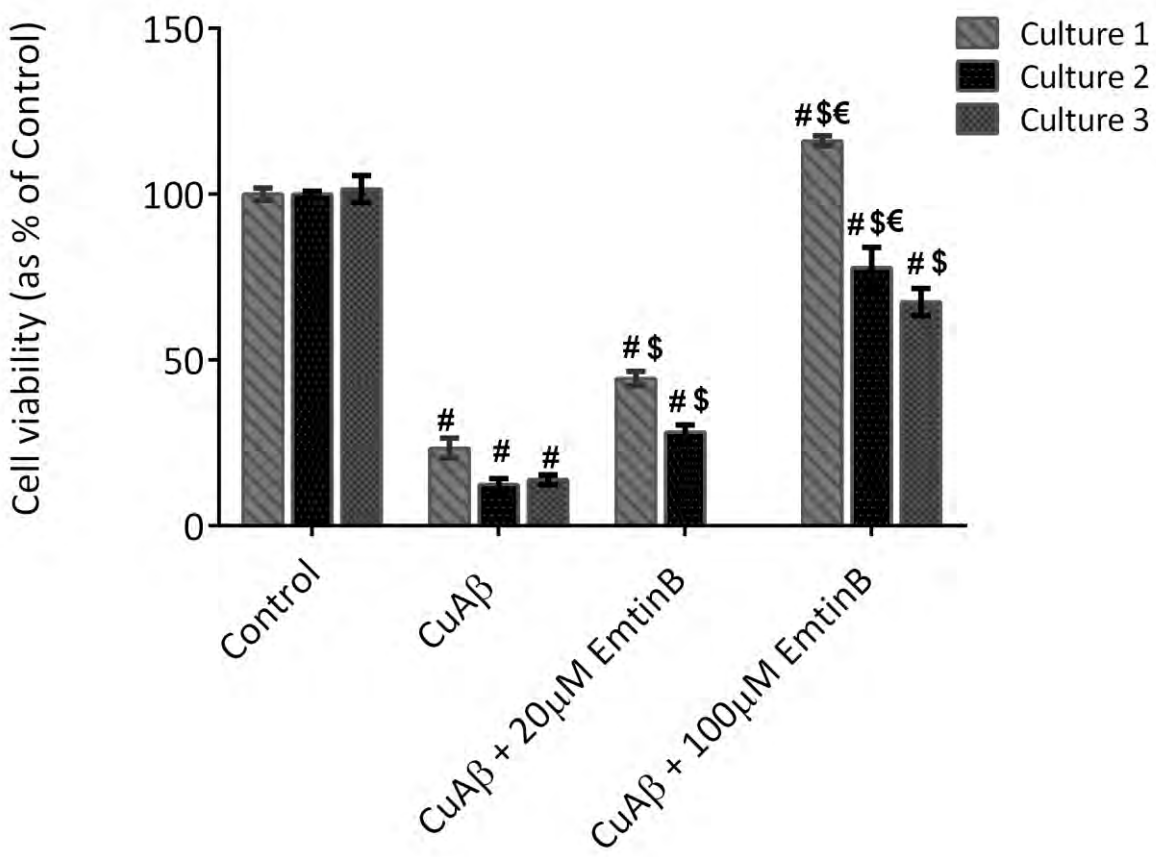

Figure 3.10 EmtinB protection against CuAβ1-42 toxicity is concentration dependent

Hippocampal neurons were treated with either 25μM CuAβ1-42 or 25μM CuAβ1-42 simultaneously with EmtinB dimer (20 or 100μM, as denoted). CuAβ1-42 significantly reduced cell viability compared to vehicle control cells. 20μM EmtinB dimer significantly improved neuronal viability of CuAβ1-42 treated cells, as did treatment with 100μM EmtinB dimer. 100μM dimeric EmtinB treatment was significantly more efficient at improving neuronal viability compared with 20μM dimeric EmtinB. One-way ANOVA with Tukey post-test. #significantly different to control neuron viability, $ significantly different to CuAβ, € significantly different to 20μM EmtinB treatment ($p<0.05$). All data are means and SEM.

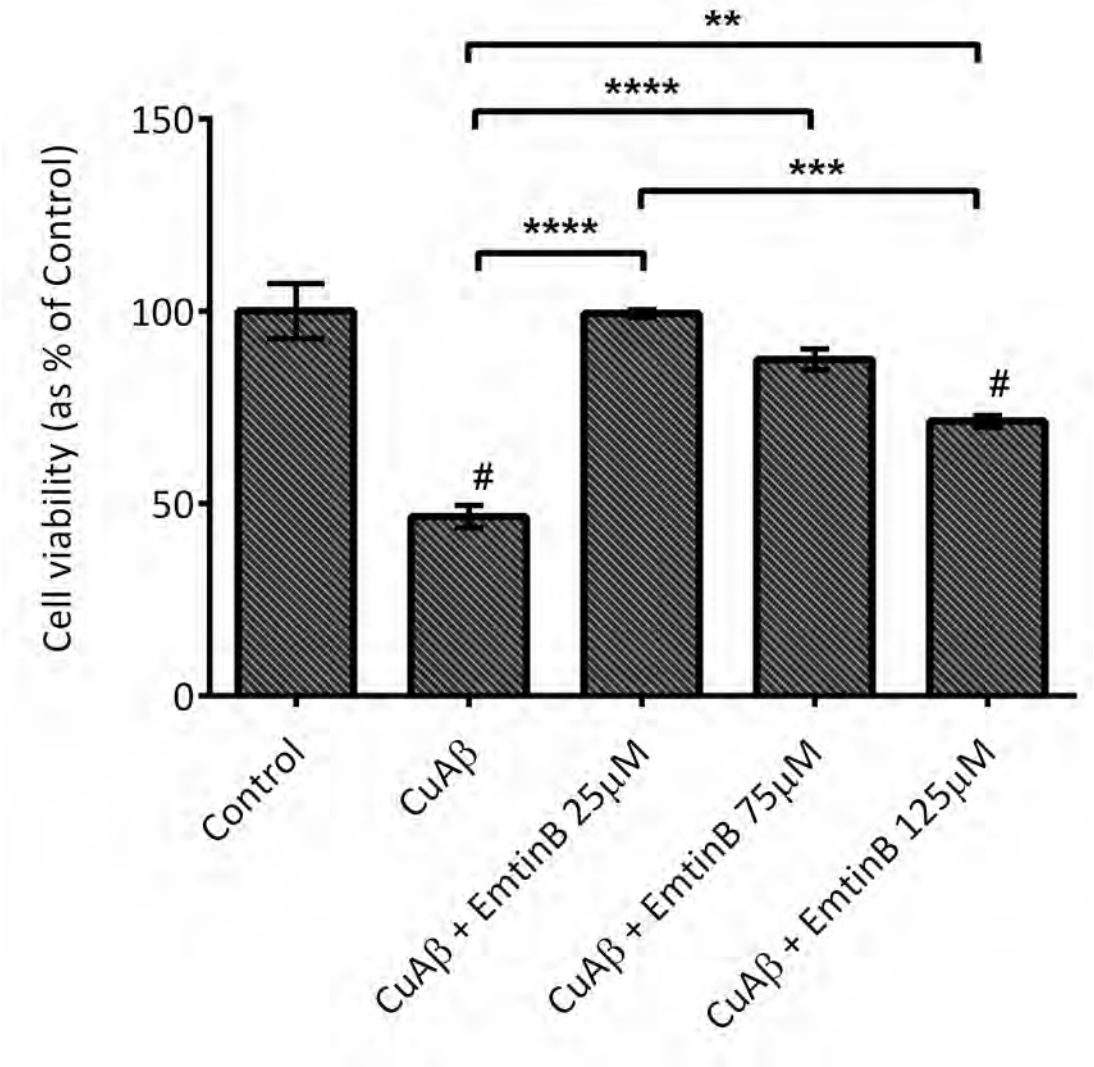

Figure 3.11 EmtinB protection against CuAβ1-42 toxicity is reduced at high EmtinB concentration

CuAβ1-42 (n=4) significantly reduced neuronal viability compared with vehicle treated control cells (n=4). EmtinB dimer fully protected hippocampal neurons for CuAβ toxicity at 25μM (n=4) and 75μM (n=4). While EmtinB at 125μM (n=4) was able to protect cultured neurons from CuAβ1-42toxicity, 125μM EmtinB was significantly less protective than 25μM EmtinB. One-way ANOVA with Tukey post-test. #significantly different to control neuron viability ($p<0.05$), ** = $p<0.01$, *** = $p<0.01$, **** = $p<0.0001$. All data are means and SEM.

3.3.10 EmtinB dimer is only effective when added concurrently with CuAβ1-42

As with any potential therapeutic for the treatment of neurodegenerative diseases, intervention at the earliest possible stage is desirable. This allows for prevention of damage to fragile neurons, which are not able to be regenerated after insult. To determine if EmtinB can be used as a pre-treatment to protect neurons against CuAβ toxicity, 7DIV primary cultured hippocampal neurons were pre-treated with 25μM EmtinB for either one day or one hour (as specified) prior to administration of CuAβ1-42 (Figure 3.12). Neither one hour nor one day pre-treatment with EmtinB produced an increase in cell viability relative to CuAβ1-42-only treated cells. EmtinB added concurrently with CuAβ1-42 was able to improve cell viability, suggesting that whatever mechanism EmtinB is acting through, it requires EmtinB to be present at the time of insult.

3.4 Discussion and conclusions

Previous work by Meloni [160] and Chung [159] has established the protective capacity of MT3 and MT2, respectively, in the CuAβ model of neurotoxicity. This chapter sought to determine which, if any, of the emtin peptides demonstrate a similar capacity to protect neurons against CuAβ-mediated toxicity. Both EmtinB and EmtinAc were found to protect cultured neurons against CuAβ, with EmtinB tetramer the more efficacious of the two peptides studied. MT2 and EmtinB tetramer had comparable efficacy against CuAβ, while EmtinB dimer was robustly more effective at protecting against CuAβ than EmtinB tetramer. EmtinB dimer appears concentration dependent, with higher concentrations improving cell viability to a greater extent than lower concentrations, however this trend was only observed at concentrations less than 100μM, with higher concentration EmtinB showing reduced efficacy. Notably, EmtinB was only effective against CuAβ toxicity when administered at the same time as the CuAβ. Pre-

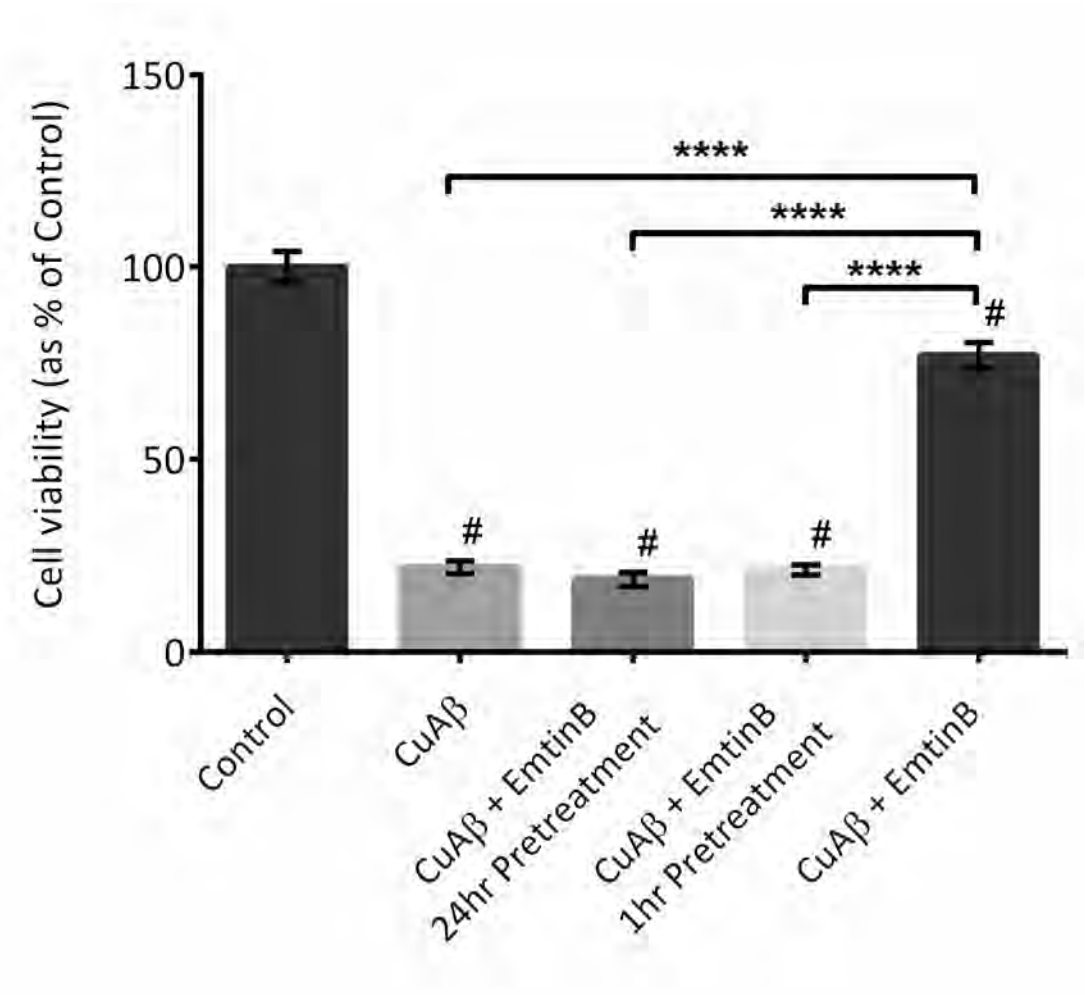

Figure 3.12 EmtinB is protective against CuAβ1-42 toxicity only when it is administered concurrently

Hippocampal neurons treated with 25µM CuAβ1-42 (n=5) had significantly lower cell viability after 24 hours treatment compared with vehicle treated control cells (n=4). The cell viability of CuAβ1-42 treated neurons was significantly improved by 25µM dimeric EmtinB (n=5) when added simultaneously with CuAβ1-42 but EmtinB did significantly improve neuronal viability when added 1 day prior to CuAβ1-42 (n=5) or 1 hour prior to CuAβ (n=5). Each culture was analysed by one-way ANOVA with Tukey post-test. # = significantly different to control neuron viability ($p<0.05$). **** = $p<0.0001$. All data are means and SEM.

treatment of hippocampal neurons with EmtinB prior to CuAβ administration has no effect on CuAβ toxicity.

3.4.1 The EmtinB/CuAβ model

A comparison of CuAβ1-40 and CuAβ1-42 showed that there was little difference in the toxicity of the two copper-bound peptides and, as such, both CuAβ1-40 and CuAβ1-42 were utilised in this work. The Aβ1-42 peptide is difficult to prepare [194] and has variable toxicity [193, 195]. In an attempt mitigate the variability exhibited by synthetic Aβ1-42, each batch of peptide was monomerised before use, using TFA/TFE monomerisation. To ensure that these chemicals left no toxic residue after monomerisation, TFA/TFE blanks were tested on hippocampal neuron cultures, showing that the toxicity that arises from the addition of the CuAβ is generated exclusively by the CuAβ. Thus, the effect of the emtin peptides results fully from an effect against CuAβ-mediated toxicity.

To demonstrate that the increase in cell viability produced by EmtinB in CuAβ treated neurons is a result of neuroprotection and not a stimulation of cell metabolism, the effect of EmtinB on cell viability under basal conditions (unstressed cells) was investigated. Addition of EmtinB tetramer (25µM) or dimer (25-100µM) had no effect on hippocampal cell viability, indicating that improvement in viability on addition of EmtinB is a direct effect of neuroprotection against CuAβ toxicity. The observation that EmtinB has no effect on the function of cells under basal conditions but is beneficial under stress is reminiscent of MT action. MT appears non-essential for normal growth and reproduction, as exemplified by the normal function of cells and organisms that lack MT [30, 31], but confers an advantage under conditions of stress such as oxidative stress or metal toxicity [4, 52, 53].

3.4.2 Comparison of emtin efficacies

Both EmtinB tetramer and EmtinAc tetramer demonstrated a capacity to protect against CuAβ-induced toxicity in cultured hippocampal neurons. Tetrameric EmtinB was able to protect hippocampal neurons against CuAβ at lower concentration than EmtinAc, suggesting that the EmtinB peptide is the more effective peptide in this context. Interestingly, the protective capacity of tetrameric EmtinB was similar to the protective capacity of MT2.

Previous emtin studies by Ambjorn [79], Asmussen [185] and Sonn [184] have utilised the tetrameric form of EmtinB, most likely because evidence from previous studies, using other peptides, has shown that tetramers have a higher affinity for the target protein than trimeric, dimeric or monomeric peptide assemblies [196, 197]. In this experimental work, the EmtinB dimer shows a much greater capacity than the tetramer to protect neurons against CuAβ-mediated toxicity.

It is unclear why EmtinB is more efficacious than EmtinAc, or why dimeric EmtinB is more efficacious than tetrameric EmtinB. One possibility is that the efficacy of these peptides relates to the aggregate state of the peptide; some peptides may have a higher propensity to aggregate than others. For example, EmtinAc may have a greater propensity than EmtinB to aggregate under experimental conditions and, similarly, the tetrameric form may be more likely to aggregate than the dimer, with aggregation rendering the peptide unable to carry out the function required. In fact, we have observed in the process of this study that EmtinB dimer does self-aggregate into higher MW SDS-resistant forms under freeze-thaw conditions (data not shown). If or how aggregation affects the capacity of emtins to act in its neuroprotective role remains to be determined.

More likely, the reason behind the difference in peptide efficacy is linked to emtin mechanism of action. There are three main candidates for emtin mechanism of action; based upon the capabilities of the parent protein MT2 (discussed in Chapter 1), emtins could potentially be

involved in free radical scavenging, Cu/Zn metal swap, or activating signalling cascades *via* LRP receptors.

Previous investigation into MT protection against CuAβ-mediated toxicity showed that MTs can perform a metal swap with CuAβ to prevent toxic ROS production [159, 160]. It is possible that the EmtinB peptide acts in a similar manner, by removal and redox silencing of the copper from CuAβ. While it is currently unknown what, if any, binding capacity EmtinB has for either zinc or copper, given that the emtin sequences have been altered to remove some cysteine residues, it is possible that EmtinB no longer has the capacity to bind metals, or has altered metal binding properties. The metal binding capabilities of the EmtinB peptide will be investigated in Chapter 4.

MT2 has also demonstrated strong free radical scavenging capabilities. The capacity of MT2 to scavenge free-radicals is a result of the high cysteine content of the protein. MT2 was unable to protect against H_2O_2 toxicity when tested in cultured cortical neurons, suggesting that in the CuAβ model of toxicity, MT2 action is not *via* scavenging of ROS. Additionally, as many cysteine residues are substituted for serine in the emtin peptides, it is unlikely that EmtinB is acting as a free radical scavenger in this model. To confirm this, the capacity of EmtinB to protect against H_2O_2 toxicity will be further explored in Chapter 4.

MT2 has also been shown to interact with the LRP family of receptors, resulting in signal transduction through MAPK signalling pathways. In accordance with this, work by Ambjorn et al. [94] suggests that EmtinB's neuroprotective activity is mediated through LRP receptors *via* a sequence specific motif. However, in a scenario involving signal transduction and activation of neuroprotective pathways, it would be expected that pre-treatment of cells with emtin might be protective against CuAβ yet neither pre-treatment of one day nor one hour prevented CuAβ toxicity (see Figure 3.12). Interestingly, Aβ is also believed to be a ligand for LRP-receptors. Hence, it is possible that MT/emtin may interfere with Aβ-LRP interactions; this

too will be explored in Chapter 4, through the use of molecular approaches that interfere with LRP receptors.

Regardless of what mechanism emtins work through, it is clear that the EmtinB peptide is better able to protect cultured hippocampal neurons than EmtinAc, and in turn that dimeric EmtinB is more efficacious than tetrameric EmtinB. While it would be informative to explore these differences further, restriction on time and resources required further investigations to focus on only one of these peptides; EmtinB dimer had greatest efficacy and the EmtinB tetramer has reported BBB penetrance, thus dimeric EmtinB was selected for further investigation.

3.4.3 Concentration determination

Investigations using low (20µM) and high (100µM) dimeric EmtinB concentrations showed that EmtinB is concentration dependent, with high concentration EmtinB improving the viability of CuAβ1-42-treated cells to 100% of non-insulted control. To further clarify the effective concentration range, EmtinB effect on CuAβ toxicity was investigated across a 25-125µM range. Once again, EmtinB improved the viability of CuAβ1-42-treated cells in concentration-dependent manner until 100% of control viability was reached. These data suggest that full protection against CuAβ1-42 can be achieved within a concentration range of 25-100µM. Interestingly, at concentrations above 100µM, the ability of EmtinB to protect cells from CuAβ1-42 appeared to be reduced, with CuAβ1-42 treated cells showing lower viability in the presence of high concentrations of EmtinB compared with concentrations within the 25-50µM range. Although the data requires repetition for a robust analysis, it suggests that at high concentration either EmtinB cannot carry out its required function, or that the EmtinB itself has a direct negative effect on the hippocampal neurons.

It is possible that, at 125µM, the concentration of emtin peptide overwhelms the ubiquitin proteasome system (UPS)/autophagy system of the neurons. Overwhelmingly high peptide

concentration within a cell causes compromised proteasome activity, which has been shown to result in neurodegeneration [198].

Additionally, while smaller MW synthetic peptides have been shown to be less cytotoxic than larger MW synthetic peptides, as previously discussed, EmtinB appears to be able to aggregate under some conditions. Theoretically, then, if the EmtinB is aggregating at high concentration, this may be creating high MW peptide aggregates and thus promotes toxicity.

Any cytotoxicity of the dendrimers could also potentially be explained by the interactions between negatively charged cell membranes and the positively charged dendrimer surface, which enables dendrimers to adhere to and damage the cell membrane, causing cell lysis [166]. While the net charge of EmtinB has not been tested experimentally, the estimated net charge of the EmtinB dimer at pH7 is +4.7, using a peptide property calculator, and thus cationic toxicity is possible.

Alternatively, EmtinB may not be negatively affecting cells, but rather may just be exhibiting reduced efficacy at high concentration. Drugs often exhibit a sigmoidal dose-response curve [199]. A dose response curve is the relationship between drug dose and biological response to that treatment. With a sigmoidal dose response, the dose curve is S-shaped, where low drug concentration elicits a very small response, a range of intermediate concentrations promotes responses that form the linear part of the s-curve and a maximal response and plateau is achieved at high concentration [199]. Some molecules, however, exhibit a bell-shaped concentration-response curve, rather than the traditional sigmoidal dose-curve. Recent work by Owen et al. [199] examined the dose response curves of three anti-cancer drugs which are known to aggregate and form colloids. These three drugs produced traditional sigmoidal dose-response curves when maintained in their monomeric state, however when allowed to generate colloids all three drugs produced bell-shaped dose-response curves [199]. The authors postulate that the formation of colloids prevents the passage of the drug across the

cell membrane, thus preventing its action [199]. While this represents a possible explanation for the suspected lower activity of EmtinB at high concentration, the data available does not allow for a definitive description of the EmtinB dimer concentration-response curve and further investigation is required to elucidate these hypotheses.

Thus taken together, the data suggest that high concentrations of EmtinB could potentially be detrimental to hippocampal neurons and that, *in vitro* at least, concentrations between 25µM and 100µM offer an optimal effect.

3.4.4 Conclusion

This work has validated that EmtinB and EmtinAc are neuroprotective against CuAβ, and that the EmtinB dimer is a suitable candidate for further *in vitro* investigation. The mechanism of its protection, in comparison to the known effects of native MT2, will be explored in Chapter 4. Furthermore, as EmtinB has been reported to readily cross the BBB (while native MT2 does not) Chapter 5 will evaluate the neuroprotective potential of EmtinB in APPswe/PS1ΔE9 mice.

Chapter 4 – EmtinB mechanism of neuroprotection against copper-Aβ

4.1 Introduction

As demonstrated in Chapter 3, the investigated MT-based, synthetic emtin peptides protect cultured hippocampal neurons from toxicity induced by CuAβ1-40 and CuAβ1-42. This chapter will explore the potential mechanisms by which emtins might be exerting their protective effect.

Aβ toxicity has been shown to be mediated by H_2O_2 in culture [108]. While the mechanism of H_2O_2 generation was unspecified in the work by Behl [108], there is mounting evidence that redox active metals, such as iron and copper, can interact with Aβ peptides to produce H_2O_2. CuAβ has been shown to generate H_2O_2 in cell-free preparations [121, 200], and the toxic effect of CuAβ in cell culture is blocked by catalase, an enzyme that breaks down H_2O_2 [121]. More recently, Meloni et al. [160] found that CuAβ exerts its neurotoxic effect through the production of ROS. These data suggest that one mechanism of CuAβ toxicity is through the production of H_2O_2 and subsequent free radical production.

As discussed in Chapter 1, MT2 exhibits number of properties which could protect neurons against CuAβ neurotoxicity. For example, MT2 has been shown under various circumstances to protect against free radicals produced in the Fenton reaction [59], act through LRP receptors to activate anti-apoptotic pathways, and to undergo a metal swap with CuAβ to prevent CuAβ toxicity. On this basis, given that EmtinB is MT2 mimetic, it could also act through any of these mechanisms to achieve neuroprotection against CuAβ toxicity in cultured hippocampal neurons.

This chapter will explore the potential of EmtinB to:

1. Participate in a metal swap with CuAβ,

2. Protect against H_2O_2-induced toxicity, and

3. Act through LRP receptors to mediate neuronal protection.

4.2 Methods

4.2.1. Metal binding and metal swap methods

4.2.1.1 ICP-MS analysis of zinc and copper associated with dimeric EmtinB

For analysis, 1mL samples in PBS were diluted 10x in ultrapure water (>18MOhm) with nitric acid and indium (as internal standard) added to a final concentration of 1% and 100ppb, respectively. Standards were prepared using 10% PBS in ultrapure water (>18MOhm) with nitric acid and indium as per the sample preparation. Raw data was blank-subtracted and dilution-factor adjusted before analysis.

Samples were prepared and then analysed using an Element 2™ ICP-MS and raw data compiled by Dr Ashley Townsend (Deputy Director of the Central Science Laboratory (CSL) Sandy Bay campus, University of Tasmania).

4.2.1.2 Zinc and copper binding by dimeric EmtinB

To determine if EmtinB dimer has any intrinsic copper or zinc bound to it after synthesis, a 1mg/mL solution of EmtinB dimer in PBS was analysed *via* ICP-MS.

To produce the copper and zinc solutions for this experiment, saturated solutions of $CuCl_2$ and $ZnCl_2$ were prepared in PBS at an estimated concentration of 670mM to add to EmtinB. To

determine the actual concentration of metals added to the EmtinB dimer, samples were prepared by adding the same volume of saturated solution to PBS alone. ICP-MS analysis of these samples empirically confirmed the concentration of Cu and Zn added to EmtinB was 640.6µM and 662.76µM, respectively.

To determine the capacity of EmtinB to bind to copper and zinc, 1mg/mL (335µM) EmtinB was incubated in the presence of $CuCl_2$ or $ZnCl_2$ at an approximate protein to metal ratio of 1:2. A 1mL reaction mixture containing 100µL of EmtinB dimer stock (10mg/mL in PBS), 10µL of saturated $CuCl_2$ or $ZnCl_2$, and 990µL of sterile PBS was prepared. The reaction mixture was incubated at room temperature for 30 minutes to allow binding of metals to the EmtinB dimer. Unbound metals were removed from the EmtinB/metal mixtures using PD-10 columns (GE Healthcare, UK). Control columns containing copper or zinc but no EmtinB were also prepared and passed through a PD-10 column.

Protein content of collected fractions was determined by BCA assay and visualised using SDS-PAGE and subsequent Coomassie stain, while copper and zinc content was determined by ICP-MS.

4.2.1.3 Free metal separation by PD-10 column

PD-10 columns were used as per manufacturer instructions. In brief, columns were equilibrated using 30mL of PBS before applying the samples (1mL). As the required sample volume for these columns is 2.5mL, after the 1mL of sample entered the column, a further 1.5mL of PBS was added to the column. All flow through for this step was discarded. The samples were then eluted from the column in ten 1mL fractions, which were collected in pre-chilled Eppendorf tubes. The sample-containing Eppendorf tubes were returned to ice immediately after sample collection.

4.2.1.4 Visualisation of protein in column fractions using SDS-PAGE and Coomassie stain

To visualise protein content in the collected column fractions, 10µL of each fraction was mixed with 2.5µL of NuPAGE LDS sample buffer (Invitrogen, Thermofisher scientific, MA, USA) and 1µL of NuPAGE reducing agent (Invitrogen, Thermofisher scientific, MA, USA) and heated to 80°C for 10 minutes before running on a NuPAGE 4-12% bis-tris gradient gel (Invitrogen, Thermofisher scientific, MA, USA).

Gels were stained overnight in Coomassie brilliant blue and then destained in Coomassie destain solution until protein bands were clear (after around 6 hours).

Stained gels were imaged using a Carestream image station 4000MM Pro (Carestream Molecular imaging, CT, USA) using Carestream MI SE software (v4.5.2).

4.2.1.5 EmtinB in the aggregation assay

The ability of EmtinB to participate in a metal swap with CuAβ1-42 was investigated using an aggregation assay developed by Meloni et al. [160]. For this aggregation, 25µM Aβ1-42 was incubated with 25µM $CuCl_2$ (in tris buffer) and 300µM ascorbate in the presence of Apo-EmtinB, Cu-EmtinB, Zn-EmtinB. Control samples were prepared with copper chloride, ascorbate, Aβ1-42 and PBS vehicle. All samples were 100µL reaction volumes and were incubated at 37°C for 72 hours at 300rpm shaking.

Samples were made to 1.9mL with tris buffer and balanced in pairs to 0.000g before centrifuging at 21,000G in a Sorvall ultracentrifuge (Thermofisher scientific, MA, USA) in a 70.1 TI rotor for one hour at 4°C. After centrifugation, the supernatant was discarded and the remaining pellets were resuspended in 20µL of NuPAGE LDS sample buffer (Invitrogen, Thermofisher scientific, MA, USA) containing 10% NuPAGE reducing agent (Invitrogen, Thermofisher scientific, MA, USA).

Samples were heated at 80°C for ten minutes, and then run on a NuPAGE 4-12% gradient gel (Invitrogen, Thermofisher scientific, MA, USA) for 15 minutes at 200 volts. Protein bands were visualised using Coomassie brilliant blue stain.

4.2.1.6 Preparation of metal bound EmtinB dimer

Metal-bound EmtinB was produced by incubating EmtinB with copper or zinc chloride. 100µL of EmtinB dimer stock (10mg/mL in PBS) was added to 10µL of saturated $CuCl_2$ or $ZnCl_2$ and 990µL of sterile PBS. The reaction mixture was incubated at room temperature for 30 minutes to allow binding of metals to the EmtinB dimer. Unbound metals were removed from the EmtinB/metal mixtures using PD-10 columns (GE healthcare, UK). Concentration of EmtinB was measured using BCA assay and the required concentration added to the 100µL reaction volume to achieve 25µM EmtinB.

4.2.2 EmtinB protection against H_2O_2-mediated toxicity

The capacity of EmtinB to protect against H_2O_2 was investigated in 7DIV hippocampal cultured neurons. Cell cultures were prepared as per method 3.2.1. At 7 DIV subsequent media was removed and replaced with Neurobasal media (subsequent, less B-27 supplement) containing 100µM H_2O_2 and 25µM EmtinB. Cells were left to incubate for 24 hours at 5% CO_2 and 37°C and cell viability assessed using an alamarBlue assay.

4.2.3 EmtinB protection via LRP-mediated mechanism

4.2.3.1 Inhibition of EmtinB action by RAP

EmtinB has been shown to act through LRP receptors to promote neuronal survival in cerebellar granule neurons [94]. To determine if EmtinB mechanism of action is mediated *via* the LRP family of receptors, the receptor-associated protein (RAP), a specific inhibitor of LRP-ligand binding, was used to block the potential interaction of EmtinB and LRP receptors.

RAP was added to 7DIV neurons and incubated for 30 minutes at 37°C and 5% CO_2. After this incubation, EmtinB and CuAβ were added at 25µM.

4.2.3.2 Knockdown of LRP1 and LRP2 using siRNA

Primary cultured hippocampal neurons were transfected using siRNA (GE Dharmacon, Thermofisher scientific, MA, USA) and Dharmafect transfection reagent-1 (GE Dharamcon, Thermofisher scientific, MA, USA). All protocols were carried out as per the manufacturer's instructions. In brief, siRNA was incubated at the desired concentration in subsequent media for five minutes at room temperature. Dharmafect transfection reagent was concurrently incubated in subsequent media at the desired concentration for five minutes. The transfection reagent and siRNA solutions were then mixed and incubated for a further 20 minutes at room temperature before adding the appropriate amount of subsequent media, pre-warmed to 37°C. The siRNA and transfection reagent media were added to primary cultured neurons and these cultures were maintained at 37°C with 5% CO_2 until cells were collected.

According to manufacturer's instruction, the recommended range for siRNA concentration is 5-50nM and the recommended range for Dharmafect transfection reagent is 0.05% to 0.5%. As an initial pass the concentrations selected for transfection were 25nM siRNA and 0.25% Dharmafect transfection reagent. To determine effective temporal conditions for knockdown, cells were transfected with siRNA for LRP1 and LRP2 at 6DIV for 24 or 5DIV for 48 hours, with cells collected for protein analysis at 7DIV. Control cells were transfected with non-targeting siRNA for 48 hours.

Subsequent experiments using 0.5% transfection reagent resulted in a loss of cell viability (data not shown) and, as such, 0.25% Dharmafect was used in all experiments.

4.2.3.3 siRNA knockdown of LRP1 and LRP2 in CuAβ model of toxicity

For all experiments, except Figure 4.22, siRNA was added concurrently at 25nM with the 0.25% Dharmafect. For experiment Figure 4.22 siRNA for LRP1 and LRP2 were added concurrently at 50nM and 0.25% Dharmafect.

4.2.3.4 Western blotting for LRP1

Western blotting was carried out as per the protocol described in general methods. Specifically, samples were run on NuPAGE 4-12% gradient gels (Invitrogen, Thermofisher scientific, MA, USA) at 200 volts for 20 minutes then blotted to nitrocellulose at 20 volts for one hour. Samples were blocked in western blot blocking solution (method 2.1.30) for 30 minutes prior to primary antibody incubation. Primary LRP1 (1:1000, Rabbit anti-LRP1, L2170, Sigma, MO, USA) antibody was incubated in western blot blocking solution for 2 hours at RT or overnight at 4°C. Secondary antibody was Anti-Rabbit-HRP (Dako, Glostrup, Denmark) incubated at 1:1000 in western blot blocking solution for 1 hour at room temperature.

4.2.3.5 Immunocytochemistry

For immunocytochemistry, cells were fixed in 4% PFA for 15 minutes then washed three times in PBS-T (method 2.1.6) for ten minutes. Cells were incubated in primary LRP1 or LRP2 antibody at 1:1000 in immuno diluent for one hour at room temperature or overnight at 4°C. Cells were washed three times for ten minutes each wash to remove primary antibody, then secondary anti-rabbit-594 antibody was incubated for one hour at room temperature in immuno diluent. Cells were washed a further three times for ten minutes before mounting in permafluor mountant (Dako, Glostrup, Denmark). Cells were allowed to dry overnight before imaging.

4.2.3.6 Microscopy

Photographs were obtained using 40x and 60x objectives on an Olympus BX50 microscope using a Photomatrix Cool Snap HQ2 camera.

4.3 Results

4.3.1 Evaluation of EmtinB metal-binding properties

Having established that EmtinB is a potent protective agent against CuAβ induced neurotoxicity in primary cultured hippocampal neurons (Chapter 3), the following experiments will attempt to determine whether this protective action is occurring through the same metal-swap mechanism reported for MT2 and MT3 [159, 160]. In these studies, zinc bound MT2 [159] and MT3 [160] were able to protect cultured neurons by swapping their endogenously bound zinc with the copper bound to Aβ. In the study by Chung et al. [159], it was demonstrated that MT could only undergo a metal swap with CuAβ when MT was in its zinc-bound state (Zn_7MT2). Attempts using other MT2 species, such as CuMT2 and apo-MT were unsuccessful, as was a carboxymethylated form (CM-MT), which is unable to bind metals. Notably, in the emtin studies detailed in Chapter 3, the peptides were not prepared in the presence of metals and the peptides are reported as being unmetallated in the literature [94], suggesting that emtin peptides have no endogenous metals to participate in a metal swap with CuAβ. Furthermore, the capacity of emtins to bind metals is unreported in the literature. To determine if the emtin mechanism of action in the CuAβ model of toxicity is, like MT, *via* a metal swap mechanism, it is important that the inherent, post synthetic metalation state of the EmtinB dimer and its capacity to bind copper and zinc, be conclusively established. As preliminary work showed EmtinB dimer to be the most efficacious, the EmtinB dimer will be the subject in this investigation.

4.3.1.1 EmtinB is not bound to copper or zinc when added to cell cultures

EmtinB dimer was analysed *via* ICP-MS to determine the inherent copper and zinc concentration of the peptide prior to its addition to tissue culture experiments. ICP-MS analysis of EmtinB prepared in PBS at 1mg/mL showed no appreciable levels of either copper or zinc in the solution (Figure 4.1).

4.3.1.2 EmtinB dimer can bind free copper and zinc

To determine if the EmtinB dimer is capable of binding copper and zinc, free copper or free zinc was incubated with EmtinB, and the unbound metals removed using a desalting column. For this analysis, the column eluent was collected in ten 1mL fractions. Fractions were also collected from a control column where only free copper or free zinc was applied to the column. Fractions were analysed for protein content by BCA Assay and SDS-PAGE, and ICP-MS was used to determine copper and zinc content.

Evaluation of copper-binding capacity of EmtinB

As no antibody is currently available for the detection of EmtinB, detection of this peptide was carried out using BCA assay to quantify protein concentration and SDS-PAGE with Coomassie stain to confirm EmtinB presence by size comparison. Protein was present in column fractions 1, 2 and 3 of the EmtinB/copper column, with the highest concentration of protein found in fraction 2 (Figure 4.2A; blue). In contrast, no protein was detected in the fractions from the copper-only control column (Figure 4.2A; orange).

Analysis of EmtinB in EmtinB/copper column fractions using SDS-PAGE and subsequent Coomassie stain confirms the presence of protein in fractions 1 and 2. Protein was not detectable in fraction 3 by Coomassie stain, likely reflecting the lower sensitivity of protein staining with Coomassie compared with BCA/Spectroscopy detection techniques. Interestingly,

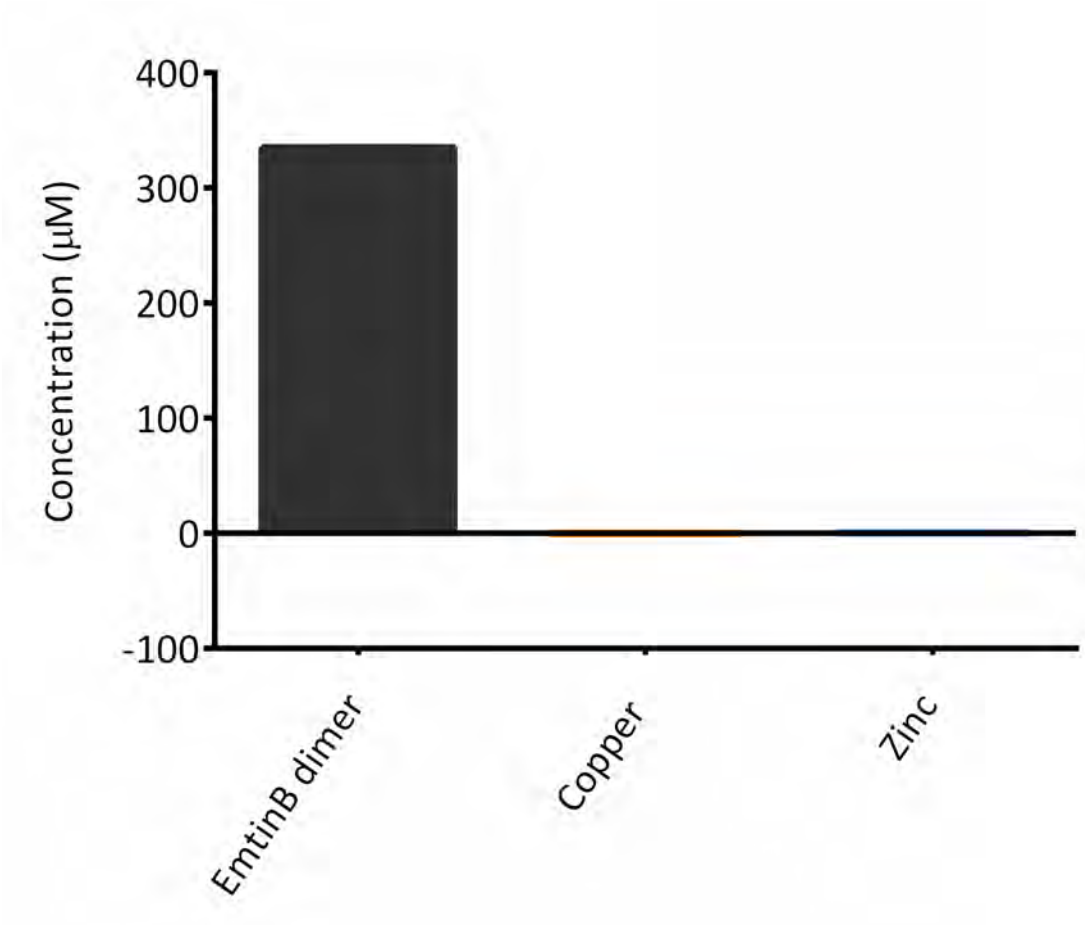

Figure 4.1 Dimeric EmtinB peptide contains no intrinsically bound copper or zinc

EmtinB dimer was reconstituted in sterile PBS at 1mg/mL (335µM). Analysis for copper and zinc content was carried out by ICP-MS and showed that the 335µM EmtinB solution contained almost no copper (-0.04µM) or zinc (0.43µM).

Figure 4.2 EmtinB is detectable in fractions 1-3 of the EmtinB/Cu column but not in copper-only control column fractions

EmtinB dimer (335µM) was co-incubated with a saturated (≈670µM) $CuCl_2$ for 30 minutes. Unbound copper was separated from EmtinB dimer on a PD-10 column. Ten 1mL fractions (F1-F10) were collected and analysed for protein content using a BCA assay (A) and SDS-PAGE/Coomassie stain (B). A) Protein was detected in fractions 1-3 of the EmtinB/Cu column. Fractions from a copper-only column contain no protein. B) A control sample of apo-EmtinB dimer is visualised at around 10kDa when resolved by SDS-PAGE. EmtinB was detectable in fractions 1 and 2 of the EmtinB/Cu column however, after incubation with copper, EmtinB in the column fractions had an apparent molecular weight of around 20kDa, twice the molecular weight of the freshly prepared EmtinB.

A

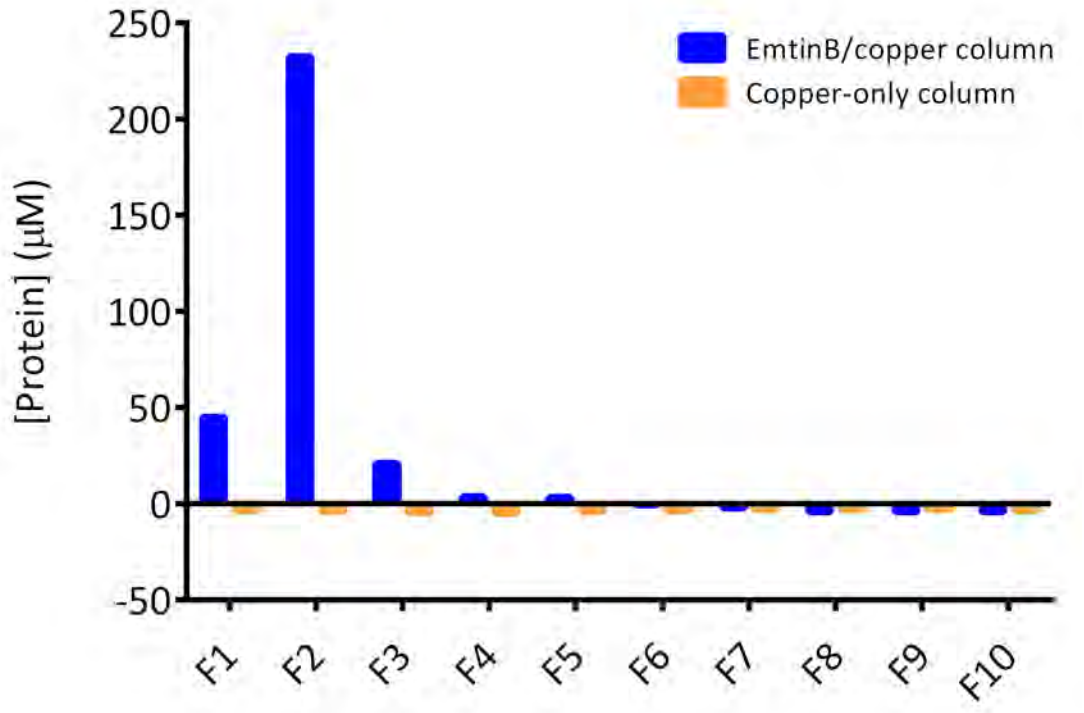
250
200
150
100
50
0
-50
[Protein] (μM)
EmtinB/copper column
Copper-only column
F1
F2
F3
F4
F5
F6
F7
F8
F9
F10

B

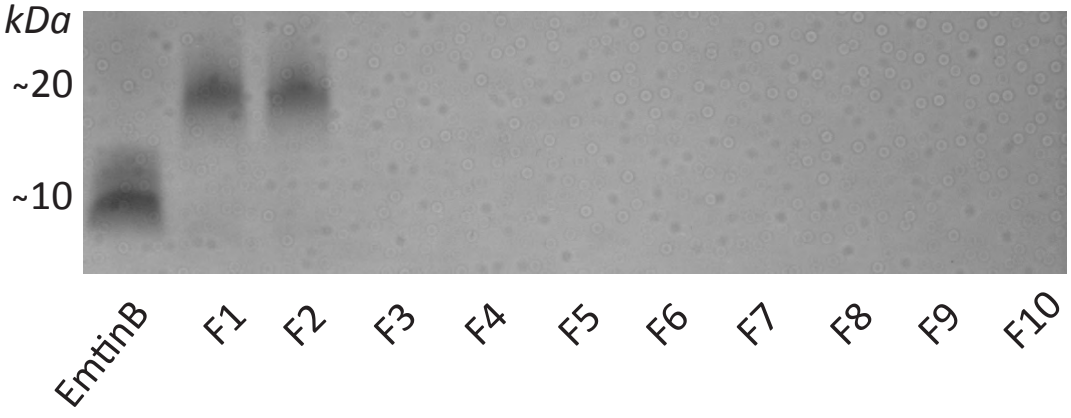
kDa
~20
~10
EmtinB
F1
F2
F3
F4
F5
F6
F7
F8
F9
F10

freshly prepared EmtinB migrated at approximately 10kDa on the gel, while EmtinB eluted from the copper-containing solution appeared to migrate at about 20kDa (Figure 4.2B).

Copper content was investigated using ICP-MS. In the copper-only control column, no copper was detectable within the first 10 column fractions (Figure 4.3; orange) in accordance with the expectation that free copper ions are retained within the column beads. In column fractions collected from the EmtinB/Cu column, copper was detected in column fraction 1, 2, 3, with the highest concentrations in fraction 2 (Figure 4.3; blue).

A direct comparison of protein and copper content from the EmtinB/copper column fractions shows that EmtinB and copper are found in the same fractions in the same molar quantities, suggesting that EmtinB has bound to the copper in a 1:1 ratio (Figure 4.4)

Zinc-binding properties of EmtinB

BCA analysis of the protein content in fractions from the EmtinB/zinc column showed that the EmtinB protein was present in fractions 1 to 3, with the highest concentration found in fraction 2 (Figure 4.5A). This pattern is consistent with findings from the EmtinB with copper column, suggesting that EmtinB elutes within fractions 1-3 of the PD-10 column under these conditions. Analysis of the EmtinB/zinc column fraction by SDS-PAGE and Coomassie stain confirmed the presence of EmtinB in fractions 1-3 (Figure 4.5B).

ICP-MS analysis showed that no zinc was detectable in the first 3 column fractions of the zinc-only control column (Figure 4.6), suggesting that free zinc does not elute in this buffer in the first three column fractions. However, zinc was found to be present in the later fractions, a finding consistent with the expected performance of the column. In column fractions collected from the EmtinB/Zn column, zinc was detected in column fraction 1, 2, 3, with the highest concentration in fraction 2 (Figure 4.6), suggesting that zinc is eluting together with EmtinB. The molar ratio of EmtinB peptide to zinc suggests a 1:1 binding ratio (Figure 4.7).

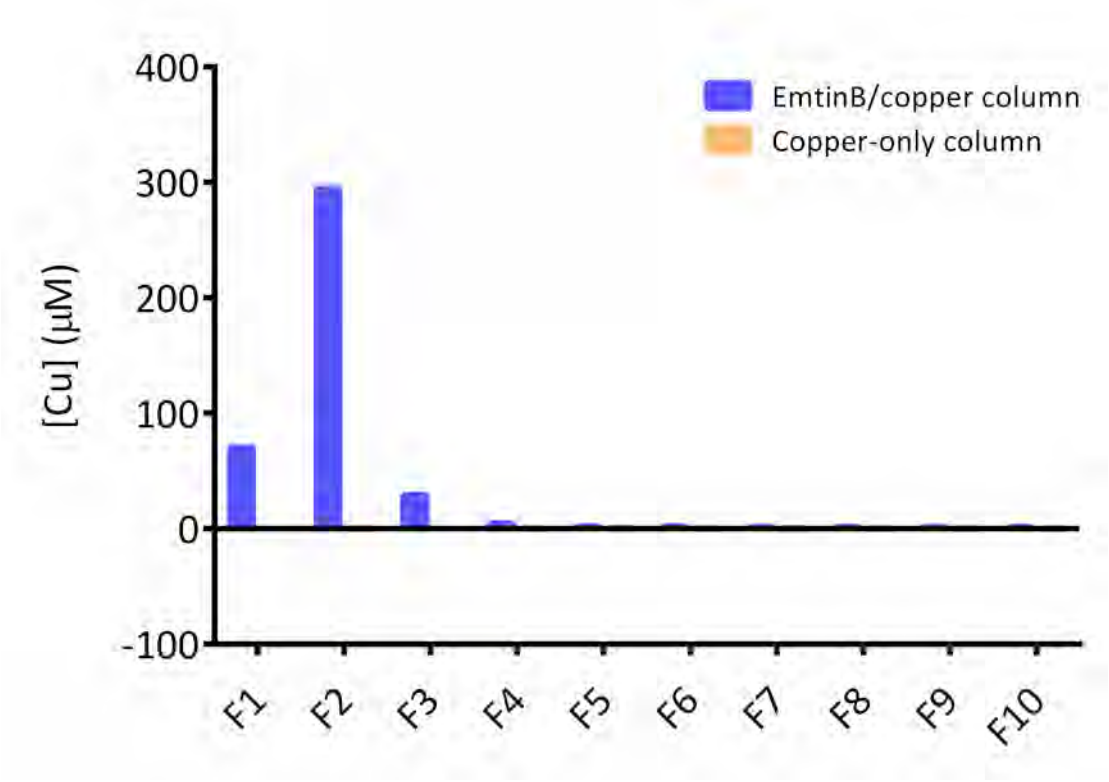

Figure 4.3 Copper is detectable in column fractions from copper incubated with EmtinB but not fractions from the copper-only column

EmtinB (335µM) was incubated with copper chloride (640µM) for 30 minutes and applied to a PD10 purification column to separate unbound copper from EmtinB protein. Ten 1mL fractions (F1-F10) were eluted and analysed for copper content using ICP-MS. ICP-MS analysis of the fractions show a marked increase in copper concentration in fractions 1-3 of the EmtinB/copper column. In control fractions from a copper-only column, where no EmtinB is present, fractions show no increase in copper concentration.

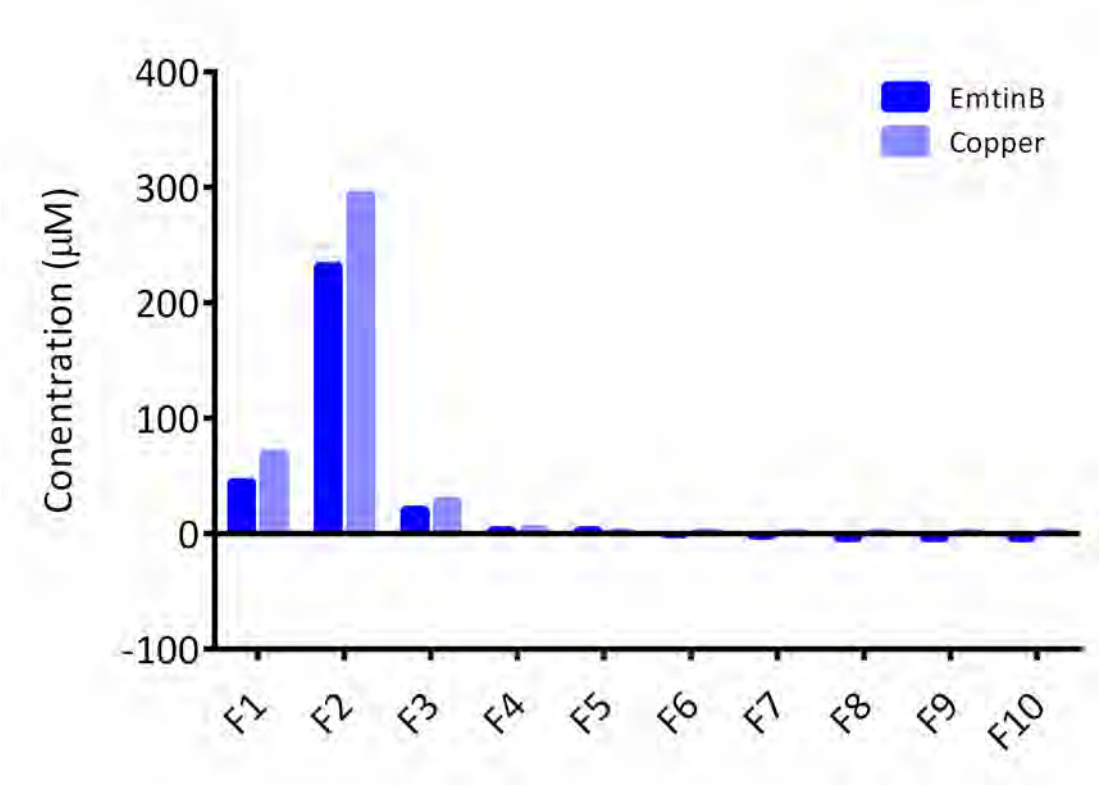

Figure 4.4 Copper concentration correlates with EmtinB presence or absence

EmtinB (335µM) and copper were co-incubated for 30 minutes and any unbound copper was then removed using a PD10 purification column. Analysis of the ten 1mL fractions (F1-F10) collected from the column show protein present in fractions 1,2, and 3, with the highest concentration in fraction 2 (see Figure 4.2). The pattern of appearance is identical for copper concentration, with the highest concentration of copper in fraction 2 with lower amounts in fractions 1 and 3 (see Figure 4.3). A direct comparison of copper and EmtinB content in these fractions indicates that EmtinB and copper appear in the same fractions (F1-3) and are present in equal concentrations.

Figure 4.5 Protein is present in fractions 1-3 of the EmtinB/zinc column but not in zinc-only column fractions

EmtinB (335µM) was incubated with zinc chloride (660µM) for 30 minutes and applied to a PD10 purification column to separate free zinc from EmtinB protein. Ten 1mL fractions were collected and analysed for protein content using BCA assay (A) and SDS-PAGE/Coomassie stain (B). A) Fractions from the zinc-only column show no protein present in any fraction, while protein was present in fractions 1-3 of the EmtinB/zinc column. B) Apo-EmtinB dimer was resolved at around 10kDa. EmtinB incubated with zinc was present in fractions 1, 2, and 3, and migrated at the same molecular weight as apo-EmtinB.

A

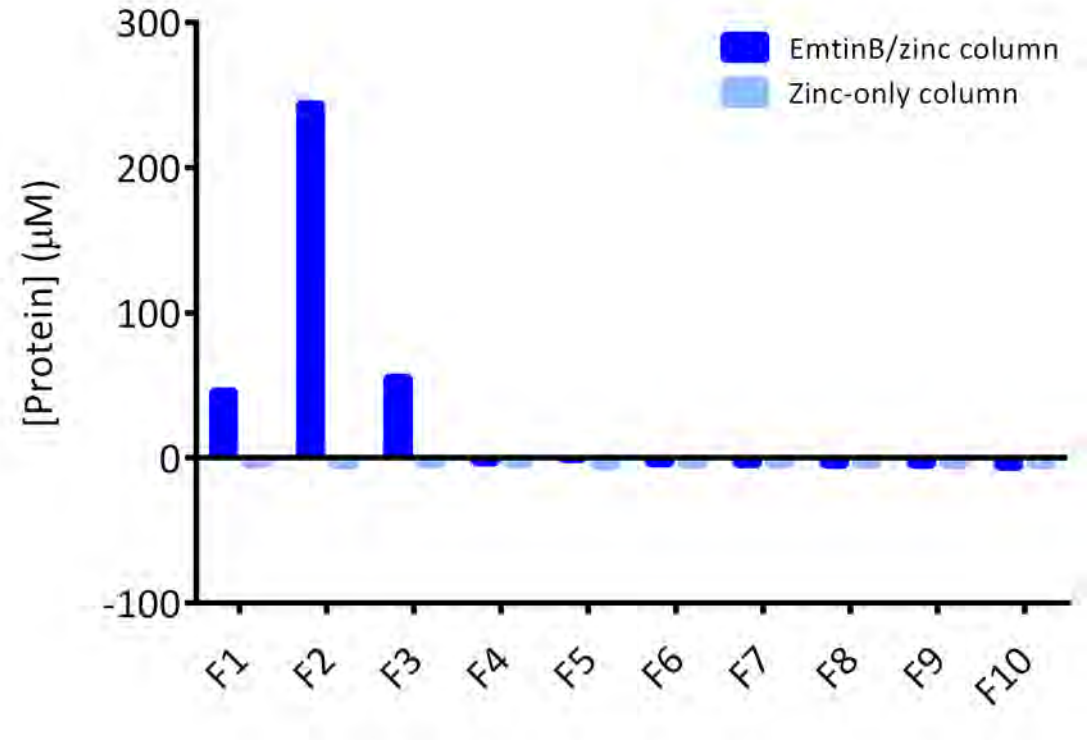
300
200
100
0
-100
[Protein] (µM)
EmtinB/zinc column
Zinc-only column
F1
F2
F3
F4
F5
F6
F7
F8
F9
F10

B

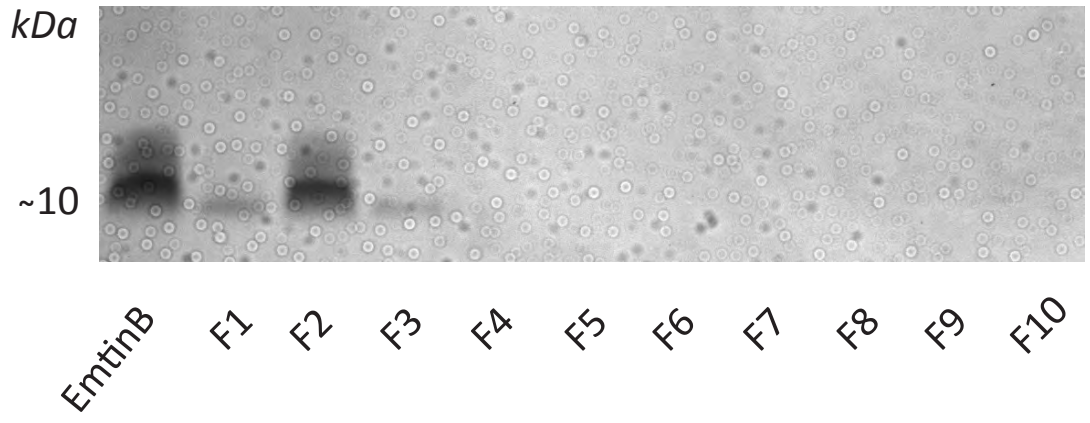
kDa
~10
EmtinB
F1
F2
F3
F4
F5
F6
F7
F8
F9
F10

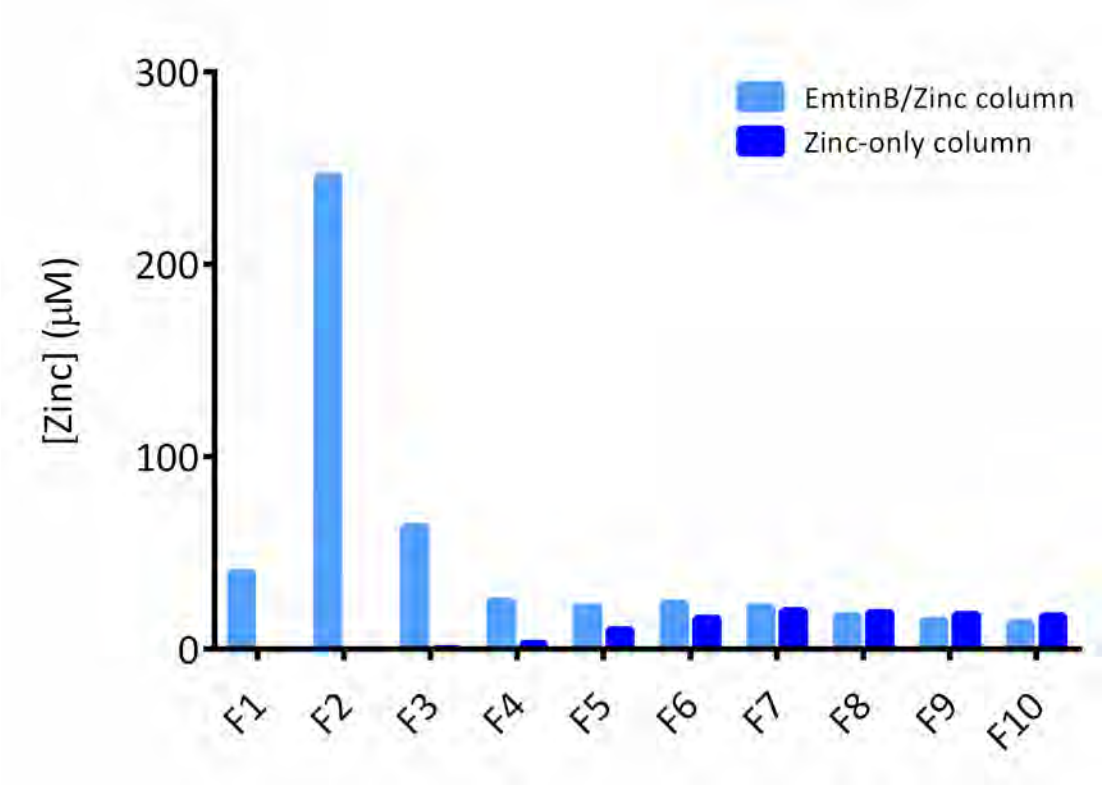

Figure 4.6 Zinc is present in fractions 1-3 from EmtinB/zinc column but is absent in fractions 1-3 of the zinc-only control column

EmtinB (335µM) was incubated with zinc chloride (660µM) for 30 minutes and applied to a PD10 purification column to separate unbound zinc from EmtinB protein. ICP-MS analysis for zinc shows zinc present predominantly in fractions 1-3 of the EmtinB/zinc column, with lower amounts detected in fractions 4-10. By comparison, fractions from the zinc-only control column show no zinc in fractions 1-3, but have similar levels to the EmtinB/zinc column in fractions 4-10, suggesting that free unbound zinc begins to be eluted around fraction 4-5.

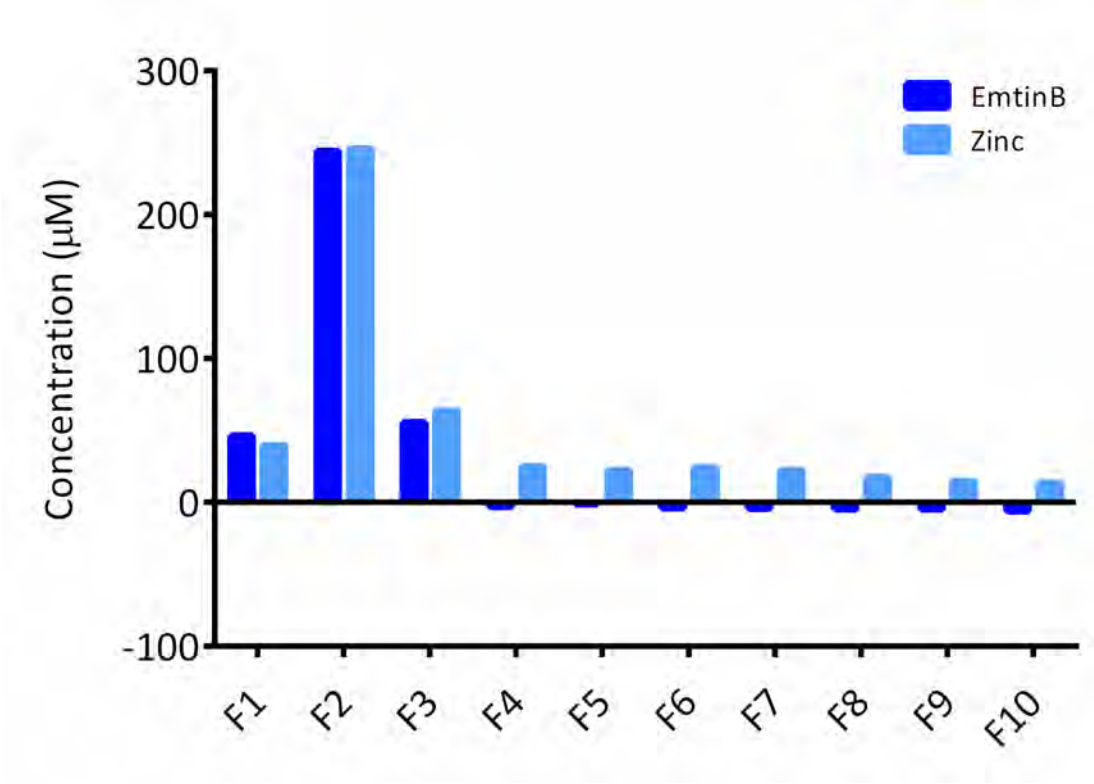

Figure 4.7 EmtinB and zinc co-elute in fractions 1-3 of the EmtinB/zinc column

EmtinB and zinc were co-incubated for 30 minutes before passing through a PD-10 column to remove unbound zinc. Ten 1mL fractions from this column were analysed for protein and zinc. Protein was found to be present in fractions 1, 2 and 3, with the highest concentration in fraction 2 (see Figure 4.6). Fractions 1-3 were also found to have the highest concentration of zinc (see Figure 4.7). A direct comparison of zinc and EmtinB in these fractions shows that EmtinB and zinc appear in the same fractions (1-3), and do so in a 1:1 ratio.

4.3.1.3 Metal bound EmtinB can undergo a metal swap with CuAβ

Having established that EmtinB can bind both copper and zinc in a 1:1 ratio, the capacity of dimeric EmtinB to undergo a metal swap with CuAβ was evaluated in the context of preventing the formation of toxic copper-bound aggregates of Aβ. This experiment used the methods developed by Meloni et al. [160] in their investigation of MT3 neuroprotection against CuAβ, and used in subsequent work by Chung et al. [159] on MT2in a similar investigation. When copper is bound to Aβ, the resulting CuAβ complex forms an SDS-insoluble aggregate that does not resolve on an SDS-PAGE gel. However, the analogous ZnAβ aggregate is SDS soluble and can be observed using this method. Accordingly, Meloni [160] and Chung [159] have independently shown that when ZnMT undergoes a metal-swap with CuAβ, the SDS soluble ZnAβ aggregate is formed.

To determine whether EmtinB can prevent the formation of an insoluble CuAβ aggregate, 25µM EmtinB was incubated in Apo, zinc-bound or copper-bound form with 25µM CuAβ1-42 for 72 hours. Following centrifugation to collect Aβ aggregates, the samples were resolved by SDS-PAGE and visualised using Coomassie stain.

No SDS-soluble Aβ was observed in samples of CuAβ alone (Figure 4.8). Similarly, no SDS-soluble Aβ was observed when CuAβ was incubated with Apo-EmtinB. Interestingly, when CuAβ was incubated with either Zn-bound or Cu-bound EmtinB, an SDS soluble Aβ aggregate was produced (Figure 4.8).

4.3.1.4 EmtinB does not readily bind metals under cell culture conditions.

While it was determined that metal bound EmtinB can prevent the formation of CuAβ aggregates in Chapter 3, EmtinB peptides, which were introduced into culture in metal free form, were found to protect against CuAβ. A possible explanation for this observation is that

Figure 4.8 EmtinB can undergo a metal swap with CuAβ, but only when bound to a metal

The capacity of EmtinB to undergo a metal swap with CuAβ was evaluated using the aggregation assay developed by Meloni et al. [160], wherein copper-bound Aβ forms an SDS-insoluble aggregate that is not resolvable by SDS-PAGE while zinc-bound Aβ forms an SDS-soluble aggregate detected by SDS-PAGE, and subsequent Coomassie stain. CuAβ was aggregated at 37°C for 72 hours alone or in the presence of Apo, Zinc-bound or copper-bound EmtinB. The resulting aggregate was collected by ultracentrifugation and analysed by SDS-PAGE/Coomassie stain. Consistent with expectations, CuAβ alone produced no soluble aggregate. Incubation of CuAβ with apo-EmtinB also produced no soluble aggregate, however, incubation of CuAβ with zinc-bound EmtinB produced an SDS soluble aggregate, indicating that zinc-bound EmtinB is able to undergo a metal swap with CuAβ. Incubation of CuAβ with CuEmtinB also appeared to produce an SDS-soluble Aβ aggregate, although potentially to a lesser degree than the ZnEmtinB.

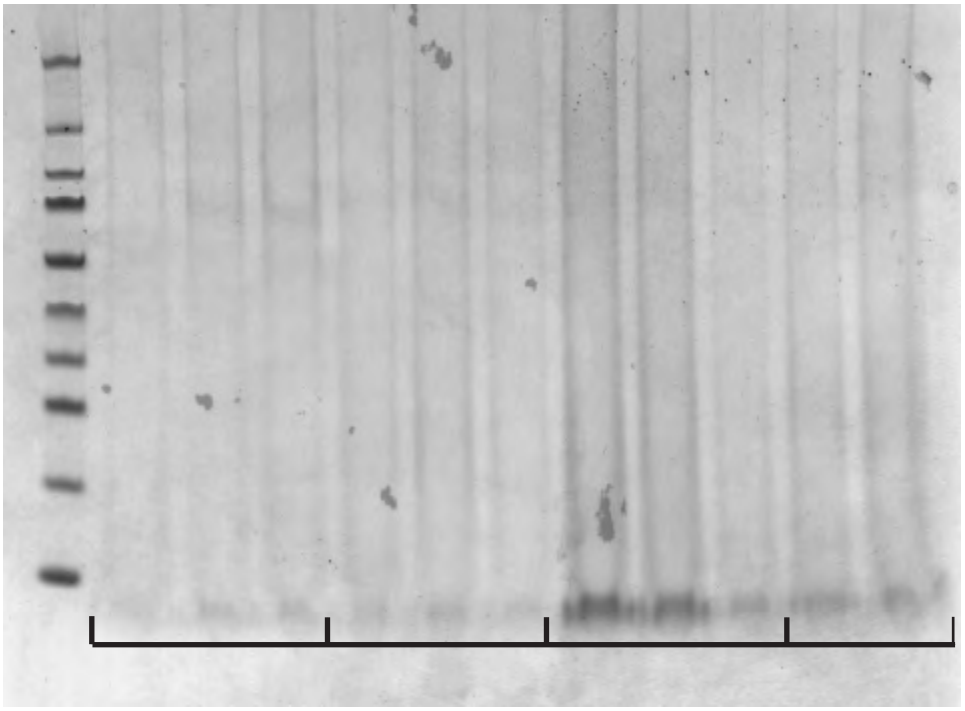
CuAβ
CuAβ + Apo EmtinB
CuAβ + ZnEmtinB
CuAβ + CuEmtinB

EmtinB peptides become metallated by scavenging zinc or copper present in the cell culture environment.

To investigate this, EmtinB was incubated in subsequent media and separated from free metals using a PD-10 column. Protein was present in fractions 1-3 of both the EmtinB/media column and the control media-only, as assessed by BCA analysis (Figure 4.9), consistent with protein being present in tissue culture media even in the absence EmtinB. However, higher protein levels observed in EmtinB/media columns compared with media-only columns suggest that EmtinB was present in these fractions. The presence of EmtinB was confirmed by SDS-PAGE analysis, with media-associated proteins found at high molecular weight and a band, most likely EmtinB observed around 10kDa (Figure 4.10A, B). EmtinB was not observable in fractions 1 and 3, as would be expected based on biochemical protein analysis (Figure 4.10B), however as mentioned previously, Coomassie stain detection of proteins appears less sensitive than detection by BCA assay.

ICP-MS analysis of copper and zinc levels in subsequent media found very low levels of both copper (0.02µM) and zinc (1.28µM), suggesting that there is very little metal available for EmtinB to scavenge (Table 4.1). Accordingly, low levels of both copper (0.27µM) and zinc (0.86µM) were found in EmtinB/media column fractions, which were similar to Cu (0.35µM) and Zn (0.62µM) levels in media-only fractions (Table 4.1).

To compare EmtinB concentration to metal content, EmtinB dimer concentrations in the fractions were analysed by BCA assay. The EmtinB concentration of the fractions was calculated to be around 106µM based on an EmtinB dimer standard curve and assumed to be zero for the media-only control (Table 4.1). By comparison, zinc and copper concentrations were less than 1µM in both media-only control and EmtinB/media fractions (Figure 4.11). Thus it appears that the presence of EmtinB in the column fractions is not associated with an increase in copper or zinc concentration and therefore the EmtinB dimer is not scavenging

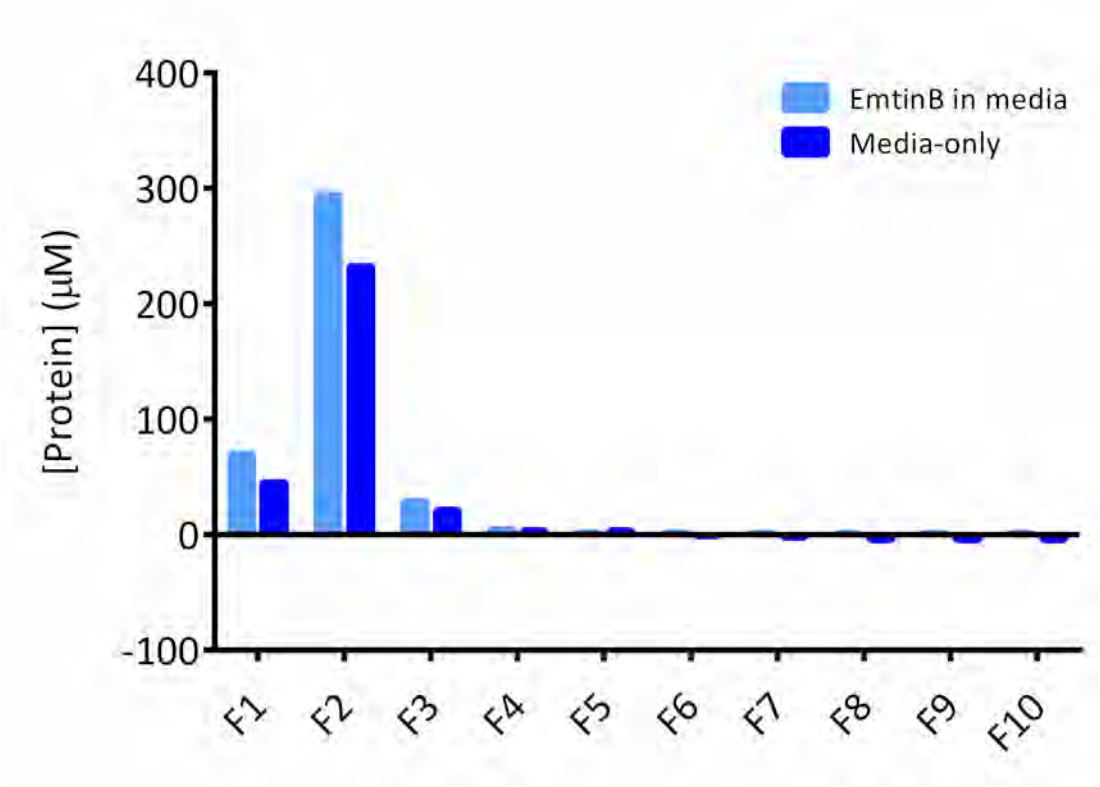

Figure 4.9 Protein concentration is higher in fractions from media with EmtinB added than fractions from media-only

Neurobasal media was incubated for two hours in the presence or absence of 335µM EmtinB dimer, before removal of free metal ions on a PD-10 column. Ten 1mL fractions (F1-F10) were collected and their protein content analysed by BCA assay. Protein was detected in fractions 1-3 of the EmtinB/media column, and was also detected in these same fractions (F1-F3) of the control media-only column. While protein was detected in fractions from both EmtinB/media and control columns, more protein was detectable in the EmtinB-containing column, suggesting EmtinB is present in these fractions.

Figure 4.10 EmtinB presence is confirmed by SDS-PAGE after incubation in media

Column fractions, from a media-only control column (A) and an EmtinB/media column (B), which were previously analysed by BCA Assay (Figure 4.9), were analysed for protein content using SDS-PAGE and subsequent Coomassie stain to confirm the presence or absence of EmtinB. High molecular weight protein bands are observed in fractions 1, 2 and 3 of both the media-only control column, and the EmtinB/media column, confirming that protein is present in media prior to EmtinB administration. EmtinB dimer was detected at around 10kDa in fraction 2 of the EmtinB/media column, which is comparable with the migration of apo-EmtinB dimer.

A

B

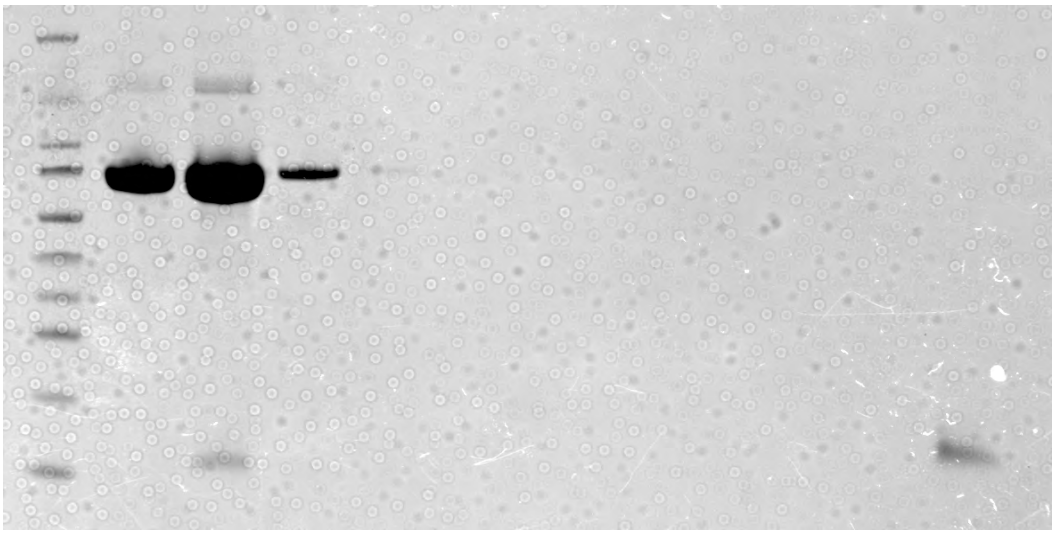

Column	[Cu]	[Zn]	Estimated [EmtinB]
Media-only	0.35	0.62	0μM
EmtinB/Media	0.27	0.86	106μM
Media (no column)	0.02	1.28	0μM

Table 4.1 Copper and zinc are not enriched in EmtinB-containing fractions after incubation with media

EmtinB dimer was incubated in Neurobasal media at 1mg/mL (335μM) for two hours before fractionating on a PD-10 column. Fractions 1 and 2, containing the highest protein content, were pooled and analysed for copper and zinc content by ICP-MS. A media sample not passed through a PD-10 column was also analysed to ascertain copper and zinc content prior to column fractionation. EmtinB content in these samples was estimated using BCA assay results for all fractions. Copper and zinc levels were below 1μM for both the media-only control fractions, and the EmtinB/media samples. EmtinB concentrations were estimated to be 0 and 106μM, respectively, suggesting that EmtinB is not scavenging metals from the media. Analysis of media with no EmtinB present, and prior to column fractionation, shows that very little copper (0.02μM) and zinc (1.28μM) are available for scavenging.

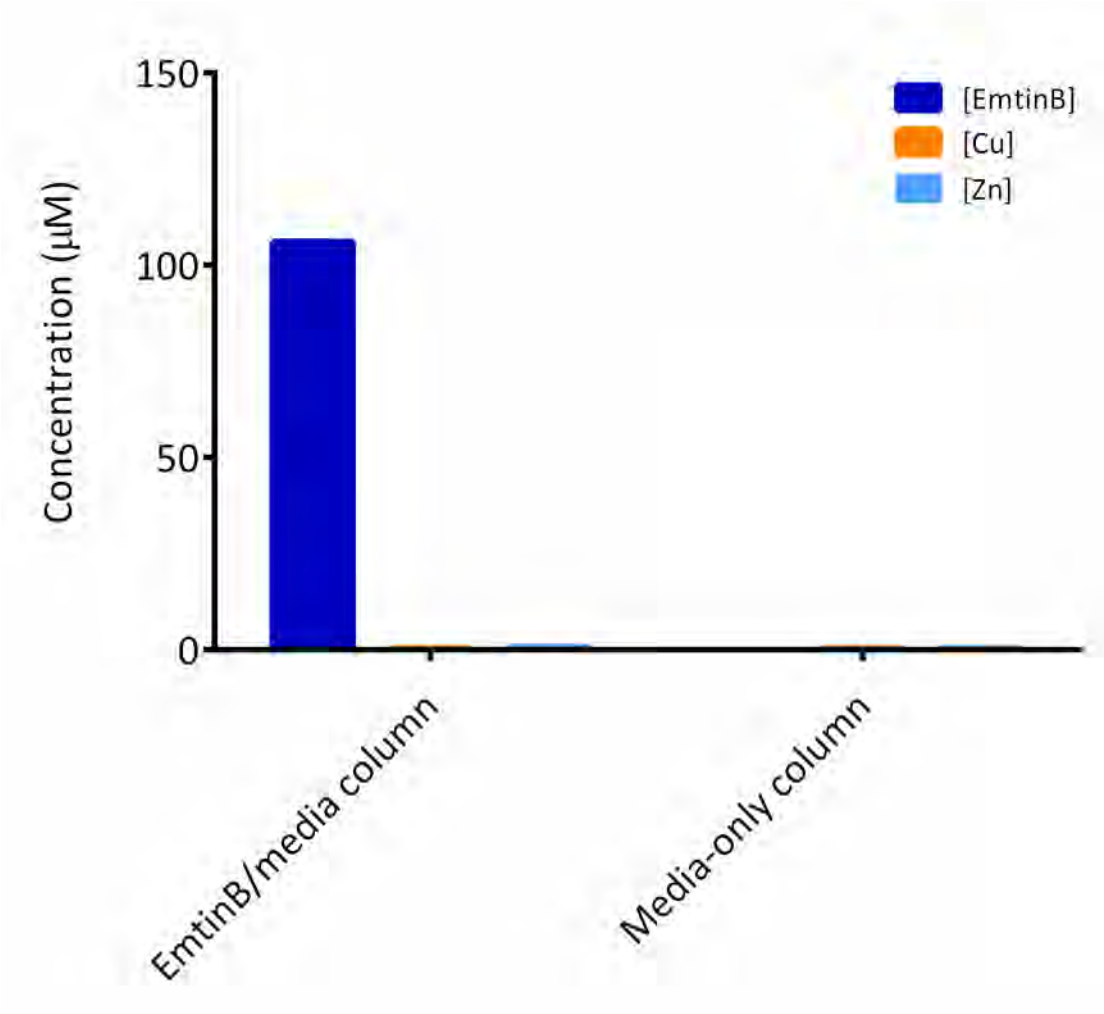

Figure 4.11 EmtinB does not scavenge copper or zinc from Neurobasal media

EmtinB dimer was incubated in Neurobasal media at 1mg/mL (335µM) for two hours before fractionating on a PD-10 column. Fractions 1 and 2, containing the highest protein content, were pooled and analysed for copper and zinc content by ICP-MS. A media sample not passed through a PD-10 column was also analysed to give copper and zinc content prior to column fractionation. EmtinB content in these samples was estimated using BCA assay results for all fractions. Copper and zinc levels were below 1µM for both the media-only control fractions and the EmtinB/media samples. EmtinB concentrations were estimated to be 0 and 106µM respectively, suggesting that EmtinB is not scavenging metals from the media.

significant amounts of either metal from the media used in these experiments.

4.3.1.5 EmtinB does not scavenge metals from tissue culture media conditioned by cortical neurons.

EmtinB was unable to scavenge metals from subsequent media, however ICP-MS analysis showed that unconditioned media has very little free metal. If EmtinB is scavenging metals to use in a copper swap mechanism with CuAβ, it must be scavenging them from metals derived from the cultured hippocampal neurons. To aid in the detection of EmtinB and metals, previous experiments have used high concentrations of EmtinB (1mg/mL; 335µM). This experiment aimed to determine if EmtinB could scavenge metals secreted from cells, and thus used 25µM EmtinB, a concentration found to be protective against CuAβ (see Chapter 3). Neurobasal media was conditioned for 24 hours on 7DIV cultured cortical neurons to potentially enrich the media in cell-secreted metals. The conditioned media was then incubated for a further 24 hours in the presence or absence of EmtinB before separating the protein from unbound metals on a desalting column. Unfractionated conditioned media samples were reserved for ICP-MS analysis to give a total metal content prior to fractionation.

In this instance only the most concentrated fractions (fractions 1-3) were selected for BCA analysis as these fractions will contain the highest EmtinB content. BCA analysis of these fractions show protein in both EmtinB/conditioned media column fractions, and in conditioned media-only column fractions (Figure 4.12), which is consistent with previous findings of protein in media-only (See Figure 4.9). On average, total protein concentration was slightly higher in EmtinB/conditioned media fractions compared to conditioned media-only fractions (see Figure 4.13). Subtracting average protein content of media-only fractions from the average protein content of EmtinB/conditioned media fractions gives an average difference of 105µg, which is roughly comparable in scale to the 75µg of EmtinB added in. Given that the slightly higher

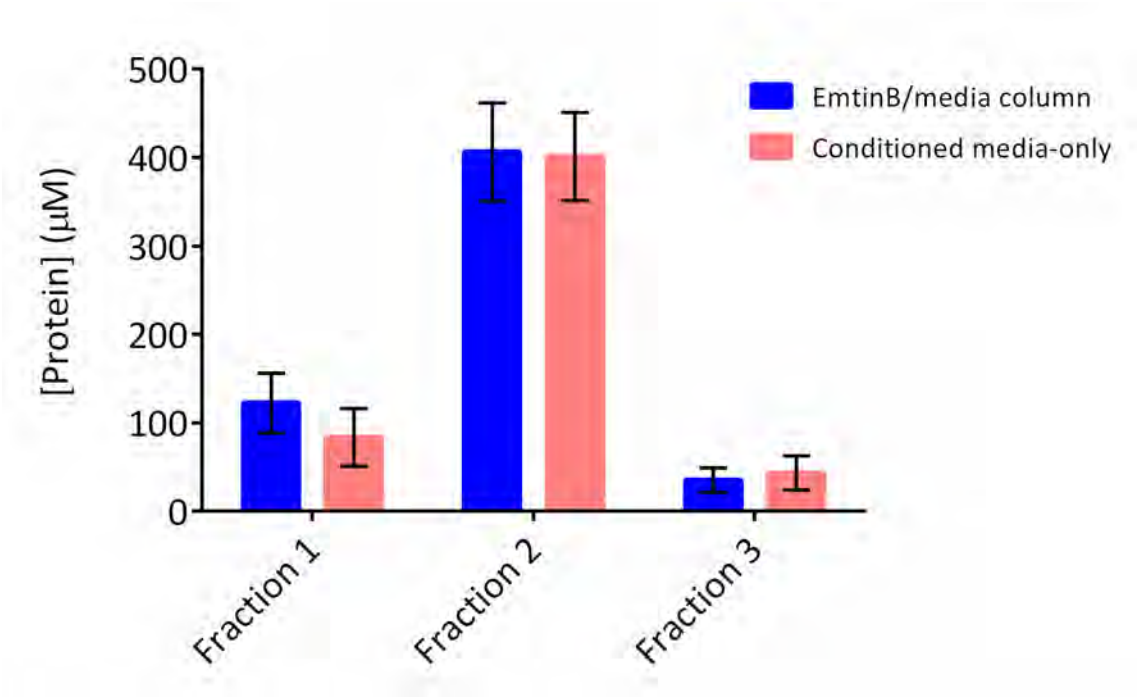

Figure 4.12 Protein is detectable in fractions 1-3 of EmtinB/conditioned media columns and conditioned media-only columns

Subsequent media was conditioned on 7DIV cortical neurons for 24 hours before EmtinB dimer was added at 25µM. EmtinB was incubated at 37°C with the conditioned media for a further 24 hours (n=4). Control conditioned media, with no EmtinB added, was incubated identically (n=4). After incubation, samples were fractionated on a PD-10 column and ten 1mL fractions collected. Fractions 1, 2 and 3 from each column were analysed for protein content by BCA assay. Protein was detected in fractions 1, 2 and 3 of both conditioned media-only and EmtinB/conditioned media columns. The pattern of elution was the same for both conditions, and similar concentrations were observed for both columns.

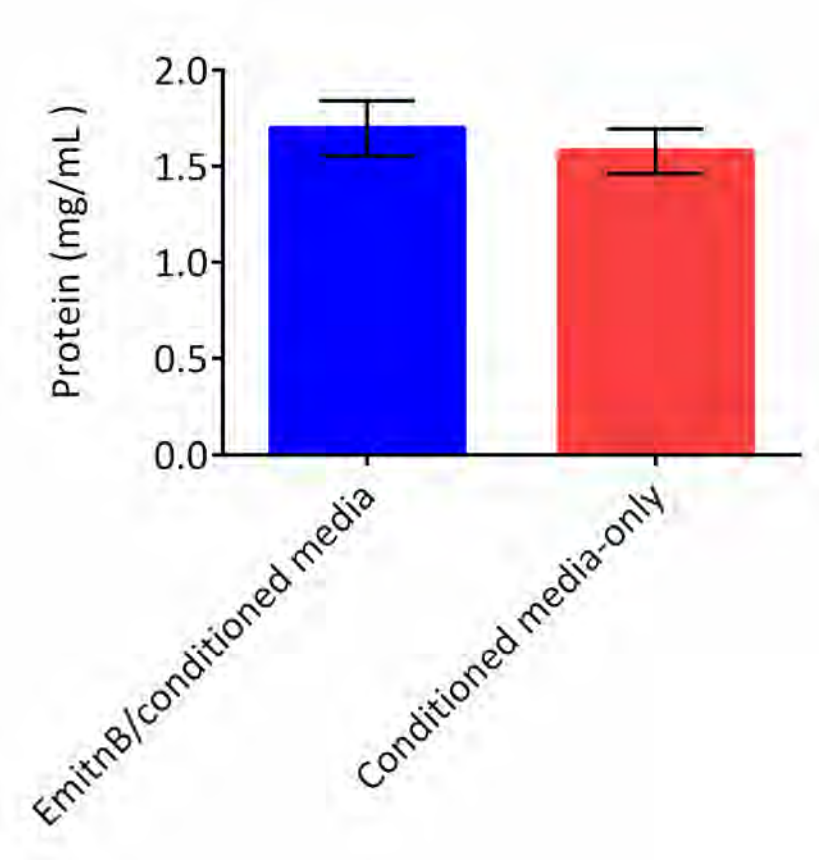

Figure 4.13 Protein is detectable in fractions 1-3 of EmtinB/conditioned media columns and conditioned media-only columns

Subsequent media was conditioned on 7DIV cortical neurons for 24 hours before EmtinB dimer was added at 25µM. EmtinB was incubated at 37°C with the conditioned media for a further 24 hours (n=4). Control conditioned media, with no EmtinB added, was incubated identically (n=4). After incubation, samples were fractionated on a PD-10 column and ten 1mL fractions collected. The protein-containing fractions from these columns, fractions 1, 2 and 3, were analysed for protein content by BCA assay. Average total protein was calculated for each PD-10 column and was slightly higher (0.105mg/mL) for EmtinB/conditioned media columns than conditioned media-only columns.

average concentration of protein in EmtinB/conditioned media columns roughly corresponds to the concentration of EmtinB added into the media, and that all previous experiments with these columns show EmtinB eluting in Fractions 1-3, it is likely that the EmtinB has passed through the columns and into the appropriate fractions. Fraction 2, the most concentrated fraction, was used for ICP-MS analysis of copper and zinc. Copper and zinc levels were not significantly different between EmtinB/conditioned media and conditioned media-only (Figure 4.14), suggesting that EmtinB dimers are not scavenging metals from conditioned media.

The accumulated evidence suggests that EmtinB is able to undergo a metal swap with CuAβ but only under conditions where it was previously bound to another metal. For the metal swap mechanism to occur in culture, EmtinB must be able to scavenge metals from the cell culture model, yet no evidence has been found that suggests this is occurring in these experiments.

While no definitive conclusion can yet be drawn from this work, the data do suggest that EmtinB could be working through a mechanism other than the metal-swap with CuAβ.

4.3.2 EmtinB protection against H_2O_2 toxicity

To investigate the ability of EmtinB to block H_2O_2-induced toxicity, EmtinB and 100µM H_2O_2 were applied concurrently to 7DIV cultured neurons for 24 hours and subsequent cell viability assessed by alamarBlue assay. It was found that 25µM hydrogen peroxide, a standard concentration used in published studies, decreased cell viability compared with control neurons (Figure 4.15). EmtinB significantly ablated hydrogen peroxide toxicity, increasing cell viability of H_2O_2 treated neurons (Figure 4.15).

At a higher H_2O_2 concentration of 100µM, which is highly neurotoxic, EmtinB had minimal protective effect (Figure 4.16).

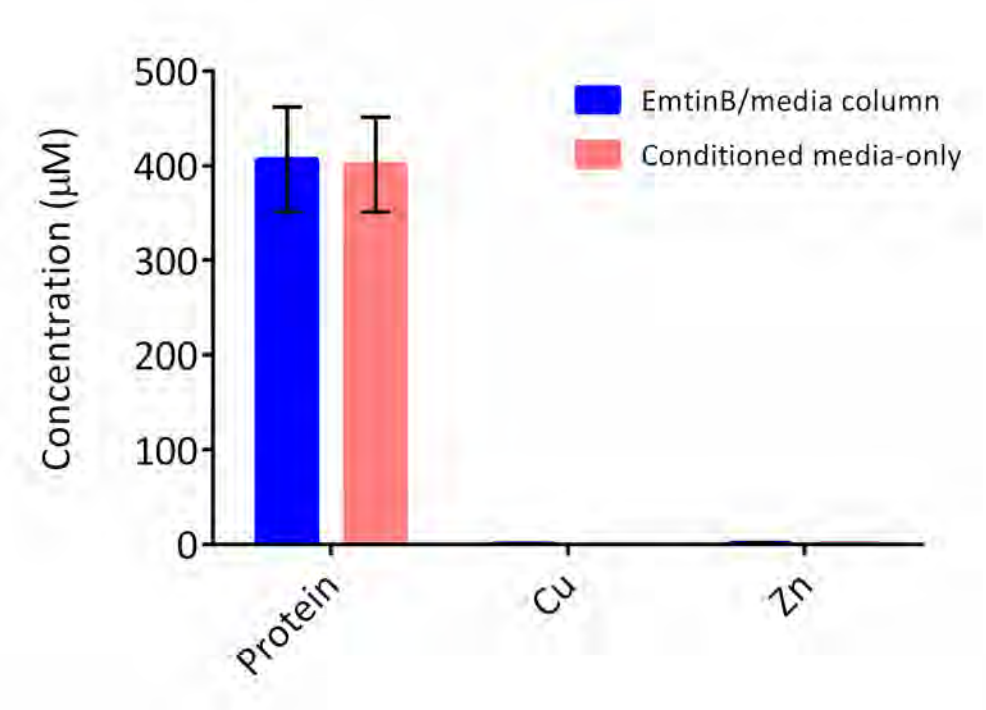

Figure 4.14 Copper and zinc are not significantly increased in EmtinB-containing fractions after incubation in conditioned media

EmtinB was incubated in conditioned media for 24 hours at 37°C (n=4). Control conditioned media, with no EmtinB added was incubated identically (n=4). Samples were fractionated on a PD-10 column and ten 1mL fractions collected. The fraction containing the most protein, fraction 2, was analysed by ICP-MS for copper and zinc. There was no significant difference in zinc content (t-test P=0.132) or copper content (t-test P=0.1904) between EmtinB/conditioned media fractions and conditioned media-only control fractions.

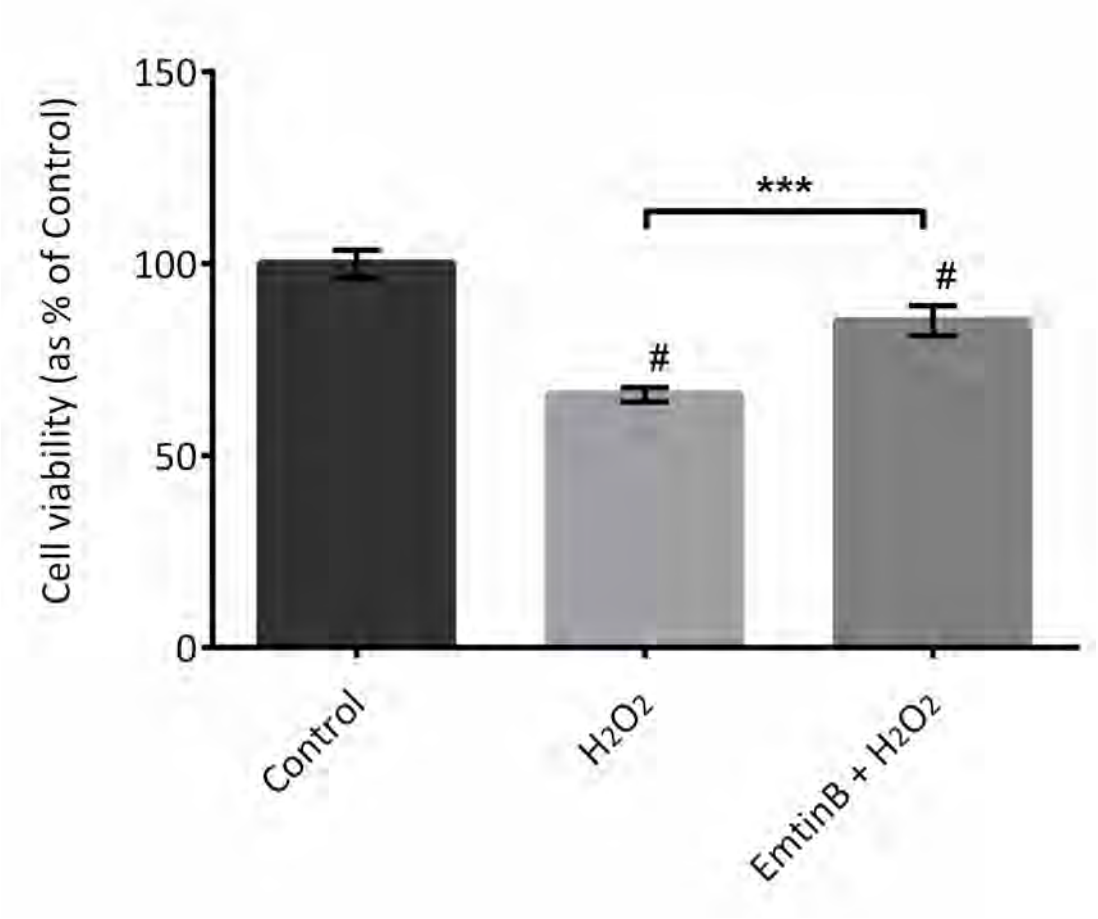

Figure 4.15 EmtinB has significant protective effect against H_2O_2 toxicity in cultured hippocampal neurons

Hippocampal neurons were treated with 25µM H_2O_2, either alone or concurrently with dimeric EmtinB (50µM). Cell viability was assessed after 24 hours using alamarBlue assay. Treatment with H_2O_2 alone (n=8) caused a decrease in cell viability compared with vehicle treated control neurons (n=8). Addition of 50µM EmtinB (n=8) to H_2O_2 treated cells resulted in a significant protective effect against H_2O_2-mediated toxicity. One-way ANOVA with Tukey post-test. # = significantly different to control neuron viability ($p<0.05$), *** = $p<0.001$. All data are means and SEM.

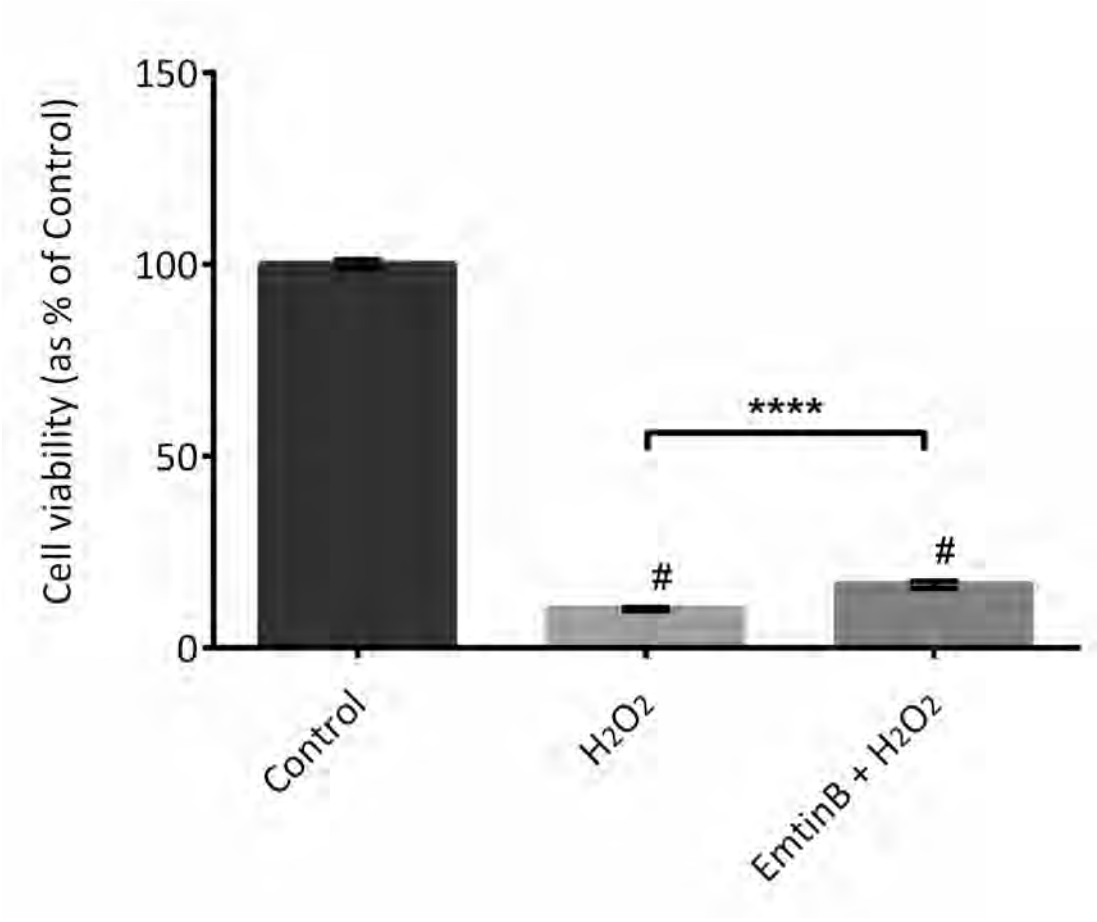

Figure 4.16 EmtinB has a small but significant protective effect against H_2O_2 toxicity in cultured hippocampal neurons

Hippocampal neurons were treated with 100µM H_2O_2, either alone or concurrently with dimeric EmtinB (50µM). Cell viability was assessed after 24 hours using alamarBlue assay. Treatment with H_2O_2 alone (n=16) caused a severe and significant decrease in cell viability compared with vehicle treated control neurons (n=16). When EmtinB (n=16) was co-administered with H_2O_2, EmtinB improved the viability of H_2O_2 treated cells by a small but significant margin. One-way ANOVA with Tukey post-test. # = significantly different to control neuron viability ($p<0.05$), **** = $p<0.0001$. All data are means and SEM.

4.3.3 LRP-mediated EmtinB protection against CuAβ1-42

While the metal-swap mechanism and protection against H_2O_2 represent two possible mechanisms of EmtinB action, a further possibility is that EmtinB is working through LRP receptors to promote neuronal survival. Both MT2 and EmtinB have demonstrated an ability to act through LRP receptors to promote survival of cerebellar granule neurons against shock induced K^+ withdrawal [94]. To determine if the protective action of EmtinB against CuAβ is mediated through the LRP family of receptors, the protective actions of EmtinB were tested in the presence of RAP, a commonly employed LRP ligand used as a competitive inhibitor to block LRP receptors, and siRNA directed specifically and LRP1 and LRP2.

4.3.3.1 RAP abrogates EmtinB neuroprotective action in the CuAβ model of toxicity

The capacity for EmtinB to protect cultured hippocampal neurons against CuAβ1-40 was tested in the presence or absence of 1μM RAP. Both EmtinB tetramers (Figure 4.17) and dimers (Figure 4.18) were able to significantly protect against CuAβ toxicity, increasing cell viability compared to CuAβ treated cells. In the presence of RAP, EmtinB was unable to effect this change and cell viability for this treatment was not significantly different from CuAβ alone (Figures 4.17 and 4.18). This suggests that inhibition of LRP receptors prevents EmtinB action. Importantly, RAP alone had no effect on the viability of CuAβ treated cells, suggesting that blocking EmtinB binding to LRP receptors prevents EmtinB action.

4.3.3.2 LRP1 and LRP2 knockdown using siRNA

MT2 has been shown to interact with LRP1 and LRP2 [89, 90, 94, 201]. Given that emtins are based on MT2 sequence, LRP1 and LRP2 represent logical investigative targets for the mechanism of EmtinB action. Ambjorn et al. [94] established that EmtinB is able to bind to LRP1 and LRP2 on the surface of neurons using an *in vitro* binding assay. To evaluate whether

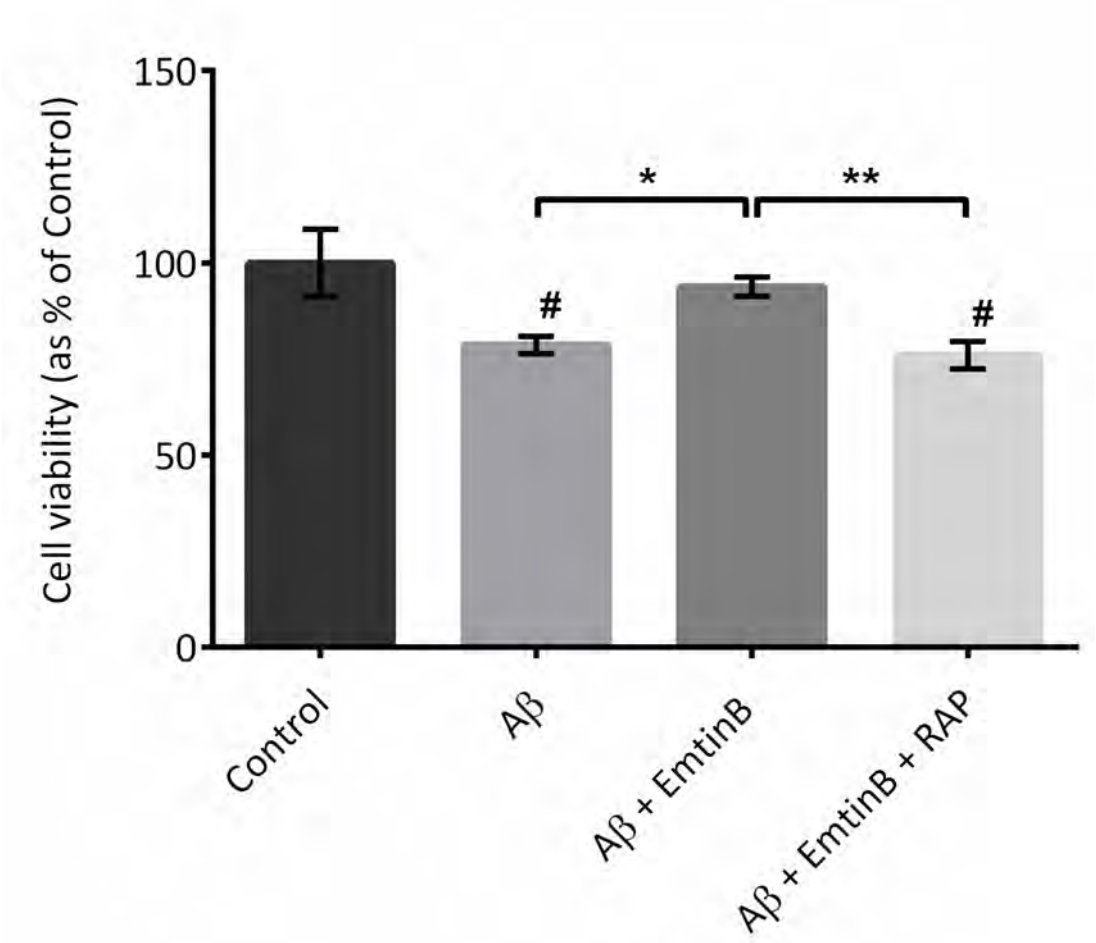

Figure 4.17 Tetrameric EmtinB cannot protect against CuAβ1-40 toxicity in the presence of RAP

EmtinB capacity to protect hippocampal neurons against CuAβ was investigated in the presence of RAP, an inhibitor of the LRP family of receptors. For inhibition of LRP, neurons were pre-incubated with RAP for 30 minutes prior to addition of EmtinB and CuAβ. CuAβ1-40 added to cultured hippocampal neurons (n=6) caused a significant decrease in neuronal viability compared to vehicle treated neurons (n=3). 25μM tetrameric EmtinB (n=6) significantly improved the viability of CuAβ1-40 treated cells compared with cell treated with CuAβ1-40 alone (n=6); however, this protective capacity was completely abrogated in the presence of RAP (n=6). One-way ANOVA with Tukey post-test. # = significantly different to control neuron viability ($p<0.05$), * = $p< 0.05$, ** = $p<0.01$. All data are means and SEM.

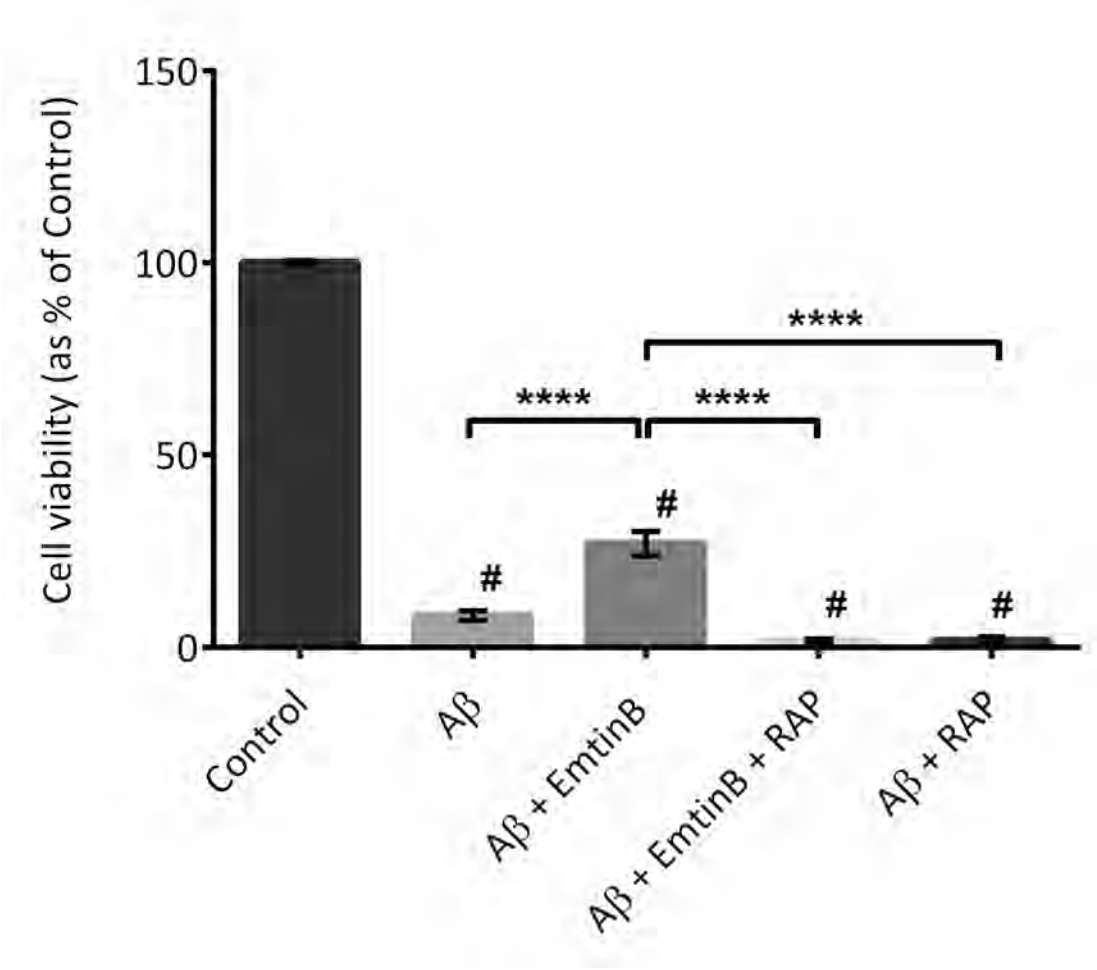

Figure 4.18 Dimeric EmtinB cannot protect against CuAβ1-42 toxicity in the presence of RAP

EmtinB protection against CuAβ1-42 was investigated in the presence of the LRP family agonist, RAP. Hippocampal neurons were pre-incubated with RAP (1µM) for 30 minutes prior to addition of EmtinB and CuAβ1-42. 25µM CuAβ1-42 (n=5) caused a significant decrease in neuronal viability compared with vehicle control treated neurons (n=4). 50µM EmtinB (n=4) improved the viability of 25µM CuAβ1-42-treated cells compared with neurons treated with CuAβ1-42 alone. In the presence of RAP (n=4), EmtinB was unable to protect neurons from CuAβ1-42 toxicity. RAP treatment in the absence of EmtinB (n=4) had no effect on the toxicity of CuAβ. One-way ANOVA with Tukey post-test. # = significantly different to control neuron viability ($p<0.05$), **** = $p<0.0001$. All data are means and SEM.

EmtinB acts specifically through these receptors to protect neurons against CuAβ-mediated toxicity, siRNA was used to knockdown expression of LRP1 and LRP2.

To ensure that the siRNA knockdown had no effect on cell viability, an alamarBlue assay was carried out prior to the collection of treated neurons. Treatment of cultured neurons with siRNA (LRP1, LRP2, or non-targeting) for either 24 or 48 hours did not alter cell viability compared to untreated control neurons (Figure 4.19), showing that these conditions are not detrimental to cultured hippocampal neurons.

Levels of LRP1 in treated neurons were investigated using both western blotting and immunocytochemistry (ICC). Analysis of treated cells by western blot showed an observable decrease in LRP1 levels in cells treated with siRNA for 24 or 48 hours compared with both untreated cells and cells treated with non-targeting siRNA (Figure 4.20 A). This depletion of LRP1 levels was confirmed by immuno-labelling (Figure 4.20 B). As expected, the prolonged siRNA treatment (48 hours) resulted in a greater degree of LRP1 knockdown.

Unfortunately, basal LRP2 was not detectable by either western blot or ICC in cultured hippocampal neurons, which are known to express LRP2 [85]. Two different antibodies were used, including one reported in prior publications. Accordingly, it was not possible for this study to evaluate the effect of the siRNA on LRP2 levels. However, this siRNA has been used in other studies carried out by Dr Lila Landowski (School of Medicine, UTAS). In this work, Landowski at al. [202] used a growth-cone turning assay to demonstrate that LRP2 siRNA induced a functional knockdown in neurons derived from dorsal root ganglia [203], see Figure A1, Appendix A. For the purposes of this work, it will be assumed that the LRP2 siRNA was equally successful at knocking down LRP2.

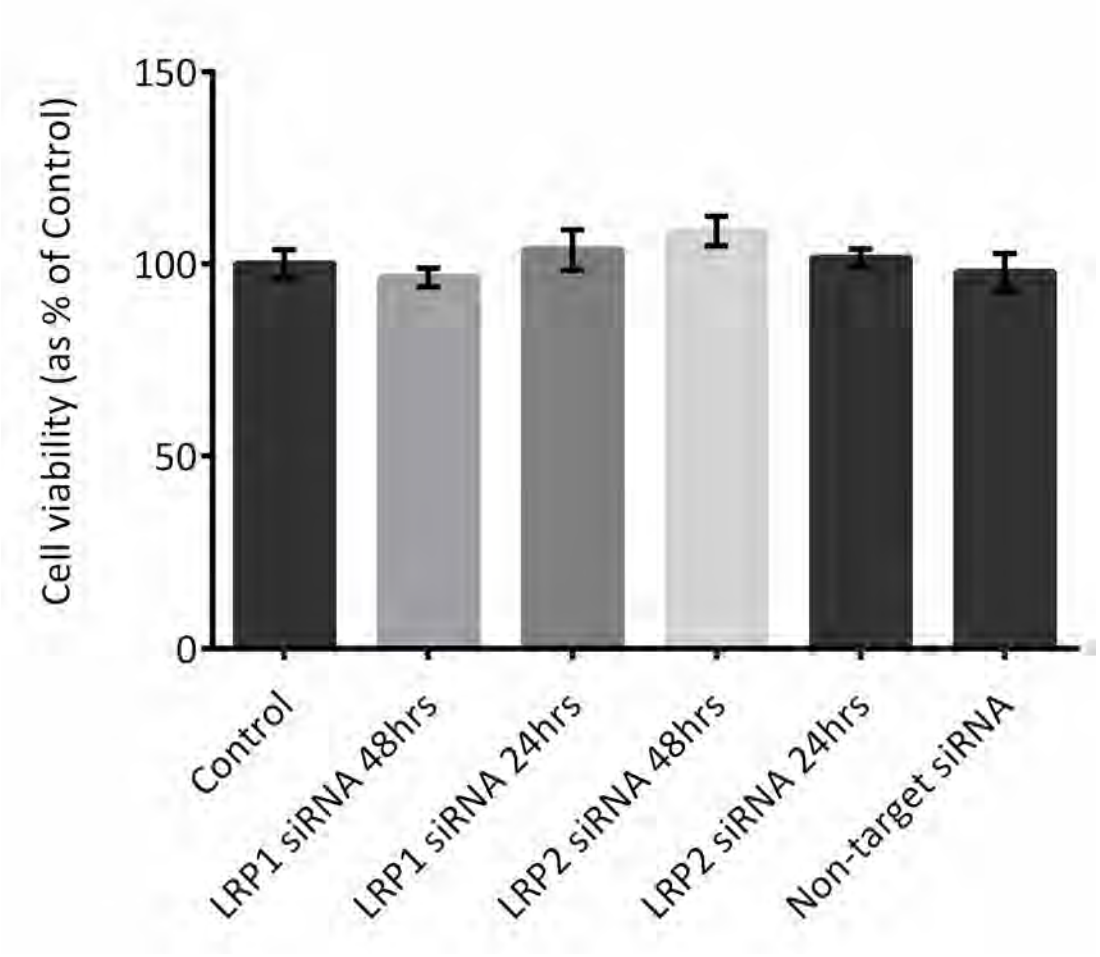

Figure 4.19 Knockdown of LRP1 and LRP2 using 25nM siRNA has no effect on cell viability

Hippocampal neurons were maintained in culture to 5DIV and 6DIV before administration of 25µM siRNA for 48 or 24 hours, respectively. Neurons treated with LRP1 or LRP2 siRNA showed no difference in cell viability compared with control untreated neurons after 24 or 48 hours incubation. Similarly, treatment of neurons with non-targeting siRNA for 48 hours did not cause any difference in cell viability compared with either control neurons or neurons treated with targeted siRNA for LRP1 or LRP2. One-way ANOVA with Tukey post-test. All data are means and standard error of the mean (SEM).

Figure 4.20 LRP1 levels are successfully decreased using 25µM LRP1 siRNA

A) Hippocampal neurons were treated with 25µM LRP1 or non-targeting siRNA for 24 or 48 hours. LRP1 levels were analysed using western blot (A) and immunocytochemistry (B). A) Western blot shows a marked decrease in LRP1 protein in cells treated for 24 or 48 hours with LRP1 siRNA. No decrease in LRP1 protein is observed after 48hrs treatment with non-targeting siRNA. B) LRP1 siRNA treated cells showing a considerable decrease in LRP1 positive staining in 24hr treated (Figure B-iii) and 48hr treated (Figure B-ii) hippocampal neurons compared with non-targeting siRNA treatment (Figure B-i). Figure B-ii shows untreated cells with no primary antibody to illustrate levels of non-specific staining. Scale bar is 25µm.

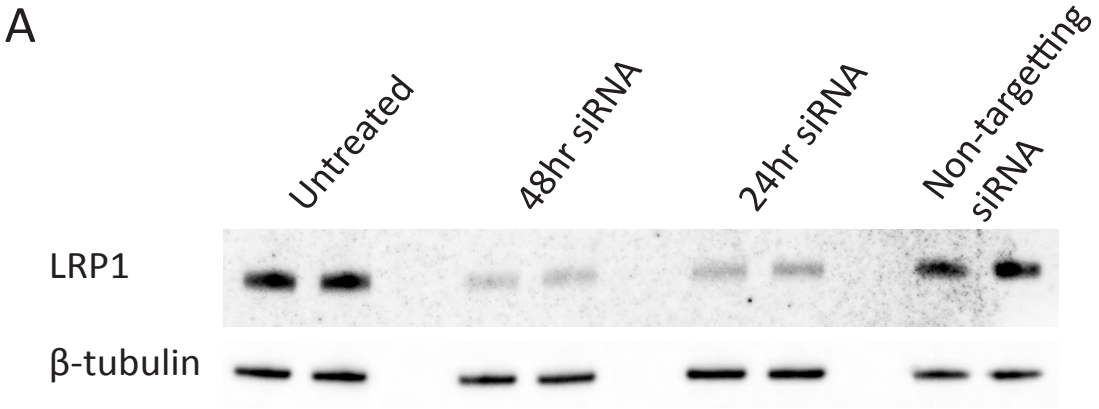
A
Untreated
48hr siRNA
24hr siRNA
Non-targetting siRNA
LRP1
β-tubulin

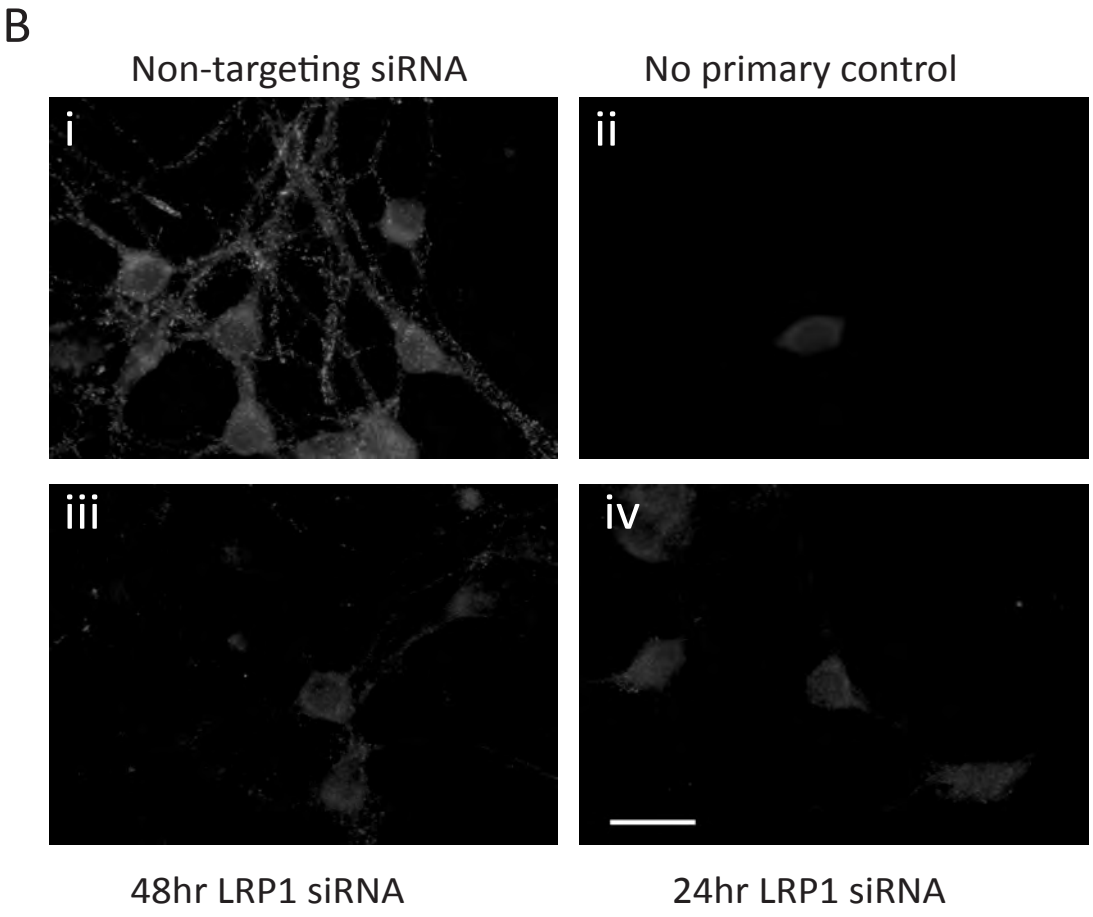
B
Non-targeting siRNA
No primary control
i
ii
iii
iv
48hr LRP1 siRNA
24hr LRP1 siRNA

4.3.3.4 Effect of combined LRP1 and LRP2 knockdown on EmtinB protection of neurons

Earlier results showing the successful blocking of EmtinB protective action by RAP (see Figures 4.17 and 4.18), suggesting the involvement of the LRP family of receptors in EmtinB mechanism of protection against CuAβ. To determine if LRP1 and LRP2 are involved in EmtinB-mediated neuronal protection, primary cultured hippocampal neurons were treated with siRNA to both LRP1 and LRP2 for 48 hours. Control cells were left untreated. Control and siRNA knockdown cells were treated with vehicle control, 25μM CuAβ1-42, or 25μM CuAβ1-42 co-administered with 25μM EmtinB dimer (Figure 4.21), or 50μM EmtinB dimer (Figure 4.22). In both experiments, knockdown of siRNA has no effect on EmtinB efficacy with EmtinB dimer exerting the same protective effect against CuAβ1-42 regardless of whether the cells had been treated with siRNA or not (Figure 4.21, Figure 4.22).

4.3.3.5 Effect of LRP1 and LRP2 knockdown on EmtinB interaction with cultured hippocampal neurons

Given that MT2 has previously been shown to interact with cultured neurons *via* an LRP-mediated mechanism [80, 90, 94, 204], EmtinB interaction with hippocampal neurons was investigated using ICC. Biotinylated dimeric EmtinB was administered to neurons at 25μM and incubated for 30 minutes or 3 hours. For control cells, no EmtinB was added. Biotinylated EmtinB was detected using ICC directed at the biotin tag. EmtinB was identified in the culture by its punctate appearance (Figure 4.23, Bii and Biii), which was not observable in the control cells (Figure 4.23, Aii). EmtinB was observed to be associated with cells 30 minutes after administration (Figure 4.23, Biii), although whether EmtinB puncta are at the surface bound to the membrane or internalised in vesicles was not established. Furthermore, EmtinB was observable in the cytosol of neurons after 3 hours incubation (Figure 4.23, Cii and Ciii), suggesting that EmtinB is rapidly internalised by neurons *via* an as yet unknown mechanism

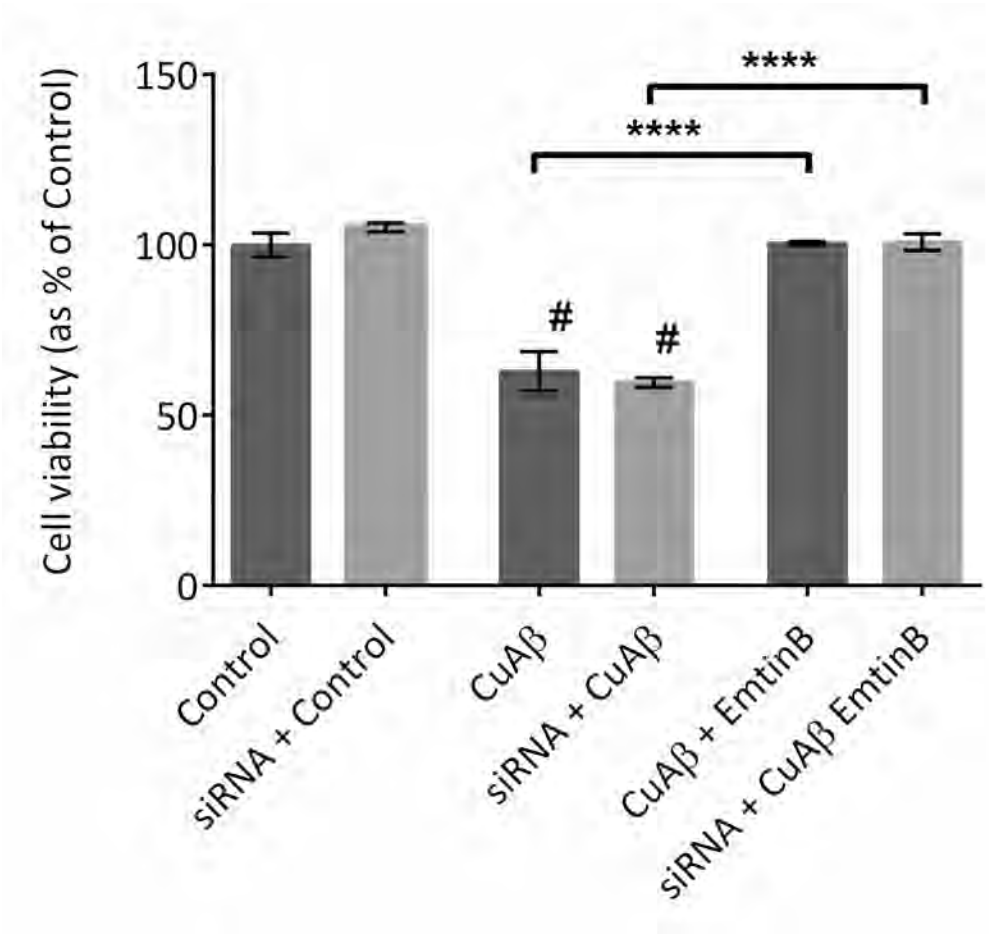

Figure 4.21 Knockdown of LRP1 and LRP2 has no effect on EmtinB protection against CuAβ1-42

Cultured hippocampal neurons either received 25nM siRNA to both LRP1 and LRP2 for 48 hours (LRP^-) or were left untreated as control neurons (LRP^+). At 7DIV control LRP^+ and LRP^-siRNA-treated neurons were treated with; vehicle control, 25µM CuAβ1-42, or 25µM CuAβ1-42 in conjunction with 25µM dimeric EmtinB. CuAβ1-42 caused reduced neuronal viability in both control LRP^+ and LRP^- neurons compared with vehicle control neurons. 25µM dimeric EmtinB improved cell viability relative to CuAβ1-42-only treatment in both LRP^+ and LRP^- neurons cells. One-way ANOVA with Tukey post-test. # = significantly different to control neuron viability ($p<0.05$), **** = $p<0.0001$. All data are means and SEM.

Figure 4.22 LRP1/LRP2 knockdown using 25nM siRNA does not abrogate EmtinB protection against CuAβ1-42 toxicity

EmtinB action against CuAβ1-42 was tested in both siRNA treated neurons and control neurons. Hippocampal neurons were either left untreated (LRP^+) or treated with 25nM LRP1 and LRP2 siRNA for 48 hours (LRP^-) before application of; vehicle control, 25µM CuAβ1-42, or 25µM CuAβ1-42 co-administered with 50µM EmtinB. CuAβ1-42 reduced neuron viability relative to vehicle control neurons and there was no significant difference in CuAβ-42 toxicity between LRP^- siRNA treated and LRP^+ control cells. EmtinB improved the viability of CuAβ1-42 cell relative to CuAβ alone however there was no difference in EmtinB ability to protect against CuAβ1-42 in LRP^- siRNA treated neurons compared with control LRP^+ control neurons. One-way ANOVA with Tukey post-test. # = significantly different to control neuron viability ($p<0.05$), *** = $p<0.001$. All data are means and SEM.

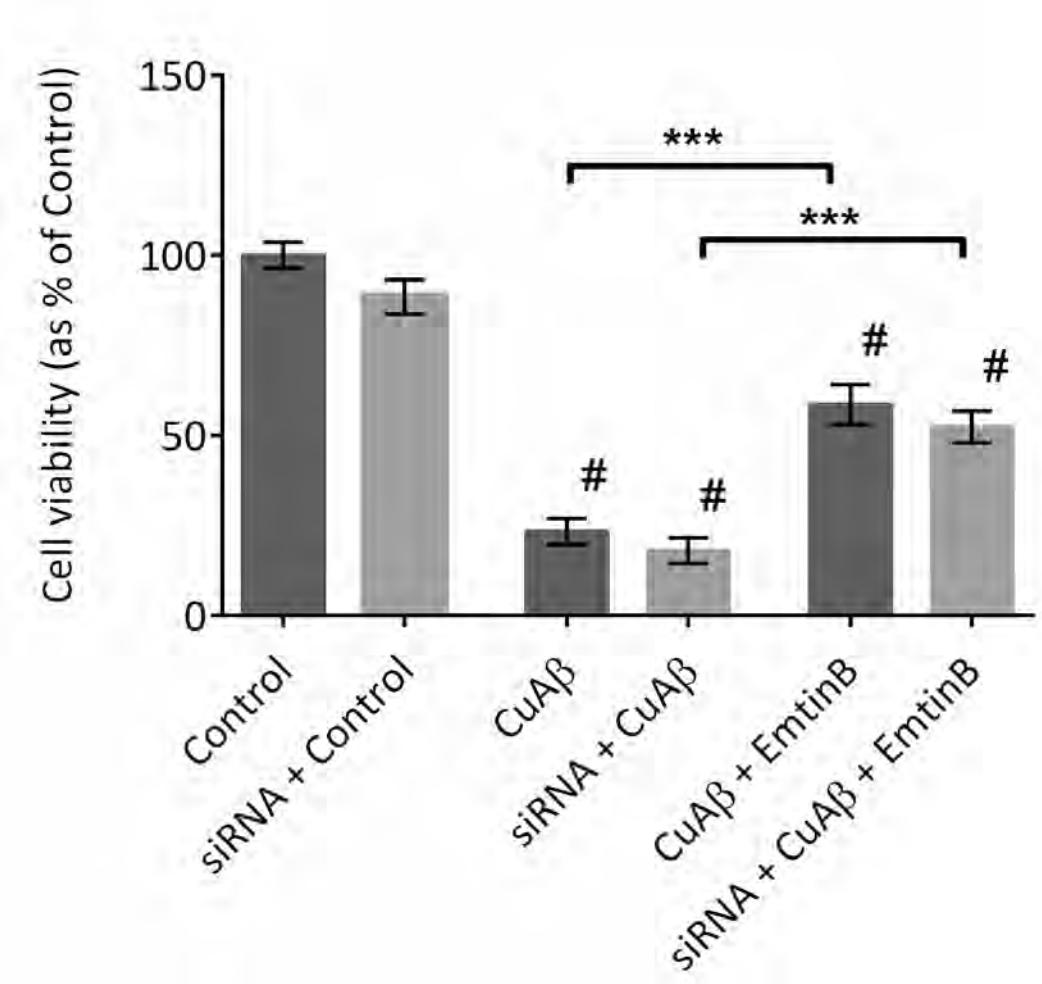
Cell viability (as % of Control)
150
100
50
0
***
***
#
#
#
#
Control
siRNA + Control
CuAβ
siRNA + CuAβ
CuAβ + EmtinB
siRNA + CuAβ + EmtinB

Figure 4.23 EmtinB is taken up into cells within 3 hours of administration

EmtinB, labelled with biotin, was administered to 7DIV cultured hippocampal neurons and fixed at 30 minutes and three hours. To determine basal fluorescence of hippocampal neurons, untreated cells were fixed at 30 minutes. Fixed neurons were immunostained for the cytoskeletal protein tau (green) and for biotinylated EmtinB (red). Untreated neurons (Ai) have minimal autofluorescence in the red channel (Aii , Aiii), while at 30 minutes post treatment (Bi) the biotinylated EmtinB is visible in punctate staining either at the cell surface or within the cell (Bii, Biii; highlighted by arrow). At three hours post EmtinB administration (Ci), diffuse EmtinB staining is observed in the cytoplasm (Cii, Ciii; highlighted by arrow). Scale bar is 25µm.

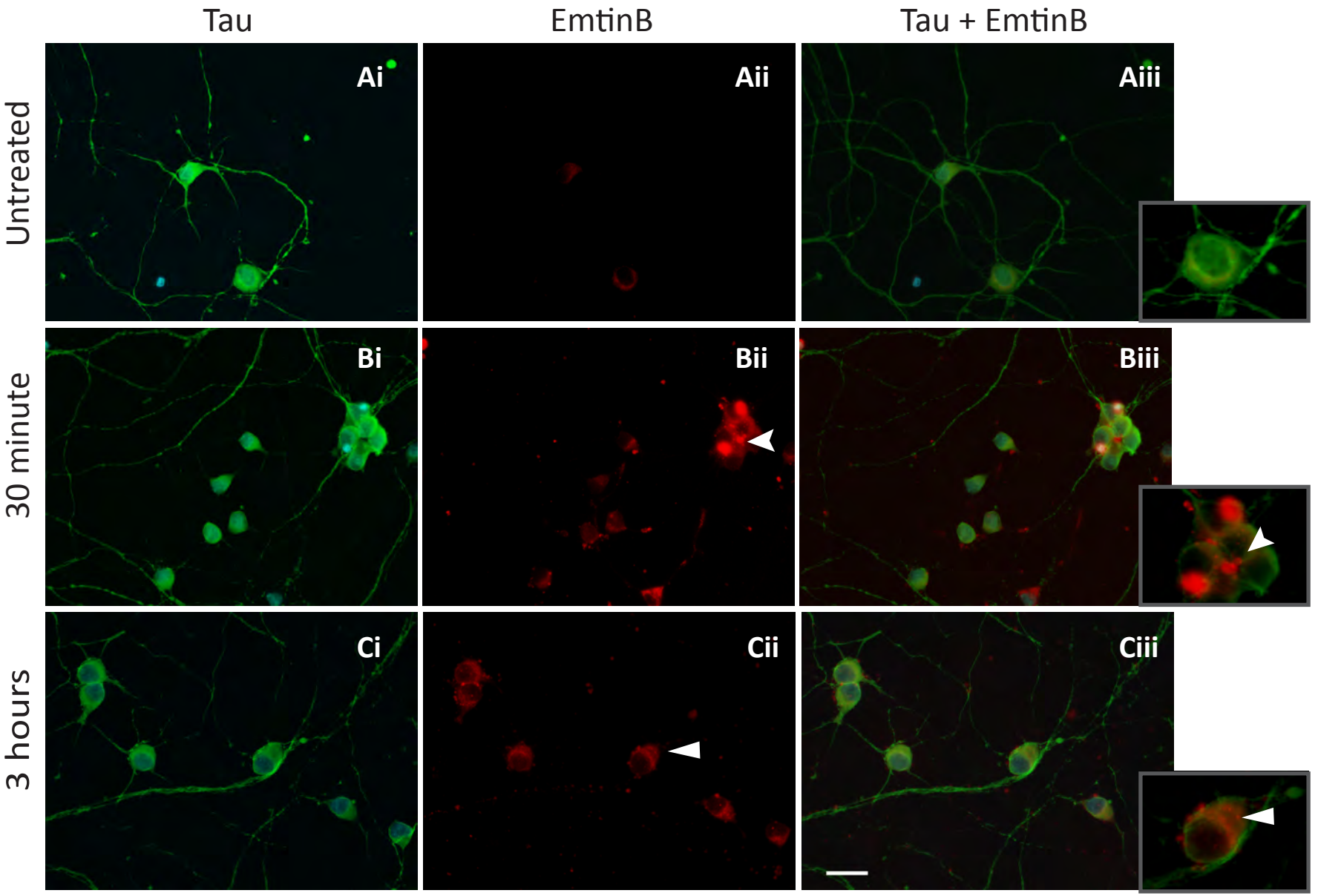
Tau
EmtinB
Tau + EmtinB
Untreated
30 minute
3 hours
Ai
Aii
Aiii
Bi
Bii
Biii
Ci
Cii
Ciii

This mechanism could potentially still be a receptor-related mechanism or perhaps, as the protein is cationic (+5.7 at pH7), could be a mechanism based on the selective uptake of cationic molecule via interaction with the negatively charged cell membrane [205]. To determine if siRNA knockdown of LRP1 and LRP2 affected EmtinB internalisation, neurons were treated with 25nM siRNA to both LRP1 and LRP2 for 48 hours. Control cells were left untreated. Biotinylated dimeric EmtinB (25µM) was added to neurons for 30 minutes or three hours before fixing in 4% paraformaldehyde and EmtinB visualised using ICC. EmtinB puncta were associated with neurons in both siRNA treated and control cells (Figure 4.24ii, i) with no observable difference. Similarly, after three hours incubation, EmtinB was evident in the cytosol of neurons which had been siRNA treated (Figure 4.24iv) and also in the cytosol of control cells (Figure 4.24iii), suggesting that siRNA knockdown of LRP1/2 has no effect on uptake of EmtinB into hippocampal neurons or that, in these experiments, despite siRNA knockdown, there is still sufficient LRP1 and/or LRP2 expressed to enable internalisation of EmtinB.

As the 25nM siRNA treatment did not prevent EmtinB action, the siRNA knockdown was repeated using the maximum siRNA concentration recommended in the manufacturer's instructions; 50nM. Consistent with previous work, CuAβ1-42 produced a decrease in cell viability relative to vehicle control neurons in both untreated and siRNA treated cells (Figure 4.25A). EmtinB (50µM) improved the neuronal viability of CuAβ1-42 treated neurons relative to cell treated with CuAβ alone (Figure 4.25A). This increase was observed equally in both untreated and siRNA treated cells, suggesting that LRP1/2 are not integral to EmtinB mechanism of action. Western blot analysis for LRP1, in control and 50nm siRNA-treated cells, showed a marked decrease in LRP1 levels in the 50nm siRNA treated cells compared with untreated control neurons (Figure 4.25B), indicating that the LRP1 is significantly decreased in these cells with no impact on EmtinB protective capacity.

Figure 4.24 siRNA knockdown of LRP1 and LRP2 has no effect on EmtinB uptake into neurons

EmtinB, labelled with biotin, was administered to control and LRP1/2 siRNA treated cultured hippocampal neurons. Cells were fixed after 30 minutes and three hours and hippocampal neurons were immunostained for Tau (green) and biotinylated EmtinB (red). Nuclei were stained with nuclear yellow (cyan). 30 minutes after EmtinB administration, both control and siRNA treated cells had observable puncta (i, ii; highlighted by arrows). At three hours post administration, both control and siRNA treated cells show more diffuse EmtinB staining in the cytosol (iii, iv; highlighted by arrows) suggesting successful EmtinB uptake. Scale bar is 25μm.

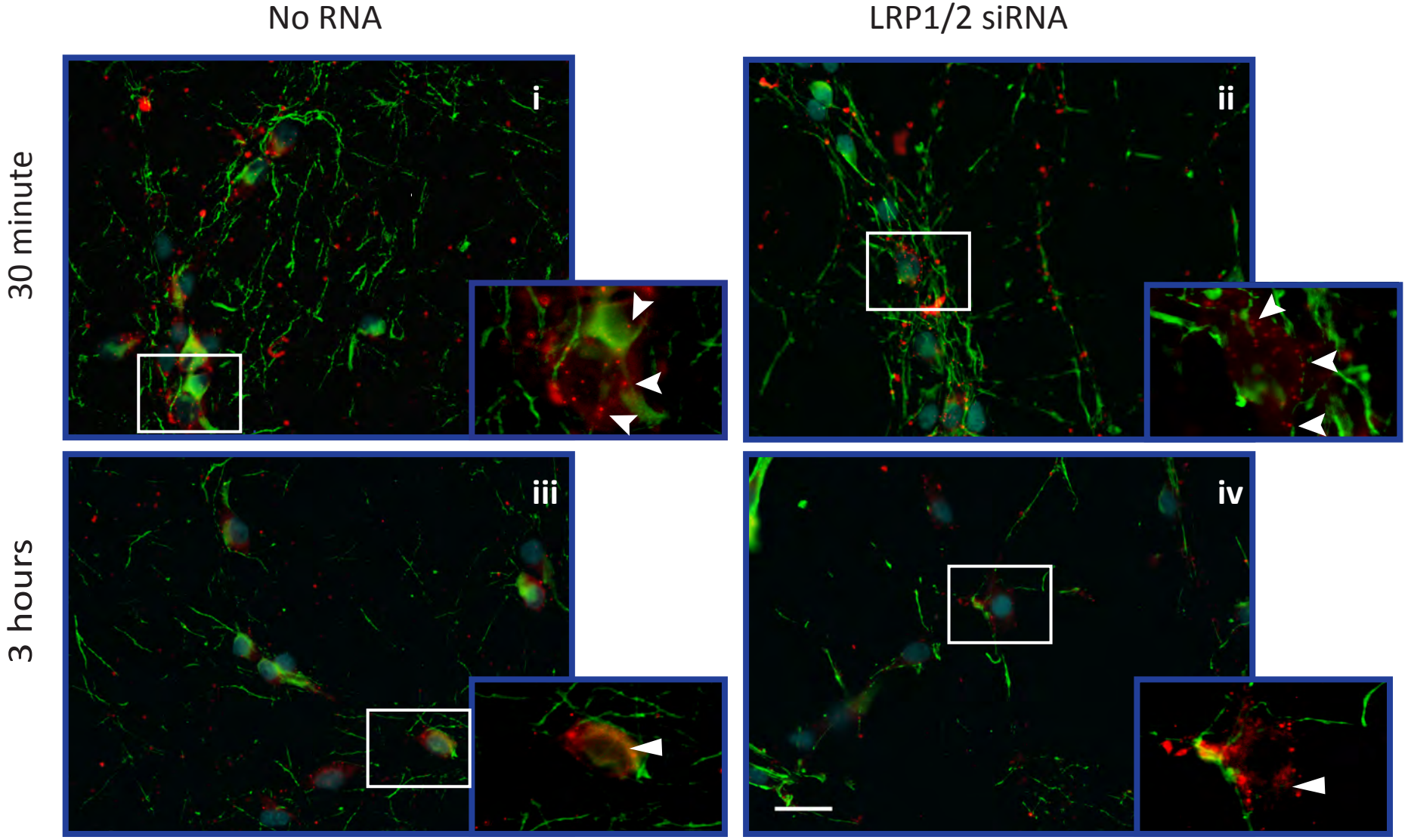
No RNA
LRP1/2 siRNA
30 minute
3 hours
i
ii
iii
iv

Figure 4.25 EmtinB efficacy is not diminished by siRNA knockdown of LRP1 and LRP2

High concentration (50nM) siRNA was used to produce a substantial reduction in LRP1 and LRP2 in 7DIV hippocampal neurons. A) Incubation of siRNA-treated and control cells with 25µM CuAβ1-42 significantly reduced neuronal viability relative to vehicle control cells. Co-incubation of the CuAβ1-42 with 50µM dimeric EmtinB improved cell viability compared with CuAβ1-42 alone, and this recovery was equally apparent in control and siRNA treated neurons. One-way ANOVA with Tukey post-test. # = significantly different to control ($p<0.05$), *** =$p<0.001$. B) Western blot of control and siRNA treated cells shows considerable knockdown of LRP1 in siRNA treated neurons.

A

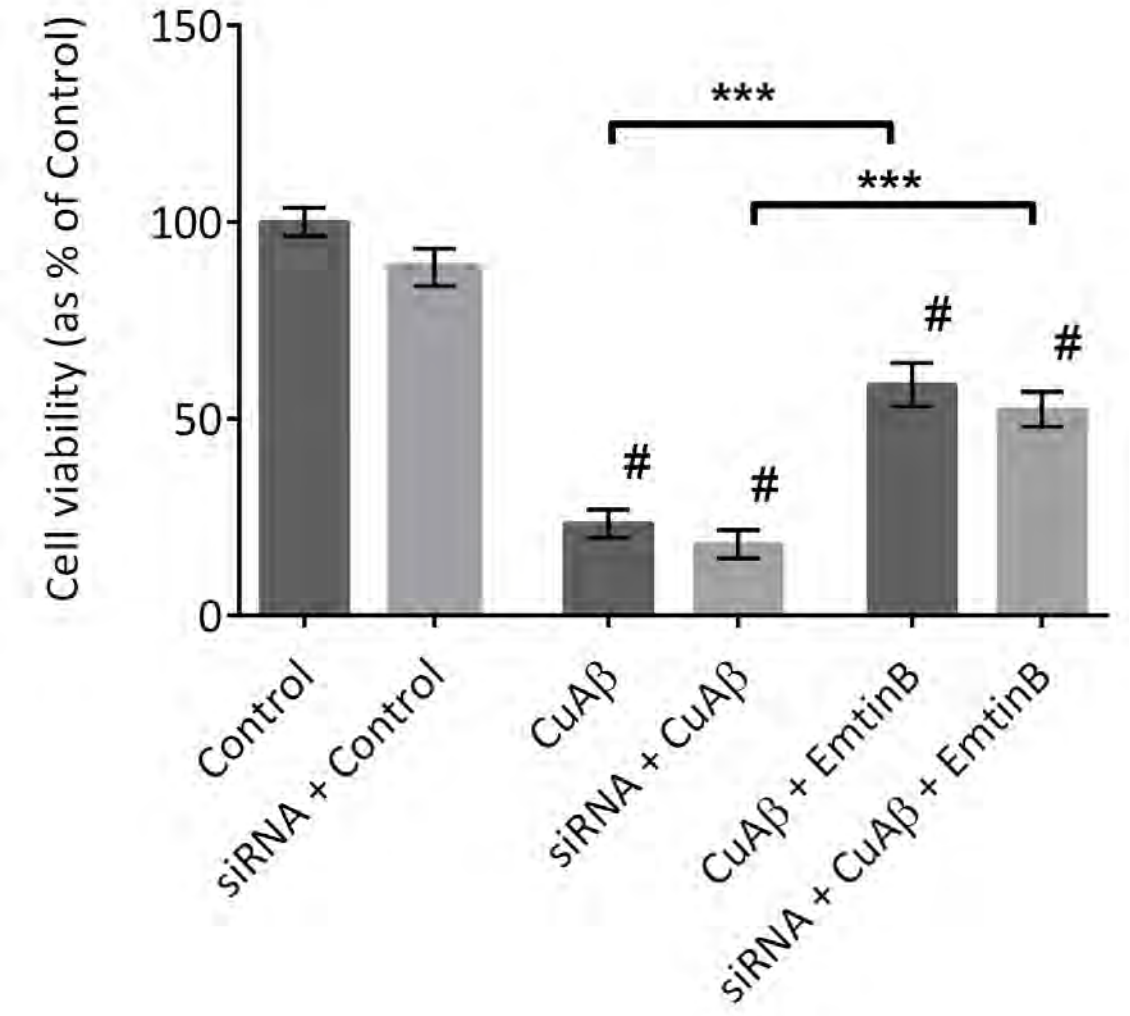
Cell viability (as % of Control)
150
100
50
0
***
***
#
#
#
#
Control
siRNA + Control
CuAβ
siRNA + CuAβ
CuAβ + EmtinB
siRNA + CuAβ + EmtinB

B

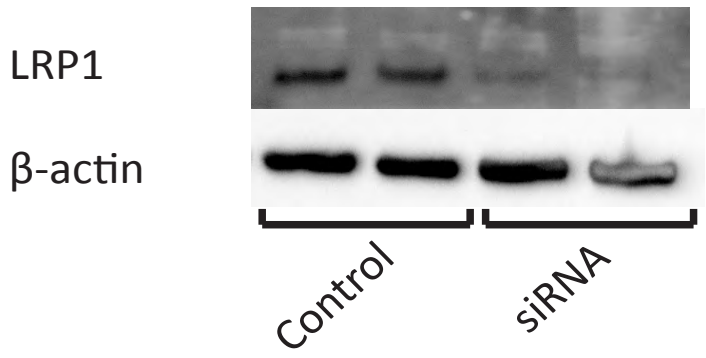
LRP1
β-actin
Control
siRNA

4.4 Discussion and conclusions

This chapter investigated the capacity of EmtinB to protect against CuAβ *via* three main mechanisms; metal swap with CuAβ, protection against reactive oxygen species, and protection *via* an LRP-mediated mechanism. It was established in this work that EmtinB was not able to undergo a metal swap with CuAβ1-42 in its metal-free form (apo), but could prevent the formation of insoluble CuAβ1-42 when metal-bound. Apo-EmtinB was able to protect hippocampal neurons against H_2O_2-induced toxicity and, additionally, LRP receptors were implicated in mediating EmtinB protection against CuAβ since the LRP competitive inhibitor, RAP, blocked EmtinB action. However, experiments using siRNA ablation of LRP1 and LRP2 failed to provide further evidence for the role of these receptors. These findings collectively provide mechanistic insight into the protective capacity of emtins.

4.4.1 EmtinB metal swap

The capacity for EmtinB to bind key biological metals such as, copper and zinc, has not previously been described. MT2 is capable of binding seven zinc ions, or around 12 copper ions, and this is mediated through highly conserved cysteine residues (cys, C), which constitute a large proportion (around 30%) of all amino acid residues. In the MT2 protein, each zinc ion (Zn^{2+}) is coordinated in a tetrahedral geometry by four cysteine residues, while copper is bound as Cu^{+} in a trigonal geometry *via* three cysteine residues [206]. In emtins, a majority of these cysteine residues have been replaced by serine to prevent self-aggregation of the peptide [185] and, consequently, for EmtinB, there are only two cysteine residues in each peptide chain available for metal binding (see Figure 1.7). Based on this decrease in cysteine residues available for metal binding, EmtinB likely has a lower metal-binding capacity than native MT2.

Consistent with this hypothesis, this study found that dimeric EmtinB can bind copper or zinc at a 1:1 ratio *in vitro*. This is in accordance with the presence of 4 cysteine residues, which

presumably supports a single metal binding site. Based upon these data, copper-bound, zinc-bound and metal free dimeric EmtinB were evaluated for their capacity to prevent CuAβ1-42 forming an SDS-insoluble aggregate. While apo-EmtinB was unable to prevent CuAβ1-42 from forming an insoluble aggregate, zinc-bound EmtinB did prevent the formation of an SDS-insoluble CuAβ1-42 aggregate, suggesting that Zn-EmtinB can undergo a metal swap with CuAβ while Apo-EmtinB cannot. Although the current work did not formally prove the existence of a metal swap between EmtinB and CuAβ1-42 *in vivo*, this is consistent with our previous studies with MT2, where zinc-bound MT2 was able to undergo a metal swap with CuAβ to promote the formation of SDS-soluble ZnAβ instead of the SDS-insoluble CuAβ aggregate, while apoMT2 and carboxymethylated MT2 were unable to participate in such a mechanism [159].

One interesting discrepancy is the action of Cu-EmtinB, which also prevented the formation of an SDS-insoluble CuAβ aggregate. In contrast to this, native copper-bound MT2 is unable to prevent the formation of insoluble CuAβ aggregates. It is not clear how Cu-EmtinB mediates this change in CuAβ, however the answer may lie in the copper binding capacity of EmtinB and the specific conformation of Cu-EmtinB.

The metal-binding capacity of MT2 is limited seven divalent metal ions, such as Zn^{2+}. However, MT can bind a larger complement of monovalent metal ions, with studies showing that MT binds around 12 (and up to 15) copper ions [207]. These copper ions are bound by bridging sulphur atoms in two clusters, an $S_{11}Cu_6$ cluster in the β-domain, and an S_9Cu_6 cluster in the α-domain [207]. This indicates that the four cysteine residues present in dimeric EmtinB could potentially support at least two copper ions. Furthermore, EmtinB was found to dimerise when bound to copper (Figure 4.2), unlike apo and Zn-EmtinB, which maintain a monomeric structure (Figure 4.5). It is possible that this conformational difference may alter the metal binding capacity of EmtinB, and/or alter the affinity of EmtinB for copper, such that it can bind additional copper and subsequently remove copper from CuAβ. Interestingly, there is some

evidence for this as EmtinB was found to bind metals at a higher than 1:1 ratio when incubated with both copper and zinc at the same time (data not shown). This phenomenon remains to be fully tested and would be an interesting theory to explore in future studies.

Notably, in Chapter 3 studies it was found that EmtinB, when prepared and applied in apo form, was protective against CuAβ1-42 toxicity. Given that only metal-bound EmtinB can prevent the formation of SDS-insoluble CuAβ aggregates, the ability of EmtinB to "scavenge" metals from media was evaluated. There was no evidence of metal scavenging by EmtinB from either basal cell culture medium or neuron-conditioned culture medium.

While EmtinB is clearly not bound to metals after incubation in media or conditioned media, this may be due to a lack of available copper and zinc in this media. Basal media (Table 4.1) and conditioned media (data not shown), were analysed for copper and zinc by ICP-MS but the results were not definitive. In basal media samples, copper levels appeared higher in media after column fractionation than before, suggesting that copper detection is impeded in whole media. This indicates a potential non-spectral interference created by a factor in the media, which is not present after fractionation of the media on a PD-10 column. This interference might prevent the accurate detection of copper in media samples. This issue may not affect zinc detection, as zinc levels in whole media are higher than total zinc detected in fractions. As we do not have an independent method of determining zinc levels in media, it is possible that zinc detection is also being depressed, however, the concentration of zinc in whole media determined by ICP-MS analysis is consistent with the concentration reported by the manufacturer (0.674µM; Technical resources, Thermofisher scientific, MA, USA).

Ostensibly, these results would indicate that EmtinB is not acting *via* a metal swap mechanism in cell culture experiments, however the data do not exclude the possibility that apo-EmtinB might bind metals when applied to cultured neurons. In adult brain, zinc concentration is approximately 200µM [208, 209] with about 90% of this existing as metalloproteins [210].

Extracellular zinc concentrations in adult brain are estimated to be around 1µM, suggesting that free zinc is not highly available [211]. However, there are some areas of the brain where ionic zinc has been detected in relatively high amounts [210]. Historically, ionic zinc has been detected in the brain using Timm's sulfide-silver staining method, a method which is not able to detect zinc which has been complexed by sequestration proteins [210, 212]. Using this histochemical stain reveals large amounts of chelatable zinc in the cerebral cortex and limbic region of the brain, including the hippocampus, and this zinc is localised in the presynaptic vesicles of neurons [210]. These neurons are termed zincergic neurons and there is evidence that zincergic neurons release sequestered zinc from presynaptic terminals in a calcium and impulse-dependent manner [209].

Zincergic neurons are a subset of glutamatergic neurons and three glutamatergic pathways are evident in the hippocampus. Neurons projecting from the entorhinal cortex to the hippocampus *via* the perforant path, dentate granular neurons projecting to the CA3 pyramidal neurons *via* mossy fibres, and CA3 pyramidal neurons projecting to the CA1 pyramidal neurons *via* the Schaffer collaterals, are all positive for zinc *via* Timm's method [209]. Of these pathways, zinc is most prominent in the synaptic boutons of the mossy fibres [209, 210]. Stimulation of these fibres prompts the release of zinc from pre-synaptic vesicles, resulting zinc release into the synaptic cleft, with estimated concentration ranging as high as 300µM [210]. While this concentration estimate is contentious, with other studies reporting zinc-concentration estimates from nil to 100µM [213, 214] most studies appear to be on agreement that chelatable zinc is produced at the synaptic cleft of zincergic neurons. Given the presence of zincergic neurons in the hippocampus, one possibility in relation to this investigation is that EmtinB is scavenging free zinc from zincergic neurons in the hippocampal neuron cultures, which have been demonstrated to contain glutamatergic neurons [215].

With high local concentrations of synaptic zinc in culture, EmtinB could potentially scavenge zinc released at the synaptic cleft, however there is no evidence to prove or disprove this in the current work. Furthermore, this concept is difficult to investigate as EmtinB is rapidly taken up in culture (see Figure 4.25), making isolating the EmtinB for further analysis without disrupting the protein-metal bond challenging. To investigate this theory, one could use biotinylated EmtinB and incubate this with hippocampal neurons. Cells could then be homogenised *via* trituration and EmtinB removed from the lysate by affinity purification using the biotin tag, and resulting metal content measured by ICP-MS.

In conclusion, EmtinB can undergo a metal swap with CuAβ and can prevent the formation of an SDS-insoluble CuAβ aggregate, but this study has been unable to find evidence that this is occurring in the cell culture model of CuAβ toxicity. As such, the metal swap mechanism cannot be confirmed as the EmtinB mechanism of action.

4.4.2 EmtinB protection against H_2O_2 toxicity

CuAβ has been demonstrated to produce H_2O_2 and then subsequent downstream radicals by Fenton and Harber-Weiss reactions [64, 216-218]. Catalase, the enzyme that catalyses the decomposition of H_2O_2, has been shown to decrease the toxicity of CuAβ in culture, suggesting that intervention to prevent H_2O_2-induced toxicity and the subsequent production of free radicals could be a viable mechanism of protection against CuAβ [121].

In this work, dimeric EmtinB was shown to protect cultured hippocampal neurons against H_2O_2-mediated toxicity, however it is not known if this occurs through direct scavenging activity. Notably, EmtinB protection against H_2O_2 is inconsistent with past work with MT2. While MT2 has a demonstrated an ability to scavenge free radicals [57], it was unable to protect cultured cortical neurons against H_2O_2 toxicity [219]. Furthermore, MT2-protective action against free radicals is mediated by the conserved cysteine residues in the MT2 sequence that form the disulphide bonds responsible for radical quenching. In EmtinB, a

majority of these cysteine residues have been substituted for serine, and it would therefore be predicted that EmtinB is likely to demonstrate lessened oxidant scavenging capacity than native MT. These factors call into question whether this protective action of EmtinB is *via* free radical scavenging or some other mechanism. To elucidate this, future studies should undertake to investigate whether EmtinB is capable of scavenging radicals downstream of H_2O_2 thought to mediate the toxic effect of H_2O_2 - for example hydroxyl radicals.

In conclusion, while EmtinB clearly works to protect cultured cells against H_2O_2, whether this protective effect is a result of free radical scavenging or some other mechanism remains to be elucidated.

4.4.2 LRP-mediated EmtinB protection

Emtins and MT2 have been shown to act through cell surface receptors, LRP1 and LRP2, to activate both MAPK and PI3K pathways, and this activation was associated with neuronal survival after insult [94]. It is therefore possible that EmtinB mechanism of action in culture against CuAβ is a not a result of EmtinB interacting directly with CuAβ, but a result of EmtinB acting on neurons to promote neuronal survival *via* LRP receptors.

Initial investigations into LRP involvement in EmtinB protective action utilised the 39kD receptor associated protein (RAP), a specific inhibitor of the low density lipoprotein receptor (LDLR) family [220], of which LRP1 and LRP2 are members. In this work, RAP prevented EmtinB action against CuAβ toxicity in cultured neurons (see Figures 4.19 and 4.20). While RAP has also been reported to interact with, and bind to, both Aβ40 and Aβ42 peptides [221], in this study RAP treatment alone had no effect on the toxicity of CuAβ, suggesting that RAP-mediated decrease in CuAβ toxicity results from an interaction of EmtinB with a member of the LDLR family of receptors.

Subsequent investigation into this mechanism using siRNA knock-down of LRPs 1 and 2 showed that combined knockdown of LRP1 and LRP2 had no effect on EmtinB action (see Figures 4.23 - 4-27).

The results of this investigation raise two main possibilities. Firstly, the knockdown of LRP1 and LRP2 may not be sufficient to impede EmtinB action. While LRP1 appeared to be significantly reduced when analysed by western blot, LRP2 knockdown could not be established. Future studies could address this by using qPCR to quantify LRP2 knockdown rather than protein detection techniques, and, additionally, by using a functional test for LRP knockdown, such as neurite extension, in response to known stimulators. A complimentary evaluation of receptor activation would be examination of downstream targets of receptor activation.

Secondly, it may be that EmtinB is not acting through LRP1 or LRP2 in this model, but through another member of the LDLR family. RAP is a known inhibitor of both LRP1 and LRP2, but has also been shown to bind strongly to the very-low-density-lipoprotein (VLDL) receptor [222] and Apolipoprotein2 (ApoER2) receptor [223]. The VLDL receptor is found in a wide variety of body tissues, including the brain, where it is found predominantly in the cortex and cerebellum (reviewed in [224]) and has been shown to play a role in neuronal migration and signal transduction [225]. ApoER2, by comparison, is found almost exclusively in the CNS and is expressed in the cerebellum, cortex, olfactory bulb and hippocampus, and plays a role in neuronal signalling (reviewed in [224]). The role of ApoER2 in the hippocampus appears to be of greater import than VLDLR, as ApoER2 KO mice have more pronounced hippocampal defects and greater deficit in hippocampal long term potentiation (LTP) than VLDLR deficient mice [224, 226]. These LDL family receptors may represent a viable alternative receptor for EmtinB action.

Conclusion

Despite intensive investigation, a definitive mechanism of action for EmtinB in the *in vitro* CuAβ model of toxicity was not determined. There is evidence that dimeric EmtinB can undergo a metal swap with CuAβ, protect hippocampal neurons against hydrogen peroxide toxicity, and potentially act through members of the LRP-family of receptors to promote neuronal survival. As EmtinB appears to be capable of working *via* more than one mechanism against CuAβ-associated toxicity, it could be acting synergistically to address CuAβ toxicity through two, or more, of these mechanisms.

Chapter 5 – EmtinB protection in a small animal model of Alzheimer's disease

5.1 Introduction

The ability of MT to protect against multiple mechanisms of Aβ toxicity *in vitro* suggests that it might be a potential modulator of disease progression in AD. However, native metallothionein has minimal brain uptake when administered peripherally [162]. For that reason, this thesis has explored the potential of metallothionein-derived synthetic peptides, Emtins, to act as neuroprotective agents. In previous chapters, EmtinB demonstrated significant protection against CuAβ-induced neurotoxicity in cell culture and, furthermore, the ability of tetrameric EmtinB to cross the BBB following peripheral administration *in vivo* has been reported [184]. The work reported in this chapter investigates the effect of EmtinB upon amyloid plaque deposition and cognitive impairment was investigated in the APPswe/PS1ΔE9 mouse model of AD.

This APPswe/PS1ΔE9 mouse model is an extensively used model of AD and incorporates both the Swedish familial double mutation (K670N, M671L) in APP (APPswe) and the ΔE9 exon deletion in presenilin 1 (PS1ΔE9), both of which are associated with early onset AD [227]. The Swedish familial APP mutation causes altered processing of APP and, subsequently, an increase in Aβ1-40 and 1-42 peptide fragments [228]. Mouse models with this APP mutation show Aβ accumulation and amyloid pathology [228]. The ΔE9 mutation in PS1 exacerbates this by promoting the formation of the Aβ1-42 peptide fragment, which, *in vivo*, is shown to be more prone to aggregation than the Aβ1-40 fragment [228].

Like other animal models of AD, the APPswe/ PS1ΔE9 mouse model does not fully recapitulate all of the pathological aspects of Alzheimer's disease as there is no frank loss of neurons [229];

however, they do display a variety of clinically relevant symptoms of AD [229]. In this model, APP levels are around two to four times higher than in non-transgenic mice [228]. Higher APP levels, along with mutant PS1, promote the early formation of plaques and deposition occurs in these mice at around six to seven months of age with abundant plaques observed in both the hippocampus and cortex by nine months of age [228]. Apart from early plaque deposition, APPswe/ PS1ΔE9 mice also exhibit memory deficits around 6 months of age, mild neuritic abnormalities, loss of neuronal activity related to plaque load, and activated astrocytes and microglia associated with plaques [229]. As such, the APPswe/ PS1ΔE9 model of AD represent a valuable device for testing therapeutic approaches, particularly those targeting plaques and inflammation [229].

To systematically evaluate the potential beneficial effects of EmtinB in APPswe/ PS1ΔE9 mice, this study tested 3 key hypotheses:

1) That EmtinB treatment will reduce the accumulation of Aβ in the APPswe/ PS1ΔE9 mouse brain,
2) That EmtinB will modify glial activation in the brains of APPswe/ PS1ΔE9 mice, and
3) That EmtinB will preserve synaptic architecture, correlating with improved cognitive outcomes, in APPswe/ PS1ΔE9 mice.

Firstly, it will be determined if EmtinB can act to decrease amyloid accumulation in the APPswe/PS1ΔE9 mouse brain. To determine if Aβ levels are altered in EmtinB treated mice, plaque load, soluble Aβ1-42 levels and APP levels will be determined in treated and control mice. As EmtinB and MT are known to act through LRP receptors, and LRP receptors are also known mediators of Aβ clearance, LRP levels will also be assessed.

Secondly, glial activation will be investigated. Aβ is known to increase activation of both astrocytes and microglia. This activation is linked with inflammation. To assess if EmtinB is able to affect glia, IBA1 and GFAP protein will be assessed for changes in microglia and astrocytes respectively.

Lastly, Aβ has been shown to interrupt long term-potentiation in culture and hippocampal brain slice. EmtinB has previously been shown protect LTP in the face of Aβ insult (Paul Adlard, Florey Institute, Vic, AUS, unpublished data). Changes in LTP have been demonstrated to coincide with changes in synaptic proteins. Potentially, then, EmtinB could be modulating synaptic changes in the hippocampus to improve memory deficits in APPswe/PS1ΔE9 mice. To investigate synaptic changes, both synaptophysin and PSD95 levels will be analysed in hippocampal enriched tissues from EmtinB treated and control APPswe/PS1ΔE9 mice.

This chapter will explore changes in cognitive outcomes, and histological and biochemical characteristics, in the APPswe/PS1ΔE9 mouse model of AD in response to dimeric EmtinB administration.

5.2 Methods

5.2.1. Injection and gavage of B6 mice with EmtinB dimer

To determine the most appropriate method of EmtinB administration for the EmtinB trial, aged B6 mice, between 8 and 11 months old, were either injected subcutaneously or gavaged with 20mg/kg biotinylated dimeric EmtinB (method 2.2.9). Three mice were used for each method of administration and two mice were used as an untreated control.

5.2.2. Analysis of EmtinB in brains of injected APPswe/PS1ΔE9 mice

Having established that EmtinB was detectable in serum after injection, it was necessary to determine if EmtinB could be detected in the brain after subcutaneous injection. In this

experiment aged APPswe/PS1ΔE9 mice between 16 and 18 months old were utilised. Four mice in total were used with two mice injected and two mice used as untreated controls.

Mice were injected and euthanised as described in method 2.2.9. In addition to serum collection, brain tissue was also collected from these animals. The mice were terminally anaesthetised with sodium pentobarbitol, injected intraperitoneally (100mg/kg), then perfused through the heart with room temperature PBS, using a 22G needle, until the liver was pale and the perfusate ran clear. The brain of each mouse was then rapidly dissected out and a small sample of cortical tissue separated from the rest of the hemisphere. The cortical sample and hemisphere were then snap-frozen in liquid nitrogen for later biochemical analyses.

5.2.3 Animal trial: Administration of dimeric EmtinB to APPswe/PS1ΔE9 mice

5.2.3.1 EmtinB trial: administration, cognitive assessment and tissue collection

Preparation, administration, behavioural analysis and tissue collection were performed by Associate professor Paul Adlard et al. (The Florey Institute of Neuroscience and Mental Health, Parkville, Vic). All protocols for the above named sections are summarised from procedural notes supplied by Associate Professor Paul Adlard and herein denoted by an asterisk, *.

*5.2.3.2 Mice for EmtinB trial**

A cohort of 44 APPswe/PS1ΔE9 mice was used to investigate the effect of EmtinB on AD pathogenesis *in vivo*. All mice were female and born on the 27/12/11. For control vs APPswe/PS1ΔE9 comparison in the Y-maze six B6 mice and ten APPswe/PS1ΔE9 mice were used.

*5.2.3.3 Preparation of EmtinB**

Dimeric EmtinB was reconstituted in sterile saline at 15mg/kg and administered at either 5mg/kg or 30mg/kg, as indicated.

*5.2.3.4 Dosing protocol**

EmtinB was administered 5 times per week, Monday-Friday, by subcutaneous injection at the nape of the neck. Mice were dosed daily for two months from nine months of age (19/9/12) until 11 months (5/12/12) of age.

*5.2.3.5 Y-maze assessment of mice**

Treated and untreated APPswe/PS1ΔE9 mice were randomised using the randomise function in Microsoft Excel. Each mouse was randomly assigned a closed arm and starting arm out of the possible arms 1, 2 or 3. Mice were placed into the start arm of the maze with the novel arm closed off, and allowed to explore the open arms (called “start” and “other” arms) of the maze for ten minutes. Mice were removed from the maze after ten minutes and returned to their cage for a period of one hour. Mice were then returned to the start arm of the Y-maze and their movement analysed for one and five minutes using Ethovision. Raw data was analysed by chi-square analysis (data falling outside two standard deviations was not included in the analysis), and by linear regression (all data included) using PRISM software (GraphPad Prism, version 6, La Jolla, CA, USA). Mice were coded and EmtinB administered in a blinded manner. Drug administration and behavioural analyses were not carried out by the same researcher.

*5.2.3.6 Tissue collection**

Blood and serum samples were collected as per method 5.2.2. The trial mice were then transcardially perfused with PBS. The brains of five animals from each group were fixed in 4% PFA overnight then transferred to 30% sucrose/PBS. The remaining animal brains were dissected to remove the left-hand hemisphere cortex, hippocampus and cerebellum, while the right hemisphere was kept intact for whole brain analysis. These unfixed tissues were snap frozen in liquid nitrogen and cryogenically stored until required.

5.2.4 Immunohistochemical (IHC) analysis of EmtinB trial brain

5.2.4.1 Paraffin embedding of EmtinB trial brain

Brains were prepared by excising a section of the right hand hemisphere of the brain between bregma -4 and bregma -0.5. Brain sections were then prepared for embedding with paraffin infiltration. Brain sections were put into labelled cassettes and processed as per the automated mouse brain protocol, in brief:

Reagent	**Incubation time (minutes)**	**Temperature (°C)**
70% ethanol	30	37
95% ethanol	40	37
Absolute ethanol	30	37
Absolute ethanol	30	37
Absolute ethanol	40	37
Xylene	45	37
Xylene	45	37
Paraplast wax	60	60
Paraplast wax	60	60
Paraplast wax	60	60

Infiltrated tissue was then placed into an embedding basin with the -4 bregma oriented toward the bottom of the basin. The basin was then partially filled with warm paraffin and the tissue held steady with forceps while the paraffin was set by placing the basin onto a cold-plate. When this layer of paraffin was set, a plastic backing was placed over the basin and the basin fully filled with paraffin. The basin was then moved to a cold-plate until completely set, then stored at 4°C overnight. Once solid, the paraffin blocks were removed and excess paraffin trimmed from the blocks using a scalpel blade. Paraffin blocks were stored at room temperature.

5.2.4.2 Sectioning of EmtinB trial fixed brains

Prior to sectioning, blocks were placed in ice for five minutes to chill. Brains were then sectioned into 5µm sections on a microtome (Microm HM325, Thermofisher scientific, MA, USA). Sections were then placed into a 37°C water bath and floated onto glass slides (FLEX ICH microscope slides Ref #8020; Dako, Glostrup, Denmark), then dried overnight in a 37°C drying oven. Sections were stored at room temperature.

5.2.4.3 Dewaxing slides

Sections for staining were taken from approximately bregma -1.34mm to -2.3mm as per the work of Wright [230]. Slides were heated to 65°C for 30 minutes prior to dewaxing to assist with paraffin removal. The dewaxing and hydration of the sections was carried out by immersion in xylene twice for three minutes each, and then 100% ethanol, 95% ethanol and 70% ethanol for two minutes each. Slides were briefly submerged in tap-water and then stored in PBS until required for staining.

5.2.4.4 Antigen retrieval

Brain sections were incubated in concentrated formic acid for eight minutes then washed six times for five minutes each time in immuno wash solution (method 2.1.32).

5.2.4.5 Immunodetection of GFAP and Aβ in trial brains

Slides were blocked for 15 minutes at room temperature using Dako serum-free block (Dako, Glostrup, Denmark). EmtinB trial brains were immunostained using MOAB2 antibody (M-1586-100, Biosensis, SA, AUS) directed against Aβ1-40 and Aβ1-42 to detect Aβ plaques.

Primary MOAB2 antibody was diluted in immuno diluent (method 2.1.31) and applied for one hour at room temperature, then incubated overnight at 4°C. Slides were washed with immuno wash solution (method 2.1.32) three times for ten minutes each wash. Secondary antibodies were diluted in immuno diluent and incubated on slides in the dark for two hours at room temperature before being washed three times in immuno diluent for ten minutes each wash.

Slides were rinsed in PBS (method 2.1.5), then briefly dried before coverslips were mounted using Dako permafluor mounting medium (Dako, Glostrup, Denmark). Slides were dried in the dark for two days, then the coverslips were sealed using clear nail polish (Cutex, clear; Priceline Pharmacy, TAS). Nail polish was dried at room temperature for four hours before the slides were transferred to a -20°C freezer for two days before imaging.

5.2.4.6 Imaging of immunostained trial brain sections

All images were taken on a spinning disk confocal Nikon TE-2000 inverted microscope with a Yokagawa CSU-22 confocal scanning unit and a Hamamatsu C9100-02 EMCCD camera using the 10x objective.

5.2.4.7 Plaque load analysis of MOAB-2 stained trial brains

Confocal images of MOAB-2 stained trial brain images were segmented using a custom plugin for the ImageJ software package [231] which used a random forest classifier, developed in-house by Aidan O'Mara (manuscript in preparation, Wicking Dementia Research and Education Centre, UTAS), to distinguish between pixels that represented Aβ pathology and background as described by [232]. The classifier was trained using a random selection of

cropped images from the data set which were annotated with examples of pathology and background pixels to produce a forest of 50 trees with a maximum depth of nine nodes. Each tree considered only a random bag of 5% of the training pixels, sampled with replacement. Aβ deposits in the segmented images were then counted and measured using ImageJ's "Analyze Particles" tool with the region of interest defined. The region of interest was drawn for each image using the cortical regions of the hemispheres down to the rhinal fissure. Significance was determined using a one-way ANOVA with Tukey post-test and PRISM software (GraphPad Prism, version 6, La Jolla, CA, USA).

5.2.5 Protein extraction from frozen trial brain whole hemispheres or hippocampal enriched samples

Protein from whole hemispheres and hippocampal enriched brain tissue was extracted in RIPA buffer using the method described previously (method 2.2.10).

5.2.6 ELISA analysis of soluble human Aβ1-42 (hAβ1-42) in trial brains

ELISA analysis of soluble hAβ1-42 was carried out on whole hemisphere RIPA extracts as per the kit instructions. In brief, each sample was diluted at 1:1, 1:2, 1:4, and 1:8 in the provided diluent. Samples were then added to the ELISA plate and an equal volume (50µL) of the provided detection solution was added to each well. These were incubated overnight at 4°C. Wells were washed with the appropriate wash buffer four times for 30 seconds each time, then the HRP antibody (100µL) was added and incubated for 30 minutes at room temperature. A further four washes of 30 seconds each were performed, and the chromagen substrate (100µL) added. After 25 minutes incubation at room temperature, the stop solution (100µL) was added to each well. The absorbance of the wells was read immediately at 450nm on a SpectraMax M2 plate reader (Molecular Devices) running the SoftMax Pro computer program (v 4.8).

Significance was determined using a one-way ANOVA with Tukey post-test and PRISM software (GraphPad Prism, version 6, La Jolla, CA, USA).

5.3 Results

5.3.1 EmtinB is present in serum after injection but not gavage.

To determine a reliable method of EmtinB administration, biotinylated dimeric EmtinB was administered to B6 mice at 20mg/kg *via* either subcutaneous injection or gavage. Serum was harvested 45 minutes after administration and biotinylated EmtinB was detected by western blot. As there is no antibody available for EmtinB, the peptide was detected using the biotin tag. An initial western blot of the samples randomised across a gel showed that serum from injected animals contained a biotinylated protein at low molecular weight (estimated to be around 4kDa), while control and gavaged animals had no bands at this molecular weight (Figure 5.1A). This suggests that biotinylated EmtinB is observable in serum 45 minutes after injection, but that dimeric EmtinB is not able to pass through the gut and into the bloodstream. To confirm that these low molecular weight bands were consistent with EmtinB, a second western blot using representative samples from each treatment group compared the small protein bands to a control sample of biotinylated EmtinB (Figure 5.1B). The low MW band observed in the EmtinB injected mouse serum was consistent with migration of the biotinylated EmtinB control, suggesting that EmtinB was present in serum from injected mice, but not in serum from control or gavaged mice.

5.3.2 EmtinB is not detected in brain after injection

The capacity for EmtinB to pass into the brain after injection was tested in APPswe/PS1ΔE9 mice. Aged APPswe/PS1ΔE9 mice were injected with biotinylated dimeric EmtinB at 20mg/kg and the serum collected along with cortical and whole-hemisphere brain samples.

Figure 5.1 EmtinB is present in serum after subcutaneous injection but not after gavage

Serum from B6 control untreated mice (n=2) was analysed by western blot alongside serum from mice injected (n=3) or gavaged (n=3) and with biotinylated EmtinB dimer (A). Low molecular weight biotinylated protein was observed in the serum of injected mice, but not gavaged or control mice. Comparison of a subset of these samples with monomeric biotinylated EmtinB dimer (B) shows that the low molecular weight protein observed in serum from injected mice is consistent in size with biotinylated EmtinB.

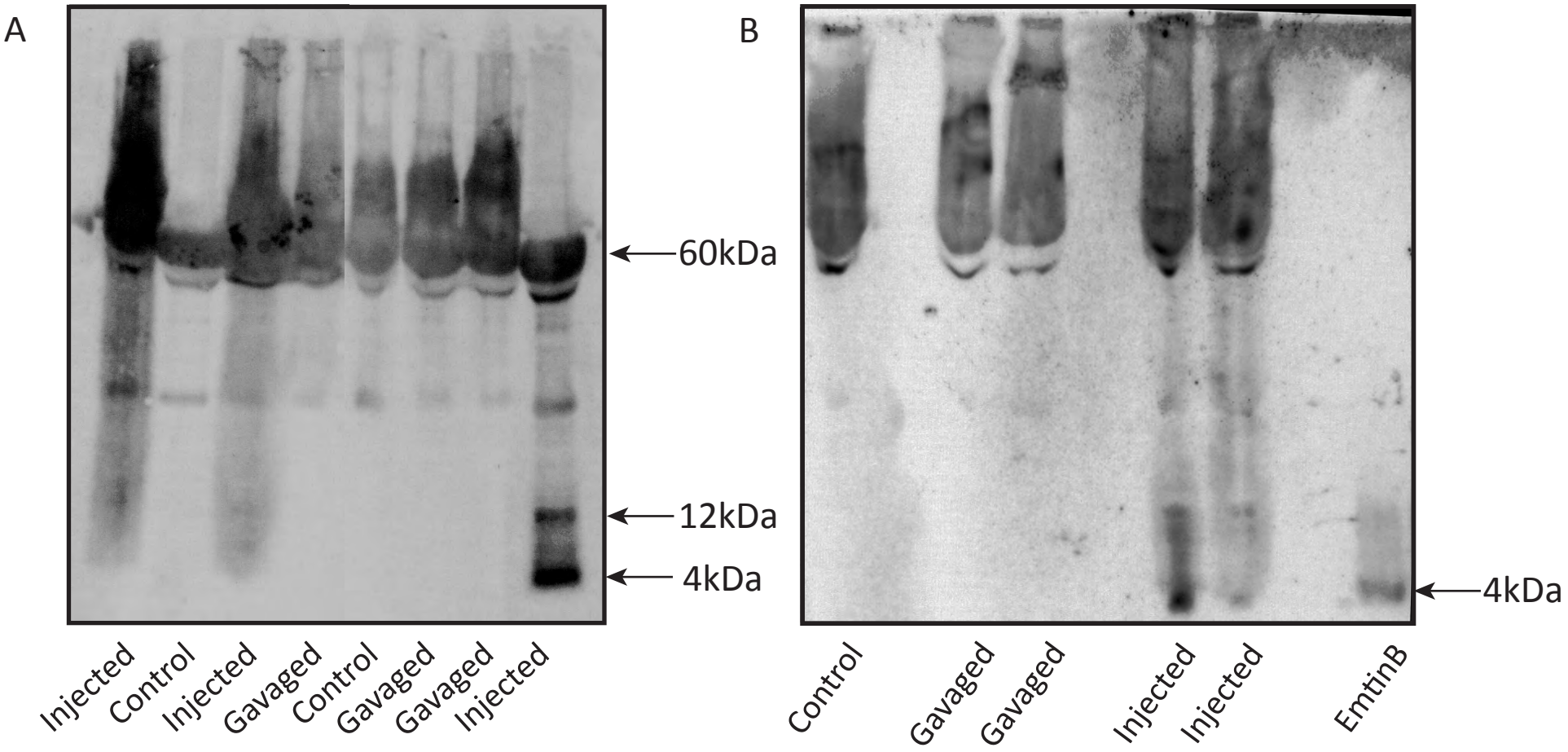
A
60kDa
12kDa
4kDa
Injected
Control
Injected
Gavaged
Control
Gavaged
Gavaged
Injected
B
4kDa
Control
Gavaged
Gavaged
Injected
Injected
EmtinB

Analysis of serum samples from control untreated and EmtinB-injected mice was carried out by western blot. Western blot analysis shows small biotinylated protein consistent with EmtinB present in the serum of injected mice, but not in untreated control mice (Figure 5.2A), showing that EmtinB is present in the serum of the EmtinB-injected APP mice 45 minutes post administration. A second western blot was carried out on cortical and whole hemisphere extracts. No EmtinB was detected in the cortical or whole hemisphere samples (Figure 5.2B).

5.3.3 EmtinB administration improves Y-Maze performance in APPswe/PS1ΔE9 mice

The effect of EmtinB administration on cognition was examined in an EmtinB animal trial using APPswe/PS1ΔE9 mice. A cohort of APPswe/PS1ΔE9 mice were treated five times per week with 5mg/kg EmtinB (n=14) or 30mg/kg EmtinB dimer (n=14) or sterile saline vehicle control (n=15). Mice were dosed with EmtinB dimer for a period of two months, from 9-11 months of age. At 11 months, trial APPswe/PS1ΔE9 mice were tested in a Y-maze to determine if EmtinB administration improved cognitive function (method 5.2.3.5). Analysis of this data was carried out using two statistical tests. In the first instance a chi-square test was performed, wherein time spent in the novel arm is compared with an expected value of 33%, which is determined based on the assumption that mice would spend an equal amount of time in each arm of the maze if they had no memory of the maze. The chi-square analysis provides information about whether the individual groups (SSV control and EmtinB treated groups) mice spent more or less time in the novel arm than expected by random chance, which gives an of indication memory loss. However, a chi-square analysis does not allow for a direct comparison of EmtinB treated and SSV control animals. A second analysis was carried out, using linear regression, where the EmtinB treatment groups were directly compared with the saline vehicle control group, with the dose of EmtinB (from zero to 30mg/kg) tested for its interaction with the dependent variable (time spent in the novel arm). To establish that APPswe/PS1ΔE9 exhibit

Figure 5.2 EmtinB is detectable in serum but not in brain after subcutaneous injection

Serum from control untreated APPswe/PS1ΔE9 mice (n=2) and APPswe/PS1ΔE9 mice injected with biotinylated dimer EmtinB (n=2) was analysed by western blot (A) 45 minutes after injection. EmtinB was detected in serum from injected, but not control, APPswe/PS1ΔE9 mice. Whole-hemisphere and cortex-only brain extracts were also analysed for EmtinB presence (B). No EmtinB was detectable in EmtinB-injected or control brain extract, in either whole hemisphere (Bi) or cortical (Bii) extracts.

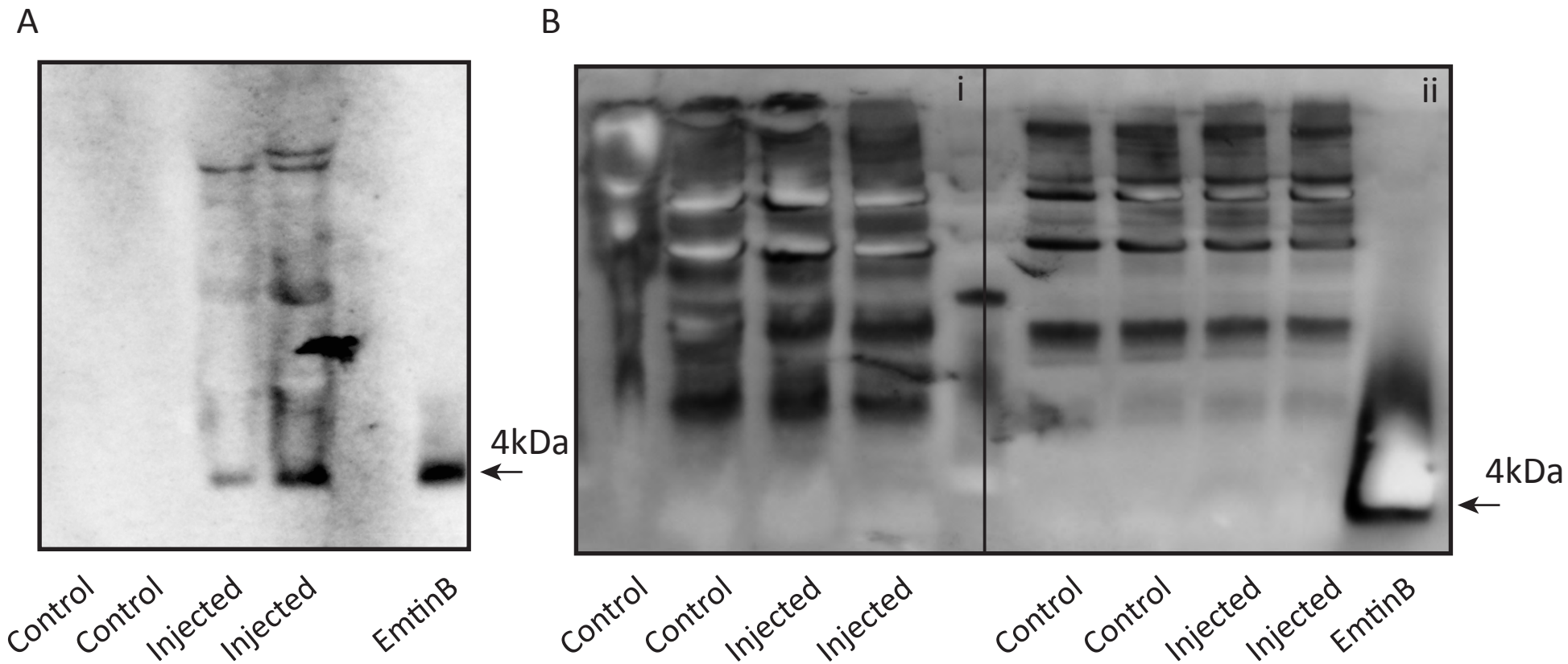
A
B
i
ii
4kDa
4kDa
Control
Control
Injected
Injected
EmtinB
Control
Control
Injected
Injected
Control
Control
Injected
Injected
EmtinB

an impairment that can be measured using Y-maze, an initial Y-maze trial was carried out by Adlard et al. (Florey Institute, VIC, AUS) to compare APPswe/PS1ΔE9 mice and B6 controls. This test showed that during the one minute test, APPswe/PS1ΔE9 mice spent significantly less time in the novel arm of the maze compared with control mice (Figure 5.3), confirming that APPswe/PS1ΔE9 mice exhibit impaired memory.

5.3.3.1 Chi-square analysis

When EmtinB treated and SSV control mice were tested in the Y-maze, chi-square analysis showed that untreated APPswe/PS1ΔE9 mice spent 35.51% (±5.23%) of their time in the novel arm of the Y-maze at one minute post entry (Figure 5.4A), which was not significantly different from the expected value of 33%, once again confirming cognitive impairment. Conversely, mice treated with EmtinB at 5mg/kg spent a significantly larger percentage of their time (62.62 ± 8.27%) in the novel arm of the maze. Mice treated with 30mg/kg also spent significantly longer in the novel arm (43.45 ± 11.56%), however the effect was not as pronounced as the 5mg/kg mice.

Chi-square analysis at five minutes post entry (Figure 5.4B), showed, that once again, untreated APPswe/PS1ΔE9 mice did not spend significantly longer in the novel arm of the Y-maze (33.88 ± 3.63%) than the expected value of 33%. Mice treated with EmtinB at 5mg/kg again spent a larger percentage of their time (46.84 ± 3.26%) in the novel arm of the maze although this was not significant. Mice treated with 30mg/kg spent 39.81% (± 3.37%) of their time in the novel arm, however this was not statistically significant compared with the chance value of 33%.

These animal studies were undertaken by A/Prof Paul Adlard (Florey Institute), and raw data and tissue samples (fixed and frozen brain) were subsequently analysed by the current author as part of this thesis.

Figure 5.3 APPswe/PS1ΔE9 mice show reduced cognitive capacity in the Y-maze compared with control B6 mice

12 month old APPswe/PS1ΔE9 mice and wild-type B6 controls were assessed for cognitive capacity using the Y- maze. To test cognitive capacity, mice were allowed to explore the two open arms (Called “start” arm and “other” arm) of the maze for ten minutes before being removed from the maze for a period of one hour. Mice were then returned to the Y-maze for one minute with all three arms of the maze accessible. Wild-type B6 control mice spent significantly longer in the novel arm of the Y-maze than their APPswe/PS1ΔE9 counterparts. Graph shows percentage of time mice spent in each of the arms. Data presented as mean and SEM. ANOVA with bonferroni post hoc analysis ($p<0.05$).

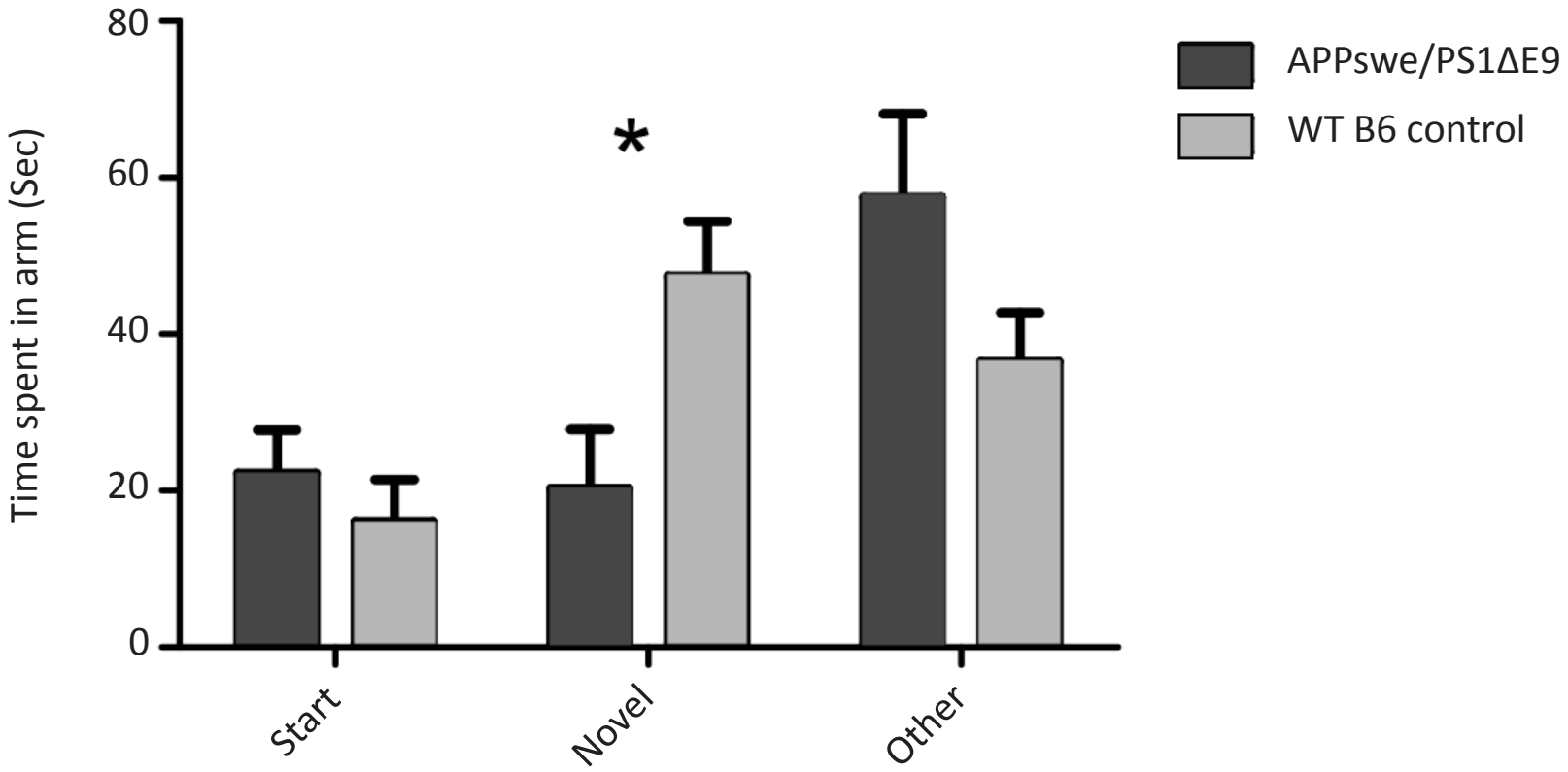
80
60
40
20
0
Time spent in arm (Sec)
*
Start
Novel
Other
APPswe/PS1ΔE9
WT B6 control

Figure 5.4 EmtinB treated APPswe/PS1ΔE9 mice show reduced cognitive impairment compared with sterile saline treated control mice

APPswe/PS1ΔE9 mice treated with either EmtinB at a low dose of 5mg/kg (n=14) or a high dose of 30mg/kg (n=11), or with a control dose of Sterile Saline Vehicle (SSV; n= 15) were assessed for cognitive capacity using the Y- maze. Mice explored the two accessible arms of the maze for ten minutes before being removed from the maze for one hour. Mice were returned to the Y-maze for A) one minute and B) five minutes, with all three arms of the maze accessible and the time spent in the novel arm of the maze was analysed using chi-square analysis, where time spent in the novel arm was compared with an expected value assuming random chance (33%). A) SSV mice did not spend significantly more time in the novel arm than the 33% expected value. Both 5mg/kg and 30mg/kg EmtinB-treated mice spent significantly longer in the novel arm of the maze than the expected 33%, with 5mg/kg treated mice performing better that the 30mg/kg treated mice. B) While there was a trend for 30mg/kg -treated mice to spend longer in the novel arm of the maze than SSV, this was not statistically significant. Mice treated with 5mg/kg EmtinB spent significantly longer in the novel arm of the maze. $p<0.05$. Values are mean and SEM.

A 1 minute post -first arm entry

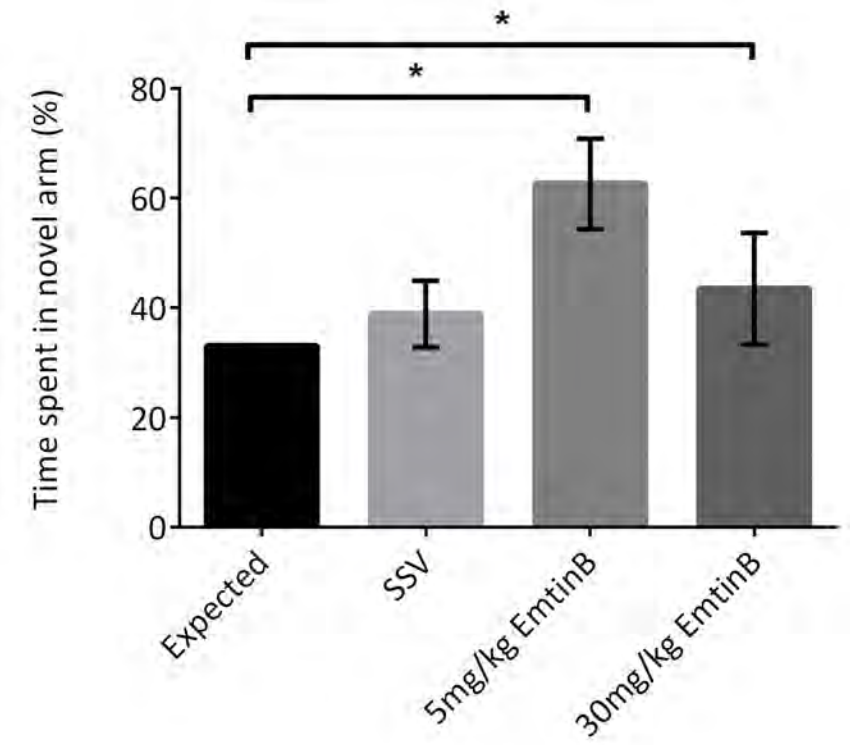

B 5 minute post -first arm entry

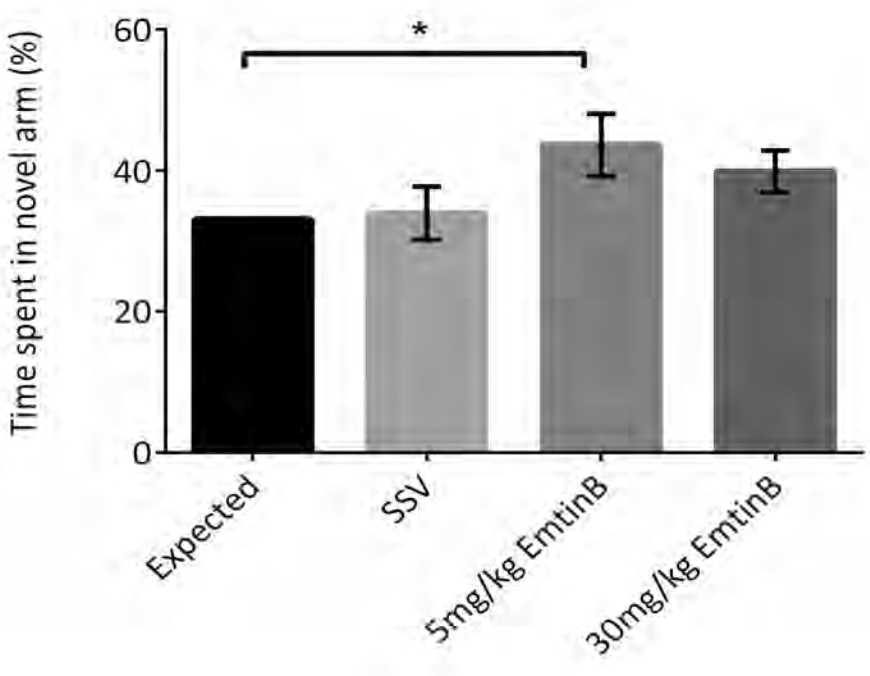

5.3.3.2 Linear regression analysis

With the help of a biostatistician (Dr Karen Wills, School of Medicine, UTAS) a linear regression model was built in R v3.1.1 (R Core Team, 2014) to analyse the data. Linear regression of the data showed that at five minutes post first arm entry there was no significant difference in time spent in the novel arm of the maze between 30mg/kg EmtinB-treated mice and control SSV mice, or between 5mg/kg EmtinB-treated mice and control mice (Figure 5.5A).

Linear regression analysis of the one minute post first arm entry data revealed a significant difference in the amount of time spent in the novel arm of the maze between 5mg/mL EmtinB-treated mice (62.62 ± 30.96) compared with SSV control mice (38.80 ± 22.77). While there was a trend for increased time in the novel arm of the maze in 30mg/mL EmtinB-treated mice (43.45 ± 38.35), compared with SSV control mice, this trend was not significant (Figure 5.5B).

5.3.4 EmtinB treatment does not alter plaque load in APPswe/PS1ΔE9 mice

Plaque load was assessed in the cortex of EmtinB treated (5mg/kg and 30mg/kg) and saline vehicle control mice. Sections were selected from the region of the brain between bregma -1.34mm and -2.3mm, and amyloid deposition assessed by determining the percentage area of the cortex containing plaque (% plaque area) and number of plaques per square millimetre of cortical tissue (plaque number). There was no significant difference in % plaque area between SSV control mice and EmtinB treated mice (Figure 5.6A, C). There was, however, a trend for lower percentage plaque area in animals treated with 5mg/kg EmtinB (Figure 5.6A, C). Interestingly, this reflects the significant improvement in cognitive capacity demonstrated by the 5mg/kg EmtinB treated mice using the Y-maze, which was comparatively less in the 30mg/kg EmtinB dosed mice (see Figure 5.4). Similarly, there was no significant difference in plaque number between saline treated mice and EmtinB treated mice; however,

Figure 5.5 EmtinB treated APPswe/PS1ΔE9 mice show reduced cognitive impairment compared with sterile saline treated control mice

APPswe/PS1ΔE9 mice treated with either EmtinB at a low dose of 5mg/kg (n=14) or a high dose of 30mg/kg (n=11), or with a control dose of Sterile Saline Vehicle (SSV; n= 15), were assessed for cognitive capacity using the Y-maze. Mice explored the two accessible arms of the maze for ten minutes before being removed from the maze for one hour. Mice were returned to the Y-maze for A) one minute and B) five minutes, with all three arms of the maze accessible and the time spent in the novel arm of the maze was analysed using linear regression. Linear regression analysis of the novel arm data shows that at one minute post first-arm entry (A) 5mg/kg treated mice spent significantly longer in the novel arm of the maze than SSV-treated mice ($p<0.05$) and, while there was a trend for 30mg/kg treated mice to spend longer in the novel arm of the maze than SSV mice, this was not statistically significant. At five minutes post first-arm entry (B), neither the 5mg/kg, nor 30mg/kg, EmtinB treated mice spent significantly longer in the novel arm of the maze compared to SSV mice. $p<0.05$. Values are mean and SEM.

A 1 minute post -first arm entry

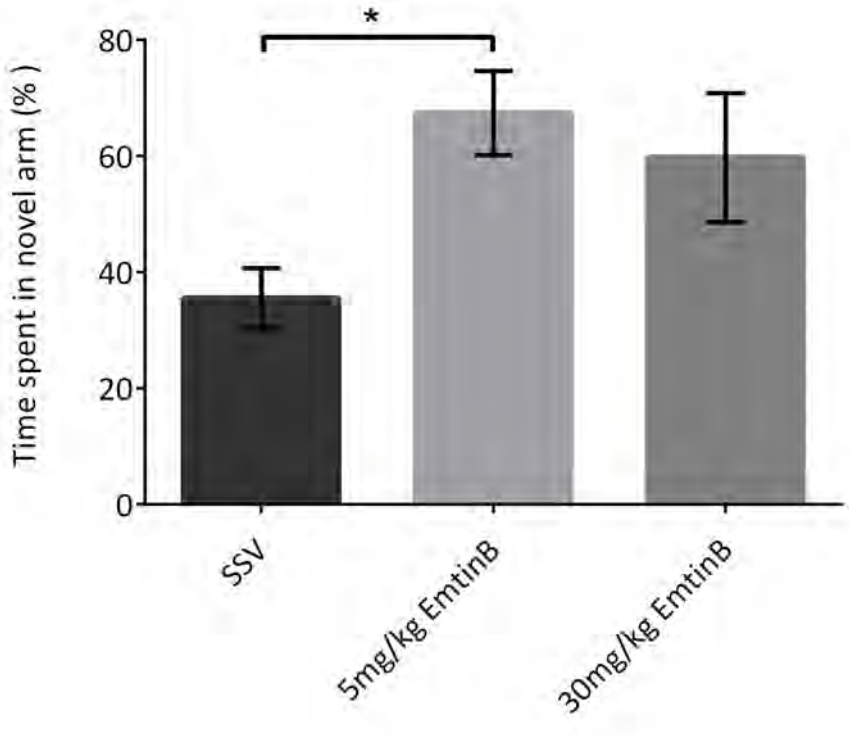

B 5 minute post -first arm entry

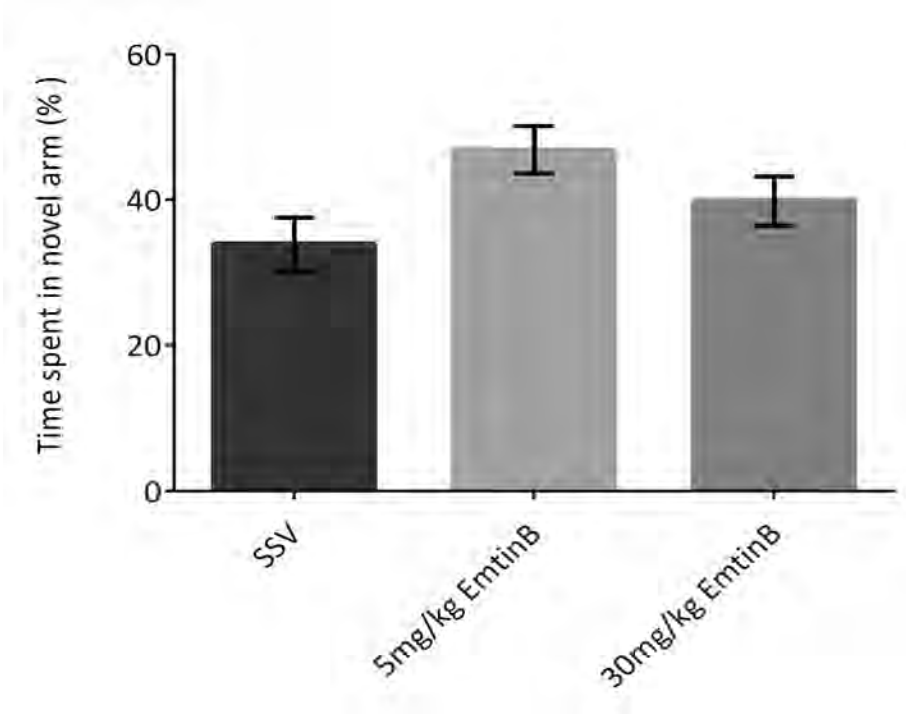

Figure 5.6 EmtinB treatment at 5mg/kg or 30mg/kg does not significantly alter Aβ deposition in APPswe/PS1ΔE9 mice

EmtinB at 5mg/kg, EmtinB at 30mg/kg, and sterile saline vehicle (SSV) control treated mouse brains (n=5) were paraffin embedded sectioned at 5µm. Three sections between bregma -1.34mm and -2.3mm were selected randomly for each brain for plaque analysis. Sections were stained with MOAB2 antibody and imaged on a spinning disk confocal microscope. The images were segmented using a random forest segmenter before analysis for plaque area and number using ImageJ. Plaque load was calculated as percent area of the cortex containing plaques (A). Based on this calculation there was no significant difference in plaque load in the cortex of 30mg/kg or 5mg/kg EmtinB treated mice compared with SSV controls. Similarly, plaque number was calculated as plaques per square mm of cortex (B), and no significant differences were observed between EmtinB-treated and control mice. Interestingly there was a trend for fewer plaques and lower plaque numbers in 5mg/kg EmtinB treated mice; representative images in (C). One-way ANOVA, p=0.05; scale bar = 500µm.

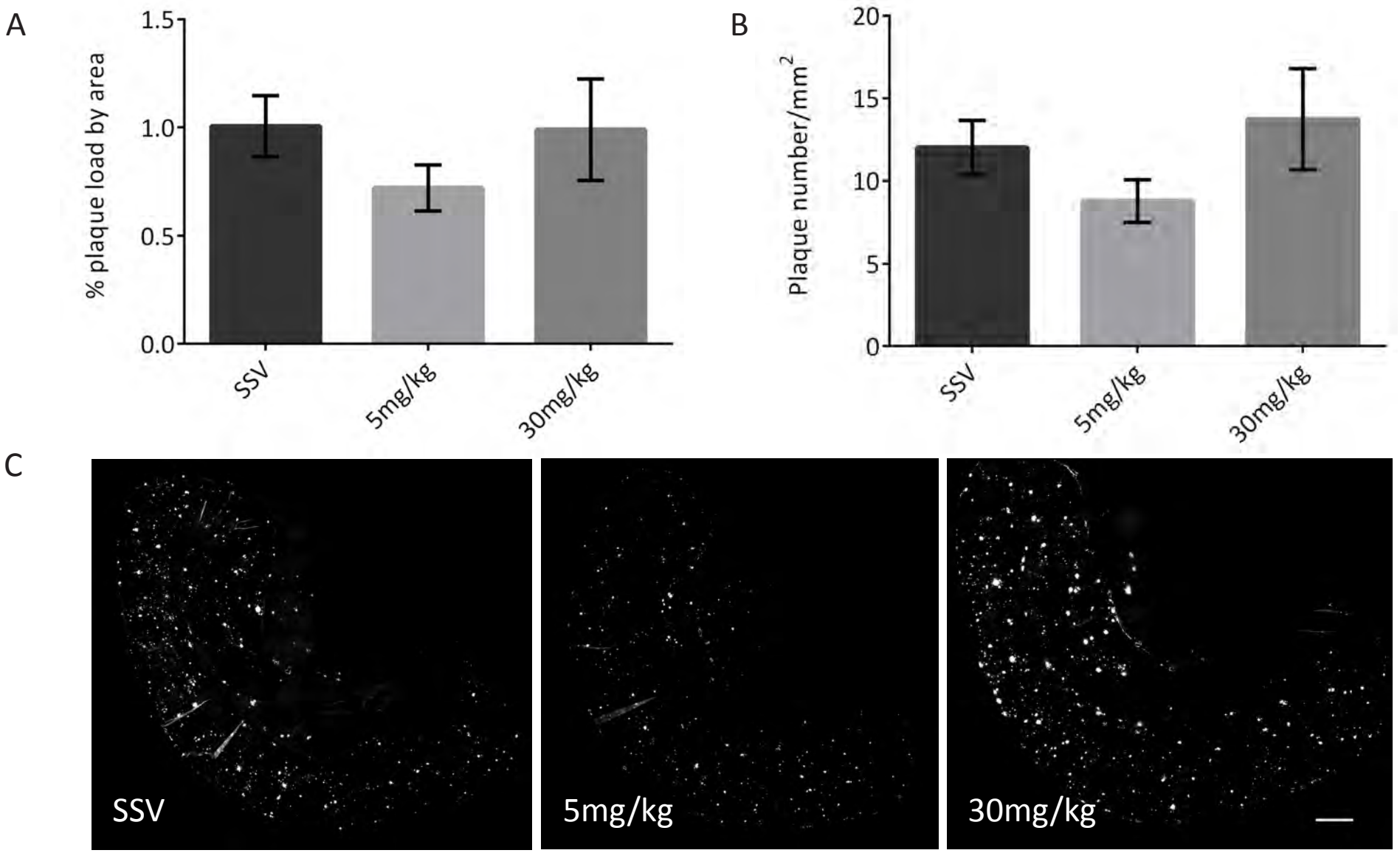
A
% plaque load by area
1.5
1.0
0.5
0.0
SSV
5mg/kg
30mg/kg
B
Plaque number/mm^2
20
15
10
5
0
SSV
5mg/kg
30mg/kg
C
SSV
5mg/kg
30mg/kg

once again there was a trend for lower plaque number in 5mg/kg EmtinB treated mice (Figure 5.6B, C). Thus, while there is a trend for lower plaque number and percentage plaque area in 5mg/kg EmtinB treated mice, there is no statistically significant difference in plaque deposition, or number, between control and EmtinB treated mice at either dose.

5.3.5 Soluble amyloid is not altered in EmtinB treated mouse brain

Soluble Aβ levels correlate well with cognitive decline in AD patients and AD mouse models. Soluble levels of human Aβ1-42 (hAβ1-42) were analysed in whole hemisphere extracts from APPswe/PS1ΔE9 mouse brains after treatment with EmtinB (5 or 30mg/kg) or sterile saline control using an ELISA (Novex by Life technologies, Thermofisher scientific, MA, USA). ELISA analysis showed no significant changes in soluble hAβ1-42 between EmtinB treated mice and saline vehicle control mice (Figure 5.7).

5.3.6 EmtinB treatment does not affect APP levels in APPswe/PS1ΔE9 mice

To determine if EmtinB modulates APP in the APPswe/PS1ΔE9 mouse model of AD, a western blot was carried out on whole-hemisphere brain samples of EmtinB treated and control mice (Figure 5.8A). Quantitation of the western blot using ImageJ showed that neither 5mg/kg nor 30mg/kg treatment with EmtinB altered brain APP levels in APPswe/PS1ΔE9 mice compared with saline vehicle control mice (Figure 5.8B).

5.3.7 EmtinB does not alter LRP1 levels in APPswe/PS1ΔE9 mice

To confirm a decrease in LRP1 in the APPswe/PS1ΔE9 model of AD, control B6 and APPswe/PS1ΔE9 mouse brains were analysed by western blot for LRP1. A decrease in LRP1 levels in APPswe/PS1ΔE9 mouse brain was confirmed by western blot (Figure 5.9A) and subsequent western blot quantitation by ImageJ (Figure 5.9B). LRP1 levels in APPswe/PS1ΔE9

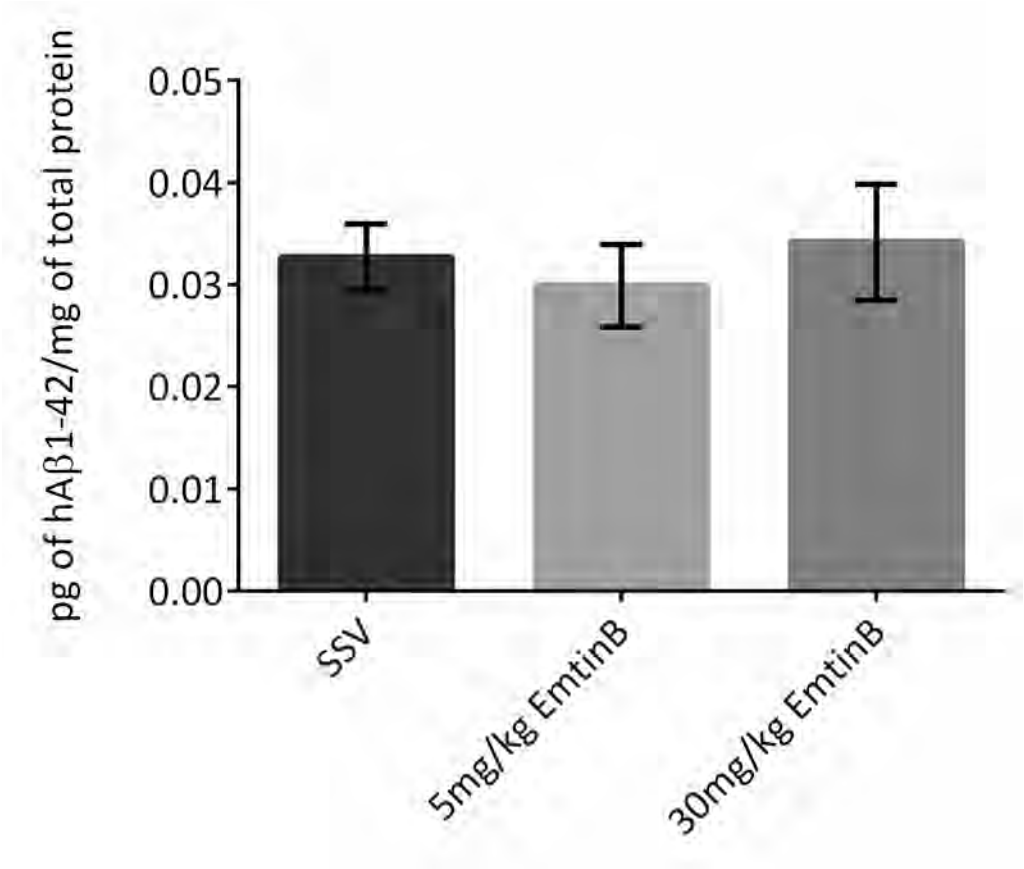

Figure 5.7 Soluble hAβ1-42 levels were not altered by EmtinB treatment at a dose of 5mg/kg or 30mg/kg

Soluble hAβ1-42 levels in 5mg/kg and 30mg/kg EmtinB-treated mouse brain were compared with soluble hAβ1-42 levels in saline vehicle-treated mouse brain by Enzyme-linked Immunosorbent Assay (ELISA). Neither 30mg/kg (n=5) nor 5mg/kg EmtinB-treated mice (n=5) showed significantly altered brain hAβ1-42 levels compared with SSV control mice (n=5). One-way ANOVA with Tukey post-test, p=0.05. Means and SEM shown.

Figure 5.8 APP is unchanged in the brains of EmtinB treated mice

Whole brain hemisphere extracts from SSV treated mice, 5mg/kg EmtinB treated mice and 30mg/kg EmtinB treated mice were analysed for APP content by western blot analysis (A) and subsequent ImageJ quantitation using ImageJ (B). There was no change in APP levels in either 5mg/kg or 30mg/kg EmtinB-treated mice compared with SSV mice. One-way ANOVA with Tukey post-test. Means and SEM shown.

A

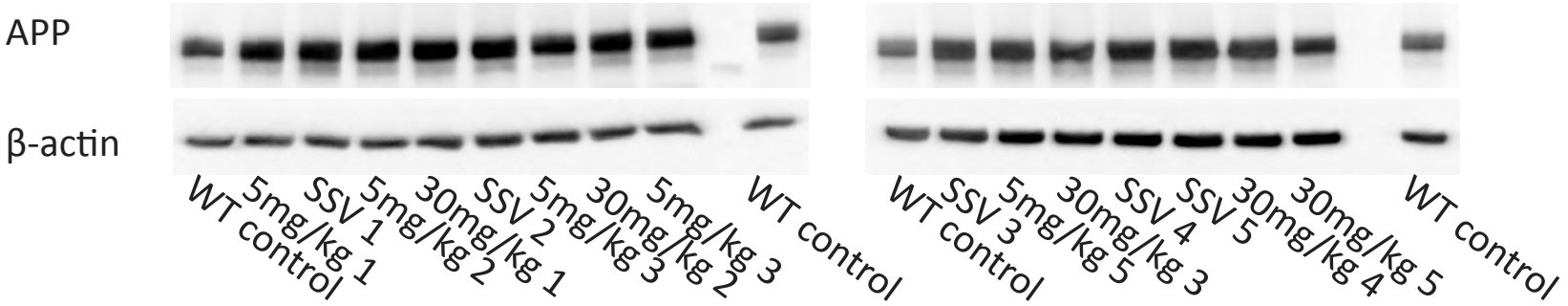
APP
β-actin
WT control
5mg/kg 1
SSV 1
5mg/kg 2
30mg/kg 1
SSV 2
5mg/kg 3
30mg/kg 2
5mg/kg 3
WT control
WT control
SSV 3
5mg/kg 5
30mg/kg 3
SSV 4
SSV 5
30mg/kg 4
30mg/kg 5
WT control

B

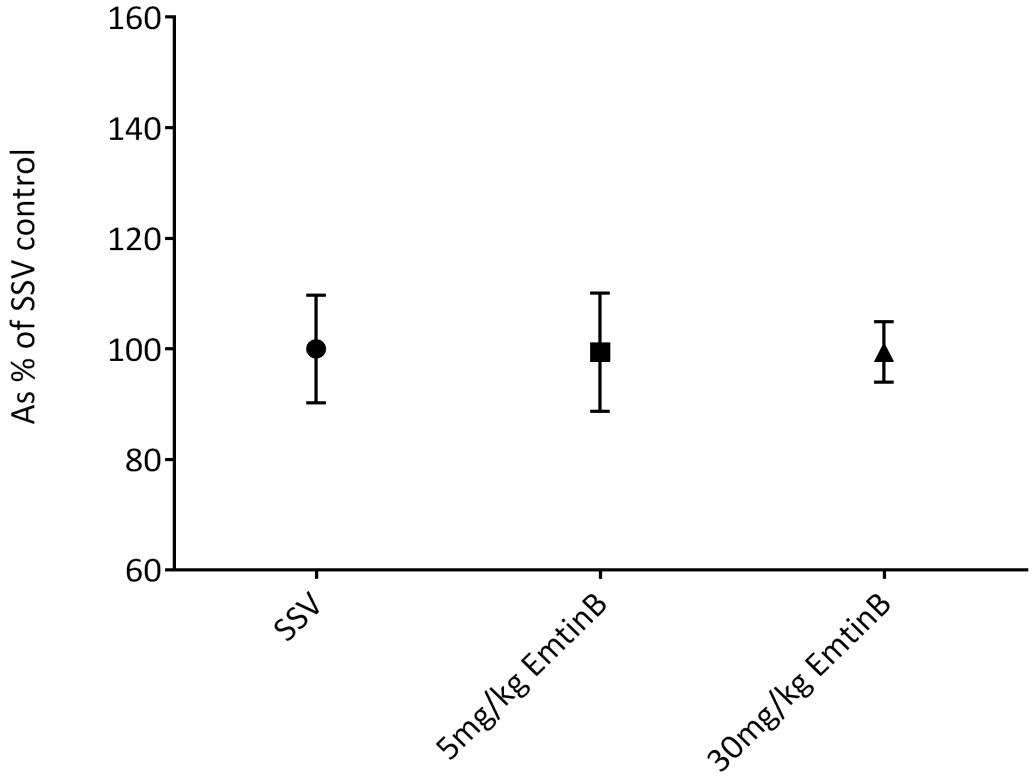
As % of SSV control
160
140
120
100
80
60
SSV
5mg/kg EmtinB
30mg/kg EmtinB

Figure 5.9 LRP1 levels are decreased in the brain of the APPswe/PS1ΔE9 mouse model

LRP1 levels in whole-hemisphere brain extracts from APPswe/PS1ΔE9 and wild-type B6 mice were analysed by western blot (A) and quantitated using ImageJ (B). LRP1 was significantly decreased in the brain of APPswe/PS1ΔE9 mice (n=3) compared with wild-type B6 mice (n=3). t-test, $p<0.05$. Values are mean and SEM.

A

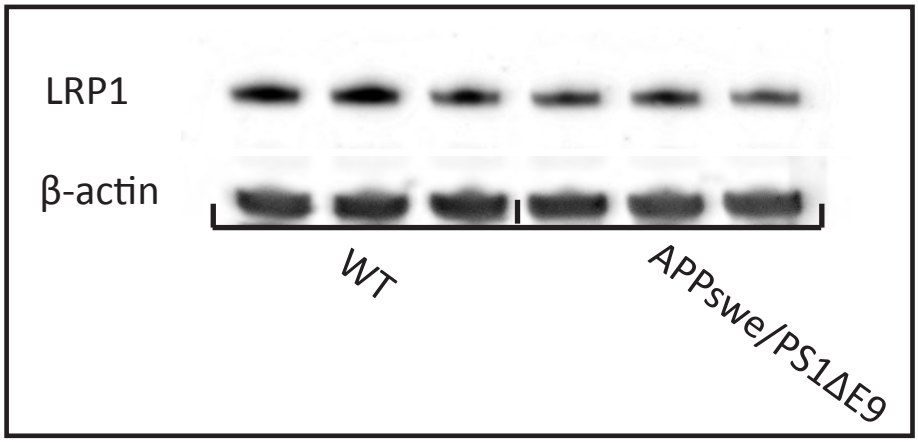
LRP1
β-actin
WT
APPswe/PS1ΔE9

B

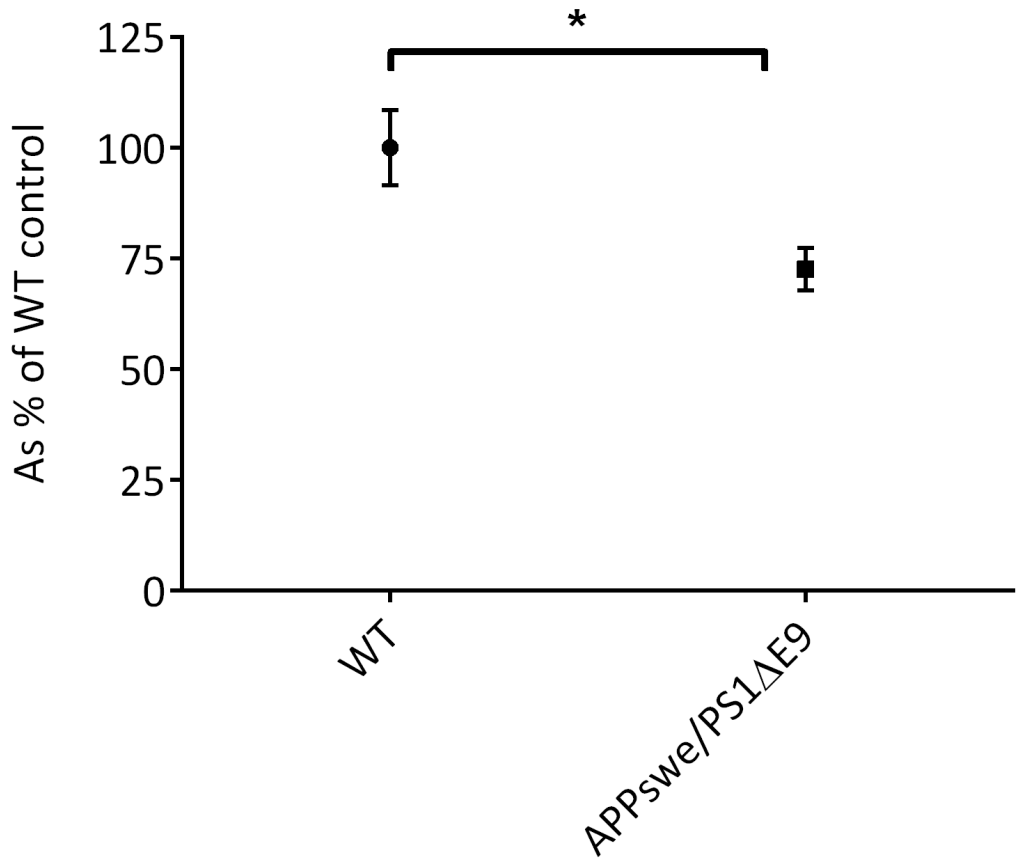
*
125
100
75
50
25
0
As % of WT control
WT
APPswe/PS1ΔE9

mice were found to be decreased by approximately 25% in the brain of APPswe/PS1ΔE9 mice compared with B6 wild-type control mice (Figure 5.9B).

To determine if EmtinB was able to modulate LRP1 levels in APPswe/PS1ΔE9 mice, whole-hemisphere extracts from 5mg/kg and 30mg/kg EmtinB treated mice and SSV control mice were analysed by western blot. Western blotting (Figure 5.10A) and subsequent analysis using ImageJ (Figure 5.10B) for LRP1 in EmtinB-treated and vehicle control mice showed no difference in LRP1 levels, suggesting that EmtinB is not acting to modulate LRP1.

5.3.8 EmtinB does not alter IBA1 levels in APPswe/PS1ΔE9 mice

Microglial changes in EmtinB treated (5mg/kg or 30mg/kg) and SSV control APPswe/PS1ΔE9 mouse brain were assessed using western blotting for IBA1 protein (Figure 5.11A). IBA-1 protein is found in all microglia and is upregulated in activated glia [233]. IBA1 levels in whole hemisphere brain extracts were quantified using ImageJ (Figure 5.11B), with no significant difference in IBA1 found between EmtinB-treated mice at either 30mg/kg or 5mg/kg treated and SSV control mice.

5.3.9 GFAP is decreased in EmtinB treated APPswe/PS1ΔE9 mice

To confirm that GFAP levels are increased in the APPswe/PS1ΔE9 model of AD, GFAP levels in APPswe/PS1ΔE9 and B6 control mouse brain were assessed using western blot (Figure 5.11A). Quantitation of the western blot showed an increase in GFAP in APPswe/PS1ΔE9 mice compared with B6 control mice (Figure 5.12B), confirming increased GFAP levels in the APPswe/PS1ΔE9 mouse model of AD.

To ascertain whether EmtinB is able to reduce astrogliosis in the APPswe/PS1ΔE9 mouse model of AD, GFAP levels were analysed in high and low dose EmtinB-treated mouse brain and SSV control brain by western blot (Figure 5.13 A) and quantitated using ImageJ analysis (Figure 5.13 B). Mice treated with EmtinB at 5 or 30mg/kg had significantly lower levels of GFAP than

Figure 5.10 EmtinB does not alter LRP1 levels in APPswe/PS1ΔE9 mouse brain

LRP1 levels in whole-hemisphere brain extracts from 30mg/kg EmtinB treated, 5mg/kg EmtinB treated, and sterile saline vehicle (SSV) treated mice were analysed by western blot (A) and subsequent ImageJ quantitation (B). LRP1 levels in 5mg/kg and 30mg/kg EmtinB-treated mice were not significantly different from SSV control animals. One-way ANOVA with Tukey post-test. Data is mean and SEM.

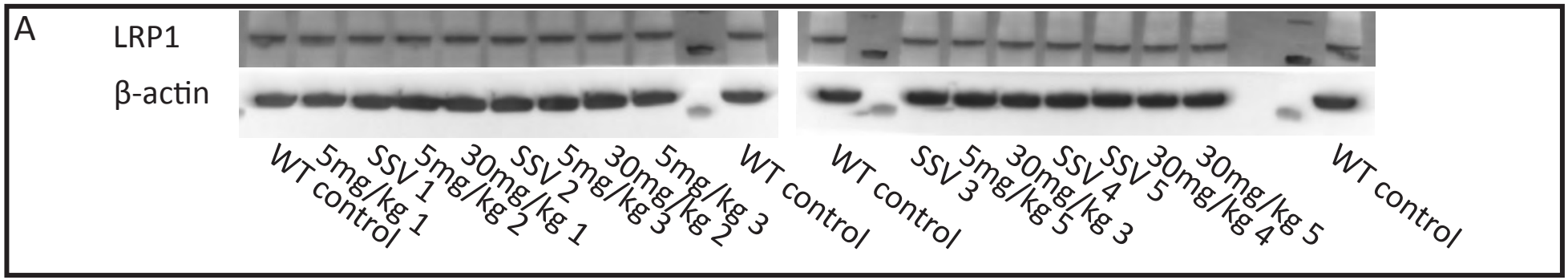
A
LRP1
β-actin
WT control
5mg/kg 1
SSV 1
5mg/kg 2
30mg/kg 1
SSV 2
5mg/kg 3
30mg/kg 3
5mg/kg 2
WT control
WT control
SSV 3
5mg/kg 5
30mg/kg 3
SSV 4
SSV 5
30mg/kg 4
30mg/kg 5
WT control

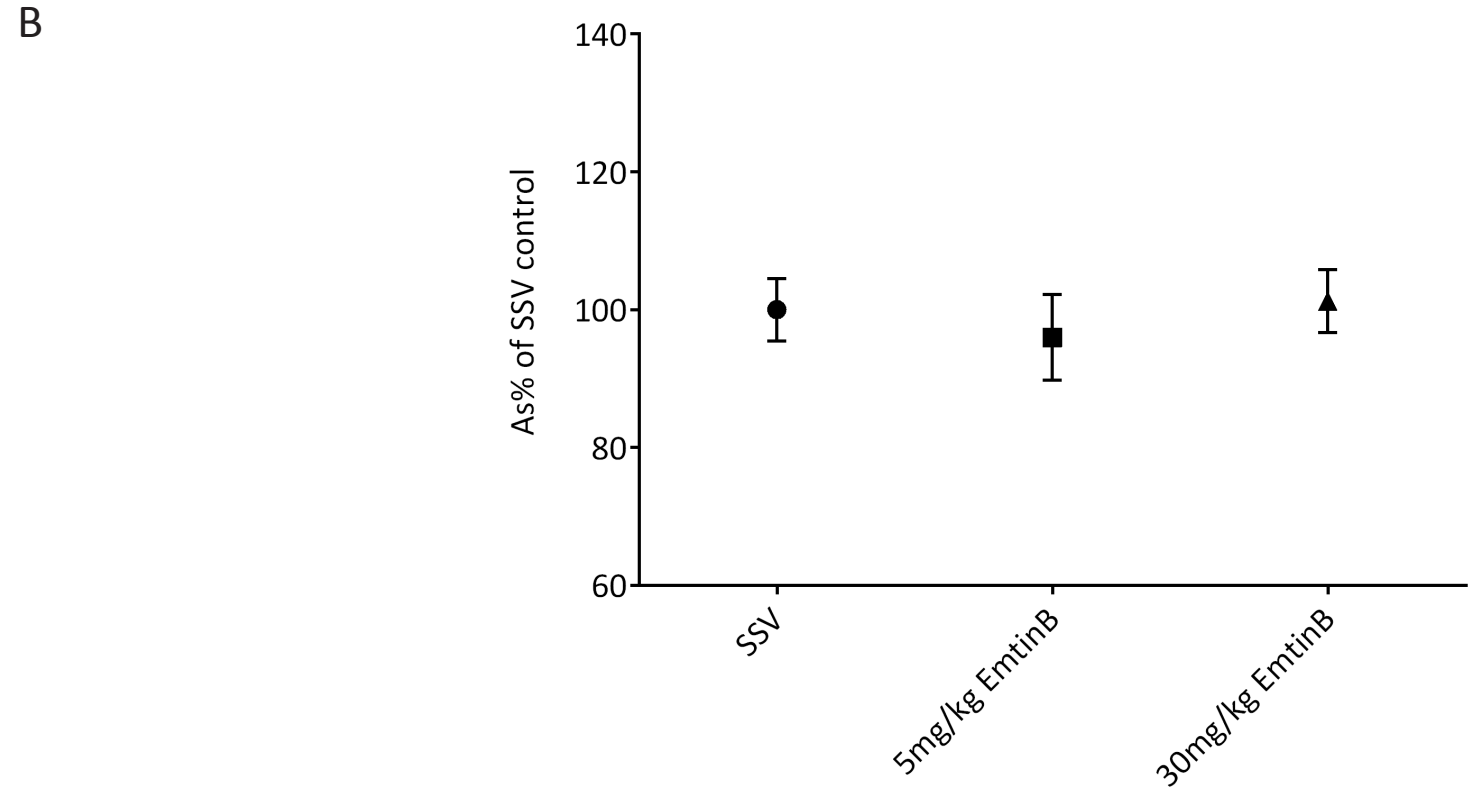
B
As% of SSV control
140
120
100
80
60
SSV
5mg/kg EmtinB
30mg/kg EmtinB

Figure 5.11 IBA1 is unchanged in the brains of EmtinB-treated mice

Whole-hemisphere brain extracts from mice treated with 30mg/kg EmtinB, 5mg/kg EmtinB and sterile saline vehicle (SSV) were analysed by western blot (A) and quantitated using ImageJ (B). IBA1 was unchanged in 5mg/kg treated mice and 30mg/kg treated mice compared with SSV treated animals. One-way ANOVA with Tukey post-test. Values are mean and SEM.

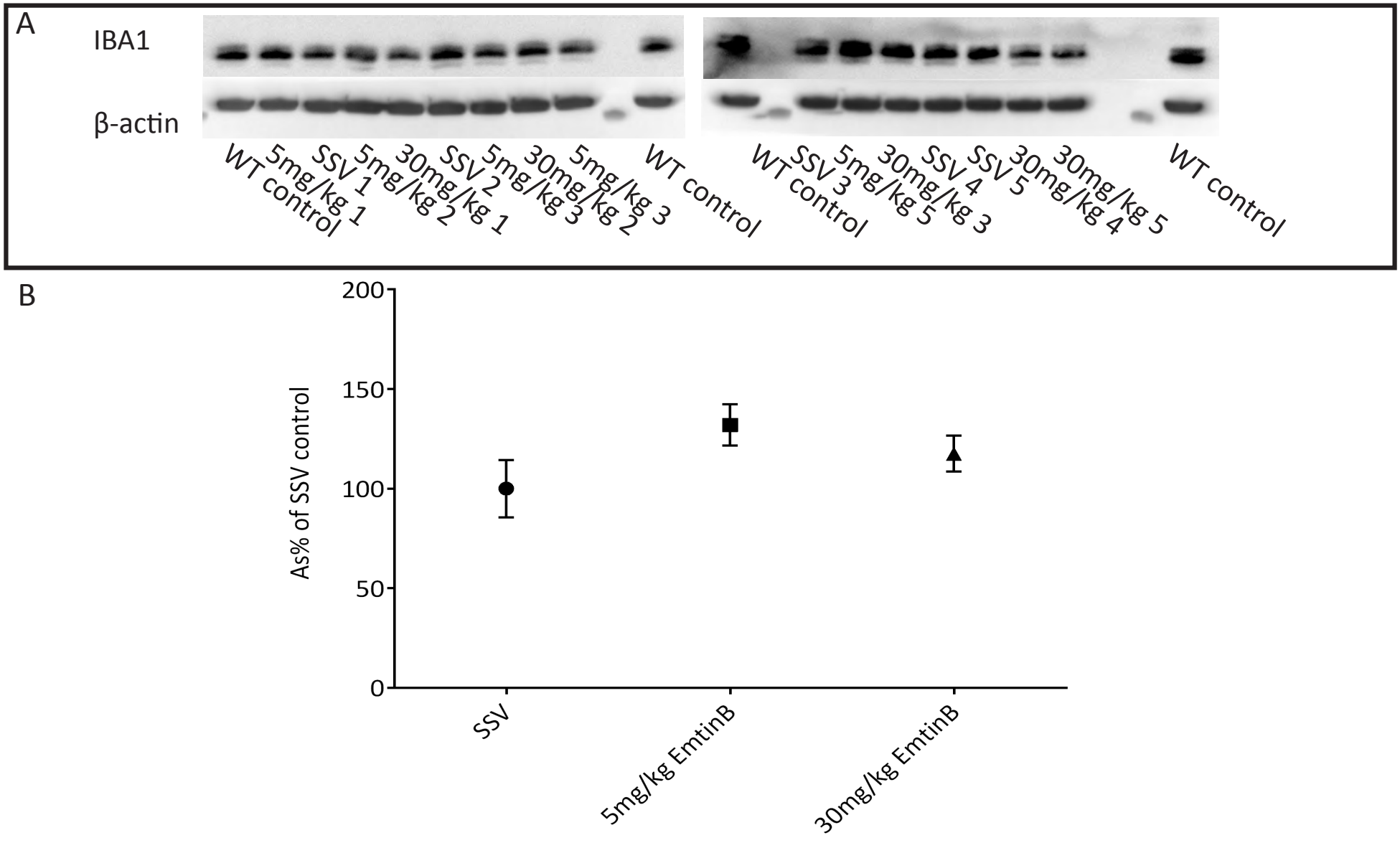
A
IBA1
β-actin
WT control
5mg/kg 1
SSV 1
5mg/kg 2
30mg/kg 1
SSV 2
5mg/kg 3
30mg/kg 2
5mg/kg 3
WT control
WT control
SSV 3
5mg/kg 5
30mg/kg 3
SSV 4
SSV 5
30mg/kg 4
30mg/kg 5
WT control
B
As% of SSV control
200
150
100
50
0
SSV
5mg/kg EmtinB
30mg/kg EmtinB

Figure 5.12 GFAP levels are increased in the APPswe/PS1ΔE9 model of AD

GFAP levels in whole brain hemisphere extracts were analysed by western blot (A) and quantitated using ImageJ analysis (B). APPswe/PS1ΔE9 mice (n=3) had significantly higher GFAP levels in whole-hemisphere brain extracts compared with wild-type B6 mice (n=3). t-test, $p<0.05$; results as mean and SEM.

A

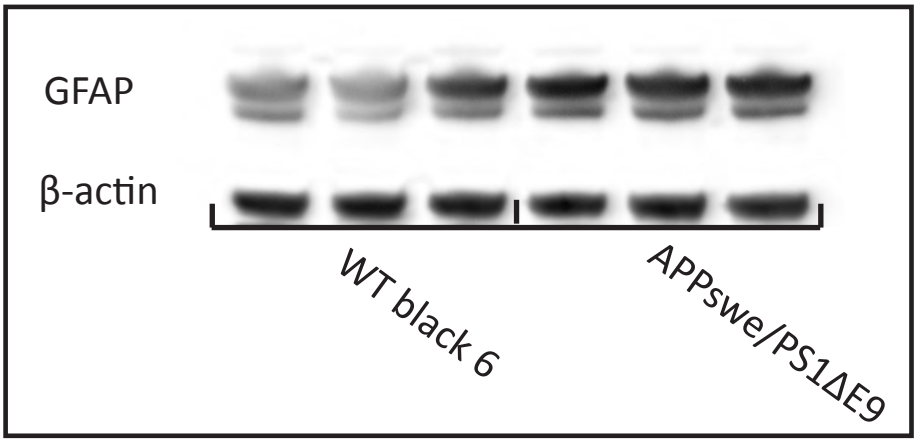
GFAP
β-actin
WT black 6
APPswe/PS1ΔE9

B

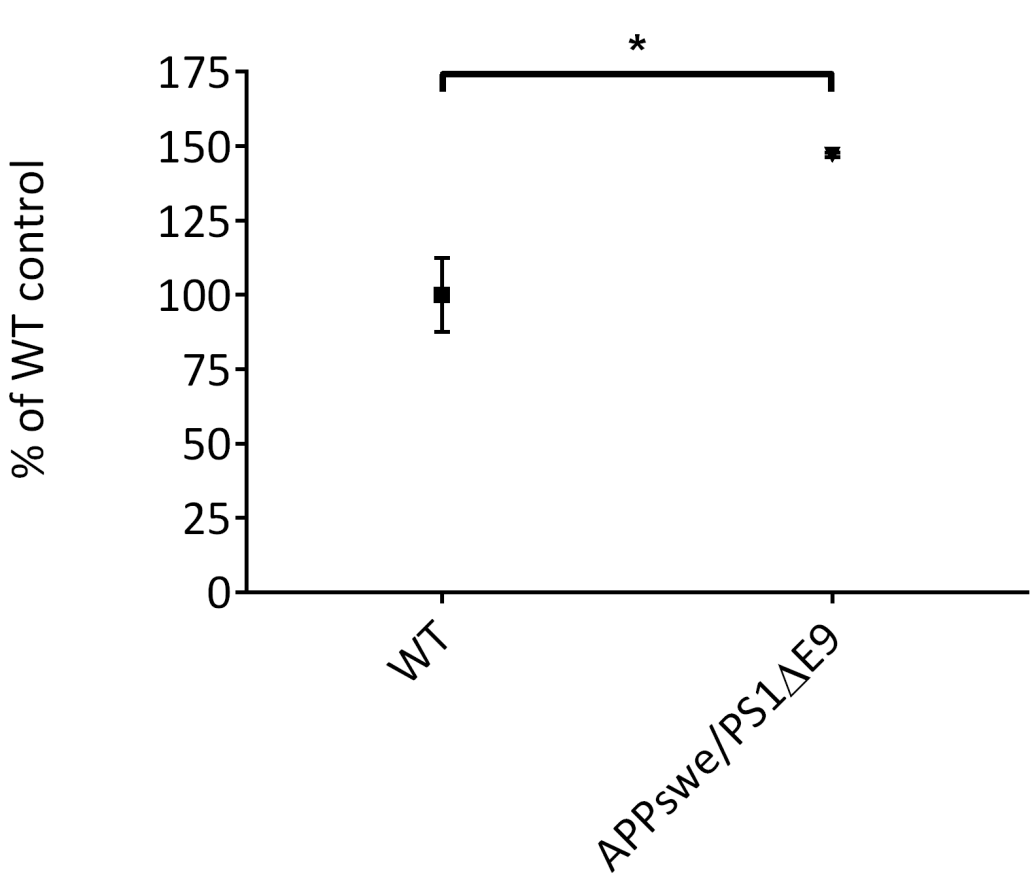
*
175
150
125
100
75
50
25
0
% of WT control
WT
APPswe/PS1ΔE9

Figure 5.13 GFAP is significantly decreased in the brains of EmtinB treated APPswe/PS1ΔE9 mice

GFAP levels in whole-hemisphere brain extracts were analysed by western blot (A) and subsequent ImageJ quantitation (B). GFAP was reduced in both 5mg/kg and 30mg/kg compared with sterile saline vehicle control animals. One-way ANOVA with Tukey post-test; * = $p < 0.05$, ** = $p<0.01$.

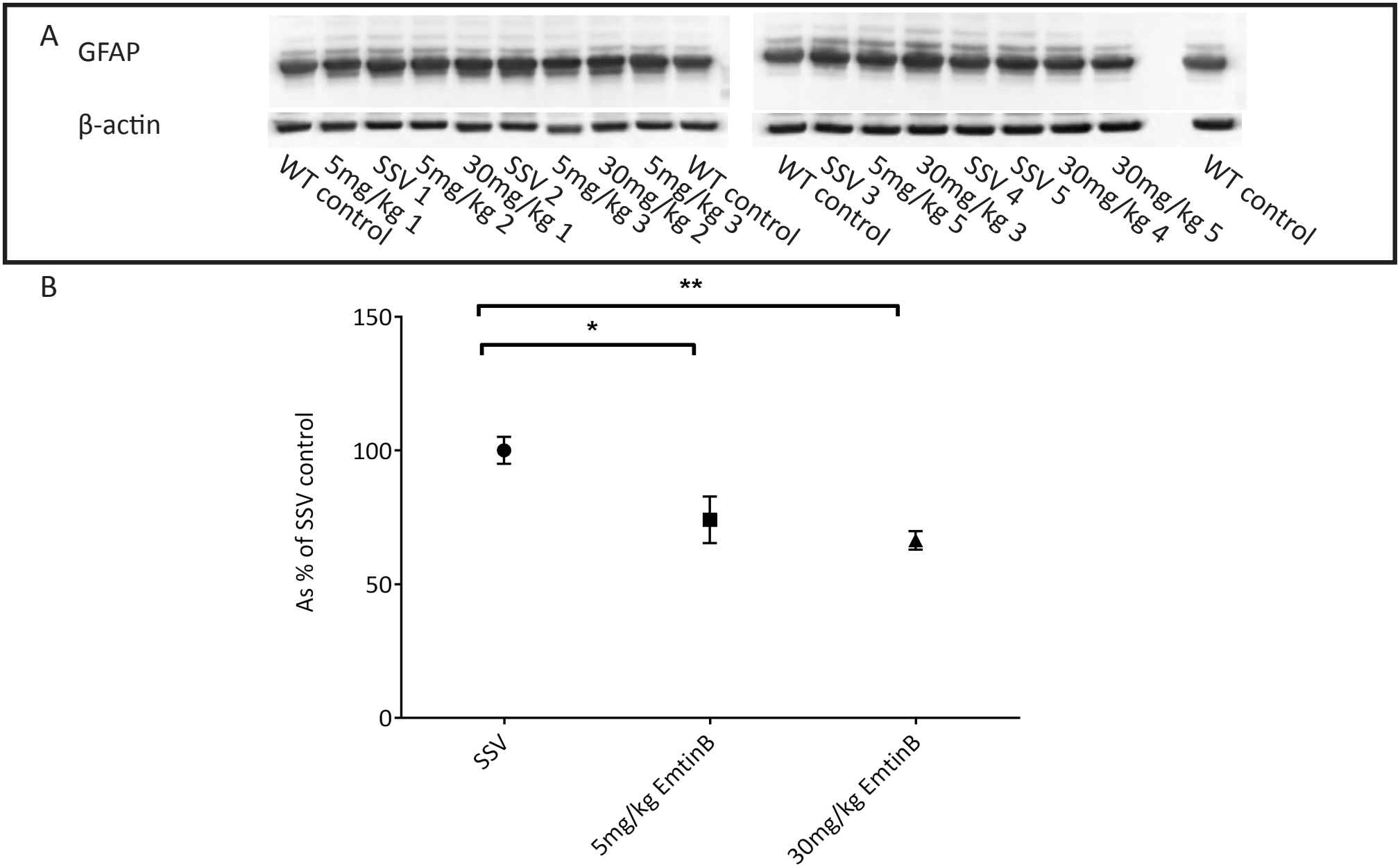
A
GFAP
β-actin
WT control
5mg/kg 1
SSV 1
5mg/kg 2
30mg/kg 1
SSV 2
5mg/kg 3
30mg/kg 2
5mg/kg 3
WT control
WT control
SSV 3
5mg/kg 5
30mg/kg 3
SSV 4
SSV 5
30mg/kg 4
30mg/kg 5
WT control
B
**
*
150
100
50
0
As % of SSV control
SSV
5mg/kg EmtinB
30mg/kg EmtinB

saline vehicle-treated mice (Figure 5.13 A, B). Thus, EmtinB is able to modulate GFAP levels in the APPswe/PS1ΔE9 mouse brain.

5.3.10 Neither Synaptophysin nor PSD-95 levels are altered in the hippocampus of APPswe/PS1ΔE9 mice after EmtinB treatment.

Western blot analysis of synaptophysin levels in high and low dose EmtinB treated brain, and SSV control brain, showed no significant difference in synaptophysin with either 30mg/kg or 5mg/kg EmtinB treatment compared to SSV control (Figure 5.14A, B).

Similarly, neither 30mg/kg EmtinB treatment nor 5mg/kg EmtinB treatment altered PSD95 levels in APPswe/PS1ΔE9 mouse brain compared to SSV control mouse brain, as analysed by western blot (Figure 5.15 A, B). Taken together, the data suggest that EmtinB does not have a direct impact on synapses.

5.4 Discussion and conclusions

The therapeutic potential of the EmtinB dimer in APPswe/PS1ΔE9 mice has been investigated. Subcutaneous administration of EmtinB improved cognitive outcome in 5mg/kg treated APPswe/PS1ΔE9 mice, but was not as efficacious in 30mg/kg treated mice. Subsequent analysis of Aβ accumulation in the EmtinB-treated and saline vehicle-treated control brains showed no changes in soluble hAβ1-42 levels. Aβ plaques were analysed by immunohistochemistry and, while a trend towards lower plaque load was observed for 5mg/kg EmtinB treated mice, this was not significant. There were no changes to levels of APP, LRP1, and IBA1 in whole-hemisphere brain extracts; however, there was a significant decrease in GFAP levels in both 5mg/kg and 30mg/kg EmtinB treated mice compared to SSV controls. Extracts from hippocampi of EmtinB-treated and SSV control mice showed no difference in synaptic markers, PSD-95 or synaptophysin.

Figure 5.14 Synaptophysin levels in the hippocampus of APPswe/PS1ΔE9 mice are not altered by EmtinB treatment

Synaptophysin levels in the hippocampus of EmtinB treated and control mice were analysed by western blot (A) and subsequent ImageJ quantitation (B). Neither 5mg/kg nor 30mg/kg treatment with EmtinB produced significant changes in synaptophysin levels in the hippocampus of treated animals compared with sterile saline vehicle control animals. One-way ANOVA with Tukey post-test.

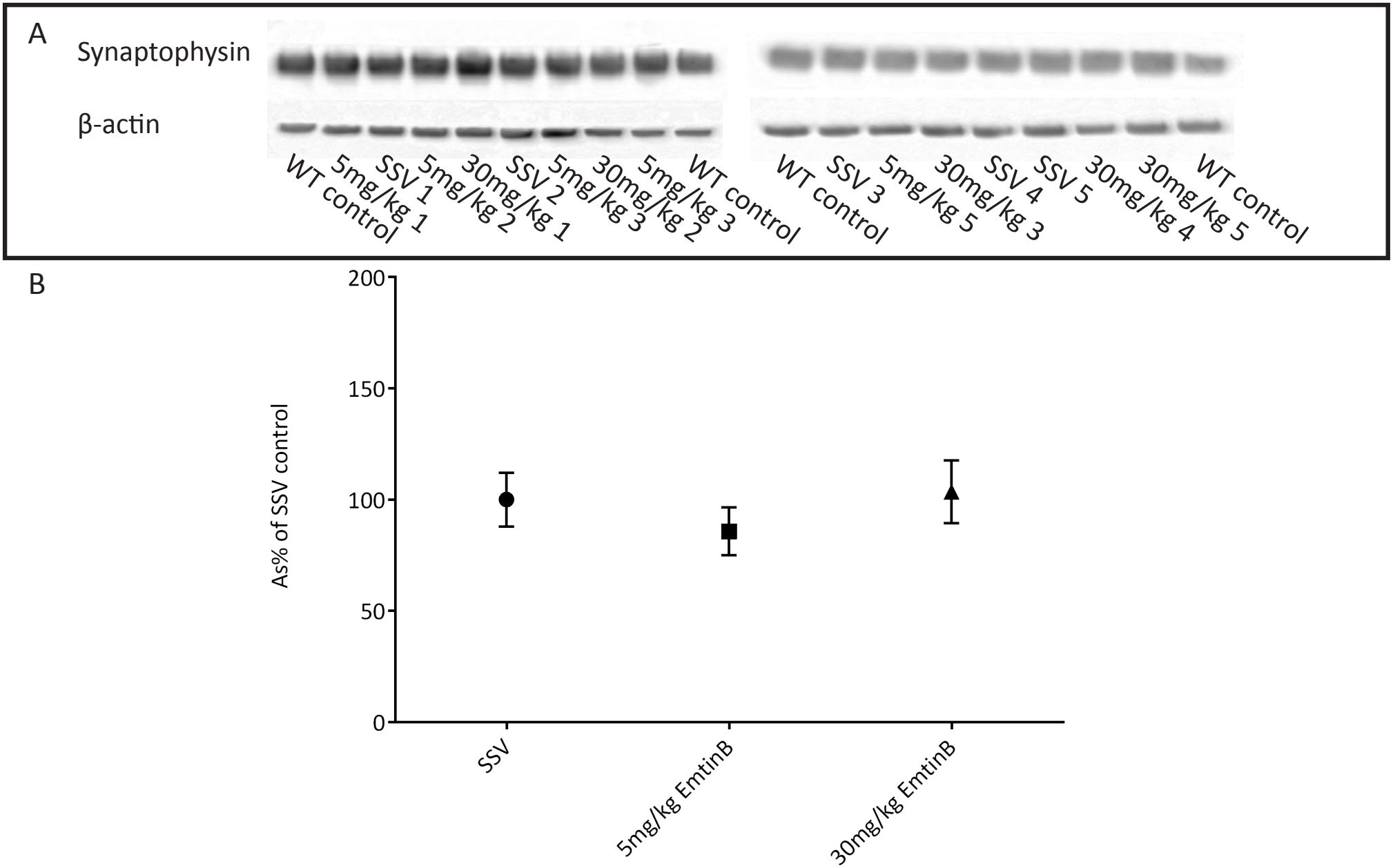
A
Synaptophysin
β-actin
WT control
5mg/kg 1
SSV 1
5mg/kg 2
30mg/kg 1
SSV 2
5mg/kg 3
30mg/kg 2
5mg/kg 3
WT control
WT control
SSV 3
5mg/kg 5
30mg/kg 3
SSV 4
SSV 5
30mg/kg 4
30mg/kg 5
WT control
B
As% of SSV control
200
150
100
50
0
SSV
5mg/kg EmtinB
30mg/kg EmtinB

Figure 5.15 EmtinB treatment does not alter PSD95 levels in the hippocampus of APPswe/PS1ΔE9 mice

PSD95 levels in protein extracts from the hippocampus of EmtinB treated and control mice were analysed by western blot (A) and subsequent quantitation using ImageJ (B). No significant changes in PSD95 were detected in EmtinB treated hippocampal sections at either 5mg/kg or 30mg/kg compared with vehicle treated controls. One-way ANOVA with Tukey post-test.

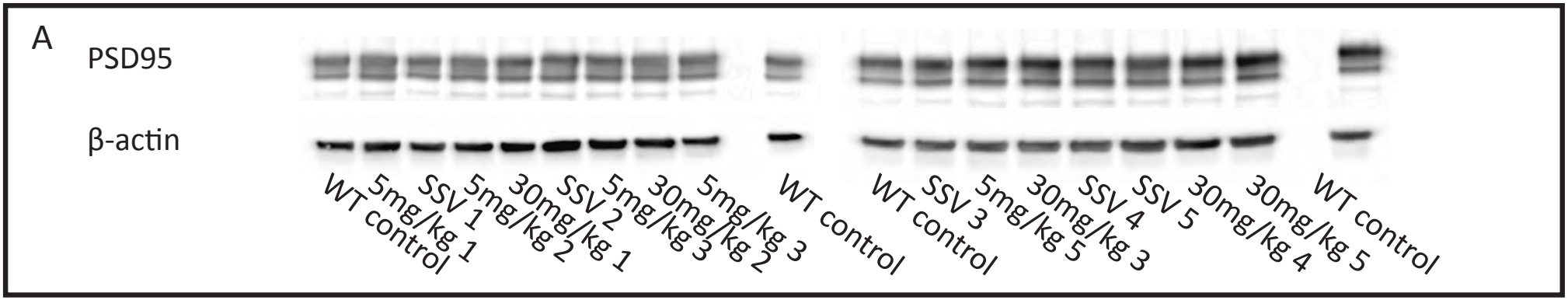
A
PSD95
β-actin
WT control
5mg/kg 1
SSV 1
5mg/kg 2
30mg/kg 1
SSV 2
5mg/kg 3
30mg/kg 2
5mg/kg 3
WT control
WT control
SSV 3
5mg/kg 5
30mg/kg 3
SSV 4
SSV 5
30mg/kg 4
30mg/kg 5
WT control

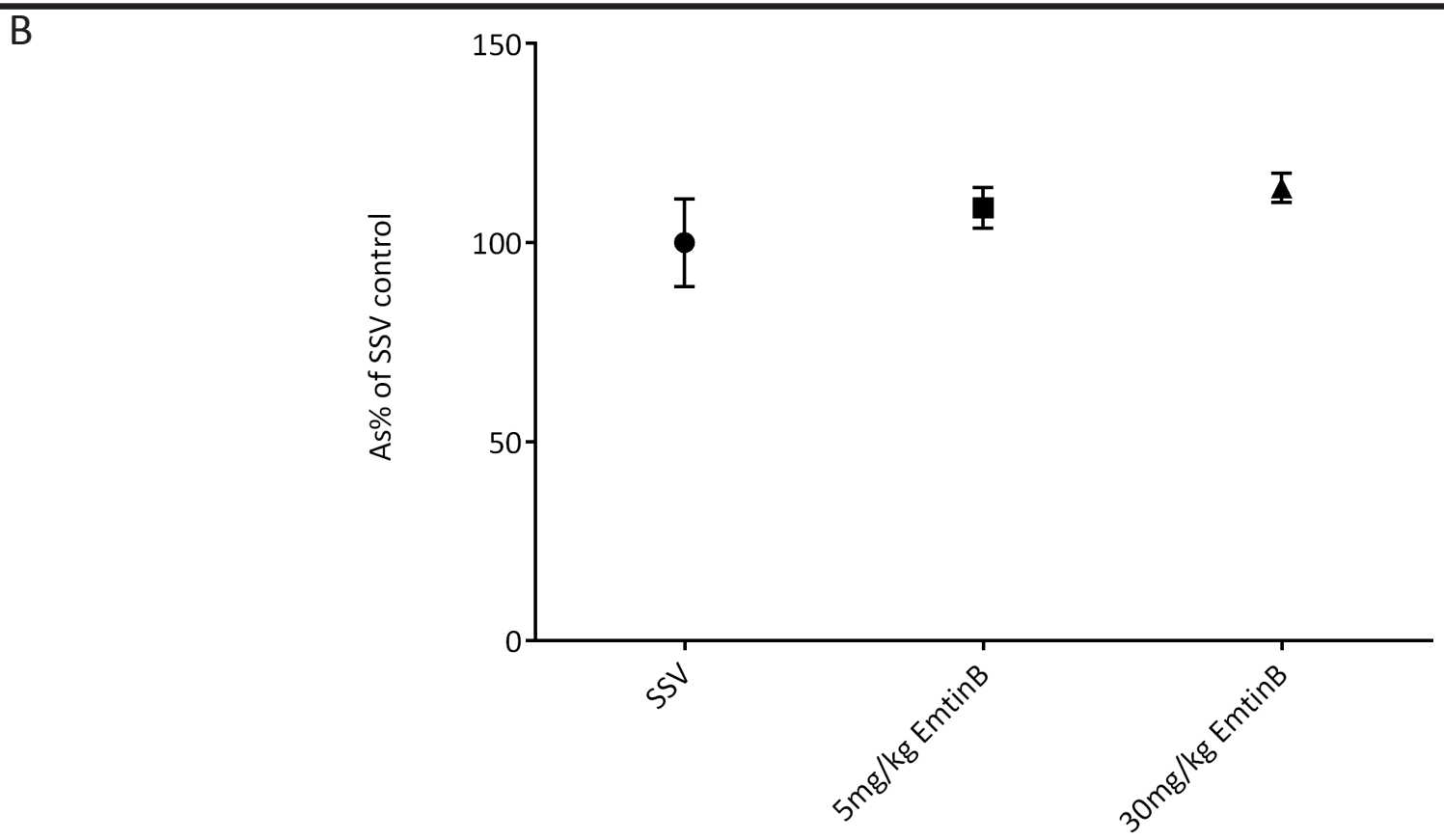
B
As% of SSV control
150
100
50
0
SSV
5mg/kg EmtinB
30mg/kg EmtinB

5.4.1 EmtinB pharmacokinetics in the APPswe/PS1ΔE9 mouse

5.4.1.1 EmtinB is not orally administrable

Peptides as therapeutics have been gaining in popularity since the 1990s [234]. Currently, most peptide drugs (approximately 75%), are administered *via* injection, however alternative administration forms, including oral, are gaining increasing prominence [165]. Oral drug administration is a preferred method in terms of convenience and safety however; using this route, the drug is required to not only be absorbed across the intestinal wall, but also pass through the liver, prior to reaching its therapeutic target [234]. For peptides, this represents a significant obstacle as the gut's specific function is to degrade peptides into their component amino acids. While emtins have not yet been tested as orally administrable peptides, there is some evidence to suggest that EmtinB might be orally administered. A recent study has shown that tetra-branched, dendrimeric peptides show decreased protease susceptibility [177]. While tetrameric EmtinB clearly falls into the category of tetra-branched dendrimeric peptide, it is unclear whether dimeric EmtinB would demonstrate similar properties in this regard. In this study, subcutaneous injection of EmtinB dimer into B6 mice resulted in detectable levels of EmtinB in serum; however, orally administered EmtinB was not detectable in serum. Recent advances in technology have created alternate methods of delivery for peptides including transdermal and intranasal, as well as methods of protecting peptides during oral delivery (reviewed in [165]); while these delivery methods may provide viable options for future trials, the only current viable method of EmtinB delivery is *via* injection.

5.4.1.2 EmtinB is detectable in the serum, but not brain, of EmtinB injected APPswe/PS1ΔE9 mice

In second experiment, looking at EmtinB crossing the blood-brain barrier in APPswe/PS1ΔE9 mice showed that, while EmtinB dimer peptide was detectable in serum of injected mice,

EmtinB was not detectable in brain. However, a prior study has reported that EmtinB tetramer peptide is detectable in CSF of mice 45 minutes after subcutaneous injection [184]. There are two reasonable explanations for this discrepancy; either EmtinB dimer is unable to cross the BBB or it is crossing the BBB but is not detectable by the methods employed.

Tetrameric EmtinB has previously been detected in the CSF of mice after subcutaneous injection at 20mg/kg [184]; the same dosage that EmtinB dimer was administered at in this current study, supporting the idea that EmtinB should be crossing the BBB in this model. Our study investigated the dimer and not the tetramer, and it may be that EmtinB dimer and tetramer possess different capacities to cross the BBB. Given that EmtinB dimer is the smaller of these two peptides, the possibility that the dimer is less able to cross the BBB is unlikely however it must be considered. While proteins often cross the blood brain barrier via receptor-mediated transcytosis, a second mechanism of CNS entry is also available to cationic proteins. Adsorptive-mediated transcytosis is a process which allows positively charged proteins to cross the blood brain barrier [235, 236]. Via this mechanism, cationic proteins bind to the negatively charged luminal surface of ECs and are transported across the BBB in clatharin coated pits [236]. As both EmtinB dimer and EmtinB tetramer are estimated to have a positive net charge at neutral pH, +4.7 and +10.5 respectively, these proteins may be candidates for adsorptive-mediated transcytosis. If indeed EmtinB entry into the CNS is facilitated by this mode of transport, the higher cationic charge of the EmtinB tetramer (+10.5) as compared with the EmtinB dimer (+4.7) could represent an advantage in terms of BBB transcytosis.

One further point of difference with these peptides is the method of biotinylation. Sonn et al. [184] developed EmtinB with a single *N*-terminal biotin, while our EmtinB has an estimated three biotins per dimer. The effect of biotin on EmtinB action has not been fully assessed, and could account for a decreased capacity to cross the BBB.

If EmtinB dimer is crossing the BBB and is present in the brain, it may be in concentrations undetectable by western blot using our conditions. In this regard, it is important to note that Sonn et al. [184] demonstrated brain uptake of EmtinB tetramer by directly sampling the CSF, a technique that was not available for this project. CSF sampling presumably provides a far more sensitive detection of BBB penetration of emtin peptide, and future studies evaluating EmtinB dimer uptake into the brain should be undertaken in a similar manner.

One of the major limitations to investigating EmtinB capacity to cross the BBB is the lack of EmtinB antibody. Currently, detection of EmtinB is only possible using the biotin tag. This poses problems such as detection of endogenous biotin in both western blot samples (observed by multiple bands present in western blots of the brain, presented in Figure 5.2), and in immunocytochemistry, where uncertain identification of the EmtinB protein, and possible alterations to EmtinB action could occur due to biotin labelling. To address these issues in future, developing an EmtinB antibody would be highly advantageous.

5.4.2 EmtinB improves cognitive performance in the APPswe/PS1ΔE9 mouse

It is well documented that APPswe/PS1ΔE9 have cognitive decline from as young as six months of age. EmtinB administration for this animal trial was started at nine months of age, post symptom onset, to better reflect post-onset administration of treatment that occurs in human patients. Changes in the cognitive decline of the mice were assessed using a Y-maze after two months of EmtinB administration. Chi-square analyses showed improved outcomes for mice treated with 5mg/kg EmtinB in both the one and five minute tests, while mice treated with 30mg/kg-only had significant outcomes in the one minute test. Using the more conservative linear regression analyses, only mice dosed at 5mg/kg EmtinB showed increased cognitive performance in the Y-maze at one minute, while a non-significant trend for improvement in 5mg/kg EmtinB-treated mice was observed in the five minute test. Taken together, the data

suggest that while there is a clear improvement in cognitive performance in mice treated with 5mg/kg EmtinB, the cognitive improvement in 30mg/kg treated animals is much less robust. Preliminary data using cultured hippocampal neurons shows that, while EmtinB concentrations up to 100µM are protective against CuAβ, concentrations above 100µM may cause a decrease in cell viability (see Figure 3.11). This suggests that EmtinB can be protective, but above threshold concentrations decrease the efficacy of EmtinB protection or may even be independently detrimental. In light of this, a key future experiment would be to determine optimal dosing of EmtinB in both culture and animal models. Additionally, it has not yet been established what effect EmtinB has on wild-type mice in terms of cognitive performance, however this is a key question and should be investigated in future studies to determine if EmtinB produces improved cognition across all animal types or acts specifically on pathological processes within the brain.

5.4.3 Aβ accumulation is unaffected by EmtinB treatment

Amyloid plaques are one of the main pathological hallmarks of AD. First described by Alouis Alzheimer in 1906 [237], the discovery of amyloid plaques and, subsequently, the identification of their main component as the β-amyloid peptide, led to intense investigation into the role of the β-amyloid peptide in AD pathogenesis [131]. These studies have confirmed the important role that Aβ plays in AD, with genetic studies showing that, in familial disease, AD is strongly associated with mutations in the amyloid precursor protein (APP) and APP processing proteins, such as presinilin 1 (PS1) [238]. More recently, it has been found that soluble Aβ levels correlate well with cognitive decline [239-243], leading to the theory that it is soluble Aβ that constitutes the main pathological form of Aβ. The implication of soluble and deposited Aβ in the pathogenesis of AD has led to amyloid pathology being the main target of a number of potential AD therapies and, while cognitive improvements are the gold-standard measure of

therapeutic efficacy, researchers commonly use hallmarks such as plaque load and soluble Aβ levels as correlates to cognitive data, or as indicators of therapeutic action themselves.

In this study, both soluble Aβ and plaque load were assessed as indicators of EmtinB action. Investigation of amyloid plaque deposition by immunohistochemistry of insoluble deposits showed no changes in amyloid plaque levels after EmtinB treatment at 5 or 30mg/kg. This lack of change was reflected in the soluble Aβ levels by ELISA analysis of soluble hAβ1-42, which similarly showed no changes in soluble Aβ levels in EmtinB treated APPswe/PS1ΔE9 mouse brains. Taken together, the data suggests that EmtinB does not modulate Aβ accumulation in the APPswe/PS1ΔE9 mouse brain.

5.4.3 EmtinB does not alter Aβ production or clearance in the APPswe/PS1ΔE9 mouse model of AD

Changes in Aβ accumulation, such as a decreased plaque load or reduced soluble Aβ load, would have indicated changes in either in Aβ production, for example by APP modulation to reduce Aβ production, or improvement in Aβ clearance, such as improved transport across the blood-brain barrier by LRP1.

APP is the parent protein for the Aβ peptide, and the APPswe/PS1ΔE9 mouse model of AD overexpresses APP as part of its generation of pathological amyloid and subsequent deposition. There is some evidence that modulation of APP can be used to reduce Aβ. Asuni et al. [244] found that using a compound called 2-PMAP, they could bring about a decrease in APP in an APP-overexpressing mouse model of AD *via* an inhibition of RNA translation to protein. Subsequently, these mice demonstrated improved memory performance and reduction in Aβ deposition in the brain. Other studies have shown that modulation of this overexpressed APP can have positive benefits in cognition and amyloid accumulation in the mouse model brain [245-247].

LRP1 is a key player in Aβ clearance from the brain, facilitating both clearance of Aβ from the brain by transportation across the BBB, and cellular uptake of Aβ for subsequent lysosomal degradation [248]. Interestingly, brain levels of LRP have been shown to be decreased in both AD brain and aged human brain [249], as well as in aged rat brain [250]. Given the pivotal role of LRP1 in Aβ clearance and the decline in LRP levels during disease and aging, LRPs have garnered interest as a therapeutic target for the treatment of AD and other diseases [251, 252].

As decreases in LRP1 are potentially an exacerbating factor in the pathogenic progression in APPswe/PS1ΔE9 mice, it is possible that EmtinB-induced cognitive improvements in APPswe/PS1ΔE9 mice could be a result of modulation of LRP1 levels in the brain.

Both APP and LRP1 levels were assessed by western blot and neither of these proteins were found to be altered in response to EmtinB treatment compared to control APPswe/PS1ΔE9 mice. As neither APP nor LRP1 levels were altered in the EmtinB-treated mice, EmtinB-induced improvement in cognitive outcomes in these mice is not likely due to reduction in Aβ pathology.

The inability of EmtinB to alter amyloid accumulation is consistent with the western blot data that shows EmtinB is not able to alter APP or LRP1 levels in the APPswe/PS1ΔE9 mouse model of AD.

5.4.4 EmtinB modulates astroglial but not microglial activation in APPswe/PS1ΔE9 mice

Gliosis is a key pathological event in the AD brain and is believed to not only be a symptom of AD, but a contributor to disease pathogenesis [253]. The Aβ peptide has been shown to activate both microglia and astrocytes and, under various circumstances, metallothioneins

have been shown to reverse this gliosis [75, 76, 83, 84], raising the possibility that EmtinB may act to decrease gliosis in the APPswe/PS1ΔE9 mouse model of AD.

5.4.4.1 EmtinB does not alter levels of microglial marker IBA1

Microglia are the immune cells of the brain and become activated in response to insult or injury. Activation of microglia induces rapid proliferation, as well as alterations, in microglial marker expression and morphology compared with quiescent microglia.

In the AD brain, changes in both molecular and morphological characteristics of microglia are observed [254]. Microglia that are in the vicinity of plaques proliferate and accumulate around plaques [255, 256] and undergo morphological changes consistent with activated microglial morphology [257]. While the activation of microglia under some circumstances has been shown to be beneficial [255, 258], there is increasing evidence that microglial activation contributes to AD pathogenesis by initiating and/or maintaining inflammation, with plaque-associated activated microglia found to express pro-inflammatory cytokines such as interleukin-1 (IL-1) and tumour necrosis factor-α (TNF-α) [255, 257]. Indeed, in vitro studies have shown that Aβ peptide can induce microglial activation [259-261] and this microglial activated subsequently potentiates neuronal cell death [259]. This evidence indicates that decreasing microglial activation could prevent Aβ-mediated damage to neurons.

Interestingly, MT2 has been shown to decrease microglial activation in rat [83] and mouse [84] models of traumatic brain injury (TBI). Further evidence for MT regulation of microglial activation comes from studies of MT-overexpressing mice and MTKO mice, wherein mice that overexpress MT show less microglial activation, and subsequent neuronal loss, after TBI [76], while increased microglial activation is observed in MTKO mice after cryolesion [75]. Given that MT2 is able to effect a change in microglial activation, it seems plausible that EmtinB might also be capable of modulating microglial activation in response to Aβ.

In this study the activation of microglia was examined by western blot analysis of IBA1 levels in whole-hemisphere brain extracts from EmtinB trial mice. Interestingly, EmtinB was not able to affect microglial activation, as measured by unaltered IBA1 protein level, suggesting that, unlike MT2, EmtinB does not modulate microglial activation state.

IBA1 expression is a commonly used marker of microglia and is upregulated during activation. Theoretically, IBA1 should reflect changes in microglial activation as microglia undergo rapid proliferation in response to insult or injury. However, IBA1 is not able to distinguish between the specific activation states of microglia. Microglia can exist in two phenotypically discrete activation states, termed M1 (classical activation) and M2 (alternate activation). Microglia can produce either cytotoxic or protective effects depending on the whether they are of M1 or M2 phenotype [262]. In AD, classically activated microglia are associated with plaques and are responsible for the pro-inflammatory environment of the AD brain [263]. Future directions for this work should include an investigation into which microglial activation state is predominant in the APPswe/PS1ΔE9 mouse brain, and whether EmtinB is able to alter this to a more favourable microglial activation phenotype. It would also be important to histologically investigate the morphology and neurochemical signature of activated microglia surrounding amyloid plaques.

5.4.4.1 EmtinB decreases GFAP levels in APPswe/PS1ΔE9 mice

Astrocytes are specialized glial cells which carry out supportive and protective roles within the central nervous system [264, 265]. As with microglia, astrocytes become reactive in response to illness or injury, and this activation induces changes in protein expression and morphology; this response is termed reactive astrogliosis [264, 265].

Astrogliosis is a common feature of AD [264], with reactive astrocytes associated with plaques in the brain parenchyma of both animal models of AD [266, 267] and human AD patients [266, 268, 269]. Much like microglia, astrocyte activation can be protective against a range of CNS

insults (reviewed in [264]), however reactive astrocytes can release pro- and anti-inflammatory cytokines [270] and thus can have beneficial or detrimental effects depending on context [264]. There is evidence that astrogliosis plays a detrimental role in AD disease progression [271] and contributes to the impairment of synaptic transmission and memory loss in the aging process [272]**.** A recent study by Garwood et al. [273] demonstrated that Aβ induced morphological changes, and inflammatory cytokine release, in primary astrocyte cultures. Furthermore, Aβ-treated astrocytes promoted neuronal cell death [273]. Modulation of astrogliosis has been propositioned as a therapeutic target for AD. GFAP expression is the prototypical marker for astrocyte identification. GFAP is highly expressed in activated astrocytes but is often not detectable in astrocytes in healthy CNS tissue [264]. As such, GFAP is regarded as a sensitive method for detecting activated astrocytes. GFAP has been found to be increased in temporal tissue from AD patient brains compared to control [274], and is increased in APPswe/PS1ΔE9 mice compared with wild-type control (see Figure 5.12).

EmtinB has been shown in this study to reduce GFAP levels compared with saline vehicle-treated APPswe/PS1ΔE9 mice, suggesting that EmtinB is reducing astrogliosis and decreasing GFAP levels back toward wild-type levels. Interestingly, GFAP levels were reduced in both 30mg/kg and 5mg/kg EmtinB dosed animals equally, while cognitive improvements were observed predominantly in 5mg/kg treated animals.

The ability of EmtinB to specifically modify astroglial activity correlates with reported observations that native metallothionein modulates astrocyte function. Metallothionein administered exogenously induces a regenerative reactive astrocyte phenotype [82] and, furthermore, reactive astrocytes have been shown to produce MT2 and promote regeneration in injured neurons [275]. To investigate the capacity of EmtinB to directly interact with astrocytes, it would be essential to look at the EmtinB/astrocyte interaction *in vitro* in primary cultured astrocytes. Preliminary investigation into the effect of EmtinB on primary cultured

astrocytes showed that treatment of astrocytes with EmtinB increased MT expression, suggesting that EmtinB can directly interact with astrocytes (data not shown). Thus, potentially, EmtinB is able to directly modify astrogliosis.

5.4.5 EmtinB does not alter synaptic markers

Loss of synapses is a hallmark of AD and is one of the strongest correlates of cognitive impairment [276]. Synaptophysin and PSD95 are widely used markers of synapses. Synaptophysin levels are decreased in the hippocampus of AD patients [277] and in transgenic AD mouse brain [278, 279]. Similarly, PSD95 levels have been found to be decreased in the hippocampus of subjects with mild cognitive impairment, in the cortex [280] and grey matter [281] of AD patients and in the hippocampus of 5xFAD transgenic mice [282]. In APP_{695}/PS1ΔE9 mice, both synaptophysin and PSD95 are markedly reduced the hippocampus and cortex at 12 months of age [283], suggesting that excitatory synapses have been lost. This is reflected in the APPswe/ PS1ΔE9 mouse model, with Mitew et al. [284] demonstrating decreased synaptophysin levels in the brains of APPswe/PS1ΔE9 at 12 months of age compared to wild-type aged-matched controls.

To determine if synaptic marker changes were observable in the hippocampus of EmtinB treated mice, compared with saline control mice, both Synaptophysin and PSD95 levels were assessed by western blot.

PSD95 and synaptophysin levels were not altered in EmtinB treated APPswe/PS1ΔE9 mice compared with control, suggesting that cognitive improvements in these mice were not a result of altered synaptic density in the hippocampus. However, changes to cognitive outcomes can be observed in the absence of synaptic changes.

Defects in a proximal area of the brain, the entorhinal cortex (ERC), have also been implicated in AD [285]. In the AD brain, the hippocampus and the ERC show the largest degree of

pathological change [286] and are among the first areas to develop plaques [285, 287]. Decosahexanoic acid (DHA) has been shown to improve cognitive outcomes in 3xTG AD mice, as measured by object recognition, with no effect on PSD95 or synaptophysin levels [285]. This improved cognition was linked to the direct effect of DHA on neuronal function, with DHA rescuing AD-related electrophysiological defects in the neurons. As changes in the entorhinal cortex pre-empt changes in the hippocampus, it is possible that EmtinB is eliciting changes in the ERC in this trial. Furthermore, while total levels of these synaptic proteins were unaltered by EmtinB treatment, this does not necessarily indicate that there has been no change in the number of functional synapses. Functional synapses can be assessed using immunohistochemistry to determine synapses where both presynaptic and postsynaptic markers co-locate. Future studies should evaluate the distribution of synaptic proteins to determine if there are differences in the colocation of pre- and post-synaptic markers in EmtinB treated mice compared with saline vehicle-treated mice.

5.4.6 Alternate theory of EmtinB action

As this work was unable to conclusively prove the presence of EmtinB in the brain, the possibility that EmtinB dimer was unable to cross the BBB must be considered. Given that the EmtinB had a significant impact on animal behaviour, it is possible the emtins may be exerting an effect on processes within the brain by a mechanism external to the CNS. An explanation of this mechanism may come from the work of Pankhurst [288]. Pankhurst observed that metallothionein plays a protective role after cryolesion brain injury as evidenced by prolonged neuronal death in MTKO mice compared to wild-type mice [288]. However, Pankhurst also noted that at least part of this action was related to peripheral effects of MT rather than direct CNS effects [288]. T cells are an important part of the immune response and when activated can infiltrate the CNS [289]. Interestingly, evidence suggests that T cells may be a contributor to the pathology of diseases such as multiple sclerosis and experimental autoimmune

encephalopathy (EAE) [290, 291] which might suggest that T cells would also contribute to the pathology of brain injury. In experiments performed by Pankhurst, the number of T cells infiltrating the cryolesion injury site was significantly higher 7 days post-injury in MTKO mice compared with wild-type mice, suggesting that immune system function is altered in the absence of MT [288].

Additionally, Pankhurst noted that MT2 was upregulated in the liver of wild-type mice that has been subjected to cryolesion as part of the acute phase response, which is the early defense system activated by stimuli such as infection or injury [288]. This response was predictably absent in MTKO mice and Pankhurst postulates that, as zinc availability affects the function of the immune system, it is possible that metallothionein modulates some aspects of immune response via zinc homeostasis [288].

If indeed MT is able to modulate the immune system response to brain injury to promote a more positive outcome in the CNS, then as an MT-mimetic it follows that emtins may also have this capacity.

5.4.7 Conclusion

EmtinB improved some features of cognitive performance in the APPswe/PS1ΔE9 AD mouse compared with SSV APPswe/PS1ΔE9 controls, as measured by the Y-maze. EmtinB was not found to alter either soluble or deposited Aβ levels, and, additionally, neither APP nor LRP1 levels were altered in whole-hemisphere extracts, suggesting that EmtinB does not influence either production or clearance in the APPswe/PS1ΔE9 mouse. No synaptic changes were detected on the hippocampus of EmtinB treated mice, with no significant changes found in either synaptophysin or PSD95 levels. Interestingly, while EmtinB did not alter microglial activation, as measured by IBA1, GFAP levels were significantly reduced, suggesting that EmtinB was able to modulate astrogliosis. The data show that EmtinB is able to positively modulate astrogliosis and improve cognitive outcomes in the APPswe/PS1ΔE9 model of AD.

Chapter 6 – Final discussion

Findings of this work

This thesis has investigated the potential of emtins to protect cultured neurons against CuAβ toxicity, the mechanism of EmtinB action in culture, and attempted to determine if EmtinB has beneficial effects in the APPswe/PS1ΔE9 model of AD.

Aim 1: Efficacy of emtin protection in the CuAβ model of Aβ insult

This work has shown that both EmtinAc and EmtinB, in tetrameric form, are capable of protecting hippocampal neuron cultures from CuAβ-mediated toxicity. In these experiments, EmtinB appeared to be more efficacious. Tetrameric EmtinB was shown to be as efficacious as parent protein MT2 in the CuAβ model of toxicity. A comparison of EmtinB tetrameric and dimeric forms showed that EmtinB dimer was significantly more efficacious in protecting cultured hippocampal neurons against CuAβ-mediated toxicity. Taken together, these data suggest that EmtinB dimer is the most promising potential therapeutic tested in this work. Interestingly, pre-treatment of hippocampal neurons with EmtinB dimer had no protective effect, suggesting that EmtinB needs to be present at the time of insult.

Aim 2: Mechanism of dimeric EmtinB protection in the CuAβ model of toxicity

While a mechanism of action was not unequivocally determined, this work has identified the capacity of EmtinB to bind both copper and zinc and to use bound zinc to undergo a metal swap with CuAβ1-42. Apo-EmtinB was unable to affect CuAβ aggregation and, as EmtinB is added to cultures in Apo form, for metal swap to be the mechanism of EmtinB action in the CuAβ model of Aβ toxicity, the EmtinB must be scavenging metals from the experimental cultures. The current study was unable to confirm that EmtinB scavenges metals from cultures,

with no metals found to be associated with EmtinB after incubation with either fresh tissue culture media or tissue culture media conditioned by cortical neurons; thus other mechanisms of action were considered.

The action of emtin peptides in previous studies have been linked to their ability to act through the LRP family of receptors [94, 185]. Consistent with this, EmtinB protective action against CuAβ toxicity could be effectively blocked when neurons were pre-incubated with RAP, indicating that EmtinB was unable to protect cells when LRP receptors were inaccessible to ligands. Receptor knockdown using siRNA against LRP1 and LRP2 was unable to block EmtinB action indicating that either, LRP1 and LRP2 are not involved in EmtinB action, or that the siRNA knockdown was insufficient to mute their activity.

EmtinB was additionally shown to protect cultured hippocampal neurons against H_2O_2 toxicity, a characteristic which has not been observed with its parent protein, MT2. Whether this was a direct result of radical scavenging or *via* a receptor mediated protective action has not yet been investigated.

Aim 3: EmtinB protective action in the APPswe/PS1ΔE9 model of AD

EmtinB administration to APPswe/PS1ΔE9 mice from 9-11 months of age improved cognitive outcomes in the AD model as assessed by the Y-maze. Analysis of soluble and deposited Aβ showed no changes in Aβ levels as a result of EmtinB treatment and, furthermore, no changes to APP or LRP1 were observed, suggesting that EmtinB does not modulate Aβ production or clearance.

No changes were observed in post or pre synaptic markers PSD95 and Synaptophysin in the hippocampus of EmtinB-treated mice, indicating that EmtinB is not altering synapses in the hippocampus to induce cognitive changes.

Interestingly, EmtinB altered astrogliosis in APPswe/PS1ΔE9 mice. While microglial activation did not appear to be altered, as per IBA1 levels, astrocyte activation was decreased in EmtinB treated mice as indicated by a significant reduction in GFAP levels. While astrocyte activation was decreased in EmtinB mice, it remains to be elucidated whether this is a direct effect of EmtinB on astrocytes or whether EmtinB affects other disease related factors and decreased glial activation is a secondary aspect of EmtinB action.

Future directions

To advance our understanding of EmtinB, as a potential therapeutic, future studies will be required to fully elucidate the mechanism of action of EmtinB. Confirmation of a mechanism of action would allow a more directed analysis of EmtinB action in the APPswe/PS1ΔE9 model of AD.

The current animal study offers scope for further investigation. Both sectioned tissue and frozen brain are available for further analysis. Analysis of these samples for other LRP family receptors or alternate receptors, markers of gliosis and synaptic dysfunction, or distribution of certain cell types may shape our understanding of the molecular mechanism of EmtinB. Additionally, given the reduction in GFAP observed in EmtinB-treated APPswe/PS1ΔE9 mice, determining the capacity of EmtinB to directly modulate astrogliosis should be a key aim of future studies.

Future animal studies looking at the EmtinB action in APPswe/PS1ΔE9 mice should encompass both temporal and dosage aspects of optimisation. Additionally, the inclusion of EmtinB treated and untreated control B6 mice would allow a more rigorous assessment of the effects of EmtinB in the APPswe/PS1ΔE9 cohort.

Final conclusion

This work has demonstrated that emtins are able to protect hippocampal neurons from CuAβ-induced toxicity in primary culture. Dimeric EmtinB was shown to be the most efficacious of the tested emtins. Comparison of tetrameric EmtinB and MT2 show that tetrameric EmtinB has a similar efficacy to MT2 and a further comparison of tetrameric and dimeric EmtinB suggest that dimeric EmtinB is the more efficacious peptide. These data suggest that the dimeric EmtinB peptide may represent a more effective therapeutic than the parent protein, MT2. While the exact mechanism of EmtinB protection is yet to be elucidated, the metal-swap mechanism, free radical scavenging and LRP-receptor mediated responses have all been implicated, raising the possibility that emtins could act synergistically *via* two or more mechanisms EmtinB has also elicited cognitive improvements and reduced astrogliosis, key clinical and pathological components of AD, in the APPswe/PS1ΔE9 mouse model of AD. Excitingly, these changes in clinical and pathological outcomes in the APPswe/PS1ΔE9 imply that EmtinB may be crossing the BBB and promoting beneficial outcomes in this mouse model of AD. Notably, these beneficial outcomes were observed in aged animals where treatment was administered post symptom onset. Given the lack of any prevention therapy currently available, emtins represent an exciting new modality to treat AD. Taken together, the data indicate that EmtinB could represent a novel therapeutic for the treatment of AD.

References

1. Margoshes, M., Vallee, B., *A cadmium protein from equine kidney cortex.* J. Am. Chem. Soc. , 1957. **79**: p. 4813-4814.
2. Ruttkay-Nedecky, B., et al., *The role of metallothionein in oxidative stress.* Int J Mol Sci, 2013. **14**(3): p. 6044-66.
3. Kagi, J.H., ed. *Metallothionein III: biological roles and medical implications*. ed. T.I. Suzuki, N; Kimura, M. 1993, Birkhauser Verlag: Basel, Switzerland. 29-55.
4. Palmiter, R.D., *The elusive function of metallothioneins.* Proc Natl Acad Sci U S A, 1998. **95**(15): p. 8428-30.
5. Masters, B.A., et al., *Metallothionein III is expressed in neurons that sequester zinc in synaptic vesicles.* J Neurosci, 1994. **14**(10): p. 5844-57.
6. Uchida, Y., *Growth-inhibitory factor, metallothionein-like protein, and neurodegenerative diseases.* Biol Signals, 1994. **3**(4): p. 211-5.
7. Acarin, L., et al., *Expression of growth inhibitory factor (metallothionein-III) mRNA and protein following excitotoxic immature brain injury.* J Neuropathol Exp Neurol, 1999. **58**(4): p. 389-97.
8. Moffatt, P. and C. Seguin, *Expression of the gene encoding metallothionein-3 in organs of the reproductive system.* DNA Cell Biol, 1998. **17**(6): p. 501-10.
9. Quaife, C.J., et al., *Induction of a new metallothionein isoform (MT-IV) occurs during differentiation of stratified squamous epithelia.* Biochemistry, 1994. **33**(23): p. 7250-9.
10. Cox, D.R. and R.D. Palmiter, *The metallothionein-I gene maps to mouse chromosome 8: implications for human Menkes' disease.* Hum Genet, 1983. **64**(1): p. 61-4.
11. Watanabe, T., et al., *Restriction fragment length variations and chromosome mapping of two mouse metallothionein genes, Mt-1 and Mt-2.* Biochem Genet, 1989. **27**(11-12): p. 689-97.
12. Liang, L., et al., *Activation of the complete mouse metallothionein gene locus in the maternal deciduum.* Mol Reprod Dev, 1996. **43**(1): p. 25-37.
13. Karin, M., et al., *Human metallothionein genes are clustered on chromosome 16.* Proc Natl Acad Sci U S A, 1984. **81**(17): p. 5494-8.
14. West, A.K., et al., *Human metallothionein genes: structure of the functional locus at 16q13.* Genomics, 1990. **8**(3): p. 513-8.
15. Garrett, S.H., et al., *Differential expression of human metallothionein isoform I mRNA in human proximal tubule cells exposed to metals.* Environ Health Perspect, 1998. **106**(12): p. 825-31.
16. Laukens, D., et al., *Human metallothionein expression under normal and pathological conditions: mechanisms of gene regulation based on in silico promoter analysis.* Crit Rev Eukaryot Gene Expr, 2009. **19**(4): p. 301-17.
17. Davis, S.R. and R.J. Cousins, *Metallothionein expression in animals: a physiological perspective on function.* J Nutr, 2000. **130**(5): p. 1085-8.
18. Kagi, J.H. and A. Schaffer, *Biochemistry of metallothionein.* Biochemistry, 1988. **27**(23): p. 8509-15.
19. Carpene, E., G. Andreani, and G. Isani, *Metallothionein functions and structural characteristics.* J Trace Elem Med Biol, 2007. **21 Suppl 1**: p. 35-9.

20. Cobbett, C. and P. Goldsbrough, *Phytochelatins and metallothioneins: roles in heavy metal detoxification and homeostasis.* Annu Rev Plant Biol, 2002. **53**: p. 159-82.
21. Li, Y. and W. Maret, *Human metallothionein metallomics.* Human metallothionein metallomics, 2008(Human metallothionein metallomics): p. 1055-1062.
22. Messerle, B.A., et al., *Three-dimensional structure of human [113Cd7]metallothionein-2 in solution determined by nuclear magnetic resonance spectroscopy.* J Mol Biol, 1990. **214**(3): p. 765-79.
23. Casini, A., et al., *Reactivity of an antimetastatic organometallic ruthenium compound with metallothionein-2: relevance to the mechanism of action.* Metallomics, 2009. **1**(5): p. 434-41.
24. Udom, A.O. and F.O. Brady, *Reactivation in vitro of zinc-requiring apo-enzymes by rat liver zinc-thionein.* Biochem J, 1980. **187**(2): p. 329-35.
25. Cano-Gauci, D.F. and B. Sarkar, *Reversible zinc exchange between metallothionein and the estrogen receptor zinc finger.* FEBS Lett, 1996. **386**(1): p. 1-4.
26. Maret, W., K.S. Larsen, and B.L. Vallee, *Coordination dynamics of biological zinc "clusters" in metallothioneins and in the DNA-binding domain of the transcription factor Gal4.* Proc Natl Acad Sci U S A, 1997. **94**(6): p. 2233-7.
27. Feng, W., et al., *Metallothionein transfers zinc to mitochondrial aconitase through a direct interaction in mouse hearts.* Biochem Biophys Res Commun, 2005. **332**(3): p. 853-8.
28. Roohani, N., et al., *Zinc and its importance for human health: An integrative review.* J Res Med Sci, 2013. **18**(2): p. 144-57.
29. Bertinato, J. and M.R. L'Abbe, *Maintaining copper homeostasis: regulation of copper-trafficking proteins in response to copper deficiency or overload.* J Nutr Biochem, 2004. **15**(6): p. 316-22.
30. Hamer, D.H., *Metallothionein.* Annu Rev Biochem, 1986. **55**: p. 913-51.
31. Michalska, A.E. and K.H. Choo, *Targeting and germ-line transmission of a null mutation at the metallothionein I and II loci in mouse.* Proc Natl Acad Sci U S A, 1993. **90**(17): p. 8088-92.
32. Durnam, D.M. and R.D. Palmiter, *Analysis of the detoxification of heavy metal ions by mouse metallothionein.* Experientia Suppl, 1987. **52**: p. 457-63.
33. Jahroudi, N., et al., *Cell-type specific and differential regulation of the human metallothionein genes. Correlation with DNA methylation and chromatin structure.* J Biol Chem, 1990. **265**(11): p. 6506-11.
34. Searle, P.F., et al., *Regulation, linkage, and sequence of mouse metallothionein I and II genes.* Mol Cell Biol, 1984. **4**(7): p. 1221-30.
35. Durnam, D.M. and R.D. Palmiter, *Transcriptional regulation of the mouse metallothionein-I gene by heavy metals.* J Biol Chem, 1981. **256**(11): p. 5712-6.
36. Miles, A.T., et al., *Induction, regulation, degradation, and biological significance of mammalian metallothioneins.* Crit Rev Biochem Mol Biol, 2000. **35**(1): p. 35-70.
37. Sato, M. and M. Kondoh, *Recent studies on metallothionein: protection against toxicity of heavy metals and oxygen free radicals.* Tohoku J Exp Med, 2002. **196**(1): p. 9-22.

38. Park, J.D., Y. Liu, and C.D. Klaassen, *Protective effect of metallothionein against the toxicity of cadmium and other metals(1).* Toxicology, 2001. **163**(2-3): p. 93-100.
39. Vallee, B.L., *Implications and inferences of metallothionein structure.* Experientia Suppl, 1987. **52**: p. 5-16.
40. Bains, M. and E.D. Hall, *Antioxidant therapies in traumatic brain and spinal cord injury.* Biochim Biophys Acta, 2012. **1822**(5): p. 675-84.
41. Pham-Huy, L.A., H. He, and C. Pham-Huy, *Free radicals, antioxidants in disease and health.* Int J Biomed Sci, 2008. **4**(2): p. 89-96.
42. Lobo, V., et al., *Free radicals, antioxidants and functional foods: Impact on human health.* Pharmacogn Rev, 2010. **4**(8): p. 118-26.
43. Mates, J.M., C. Perez-Gomez, and I. Nunez de Castro, *Antioxidant enzymes and human diseases.* Clin Biochem, 1999. **32**(8): p. 595-603.
44. Aouffen, M., et al., *Deglycosylated ceruloplasmin maintains its enzymatic, antioxidant, cardioprotective, and neuronoprotective properties.* Biochem Cell Biol, 2001. **79**(4): p. 489-97.
45. Taverne, Y.J., et al., *Reactive oxygen species and the cardiovascular system.* Oxid Med Cell Longev, 2013. **2013**: p. 862423.
46. Poljsak, B., D. Suput, and I. Milisav, *Achieving the balance between ROS and antioxidants: when to use the synthetic antioxidants.* Oxid Med Cell Longev, 2013. **2013**: p. 956792.
47. Dalton, T., R.D. Palmiter, and G.K. Andrews, *Transcriptional induction of the mouse metallothionein-I gene in hydrogen peroxide-treated Hepa cells involves a composite major late transcription factor/antioxidant response element and metal response promoter elements.* Nucleic Acids Res, 1994. **22**(23): p. 5016-23.
48. Cai, L., et al., *Metallothionein induction in human CNS in vitro: neuroprotection from ionizing radiation.* Int J Radiat Biol, 2000. **76**(7): p. 1009-17.
49. Nakagawa, I., et al., *Involvement of oxidative stress in paraquat-induced metallothionein synthesis under glutathione depletion.* Free Radic Biol Med, 1998. **24**(9): p. 1390-5.
50. Sato, M. and I. Bremner, *Oxygen free radicals and metallothionein.* Free Radic Biol Med, 1993. **14**(3): p. 325-37.
51. Andrews, G.K., *Regulation of metallothionein gene expression by oxidative stress and metal ions.* Biochem Pharmacol, 2000. **59**(1): p. 95-104.
52. Lazo, J.S., et al., *Enhanced sensitivity to oxidative stress in cultured embryonic cells from transgenic mice deficient in metallothionein I and II genes.* J Biol Chem, 1995. **270**(10): p. 5506-10.
53. Colangelo, D., et al., *Protective effect of metallothioneins against oxidative stress evaluated on wild type and MT-null cell lines by means of flow cytometry.* Biometals, 2004. **17**(4): p. 365-70.
54. Liu, J., et al., *Metallothionein-I/II knockout mice are sensitive to acetaminophen-induced hepatotoxicity.* J Pharmacol Exp Ther, 1999. **289**(1): p. 580-6.
55. You, H.J., K.J. Lee, and H.G. Jeong, *Overexpression of human metallothionein-III prevents hydrogen peroxide-induced oxidative stress in human fibroblasts.* FEBS Lett, 2002. **521**(1-3): p. 175-9.
56. Wanpen, S., et al., *Salsolinol, a dopamine-derived tetrahydroisoquinoline, induces cell death by causing oxidative stress in dopaminergic SH-SY5Y cells,*

and the said effect is attenuated by metallothionein. Brain Research, 2004. **1005**(1-2): p. 67-76.
57. Thornalley, P.J. and M. Vasak, *Possible role for metallothionein in protection against radiation-induced oxidative stress. Kinetics and mechanism of its reaction with superoxide and hydroxyl radicals.* Biochim Biophys Acta, 1985. **827**(1): p. 36-44.
58. Hussain, S., W. Slikker, Jr., and S.F. Ali, *Role of metallothionein and other antioxidants in scavenging superoxide radicals and their possible role in neuroprotection.* Neurochem Int, 1996. **29**(2): p. 145-52.
59. Kumari, M.V., M. Hiramatsu, and M. Ebadi, *Free radical scavenging actions of metallothionein isoforms I and II.* Free Radic Res, 1998. **29**(2): p. 93-101.
60. Schwarz, M.A., et al., *Metallothionein protects against the cytotoxic and DNA-damaging effects of nitric oxide.* Proc Natl Acad Sci U S A, 1995. **92**(10): p. 4452-6.
61. Anderson, R.S., K.M. Patel, and G. Roesijadi, *Oyster metallothionein as an oxyradical scavenger: implications for hemocyte defense responses.* Dev Comp Immunol, 1999. **23**(6): p. 443-9.
62. Kang, Y.J., *Metallothionein redox cycle and function.* Exp Biol Med (Maywood), 2006. **231**(9): p. 1459-67.
63. Rodriguez-Rodriguez, A., et al., *Oxidative stress in traumatic brain injury.* Current Medicinal Chemistry, 2014. **21**(10): p. 1201-11.
64. Uttara, B., et al., *Oxidative stress and neurodegenerative diseases: a review of upstream and downstream antioxidant therapeutic options.* Curr Neuropharmacol, 2009. **7**(1): p. 65-74.
65. Cornelius, C., et al., *Traumatic brain injury: oxidative stress and neuroprotection.* Antioxid Redox Signal, 2013. **19**(8): p. 836-53.
66. Barnham, K.J., C.L. Masters, and A.I. Bush, *Neurodegenerative diseases and oxidative stress.* Nat Rev Drug Discov, 2004. **3**(3): p. 205-14.
67. Facecchia, K., et al., *Oxidative toxicity in neurodegenerative diseases: role of mitochondrial dysfunction and therapeutic strategies.* J Toxicol, 2011. **2011**: p. 683728.
68. Juurlink, B.H. and P.G. Paterson, *Review of oxidative stress in brain and spinal cord injury: suggestions for pharmacological and nutritional management strategies.* J Spinal Cord Med, 1998. **21**(4): p. 309-34.
69. Rink, A., et al., *Evidence of apoptotic cell death after experimental traumatic brain injury in the rat.* Am J Pathol, 1995. **147**(6): p. 1575-83.
70. Hutchison, J.S., et al., *Neuronal apoptosis inhibitory protein expression after traumatic brain injury in the mouse.* J Neurotrauma, 2001. **18**(12): p. 1333-47.
71. Zhou, H., et al., *Moderate traumatic brain injury triggers rapid necrotic death of immature neurons in the hippocampus.* J Neuropathol Exp Neurol, 2012. **71**(4): p. 348-59.
72. Anderson, D.K., et al., *Effects of treatment with U-74006F on neurological outcome following experimental spinal cord injury.* J Neurosurg, 1988. **69**(4): p. 562-7.
73. Hall, E.D., J.M. Braughler, and J.M. McCall, *Antioxidant effects in brain and spinal cord injury.* J Neurotrauma, 1992. **9 Suppl 1**: p. S165-72.

74. Xu, W., et al., *Increased production of reactive oxygen species contributes to motor neuron death in a compression mouse model of spinal cord injury.* Spinal Cord, 2005. **43**(4): p. 204-13.
75. Penkowa, M., et al., *CNS wound healing is severely depressed in metallothionein I- and II-deficient mice.* J Neurosci, 1999. **19**(7): p. 2535-45.
76. Giralt, M., et al., *Metallothionein-1+2 protect the CNS after a focal brain injury.* Exp Neurol, 2002. **173**(1): p. 114-28.
77. Chung, R.S., et al., *Metallothionein-IIA promotes initial neurite elongation and postinjury reactive neurite growth and facilitates healing after focal cortical brain injury.* J Neurosci, 2003. **23**(8): p. 3336-42.
78. Kohler, L.B., et al., *The role of metallothionein II in neuronal differentiation and survival.* Brain Research, 2003. **992**(1): p. 128-36.
79. Ambjørn, M., et al., *Metallothionein and a peptide modeled after metallothionein , EmtinB , induce neuronal differentiation and survival through binding to receptors of the low-density lipoprotein receptor family.* Journal of Neurochemistry, 2008: p. 21-37.
80. Chung, R.S., et al., *Redefining the role of metallothionein within the injured brain: extracellular metallothioneins play an important role in the astrocyte-neuron response to injury.* J Biol Chem, 2008. **283**(22): p. 15349-58.
81. Yu, P., et al., *An in vitro model of reactive astrogliosis and its effect on neuronal growth.* Methods Mol Biol, 2012. **814**: p. 327-40.
82. Leung, Y.K., et al., *Metallothionein induces a regenerative reactive astrocyte phenotype via JAK/STAT and RhoA signalling pathways.* Exp Neurol, 2010. **221**(1): p. 98-106.
83. Chung, R.S., et al., *Metallothionein treatment attenuates microglial activation and expression of neurotoxic quinolinic acid following traumatic brain injury.* Neurotox Res, 2009. **15**(4): p. 381-9.
84. Potter, E.G., et al., *Basic science; metallothionein I and II attenuate the thalamic microglial response following traumatic axotomy in the immature brain.* J Neurotrauma, 2007. **24**(1): p. 28-42.
85. Spuch, C., S. Ortolano, and C. Navarro, *LRP-1 and LRP-2 receptors function in the membrane neuron. Trafficking mechanisms and proteolytic processing in Alzheimer's disease.* Front Physiol, 2012. **3**: p. 269.
86. Gent, J. and I. Braakman, *Low-density lipoprotein receptor structure and folding.* Cell Mol Life Sci, 2004. **61**(19-20): p. 2461-70.
87. Dieckmann, M., M.F. Dietrich, and J. Herz, *Lipoprotein receptors--an evolutionarily ancient multifunctional receptor family.* Biol Chem, 2010. **391**(11): p. 1341-63.
88. Pedersen, M.O., et al., *Metallothionein-I+II in neuroprotection.* Biofactors, 2009. **35**(4): p. 315-25.
89. Klassen, R.B., et al., *Megalin mediates renal uptake of heavy metal metallothionein complexes.* Am J Physiol Renal Physiol, 2004. **287**(3): p. F393-403.
90. Fitzgerald, M., et al., *Metallothionein-IIA promotes neurite growth via the megalin receptor.* Exp Brain Res, 2007. **183**(2): p. 171-80.
91. Lu, Z. and S. Xu, *ERK1/2 MAP kinases in cell survival and apoptosis.* IUBMB Life, 2006. **58**(11): p. 621-31.

92. Song, G., G. Ouyang, and S. Bao, *The activation of Akt/PKB signaling pathway and cell survival.* J Cell Mol Med, 2005. **9**(1): p. 59-71.
93. Wasan, K.M., et al., *Impact of lipoproteins on the biological activity and disposition of hydrophobic drugs: implications for drug discovery.* Nat Rev Drug Discov, 2008. **7**(1): p. 84-99.
94. Ambjorn, M., et al., *Metallothionein and a peptide modeled after metallothionein, EmtinB, induce neuronal differentiation and survival through binding to receptors of the low-density lipoprotein receptor family.* Journal of Neurochemistry, 2008. **104**(1): p. 21-37.
95. O'Brien, R.J. and P.C. Wong, *Amyloid precursor protein processing and Alzheimer's disease.* Annu Rev Neurosci, 2011. **34**: p. 185-204.
96. Haass, C., et al., *Trafficking and Proteolytic Processing of APP.* Cold Spring Harb Perspect Med, 2012. **2**(5).
97. Roch, J.M., et al., *Increase of synaptic density and memory retention by a peptide representing the trophic domain of the amyloid beta/A4 protein precursor.* Proc Natl Acad Sci U S A, 1994. **91**(16): p. 7450-4.
98. Meziane, H., et al., *Memory-enhancing effects of secreted forms of the beta-amyloid precursor protein in normal and amnestic mice.* Proc Natl Acad Sci U S A, 1998. **95**(21): p. 12683-8.
99. Qiu, W.Q., et al., *Cell-surface beta-amyloid precursor protein stimulates neurite outgrowth of hippocampal neurons in an isoform-dependent manner.* J Neurosci, 1995. **15**(3 Pt 2): p. 2157-67.
100. Wong, B.X., et al., *beta-Amyloid precursor protein does not possess ferroxidase activity but does stabilize the cell surface ferrous iron exporter ferroportin.* Plos One, 2014. **9**(12): p. e114174.
101. Thinakaran, G. and E.H. Koo, *Amyloid precursor protein trafficking, processing, and function.* J Biol Chem, 2008. **283**(44): p. 29615-9.
102. Lehman, E.J., et al., *Genetic background regulates beta-amyloid precursor protein processing and beta-amyloid deposition in the mouse.* Hum Mol Genet, 2003. **12**(22): p. 2949-56.
103. Nag, S., et al., *Nature of the amyloid-beta monomer and the monomer-oligomer equilibrium.* J Biol Chem, 2011. **286**(16): p. 13827-33.
104. Zhao, Y. and B. Zhao, *Oxidative stress and the pathogenesis of Alzheimer's disease.* Oxid Med Cell Longev, 2013. **2013**: p. 316523.
105. Zhao, Y., et al., *Mimicry of high-density lipoprotein: functional peptide-lipid nanoparticles based on multivalent peptide constructs.* Journal of the American Chemical Society, 2013. **135**(36): p. 13414-24.
106. Butterfield, D.A. and D. Boyd-Kimball, *Amyloid beta-peptide(1-42) contributes to the oxidative stress and neurodegeneration found in Alzheimer disease brain.* Brain Pathol, 2004. **14**(4): p. 426-32.
107. Hensley, K., et al., *A model for beta-amyloid aggregation and neurotoxicity based on free radical generation by the peptide: relevance to Alzheimer disease.* Proc Natl Acad Sci U S A, 1994. **91**(8): p. 3270-4.
108. Behl, C., et al., *Hydrogen peroxide mediates amyloid beta protein toxicity.* Cell, 1994. **77**(6): p. 817-27.
109. Marcus, D.L., et al., *Increased peroxidation and reduced antioxidant enzyme activity in Alzheimer's disease.* Exp Neurol, 1998. **150**(1): p. 40-4.

110. Omar, R.A., et al., *Increased Expression but Reduced Activity of Antioxidant Enzymes in Alzheimer's Disease.* J Alzheimers Dis, 1999. **1**(3): p. 139-145.
111. Pappolla, M.A., et al., *Immunohistochemical evidence of oxidative [corrected] stress in Alzheimer's disease.* Am J Pathol, 1992. **140**(3): p. 621-8.
112. Tamagno, E., et al., *Oxidative stress activates a positive feedback between the gamma- and beta-secretase cleavages of the beta-amyloid precursor protein.* Journal of Neurochemistry, 2008. **104**(3): p. 683-95.
113. Feng, Y. and X. Wang, *Antioxidant therapies for Alzheimer's disease.* Oxid Med Cell Longev, 2012. **2012**: p. 472932.
114. Sano, M., et al., *A controlled trial of selegiline, alpha-tocopherol, or both as treatment for Alzheimer's disease. The Alzheimer's Disease Cooperative Study.* N Engl J Med, 1997. **336**(17): p. 1216-22.
115. Dysken, M.W., et al., *Effect of vitamin E and memantine on functional decline in Alzheimer disease: the TEAM-AD VA cooperative randomized trial.* JAMA, 2014. **311**(1): p. 33-44.
116. Ikeda, T., et al., *Treatment of Alzheimer-type dementia with intravenous mecobalamin.* Clin Ther, 1992. **14**(3): p. 426-37.
117. Lovell, M.A., et al., *Copper, iron and zinc in Alzheimer's disease senile plaques.* J Neurol Sci, 1998. **158**(1): p. 47-52.
118. Drago, D., S. Bolognin, and P. Zatta, *Role of metal ions in the abeta oligomerization in Alzheimer's disease and in other neurological disorders.* Curr Alzheimer Res, 2008. **5**(6): p. 500-7.
119. Tougu, V., A. Tiiman, and P. Palumaa, *Interactions of Zn(II) and Cu(II) ions with Alzheimer's amyloid-beta peptide. Metal ion binding, contribution to fibrillization and toxicity.* Metallomics, 2011. **3**(3): p. 250-61.
120. Smith, D.G., R. Cappai, and K.J. Barnham, *The redox chemistry of the Alzheimer's disease amyloid beta peptide.* Biochim Biophys Acta, 2007. **1768**(8): p. 1976-90.
121. Huang, X., et al., *Cu(II) potentiation of alzheimer abeta neurotoxicity. Correlation with cell-free hydrogen peroxide production and metal reduction.* J Biol Chem, 1999. **274**(52): p. 37111-6.
122. Adlard, P.A. and A.I. Bush, *Metals and Alzheimer's disease.* J Alzheimers Dis, 2006. **10**(2-3): p. 145-63.
123. Kaden, D., et al., *Disturbed copper bioavailability in Alzheimer's disease.* Int J Alzheimers Dis, 2011. **2011**: p. 345614.
124. Manso, Y., et al., *Copper modulation as a therapy for Alzheimer's disease?* Int J Alzheimers Dis, 2011. **2011**: p. 370345.
125. Adlard, P.A., et al., *Rapid restoration of cognition in Alzheimer's transgenic mice with 8-hydroxy quinoline analogs is associated with decreased interstitial Abeta.* Neuron, 2008. **59**(1): p. 43-55.
126. Cherny, R.A., et al., *Treatment with a copper-zinc chelator markedly and rapidly inhibits beta-amyloid accumulation in Alzheimer's disease transgenic mice.* Neuron, 2001. **30**(3): p. 665-76.
127. Ritchie, C.W., et al., *Metal-protein attenuation with iodochlorhydroxyquin (clioquinol) targeting Abeta amyloid deposition and toxicity in Alzheimer disease: a pilot phase 2 clinical trial.* Arch Neurol, 2003. **60**(12): p. 1685-91.

128. Lannfelt, L., et al., *Safety, efficacy, and biomarker findings of PBT2 in targeting Abeta as a modifying therapy for Alzheimer's disease: a phase IIa, double-blind, randomised, placebo-controlled trial.* Lancet Neurol, 2008. **7**(9): p. 779-86.
129. Niikura, T., H. Tajima, and Y. Kita.
130. Simoncini, C., et al., *Alzheimer's Pathogenesis and Its Link to the Mitochondrion.* Oxid Med Cell Longev, 2015. **2015**: p. 803942.
131. Hardy, J.A. and G.A. Higgins, *Alzheimer's disease: the amyloid cascade hypothesis.* Science, 1992. **256**(5054): p. 184-5.
132. Cummings, B.J. and C.W. Cotman, *Image analysis of beta-amyloid load in Alzheimer's disease and relation to dementia severity.* Lancet, 1995. **346**(8989): p. 1524-8.
133. Arriagada, P.V., et al., *Neurofibrillary tangles but not senile plaques parallel duration and severity of Alzheimer's disease.* Neurology, 1992. **42**(3 Pt 1): p. 631-9.
134. Schmitz, C., et al., *Hippocampal neuron loss exceeds amyloid plaque load in a transgenic mouse model of Alzheimer's disease.* Am J Pathol, 2004. **164**(4): p. 1495-502.
135. Pike, C.J., et al., *In vitro aging of beta-amyloid protein causes peptide aggregation and neurotoxicity.* Brain Research, 1991. **563**(1-2): p. 311-4.
136. Busciglio, J., A. Lorenzo, and B.A. Yankner, *Methodological variables in the assessment of beta amyloid neurotoxicity.* Neurobiol Aging, 1992. **13**(5): p. 609-12.
137. Mattson, M.P., K.J. Tomaselli, and R.E. Rydel, *Calcium-destabilizing and neurodegenerative effects of aggregated beta-amyloid peptide are attenuated by basic FGF.* Brain Research, 1993. **621**(1): p. 35-49.
138. Kowall, N.W., et al., *An in vivo model for the neurodegenerative effects of beta amyloid and protection by substance P.* Proc Natl Acad Sci U S A, 1991. **88**(16): p. 7247-51.
139. Dahlgren, K.N., et al., *Oligomeric and fibrillar species of amyloid-beta peptides differentially affect neuronal viability.* J Biol Chem, 2002. **277**(35): p. 32046-53.
140. Kumar-Singh, S., et al., *Mean age-of-onset of familial alzheimer disease caused by presenilin mutations correlates with both increased Abeta42 and decreased Abeta40.* Hum Mutat, 2006. **27**(7): p. 686-95.
141. Sakono, M. and T. Zako, *Amyloid oligomers: formation and toxicity of Abeta oligomers.* FEBS J, 2010. **277**(6): p. 1348-58.
142. Glabe, C.G. and R. Kayed, *Common structure and toxic function of amyloid oligomers implies a common mechanism of pathogenesis.* Neurology, 2006. **66**(2 Suppl 1): p. S74-8.
143. Sondag, C.M., G. Dhawan, and C.K. Combs, *Beta amyloid oligomers and fibrils stimulate differential activation of primary microglia.* J Neuroinflammation, 2009. **6**: p. 1.
144. Caughey, B. and P.T. Lansbury, *Protofibrils, pores, fibrils, and neurodegeneration: separating the responsible protein aggregates from the innocent bystanders.* Annu Rev Neurosci, 2003. **26**: p. 267-98.
145. Glabe, C.G., *Common mechanisms of amyloid oligomer pathogenesis in degenerative disease.* Neurobiol Aging, 2006. **27**(4): p. 570-5.

146. Zhu, Y.J., H. Lin, and R. Lal, *Fresh and nonfibrillar amyloid beta protein(1-40) induces rapid cellular degeneration in aged human fibroblasts: evidence for AbetaP-channel-mediated cellular toxicity.* FASEB J, 2000. **14**(9): p. 1244-54.
147. Gong, Y., et al., *Alzheimer's disease-affected brain: presence of oligomeric A beta ligands (ADDLs) suggests a molecular basis for reversible memory loss.* Proc Natl Acad Sci U S A, 2003. **100**(18): p. 10417-22.
148. Koudinov, A., et al., *The soluble form of Alzheimer's amyloid beta protein is complexed to high density lipoprotein 3 and very high density lipoprotein in normal human plasma.* Biochem Biophys Res Commun, 1994. **205**(2): p. 1164-71.
149. Ghiso, J., et al., *The cerebrospinal-fluid soluble form of Alzheimer's amyloid beta is complexed to SP-40,40 (apolipoprotein J), an inhibitor of the complement membrane-attack complex.* Biochem J, 1993. **293 (Pt 1)**: p. 27-30.
150. Naslund, J., et al., *Correlation between elevated levels of amyloid beta-peptide in the brain and cognitive decline.* JAMA, 2000. **283**(12): p. 1571-7.
151. McLean, C.A., et al., *Soluble pool of Abeta amyloid as a determinant of severity of neurodegeneration in Alzheimer's disease.* Ann Neurol, 1999. **46**(6): p. 860-6.
152. Lue, L.F., et al., *Soluble amyloid beta peptide concentration as a predictor of synaptic change in Alzheimer's disease.* Am J Pathol, 1999. **155**(3): p. 853-62.
153. Yankner, B.A. and T. Lu, *Amyloid beta-protein toxicity and the pathogenesis of Alzheimer disease.* J Biol Chem, 2009. **284**(8): p. 4755-9.
154. Ladiwala, A.R., et al., *Resveratrol selectively remodels soluble oligomers and fibrils of amyloid Abeta into off-pathway conformers.* J Biol Chem, 2010. **285**(31): p. 24228-37.
155. Hidalgo, J., et al., *Expression of metallothionein-I, -II, and -III in Alzheimer disease and animal models of neuroinflammation.* Exp Biol Med (Maywood), 2006. **231**(9): p. 1450-8.
156. Carrasco, J., et al., *Metallothionein-I and -III expression in animal models of Alzheimer disease.* Neuroscience, 2006. **143**(4): p. 911-22.
157. Adlard, P.A., A.K. West, and J.C. Vickers, *Increased density of metallothionein I/II-immunopositive cortical glial cells in the early stages of Alzheimer's disease.* Neurobiol Dis, 1998. **5**(5): p. 349-56.
158. Irie, Y. and W.M. Keung, *Metallothionein-III antagonizes the neurotoxic and neurotrophic effects of amyloid beta peptides.* Biochem Biophys Res Commun, 2001. **282**(2): p. 416-20.
159. Chung, R.S., et al., *The Native Copper- and Zinc- Binding Protein Metallothionein Blocks Copper-Mediated A beta Aggregation and Toxicity in Rat Cortical Neurons.* Plos One, 2010. **5**(8).
160. Meloni, G., et al., *Metal swap between Zn7-metallothionein-3 and amyloid-beta-Cu protects against amyloid-beta toxicity.* Nature Chemical Biology, 2008. **4**(6): p. 366-72.
161. Howells, C., A.K. West, and R.S. Chung, *Neuronal growth-inhibitory factor (metallothionein-3): evaluation of the biological function of growth-inhibitory factor in the injured and neurodegenerative brain.* Febs Journal, 2010. **277**(14): p. 2931-2939.

162. Lewis, K.E., et al., *Distribution of exogenous metallothionein following intraperitoneal and intramuscular injection of metallothionein-deficient mice.* Histol Histopathol, 2012. **27**(11): p. 1459-70.
163. Ali, A., Rani, R., Kumar, S., *New Peptide Based Therapeutic Approaches*, in *Advances is Protein Chemistry* G.M. Ashraf, Sheikh, I. A. , Editor. 2013, Omics Group International
164. Uhlig, T., et al., *The emergence of peptides in the pharmaceutical business: From exploration to exploitation.* EuPA Open Proteomics, 2014. **4**: p. 58-69.
165. Fosgerau, K. and T. Hoffmann, *Peptide therapeutics: current status and future directions.* Drug Discov Today, 2015. **20**(1): p. 122-8.
166. Boas, U. and P.M. Heegaard, *Dendrimers in drug research.* Chem Soc Rev, 2004. **33**(1): p. 43-63.
167. Abbasi, E., et al., *Dendrimers: synthesis, applications, and properties.* Nanoscale Res Lett, 2014. **9**(1): p. 247.
168. Hawker, C.J. and J.M. Frechet, *Preparation of polymers with controlled molecular architecture. A new convergent approach to dendritic macromolecules.* J. Am. Chem. Soc., 1990. **112**(21): p. 7638-7647.
169. Grayson, S.M. and J.M. Frechet, *Convergent dendrons and dendrimers: from synthesis to applications.* Chem Rev, 2001. **101**(12): p. 3819-68.
170. Klajnert, B., et al., *Biological properties of low molecular mass peptide dendrimers.* Int J Pharm, 2006. **309**(1-2): p. 208-17.
171. Mintzer, M.A. and M.W. Grinstaff, *Biomedical applications of dendrimers: a tutorial.* Chem Soc Rev, 2011. **40**(1): p. 173-90.
172. Aulenta, F., W. Hayes, and S. Rannard, *Dendrimers: a new class of nanoscopic containers and delivery devices.* European Polymer Journal, 2003. **39**(9): p. 1741-1771.
173. McGregor, D.P., *Discovering and improving novel peptide therapeutics.* Curr Opin Pharmacol, 2008. **8**(5): p. 616-9.
174. Vlieghe, P., et al., *Synthetic therapeutic peptides: science and market.* Drug Discov Today, 2010. **15**(1-2): p. 40-56.
175. Boas, U., J. Christensen, and P.M. Heegaard, eds. *Dendrimers in Medicine and Biotechnology*. 2006, The Royal Society of Chemistry.
176. Francis, M.J., et al., *Immunological evaluation of the multiple antigen peptide (MAP) system using the major immunogenic site of foot-and-mouth disease virus.* Immunology, 1991. **73**(3): p. 249-54.
177. Bracci, L., et al., *Synthetic peptides in the form of dendrimers become resistant to protease activity.* J Biol Chem, 2003. **278**(47): p. 46590-5.
178. Jain, K., et al., *Dendrimer toxicity: Let's meet the challenge.* Int J Pharm, 2010. **394**(1-2): p. 122-42.
179. Pini, A., et al., *Antimicrobial activity of novel dendrimeric peptides obtained by phage display selection and rational modification.* Antimicrob Agents Chemother, 2005. **49**(7): p. 2665-72.
180. Rodrigo, A.C., et al., *Efficient, non-toxic hybrid PPV-PAMAM dendrimer as a gene carrier for neuronal cells.* Biomacromolecules, 2011. **12**(4): p. 1205-13.
181. Chauhan, A.S., N.K. Jain, and P.V. Diwan, *Pre-clinical and behavioural toxicity profile of PAMAM dendrimers in mice.* Proceedings of the Royal Society, 2010(466): p. 1535–1550.

182. Wooldridge, L., et al., *Tricks with tetramers: how to get the most from multimeric peptide-MHC.* Immunology, 2009. **126**(2): p. 147-64.
183. Wiwattanapatapee, R., et al., *Anionic PAMAM dendrimers rapidly cross adult rat intestine in vitro: a potential oral delivery system?* Pharm Res, 2000. **17**(8): p. 991-8.
184. Sonn, K., et al., *A metallothionein mimetic peptide protects neurons against kainic acid-induced excitotoxicity.* J Neurosci Res, 2010. **88**(5): p. 1074-82.
185. Asmussen, J.W., et al., *Peptides modeled after the alpha-domain of metallothionein induce neurite outgrowth and promote survival of cerebellar granule neurons.* Eur J Cell Biol, 2009. **88**(8): p. 433-43.
186. Pankratova, S., et al., *Neuroprotective properties of a novel, non-haematopoietic agonist of the erythropoietin receptor.* Brain, 2010. **133**: p. 2281-2294.
187. Pulido, P., J.H. Kagi, and B.L. Vallee, *Isolation and some properties of human metallothionein.* Biochemistry, 1966. **5**(5): p. 1768-77.
188. Atcha, Z., et al., *Alternative method of oral dosing for rats.* J Am Assoc Lab Anim Sci, 2010. **49**(3): p. 335-43.
189. Huang, X., et al., *Redox-active metals, oxidative stress, and Alzheimer's disease pathology.* Ann N Y Acad Sci, 2004. **1012**: p. 153-63.
190. Fletcher, T.L., P. De Camilli, and G. Banker, *Synaptogenesis in hippocampal cultures: evidence indicating that axons and dendrites become competent to form synapses at different stages of neuronal development.* J Neurosci, 1994. **14**(11 Pt 1): p. 6695-706.
191. Mundy, W.R. and T.M. Freudenrich, *Sensitivity of immature neurons in culture to metal-induced changes in reactive oxygen species and intracellular free calcium.* Neurotoxicology, 2000. **21**(6): p. 1135-44.
192. Cullen, D.K., et al., *Synapse-to-neuron ratio is inversely related to neuronal density in mature neuronal cultures.* Brain Research, 2010. **1359**: p. 44-55.
193. Brining, S.K., *Predicting the in vitro toxicity of synthetic beta-amyloid (1-40).* Neurobiol Aging, 1997. **18**(6): p. 581-9.
194. Zarandi, M., et al., *Synthesis of Abeta[1-42] and its derivatives with improved efficiency.* J Pept Sci, 2007. **13**(2): p. 94-9.
195. May, P.C., et al., *beta-Amyloid peptide in vitro toxicity: lot-to-lot variability.* Neurobiol Aging, 1992. **13**(5): p. 605-7.
196. Li, S., et al., *Synthesis and characterization of a high-affinity {alpha}v{beta}6-specific ligand for in vitro and in vivo applications.* Mol Cancer Ther, 2009. **8**(5): p. 1239-49.
197. Cheng, Z., et al., *Near-infrared fluorescent RGD peptides for optical imaging of integrin alphavbeta3 expression in living mice.* Bioconjug Chem, 2005. **16**(6): p. 1433-41.
198. Cohen, E. and A. Dillin, *The insulin paradox: aging, proteotoxicity and neurodegeneration.* Nat Rev Neurosci, 2008. **9**(10): p. 759-67.
199. Owen, S.C., et al., *Colloidal drug formulations can explain "bell-shaped" concentration-response curves.* ACS Chem Biol, 2014. **9**(3): p. 777-84.
200. Cuajungco, M.P., et al., *Evidence that the beta-amyloid plaques of Alzheimer's disease represent the redox-silencing and entombment of abeta by zinc.* J Biol Chem, 2000. **275**(26): p. 19439-42.

201. West, A.K., J.Y. Leung, and R.S. Chung, *Neuroprotection and regeneration by extracellular metallothionein via lipoprotein-receptor-related proteins.* J Biol Inorg Chem, 2011. **16**(7): p. 1115-22.
202. Landowski, L.M., et al., *Low-density lipoprotein receptor-related proteins in a novel mechanism of axon guidance and peripheral nerve regeneration.* J Biol Chem, 2015.
203. Landowski, L., *LRP receptors in a novel mechanism of axon pathfinding and peripheral nerve regeneration*, in *Menzies Research Institute Tasmania*. 2014, University of Tasmania: Hobart. p. 278.
204. Leung, J.Y., et al., *Metallothionein promotes regenerative axonal sprouting of dorsal root ganglion neurons after physical axotomy.* Cell Mol Life Sci, 2012. **69**(5): p. 809-17.
205. Yeung, T., et al., *Membrane phosphatidylserine regulates surface charge and protein localization.* Science, 2008. **319**(5860): p. 210-3.
206. Milanino, R., K.D. Rainsford, and G.P. Velo, eds. *Copper and zinc in inflammation*. 1989, Kluwer Academic Publishers Group: DordrechtNetherlands. 150.
207. Stillman, M.J., et al., *Spectroscopic studies of copper, silver and gold-metallothioneins.* Met Based Drugs, 1994. **1**(5-6): p. 375-94.
208. Markesbery, W.R., et al., *Brain trace element concentrations in aging.* Neurobiol Aging, 1984. **5**(1): p. 19-28.
209. Takeda, A., *Insight into glutamate excitotoxicity from synaptic zinc homeostasis.* Int J Alzheimers Dis, 2010. **2011**: p. 491597.
210. Huang, E.P., *Metal ions and synaptic transmission: think zinc.* Proc Natl Acad Sci U S A, 1997. **94**(25): p. 13386-7.
211. Weiss, J.H., S.L. Sensi, and J.Y. Koh, *Zn(2+): a novel ionic mediator of neural injury in brain disease.* Trends Pharmacol Sci, 2000. **21**(10): p. 395-401.
212. McRae, R., et al., *In situ imaging of metals in cells and tissues.* Chem Rev, 2009. **109**(10): p. 4780-827.
213. Paoletti, P., et al., *Zinc at glutamatergic synapses.* Neuroscience, 2009. **158**(1): p. 126-36.
214. Perez-Rosello, T., et al., *Synaptic Zn2+ inhibits neurotransmitter release by promoting endocannabinoid synthesis.* J Neurosci, 2013. **33**(22): p. 9259-72.
215. Bjorklund, U., et al., *Primary cultures from cerebral cortex and hippocampus enriched in glutamatergic and GABAergic neurons.* Neurochem Res, 2010. **35**(11): p. 1733-42.
216. Opazo, C., et al., *Metalloenzyme-like activity of Alzheimer's disease beta-amyloid. Cu-dependent catalytic conversion of dopamine, cholesterol, and biological reducing agents to neurotoxic H(2)O(2).* J Biol Chem, 2002. **277**(43): p. 40302-8.
217. Mayes, J., et al., *beta-amyloid fibrils in Alzheimer disease are not inert when bound to copper ions but can degrade hydrogen peroxide and generate reactive oxygen species.* J Biol Chem, 2014. **289**(17): p. 12052-62.
218. Dikalov, S.I., M.P. Vitek, and R.P. Mason, *Cupric-amyloid beta peptide complex stimulates oxidation of ascorbate and generation of hydroxyl radical.* Free Radic Biol Med, 2004. **36**(3): p. 340-7.

219. Howells, C., *Interactions between metallothionein-2A and B-amyloid in a cortical neuron model*, in *Discipline of Biochemistry*. 2009, University of Tasmania: Hobart.
220. Godyna, S., et al., *Identification of the low density lipoprotein receptor-related protein (LRP) as an endocytic receptor for thrombospondin-1.* J Cell Biol, 1995. **129**(5): p. 1403-10.
221. Kanekiyo, T. and G. Bu, *Receptor-associated protein interacts with amyloid-beta peptide and promotes its cellular uptake.* J Biol Chem, 2009. **284**(48): p. 33352-9.
222. Willnow, T.E., et al., *RAP, a specialized chaperone, prevents ligand-induced ER retention and degradation of LDL receptor-related endocytic receptors.* EMBO J, 1996. **15**(11): p. 2632-9.
223. Hiesberger, T., et al., *Direct binding of Reelin to VLDL receptor and ApoE receptor 2 induces tyrosine phosphorylation of disabled-1 and modulates tau phosphorylation.* Neuron, 1999. **24**(2): p. 481-9.
224. Reddy, S.S., et al., *Similarities and differences in structure, expression, and functions of VLDLR and ApoER2.* Mol Neurodegener, 2011. **6**: p. 30.
225. Takahashi, S., et al., *The very low-density lipoprotein (VLDL) receptor: characterization and functions as a peripheral lipoprotein receptor.* J Atheroscler Thromb, 2004. **11**(4): p. 200-8.
226. Weeber, E.J., et al., *Reelin and ApoE receptors cooperate to enhance hippocampal synaptic plasticity and learning.* J Biol Chem, 2002. **277**(42): p. 39944-52.
227. Magga, J., et al., *Human intravenous immunoglobulin provides protection against Abeta toxicity by multiple mechanisms in a mouse model of Alzheimer's disease.* J Neuroinflammation, 2010. **7**: p. 90.
228. Jankowsky, J.L., et al., *Mutant presenilins specifically elevate the levels of the 42 residue beta-amyloid peptide in vivo: evidence for augmentation of a 42-specific gamma secretase.* Hum Mol Genet, 2004. **13**(2): p. 159-70.
229. Malm, T., J. Koistinaho, and K. Kanninen, *Utilization of APPswe/PS1dE9 Transgenic Mice in Research of Alzheimer's Disease: Focus on Gene Therapy and Cell-Based Therapy Applications.* Int J Alzheimers Dis, 2011. **2011**: p. 517160.
230. Wright, A.L., et al., *Neuroinflammation and neuronal loss precede Abeta plaque deposition in the hAPP-J20 mouse model of Alzheimer's disease.* Plos One, 2013. **8**(4): p. e59586.
231. Schneider, C.A., W.S. Rasband, and K.W. Eliceiri, *NIH Image to ImageJ: 25 years of image analysis.* Nat Methods, 2012. **9**(7): p. 671-5.
232. Sommer, C., et al., *Ilastik: Interactive learning and segmentation toolkit*, in *Biomedical Imaging: From Nano to Macro, 2011 IEEE International Symposium on*. 2011, IEEE: Chicago, IL. p. 230-233.
233. Ito, D., et al., *Enhanced expression of Iba1, ionized calcium-binding adapter molecule 1, after transient focal cerebral ischemia in rat brain.* Stroke, 2001. **32**(5): p. 1208-15.
234. Kaspar, A.A. and J.M. Reichert, *Future directions for peptide therapeutics development.* Drug Discov Today, 2013. **18**(17-18): p. 807-17.
235. Villegas, J.C. and R.D. Broadwell, *Transcytosis of protein through the mammalian cerebral epithelium and endothelium. II. Adsorptive transcytosis of*

WGA-HRP and the blood-brain and brain-blood barriers. J Neurocytol, 1993. **22**(2): p. 67-80.
236. Herve, F., N. Ghinea, and J.M. Scherrmann, *CNS delivery via adsorptive transcytosis.* AAPS J, 2008. **10**(3): p. 455-72.
237. Hippius, H. and G. Neundorfer, *The discovery of Alzheimer's disease.* Dialogues Clin Neurosci, 2003. **5**(1): p. 101-8.
238. Tang, Y.P. and E.S. Gershon, *Genetic studies in Alzheimer's disease.* Dialogues Clin Neurosci, 2003. **5**(1): p. 17-26.
239. Zhang, W., et al., *Soluble Abeta levels correlate with cognitive deficits in the 12-month-old APPswe/PS1dE9 mouse model of Alzheimer's disease.* Behav Brain Res, 2011. **222**(2): p. 342-50.
240. Tomic, J.L., et al., *Soluble fibrillar oligomer levels are elevated in Alzheimer's disease brain and correlate with cognitive dysfunction.* Neurobiol Dis, 2009. **35**(3): p. 352-8.
241. Klein, W.L., *Abeta toxicity in Alzheimer's disease: globular oligomers (ADDLs) as new vaccine and drug targets.* Neurochem Int, 2002. **41**(5): p. 345-52.
242. Cleary, J.P., et al., *Natural oligomers of the amyloid-beta protein specifically disrupt cognitive function.* Nat Neurosci, 2005. **8**(1): p. 79-84.
243. Liu, L., et al., *Abeta levels in serum, CSF and brain, and cognitive deficits in APP + PS1 transgenic mice.* Neuroreport, 2003. **14**(1): p. 163-6.
244. Asuni, A.A., et al., *Modulation of amyloid precursor protein expression reduces beta-amyloid deposition in a mouse model.* Ann Neurol, 2014. **75**(5): p. 684-99.
245. Greig, N.H., et al., *An overview of phenserine tartrate, a novel acetylcholinesterase inhibitor for the treatment of Alzheimer's disease.* Curr Alzheimer Res, 2005. **2**(3): p. 281-90.
246. Lahiri, D.K., et al., *The experimental Alzheimer's disease drug posiphen [(+)-phenserine] lowers amyloid-beta peptide levels in cell culture and mice.* J Pharmacol Exp Ther, 2007. **320**(1): p. 386-96.
247. Klein, J., *Phenserine.* Expert Opin Investig Drugs, 2007. **16**(7): p. 1087-97.
248. Kanekiyo, T. and G. Bu, *The low-density lipoprotein receptor-related protein 1 and amyloid-beta clearance in Alzheimer's disease.* Front Aging Neurosci, 2014. **6**: p. 93.
249. Kang, D.E., et al., *Modulation of amyloid beta-protein clearance and Alzheimer's disease susceptibility by the LDL receptor-related protein pathway.* J Clin Invest, 2000. **106**(9): p. 1159-66.
250. Silverberg, G.D., et al., *Amyloid efflux transporter expression at the blood-brain barrier declines in normal aging.* J Neuropathol Exp Neurol, 2010. **69**(10): p. 1034-43.
251. Vana, K., et al., *LRP/LR as an alternative promising target in therapy of prion diseases, Alzheimer's disease and cancer.* Infect Disord Drug Targets, 2009. **9**(1): p. 69-80.
252. Hong-Qi, Y., S. Zhi-Kun, and C. Sheng-Di, *Current advances in the treatment of Alzheimer's disease: focused on considerations targeting Abeta and tau.* Transl Neurodegener, 2012. **1**(1): p. 21.
253. Bates, K.A., et al., *Chronic gliosis triggers Alzheimer's disease-like processing of amyloid precursor protein.* Neuroscience, 2002. **113**(4): p. 785-96.

254. Mosher, K.I. and T. Wyss-Coray, *Microglial dysfunction in brain aging and Alzheimer's disease.* Biochem Pharmacol, 2014. **88**(4): p. 594-604.
255. Monif, M., G. Burnstock, and D.A. Williams, *Microglia: proliferation and activation driven by the P2X7 receptor.* Int J Biochem Cell Biol, 2010. **42**(11): p. 1753-6.
256. McGeer, P.L., et al., *Reactive microglia are positive for HLA-DR in the substantia nigra of Parkinson's and Alzheimer's disease brains.* Neurology, 1988. **38**(8): p. 1285-91.
257. Mrak, R.E., *Microglia in Alzheimer brain: a neuropathological perspective.* Int J Alzheimers Dis, 2012. **2012**: p. 165021.
258. Dowding, A.J., A. Maggs, and J. Scholes, *Diversity amongst the microglia in growing and regenerating fish CNS: immunohistochemical characterization using FL.1, an anti-macrophage monoclonal antibody.* Glia, 1991. **4**(4): p. 345-64.
259. Maezawa, I., et al., *Amyloid-beta protein oligomer at low nanomolar concentrations activates microglia and induces microglial neurotoxicity.* J Biol Chem, 2011. **286**(5): p. 3693-706.
260. McLarnon, J.G., et al., *Upregulated expression of purinergic P2X(7) receptor in Alzheimer disease and amyloid-beta peptide-treated microglia and in peptide-injected rat hippocampus.* J Neuropathol Exp Neurol, 2006. **65**(11): p. 1090-7.
261. Garcao, P., C.R. Oliveira, and P. Agostinho, *Comparative study of microglia activation induced by amyloid-beta and prion peptides: role in neurodegeneration.* J Neurosci Res, 2006. **84**(1): p. 182-93.
262. Tang, Y. and W. Le, *Differential Roles of M1 and M2 Microglia in Neurodegenerative Diseases.* Mol Neurobiol, 2015.
263. Cameron, B. and G.E. Landreth, *Inflammation, microglia, and Alzheimer's disease.* Neurobiol Dis, 2010. **37**(3): p. 503-9.
264. Sofroniew, M.V. and H.V. Vinters, *Astrocytes: biology and pathology.* Acta Neuropathol, 2010. **119**(1): p. 7-35.
265. Rodriguez, J.J., et al., *Astroglia in dementia and Alzheimer's disease.* Cell Death and Differentiation, 2009. **16**(3): p. 378-85.
266. Thomason, L.A., et al., *Reactive astrocytes associated with plaques in TgCRND8 mouse brain and in human Alzheimer brain express phosphoprotein enriched in astrocytes (PEA-15).* FEBS Lett, 2013. **587**(15): p. 2448-54.
267. Matsuoka, Y., et al., *Inflammatory responses to amyloidosis in a transgenic mouse model of Alzheimer's disease.* Am J Pathol, 2001. **158**(4): p. 1345-54.
268. Mrak, R.E. and W.S. Griffin, *Role of Activated Glia and of Glial Cytokines in Alzheimer's Disease: A Review.* EOS, 1996. **16**(3-4): p. 80-84.
269. Pike, C.J., B.J. Cummings, and C.W. Cotman, *Early association of reactive astrocytes with senile plaques in Alzheimer's disease.* Exp Neurol, 1995. **132**(2): p. 172-9.
270. Jang, E., et al., *Phenotypic polarization of activated astrocytes: the critical role of lipocalin-2 in the classical inflammatory activation of astrocytes.* J Immunol, 2013. **191**(10): p. 5204-19.
271. Verkhratsky, A., et al., *Astrocytes in Alzheimer's disease.* Neurotherapeutics, 2010. **7**(4): p. 399-412.

272. Watson, R.R., ed. *Foods and Dietary Supplements in the Prevention and Treatment of Disease in Older Adults*. 2015, Academic Press. 398.
273. Garwood, C.J., et al., *Astrocytes are important mediators of Abeta-induced neurotoxicity and tau phosphorylation in primary culture.* Cell Death Dis, 2011. **2**: p. e167.
274. Panter, S.S., et al., *Glial fibrillary acidic protein and Alzheimer's disease.* Neurochem Res, 1985. **10**(12): p. 1567-76.
275. Miyazaki, I., et al., *Astrocyte-derived metallothionein protects dopaminergic neurons from dopamine quinone toxicity.* Glia, 2011. **59**(3): p. 435-51.
276. Terry, R.D., et al., *Physical basis of cognitive alterations in Alzheimer's disease: synapse loss is the major correlate of cognitive impairment.* Ann Neurol, 1991. **30**(4): p. 572-80.
277. Sze, C.I., et al., *Loss of the presynaptic vesicle protein synaptophysin in hippocampus correlates with cognitive decline in Alzheimer disease.* J Neuropathol Exp Neurol, 1997. **56**(8): p. 933-44.
278. Mucke, L., et al., *High-level neuronal expression of abeta 1-42 in wild-type human amyloid protein precursor transgenic mice: synaptotoxicity without plaque formation.* J Neurosci, 2000. **20**(11): p. 4050-8.
279. Tampellini, D., et al., *Effects of synaptic modulation on beta-amyloid, synaptophysin, and memory performance in Alzheimer's disease transgenic mice.* J Neurosci, 2010. **30**(43): p. 14299-304.
280. Gylys, K.H., et al., *Synaptic changes in Alzheimer's disease: increased amyloid-beta and gliosis in surviving terminals is accompanied by decreased PSD-95 fluorescence.* Am J Pathol, 2004. **165**(5): p. 1809-17.
281. Yuki, D., et al., *DHA-PC and PSD-95 decrease after loss of synaptophysin and before neuronal loss in patients with Alzheimer's disease.* Sci Rep, 2014. **4**: p. 7130.
282. Shao, C.Y., et al., *Postsynaptic degeneration as revealed by PSD-95 reduction occurs after advanced Abeta and tau pathology in transgenic mouse models of Alzheimer's disease.* Acta Neuropathol, 2011. **122**(3): p. 285-92.
283. Xu, Z., et al., *Deletion of aquaporin-4 in APP/PS1 mice exacerbates brain Abeta accumulation and memory deficits.* Mol Neurodegener, 2015. **10**(1): p. 58.
284. Mitew, S., et al., *Altered synapses and gliotransmission in Alzheimer's disease and AD model mice.* Neurobiol Aging, 2013. **34**(10): p. 2341-51.
285. Arsenault, D., et al., *DHA improves cognition and prevents dysfunction of entorhinal cortex neurons in 3xTg-AD mice.* Plos One, 2011. **6**(2): p. e17397.
286. Du, A.T., et al., *Magnetic resonance imaging of the entorhinal cortex and hippocampus in mild cognitive impairment and Alzheimer's disease.* J Neurol Neurosurg Psychiatry, 2001. **71**(4): p. 441-7.
287. Serrano-Pozo, A., et al., *Neuropathological alterations in Alzheimer disease.* Cold Spring Harb Perspect Med, 2011. **1**(1): p. a006189.
288. Pankhurst, M.W., *Immune system modulation in the brain injury of the metallothionein-I/II null mutant mouse* in *Faculty of Health Science*. 2011, Universoty of Tasmania: Hobart. p. 180.
289. Ling, C., et al., *Traumatic injury and the presence of antigen differentially contribute to T-cell recruitment in the CNS.* J Neurosci, 2006. **26**(3): p. 731-41.

290. Huseby, E.S., et al., *A pathogenic role for myelin-specific CD8(+) T cells in a model for multiple sclerosis.* J Exp Med, 2001. **194**(5): p. 669-76.
291. Hauser, S.L., et al., *Immunohistochemical analysis of the cellular infiltrate in multiple sclerosis lesions.* Ann Neurol, 1986. **19**(6): p. 578-87.

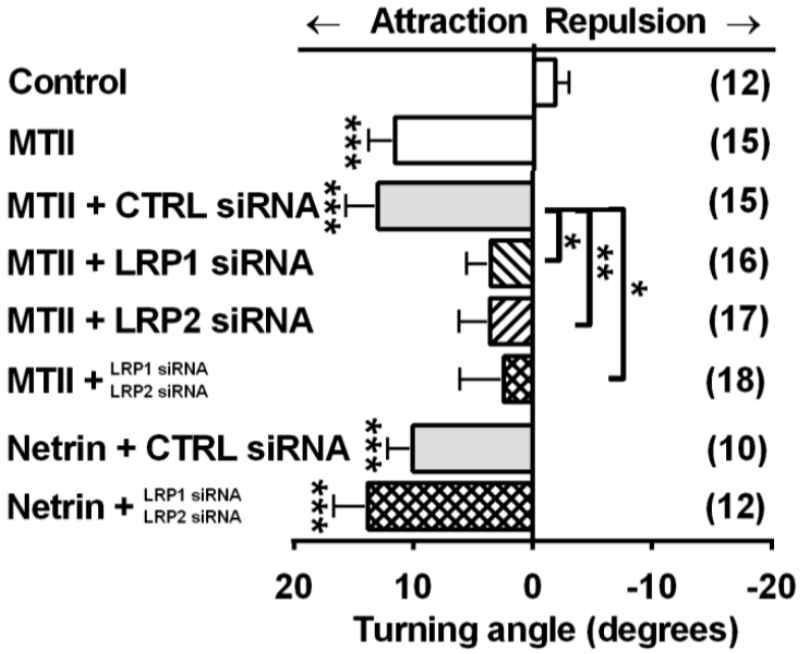

Figure A1. Knockdown of LRP1 and LRP2 using siRNA perturbs MT2-induced growth cone chemoattraction

MT2 is a chemoattractant and induces growth cone turning of DRG neurons towards the MT2 concentration gradient. siRNA targeted to LRP1 and LRP2 abolished the response of growth cones to MT2. Reproduced from [202, 203] with permission.